SUPERPARAMAGNETIC IRON OXIDE NANOPARTICLES AS ARSENIC ADSORBENT

Development of Nanofiber SPION Supports and Arsenic Speciation Using Synchrotron and Hyphenated Techniques

Diego Morillo Martín

Tesis doctoral

Doctorado en Química

Directores: Manuel Valiente Malmagro
Gustavo Pérez González

Departamento de Química

Facultad de Ciencias

2013

Memoria presentada para aspirar al Grado de Doctor por

Diego Morillo Martín

Visto bueno, los directores

Dr. Manuel Valiente Malmagro   **Dr. Gustavo Pérez González**

Bellaterra (Cerdanyola del Vallès) a 27 de Septiembre de 2013

UAB
Universitat Autònoma
de Barcelona

In addition, the congresses and scientific meeting were the PhD. thesis results have been presented are detailed:

➤ **Trends in NanoTechnology 2009 (TNT)**. Poster communication: "*Fe$_3$O$_4$ nanoparticles-Loaded Cellulose Sponge: Novel system for the Arsenic removal from aqueous solution*". 7th to 11th September, 2009. Barcelona (Spain).

➤ **Sisena Trobada de Joves Investigadors dels Països Catalans.** Oral communication: "*Avanços en l'adsorció d'arsenic sobre nanopartícules*". 1st to 2nd February, 2010. Valencia (Spain).

➤ **Higher European Research Course for Users of Large Experimental Systems: Synchrotron radiation and neutrons techniques in physics and chemistry of condensed matter (HERCULES 2011)**. Oral communication: "*Arsenic Speciation in SPION Loaded Cellulose Sponge by XAS*". 28th February to 31st March, 2011**.** European Synchrotron Radiation Facility (ESRF), Grenoble (France).

➤ **13th Workshop on Progress in Trace Metal Speciation for Environmental Analytical Chemistry (TraceSpec).** Oral communication: "*Direct arsenic speciation in SPION loaded cellulose sponge by XAS*". 18th to 20th May, 2011. Pau (France)

➤ **International Symposium on Metal Complexes (ISMEC)**. Oral communication: "*SPION-Loaded Cellulose Sponge, a System for Arsenic Removal from Aqueous Solutions*". 11th to 13th July, 2011. Messina (Italy).

➤ **International Workshop "Hadrumetum Eco-Industries"**. Oral communication: "*SPION-Loaded Cellulose Sponge, a System for Arsenic Removal from Aqueous Solutions*". 10th to 15th November, 2011. Sousse-Hammamet (Tunisia)

➤ **SOWAEUMED International Workshop "ITS2WAT-2012"**. Poster communication: "*SPION-loaded Cellulose Sponge, as Novel System for Arsenic Removal from Aqueous Solutions regarding non-supported SPION*". 23-26/05/2012. Marrakech (Morocco).

A mis padres,

a mi hermana y

a mi Amorsito

SUMMARY - RESUMEN

SUMMARY

The studies that have been carried out in the present PhD thesis Project are based in the development of a synthesis methodology and characterization of nanostructured systems as an innovative facility for the recovery of arsenic from contaminated effluents and the purification of these effluents. These adsorbent materials have a base element, *Superparamagnetic Iron Oxide Nanoparticles* (**SPION**). Using these nanoparticles arsenic adsorption experiments were carried out to evaluate the optimum adsorption parameters (contact time, pH effect and concentration effect). These studies have determine the maximum adsorption capacity of SPION when the contaminant element is adsorbed, indicating the adsorption capacity to be dependent of the chemical form of the arsenic present in the target solution.

It is expected to use the high affinity and string interaction between Fe-As as it is proved in several natural compounds. The results obtained in this work involve the improvement of SPION synthesis and the development of new adsorbent systems, based on SPION including, SPION in suspension, surface modified SPION, SPION loaded in either Forager® Sponge or CA and PAN nanofibers. Materials fully characterized and applied to evaluate their arsenic adsorption properties. Inorganic arsenic species, arsenite and arsenate, have been studied in order to determine the influence of adsorption conditions (contact time, pH and As concentration)

Analytical techniques such as ICP-MS, ICP-AES and FP-XRF were used to obtain relevant information regarding the arsenic content in solution and in the adsorbents. Microscopy techniques such as TEM and SEM were applied to characterize the nanoparticles and nanofibers size, morphology and distribution, their magnetic properties were determined by SQUID and structural properties by TGA and ATR-FTIR.

Specific results can be summarized as follows:

The maximum adsorption for arsenate on SPION suspensions was obtained in an acid media (pH 3.6), while arsenite adsorption is not pH dependent of pH, what is consequence of their different acidic properties. Selectivity against cations, Zinc, Nickel and Copper in As(III)/As(V) mixtures was very high while in presence of interfering anions, selectivity decreases in the order: phosphate >> sulphate ~ nitrate ~ chloride, being phosphate the

most interfering anion (adsorption capacity decrease in a 68%) due to the similar affinity for Iron hydroxide compounds. The nanometric size of SPION produces a remarkable higher adsorption than bulk Fe_3O_4 or other iron oxides, making SPION more reactive. However, the main observed drawback is due to the partial aggregation of SPION that reduces their potential adsorption capacity.

3-mercaptopropionic acid was selected as surface modifier to decrease the SPION aggregation. The SPION functionalization with 3-MPA was successfully developed with an optimized 3.7 mmol 3-MPA/ g SPION coating the SPION surface. The optimum parameters for Arsenic adsorption were similar to those with SPION suspension. However, a pH dependence in As(III) adsorption is observed contrary to corresponding results on SPION suspension. The presence of thiol groups is the responsible of these effects. The adsorption capacities are 1.03 mmol As/g SPION and 1.60 mmol As /g SPION for arsenite and arsenate, respectively and improving the SPION suspension adsorption. In this case, selectivity against cations and anions follows the pattern of SPION suspensions but increasing their efficiency due to the presence of thiol groups. 3-MPA coated SPION provide an increase in the adsorption capacity against SPION suspension attributed to the reduction of nanoparticles aggregation because of the role of the organic functionalizing compound.

To overcome the drawbacks of aggregation, SPION was loaded on sponge (Forager® Sponge), successfully developed and optimized to obtain a new adsorbent system with a fine and homogeneous SPION layer over the Forager® Sponge surface. The optimum adsorption parameters were determined to be of similar pattern than those obtained in SPION suspensions. However, the adsorption capacities being 2.11 mmol As/g SPION and 12.09 mmol As /g SPION for arsenite and arsenate, respectively, much higher than those for corresponding suspensions. Selectivity against cations and anions followed previous described behavior for suspensions of SPION.

Novel support based on nanofiber produced from of 15% CA spinning solution with DMAc/Acetone mixture as solvent was determined to have most suitable characteristic as SPION support, with fiber diameter ranged from 200-300 nm.

Other nanofibers prepared from 7.5–15 wt% PAN spinning solution with DMF as solvent was identified as the conditions for best spinnability with the diameter ranged among 300 nm to 1.5 μm. Hydrolyzed HPAN nanofiber from 10 wt% solutions represents the

optimum nanofibers that can be electrospun as SPION supports with a diameter size of 350 nm being the SPION fixation 2.9-144 mg per gram of HPAN nanofiber. The adsorption capacity increases to a very high values with adsorption capacity of 32 mmol As(V) / g SPION, almost three times higher than the SPION loaded Forager® Sponge, with a SPION concentration of 2.9 mg SPION / g HPAN. Continuous process performed by counterflow to avoid nanofiber compression reached an adsorption capacity about 63 mmol As(V) / g SPION. The achieved figures, in terms of adsorbent, means an adsorption capacity up to the 850mg of As(V) / g of adsorbent system, the highest never obtained before. Application to industrial water samples was carried out Under the experimental conditions employed, just one hour is required to remove all the As(V) entering the column..

Indirect speciation by HPLC-ICP-MS has been verified as a useful technique for the arsenic speciation in liquid samples. Retention times were determined with a significant chromatographic resolution, being of 3.0 min for arsenite while arsenate has a retention time of 6.6 min. A good correlation is obtained between the speciation results for As(III) and As(V) by HPLC-ICP-MS and the total content by ICP-MS, with recoveries ranging from 95% to 100%.

Direct arsenic speciation by synchrotron radiation techniques has been carried out on adsorbent solid samples. Principal Components Analysis (PCA) and linear combination fit of corresponding reference samples were applied to spectral data to evaluate the arsenic species content in the different target samples of SPION loaded Forager® Sponge at different pH values, revealing arsenate species to be predominant, and reaching up to a 97% of the total adsorbed Arsenic. These results confirm arsenate to be selectively removed from the contaminated water with the indicated adsorbent system. Direct speciation study of iron in the SPION samples reveals that SPION maintains its structure after the Arsenic adsorption process in all cases, independently of the adsorbed species, As(III), As(V) or a mixture of both species.This work provides knowledge, demonstrated advances and different nanostructured adsorbent systems that can be potentially applied to remove highly toxic contaminants such as arsenic. An example of the appropriate technologic transference derived from the PhD. Thesis is the Spanish Patent "*Filtro de tratamiento de líquidos con nanopartículas de magnetita y procedimientos correspondientes*". Ref: *P201330144* with priority date on Febrery 6th, 2013.

RESUMEN

Los estudios que se han llevado a cabo en la presente tesis doctoral se basan en el desarrollo de una metodología de síntesis y caracterización de sistemas nanoestructurados como recurso innovador para la recuperación de arsénico en efluentes contaminados y la depuración de dichos efluentes. Estos materiales tienen como elemento común, el uso de las *Superparamagnetic Iron Oxide Nanoparticles* (**SPION**), con las que se han realizado diferentes estudios de adsorción para evaluar los parámetros de adsorción óptimos (tiempo de contacto, efecto del pH y de la concentración). Dichos estudios han permitido determinar la máxima capacidad de adsorción del SPION a la hora de extraer el elemento contaminante y observar como se ve afectada dicha capacidad de adsorción, en función de la especie existente del elemento contaminante, lo que indica que la capacidad de adsorción es dependiente de la forma química del arsénico presente en la solución objetivo.

La elección de SPION se fundamenta en el empleo de la fuerte interacción Fe-As demostrada en muchos compuestos naturales, así como por su capacidad magnética. A partir de éste estudio, se han desarrollado diferentes sistemas adsorbentes en modo no soportados, basados en la funcionalización del SPION (**NanoComposites**) o bien empleando sistemas soportados, ya sean con esponja de celulosa (**Forager® Sponge**) impregnada de SPION o los más novedosos, sistemas basados en **nanofibras** (de acetato de celulosa y poliacrilonitrilo). En este último caso, dichos sistemas son sintetizados vía electrospinning y cargados con SPION con el objetivo de incrementar la superficie específica de adsorción y de este modo, facilitar su posible aplicación en muestras reales.

Además, todos los sistemas desarrollados disponen de un valor añadido, ya que las propiedades magnéticas del SPION permiten recuperar las nanopartículas que pueden quedar expuestas en las disoluciones contaminadas de una manera rápida y efectiva, evitando así, una contaminación con nanopartículas del efluente tratado.

El trabajo realizado, ha permitido optimizar tanto la síntesis de SPION, vía co-precipitación, como el desarrollo y caracterización completa de los sistemas adsorbentes para evaluar sus propiedades frente a la adsorción de Arsénico. Las especies inorgánicas de arsénico, arsenito y arsenato, se han evaluado con el fin de determinar la influencia de las condiciones de adsorción.

Técnicas analíticas, tales como ICP-MS, ICP-AES y FP-XRF se utilizaron para obtener la información pertinente sobre el contenido de arsénico en solución y en los adsorbentes. Técnicas de microscopía como SEM y TEM, se aplicaron para caracterizar las nanopartículas y las nanofibras permitiendo conocer su tamaño, distribución y morfología. Sus propiedades magnéticas se determinaron por SQUID y las propiedades estructurales por TGA, XRD y ATR-FTIR.

Los resultados específicos se pueden resumir de la siguiente manera:

La máxima adsorción para el arsenato con SPION en suspensión se obtuvo en un medio ácido (pH 3,6), mientras que la adsorción de arsenito es independiente del pH, lo que es consecuencia de sus diferentes propiedades ácidas. La selectividad frente a la presencia de cationes metálicos tales como Zinc, Níquel y Cobre en las mezclas As(III)/As(V) es muy elevada mientras que en presencia de aniones interferentes, la selectividad disminuye en el orden: fosfato >> sulfato ~ nitrato ~ cloruro, siendo el fosfato el anión más interferente (la disminución de la capacidad de adsorción es de un 68 %) debido a la afinidad similar al arsenato hacia los Fe(III) del SPION. El tamaño nanométrico de SPION produce un notable incremento de la capacidad de adsorción frente a la magnetita (Fe$_3$O$_4$) bulk u otros óxidos de hierro, haciendo al SPION más reactivo. Sin embargo, el principal inconveniente observado es debido a la agregación parcial de SPION que reduce su potencial capacidad de adsorción.

El ácido 3-mercaptopropiónico fue seleccionado como modificador superficial para disminuir la agregación del SPION. La funcionalización del SPION con 3-MPA se desarrolló con éxito con un recubrimiento optimizado de 3,7 mmol de 3-MPA / g SPION en la superficie del SPION. Los parámetros óptimos para la adsorción de As(V) fueron similares a los obtenidos con el SPION en suspensión. Sin embargo, se observó una dependencia del pH en la adsorción de As(III) al contrario de lo que sucedía en los resultados correspondientes con el SPION en suspensión. La presencia de grupos tiol es la responsable de estos efectos. Las capacidades de adsorción son de 1,03 mmol As(III)/g SPION y 1,60 mmol As(V)/g SPION para arsenito y arsenato , respectivamente, y la mejorando la adsorción del SPION en suspensión. En este caso, la selectividad frente a cationes metálicos y aniones sigue el patrón de las suspensiones de SPION pero incrementando su eficiencia debido a la presencia de grupos

tiol. SPION modificado con 3-MPA proporciona un aumento en la capacidad de adsorción atribuida a la reducción de la agregación de nanopartículas debido a la función del compuesto de funcionalización orgánica.

Para superar los inconvenientes de la agregación, el SPION se cargó en esponja (Forager® Sponge), satisfactoriamente desarrollada y optimizada para obtener un nuevo sistema de adsorbente con una fina y homogénea capa de SPION sobre la superficie de la Forager® Sponge. Los parámetros óptimos de adsorción que se determinaron eran de un patrón similar a los obtenidos en suspensiones SPION. Sin embargo, las capacidades de adsorción de ser 2,11 mmol As(III)/g SPION y 12,09 mmol As(V)/g SPION para arsenito y arsenato , respectivamente , mucho más alto que los de las suspensiones correspondientes. Selectividad frente cationes metálicos y aniones sigue el comportamiento descrito anterior para las suspensiones de SPION.

Un innovador soporte basad en nanofibras producido vía electrospinning a partir de una disolución de Acetato de Celulosa 15% en una mezcla de DMAc/Acetona se determinó de tener las características más adecuadas para poder depositar SPION , con un diámetro de fibra entre 200-300 nm.

Otras nanofibras fueron sintetizadas vía electrospinning a partir disoluciones entre 7,5 y 15 % de Poliacrilonitrilo en DMF y se identificaron las condiciones para la mejor síntesis con un diámetro de fibra entre 300 nm y 1,5 µm. La hidrolisis de las nanofibras de PAN, HPAN, al 10% representa a las nanofibras óptimas que pueden soportar al SPION, presentando un diámetro de 350 nm y una carga de SPION variable entre 2 a 144 mg de SPION por gramo de nanofibras de HPAN. La capacidad de adsorción aumenta a elevados valores de capacidad de adsorción de 32 mmol As(V) / g SPION , casi tres veces más alta que la Forager® Sponge cargada con SPION, con una concentración de 2.9 mg SPION / g HPAN. Procesos de adsorción en continuo realizados a contracorriente para evitar la compresión de nanofibras alcanzaron una capacidad de adsorción de 63 mmol As(V)/ g SPION. Las cifras obtenidos, en términos del adsorbente, significan una capacidad de adsorción hasta la 850 mg de As (V)/g de sistema adsorbente, el más alto obtenido nunca antes. Se llevó a cabo su aplicación a muestras de agua industrial en las condiciones experimentales empleadas anteriormente, requiriéndose solamente una hora para eliminar todo el As (V) que entra en la columna.

Se ha verificado la especiación indirecta por HPLC-ICP-MS como una técnica útil para la especiación de arsénico en muestras líquidas. Los tiempos de retención se determinaron con una significativa resolución cromatográfica, siendo de 3,0 min para arsenito mientras que el arsenato tiene un tiempo de retención de 6,6 min. Se obtiene una buena correlación entre los resultados de especiación de As(III) y As(V) por HPLC-ICP-MS y el contenido total por ICP-MS , con recuperaciones que van desde 95 % a 100 % .

Se ha llevado a cabo la especiación directa de Arsénico mediante técnicas de radiación sincrotrón en muestras sólidas de adsorbente. Análisis de Componentes Principales (PCA) y ajuste de mínimos cuadrados se aplicaron a los datos espectrales de las muestras de referencia para evaluar el contenido de especies de arsénico en las diferentes muestras de Forager® Sponge cargadas con SPION procedentes de ensayos a diferentes pHs, revelando que arsenato es la especie predominante y que alcanza hasta un 97 % del total de arsénico adsorbido.

Estos resultados confirman que el arsenato es eliminado selectivamente del agua contaminada con el sistema adsorbente descrito anteriormente. El estudio de especiación directa de hierro en las muestras de SPION revela que, en todos los casos, el SPION mantiene su estructura después del proceso de adsorción de arsénico, independientemente de las especies adsorbidas (As(III), As(V) o mezcla de ambas). Este trabajo proporciona conocimientos, demostrando avances y diferentes sistemas adsorbentes nanoestructurados que pueden ser potencialmente aplicados para eliminar los contaminantes altamente tóxicos tales como arsénico.

Un ejemplo de la transferencia tecnológica derivada de esta tesis doctoral, es la patente solicitada "*Filtro de tratamiento de líquidos con nanopartículas de magnetita y procedimientos correspondientes*". Ref: *P201330144* y con fecha de prioridad del 6 de Febrero de 2013.

INDEX

General Index

Abbreviations

ATR-FTIR	Attenuated Total Reflectance Fourier Transform Infrared Spectroscopy.
CA	Cellulose Acetate.
DESY	Deutsches Elektronen-Synchrotron (German Electron Synchrotron).
DMAc	Dimethylacetamide.
DMF	Dimethylformamide.
EDA	Ethylenediamine.
EDS/EDX	Energy-dispersive X-ray Spectroscopy.
ESRF	European Synchrotron Radiation Facility.
EXAFS	Extended X-ray Absorption Fine Structure.
FP-XRF	Field Portable X-ray Fluorescence.
GA	Gauge.
hcp	Hexagonal Close-Packed.
HASYLAB	Hamburger Synchrotronstrahlungslabor (Hamburg Synchrotron Radiation Laboratory).
HPAN	Hydrolyzed Polyacrylonitrile.
HPAN-EDA	EDA modified Hydrolyzed Polyacrylonitrile.
HPLC	High Pressure Liquid Chromatography.
HR-TEM	High-Resolution Transmission Electron Microscopy.
ICP-AES	Inductively Coupled Plasma Atomic Emission Spectrometry.
ICP-MS	Inductively Coupled Plasma Mass Spectrometry.
IONMs	Iron Oxide Nanomaterials
NMs	Nanomaterials.
NPs	Nanoparticles.
PAN	Polyacrylonitrile.
PCA	Principal component analysis.

ppb   Parts per billion.

ppm   Parts per million.

ppt   Parts per trillion.

psi   Pound-force per square inch.

pzc   Point of zero change.

SSA   Specific surface area.

SEM   Scanning Electron Microscopy.

SQUID   Superconducting Quantum Interference Device.

SPION   Superparamagnetic Iron Oxide Nanoparticles.

TEM   Transmission Electron Microscopy.

TGA   Thermogravimetric Analysis.

XAS   X-ray Adsorption Spectroscopy.

XANES   X-ray Absorption Near Edge Structure.

XRD   X-Ray Diffraction.

3-MPA   3-mercaptopropionic acid.

1

Introduction

.

1. INTRODUCTION

1.1. Problem statement

Arsenic is the 20th most abundant element found in the earth's crust.[1] Arsenic inorganic forms arise in most natural waters and mainly comprise arsenite and arsenate. These two ions are either naturally occurring or byproducts of industrial waste. The predominant species for ions are, in case of arsenite, arsenous acid (H_3AsO_3) and in case of arsenate, deprotonated species of arsenic acid, $H_2AsO_4^-$ and $HAsO_4^{2-}$. Ingestion of inorganic arsenic results in both cancer and non-cancer related health effects.[2] The USEPA has classified arsenic as a Class A carcinogen. Chronic exposure to low arsenic levels (less than 50 ppb) has been linked to health complications, including skin, kidney, lung, and bladder cancers, as well as other diseases of the skin, and the neurological and cardiovascular systems.[3,4]

Natural oxidation and/or reduction reactions involving arsenic bearing rocks under favorable Eh and pH conditions may mobilize the arsenic and increase arsenic concentrations in groundwater. There are several human activities that could increase arsenic concentrations in groundwater and surface waters as Table 1.1 shows

Table 1.1. Human activities that could increase arsenic concentrations in groundwater and surface water.

Arsenic contaminant human activities [5,6,7,8]	
➢ Oil and coal burning power plants	➢ Waste incineration
➢ Cement works	➢ Disinfectants
➢ Household waste disposal	➢ Glassware production
➢ Electronics industries	➢ Ore production and processing
➢ Metal treatment	➢ Galvanizing
➢ Ammunition factories	➢ Dyes and colours
➢ Wood preservatives	➢ Pesticides, pyrotechnics
➢ Drying agents for cotton	➢ Oil and solvent recycling
➢ Pharmaceutical works	

It is important to note that the most effective way to overcome the adverse health effects of arsenic is prevention of further exposure by providing safe drinking water, because there is no effective treatment to counteract arsenic toxicity. Therefore, The USEPA has

reduced the maximum contaminant level (MCL) of arsenic in drinking water from 50 ppb to 10 ppb, by 23rd January 2006. Since nearly 97% of the water systems affected by the new regulatory standard are small systems, it is vital that cost effective and affordable treatment technologies are developed. The major concern that faces any small community is whether the treatment of arsenic is going to require the construction of a centralized treatment facility or whether treatment is to be accomplished at the point-of-use. In either case, there are major decisions that must be made that require a significant community investment.[9,10]

Several technologies are effective in lowering total arsenic in aqueous solutions namely, coagulation/precipitation,[11,12] ion exchange,[13] adsorption processes,[14,15] and reverse osmosis.[16] Materials that have shown capacities for arsenic sorption include activated alumina;[17] iron media (granular ferric hydroxide, iron oxide coated sand, iron pyrites),[18] synthetic ion exchange resins[19]….

Both arsenite and arsenate have a high affinity for Fe-oxides,[20,21] but the cost of the adsorptive metal removal process is high when pure sorbents (either activated carbon or hydrated Fe and Al oxides) are used.[22] Consequently, the cost of pure adsorbents may be a limitation for many water treatment applications and there is a strong motivation to find cost-effective alternatives.

1.2. Arsenic in the environment

Arsenic is a naturally occurring element present in food, water, and air. Known for centuries to be an effective poison; however, some animal studies suggest that arsenic may be an essential nutrient at low concentrations.[2] It is ubiquitous in the environment and occupies approximately 5×10^{-5} % of the earth's crust and its presence has been reported in several parts of the world, like USA, China, Chile, Bangladesh, Taiwan, Mexico, Argentina, Poland, Canada, Hungary, Japan, and India as Figure 1.1 shows.[23]

Figure 1.1. Probability of occurrence of excessive arsenic concentrations in groundwater. [24]

1.2.1. Arsenic chemistry

Arsenic is a metallic chemical element with a molecular weight of 74.92 and an atomic number of 33. Earth's crust is the source of arsenic, and it exists as various minerals including arsenopyrite (FeAsS), orpiment (As_2S_3), realgar (AsS), and loellingite ($FeAs_2$).[25] Arsenic is found both in organic and inorganic forms. Organic arsenic compounds include CH_5AsO_2 (monomethylarsenic acid, MMA), $C_2HAs_7O_2$ (dimethylarsinic acid, DMA) and arseno-sugars, while inorganic arsenic compounds include H_3AsO_3 (arsenous acid) and H_3AsO_4 (arsenic acid) as Figure 1.2[26] shows. These acids can release hydrogen ions and form a number of anionic forms of inorganic arsenic. Arsenic exists in a variety of oxidations states, such as As(-I) in arsenopyrite (FeAsS), As(II) in realgar (AsS), As(III) in arsenic trioxide (As_2O_3), and As(V) in arsenic pentoxide (As_2O_5) (As(III) which is lightly soluble in water forming arsenious acid and arsenic acid by oxidation of As(III), respectively).[27,28,29,30] In general, it is easily found in combination with Sulphur, Oxygen or Iron.
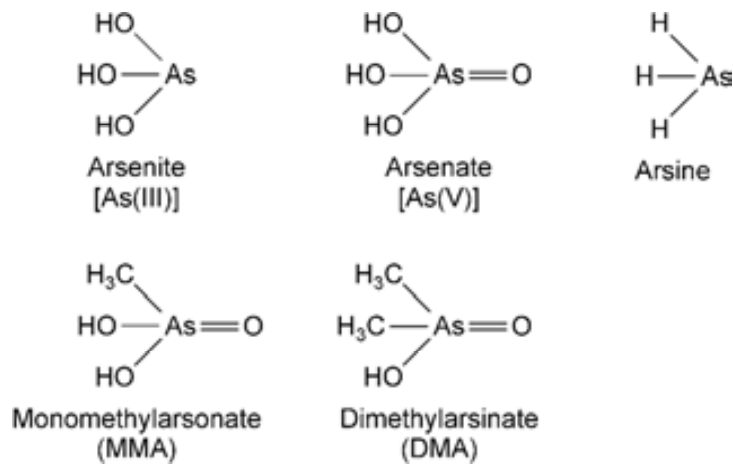
Figure 1.2. Chemical structures of some environmental arsenic compounds.[31]

The most prevalent species of inorganic arsenic in the environment are arsenite and arsenate. It is important to be able to distinguish concentrations of As(III) and As(V) because of their different properties, i.e. As(III) is a carcinogen and is more toxic than As(V). The primary forms of As(III) are uncharged below pH 9.2, because the pK_a of arsenous acid is 9.2. On the other hand, the primary forms of As(V) are anionic above pH 2.2, because the first pK_a for arsenic acid is 2.2. The second and third values of pK_a on As(V) are 7.0, and 11.4 (Table 1.2). Such facts induce a higher mobility of As(III) in front of As(V).

Table 1.2. Dissociation constants of inorganic and organic arsenic compounds.[i][Error! Marcador no definido.]

Compound	pK_1	pK_2	pK_3
H_3AsO_3	9.2	12.2	13.4
H_3AsO_4	2.2	7.0	11.5
MMAA	3.6	8.2	-
DMAA	6.3	-	-

Most natural waters contain the more toxic inorganic forms of arsenic rather than organic species.[32,31] Ground waters contain predominantly As(III) since reducing conditions prevail, while natural surface waters contain As(V) as the dominant species. The aqueous chemistry of arsenic is important, since the chemistry of speciation of arsenic controls the selection of treatment processes.

Typically, the primary method to remove arsenic from waters is to convert As(III) to As(V), because it is easier to remove As(V) than As(III). The dominant arsenic species at each pH are presented in Figure 1.3a and Figure 1.3b.
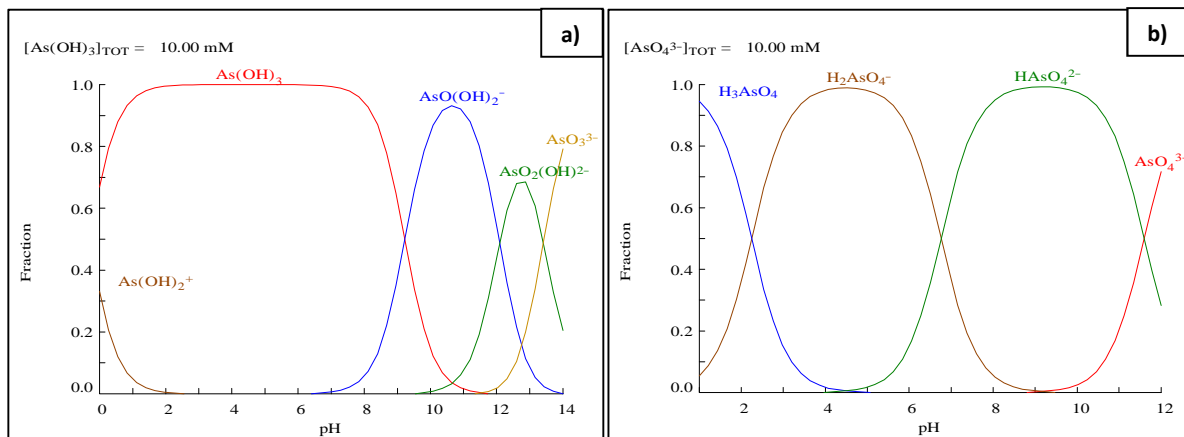
Figure 1.3. Arsenic speciation as pH function for As(III) (a) and As(V) (b). (Ionic strength about 10mM).

The Eh-pH diagram for arsenic species is shown in Figure 1.4. As(III) is thermodynamically stable under reducing conditions, while As(V) is prevalent under oxidized conditions. Arsenic acid and its ionization products are of prime importance for arsenic transport under a wide range of Eh and pH.
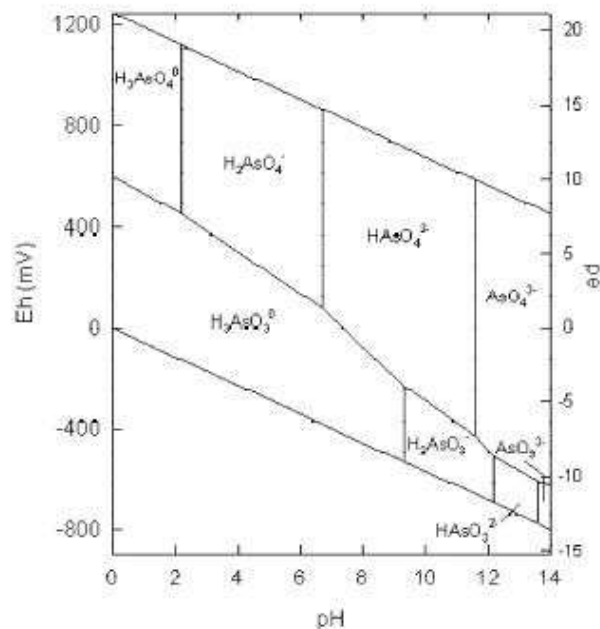
Figure 1.4. Eh-pH diagram for aqueous arsenic species in the As-O_2-H_2O system at 25ºC and 1 bar of pressure.[33]

1.2.2. Arsenic toxicity

Significant exposure to arsenic occurs through both anthropogenic and natural

7

sources. Arsenic in the earth's surface is re-released into the air by volcanoes and is a natural contaminant of some deep-water wells. The primary route of exposure to arsenic for humans is ingestion. However, exposure via inhalation while considered minimal, occurs periodically in some regions.[34] Occupational exposure to arsenic is common in the smelting industry and is increasing in the microelectronics industry. The general population is exposed to low levels of arsenic through the commercial use of inorganic arsenic compounds in common products such as wood preservatives, pesticides, herbicides, fungicides, and paints; and also through the burning of fossil fuels in which arsenic is a contaminant.[35]

As(III) is more toxic than As(V), but both As(III) and As(V) are known human carcinogen by both the inhalation and oral routes. There are several ways for arsenic to enter our body i.e. breathing, eating, or drinking the substance, or by skin contact. The degree of harmfulness of arsenic is measured by the dose, the duration of exposure, and the nature of contact with the arsenic.

The most important threat of environmental arsenic contamination is in the water, especially in drinking water due to the diversity of sources as Table 1.3 shows. [36,37] Arsenic concentrations in natural water are low, but elevated arsenic concentrations are common in groundwater as a result of natural conditions or anthropogenic impacts. [38]

Table 1.3. Arsenic availability in different water sources.

Source	Availability (µg/L)	Arsenic concentration reasons
River	0,1 – 0,8	Geothermal sources, groundwater and industrial contamination.
Lake	0,1 – 0,8	Geothermal sources, microbial activity and mining.
Sea and ocean	1,5	Geothermal sources, industrial activity and river mouth.
Groundwater	<0,5 – 5000	Geothermal sources, agricultural activity and mining.

All in all, concentration and oxidation state are two parameters that affect to the different arsenic toxicity processes. Thereby, it is necessary to understand and determine these processes to be treated in case of health emergency.

1.2.3. Health effects

There are different sources of arsenic toxicity as the Figure 1.5[39] shows. People

exposed to water contaminated with arsenic generally show arsenical skin lesions, which are a late manifestation of arsenic toxicity. Long-term exposure to arsenic contaminated water may lead to various diseases such as conjunctivitis, hyperkeratosis, hyperpigmentation, cardiovascular diseases, disturbance in the peripheral vascular and nervous systems and skin cancer.[40,41,42] Arsenic contamination in ground water is well known[43,44] and has resulted, in many situations, in arsenism and black-foot disease. The effects on the lungs, uterus, genito-urinary tract, and other parts of the body have been also detected in the advance stages of arsenic toxicity. Additionally, high concentrations of arsenic in drinking water also result in an increase in stillbirths and spontaneous abortions.[45]
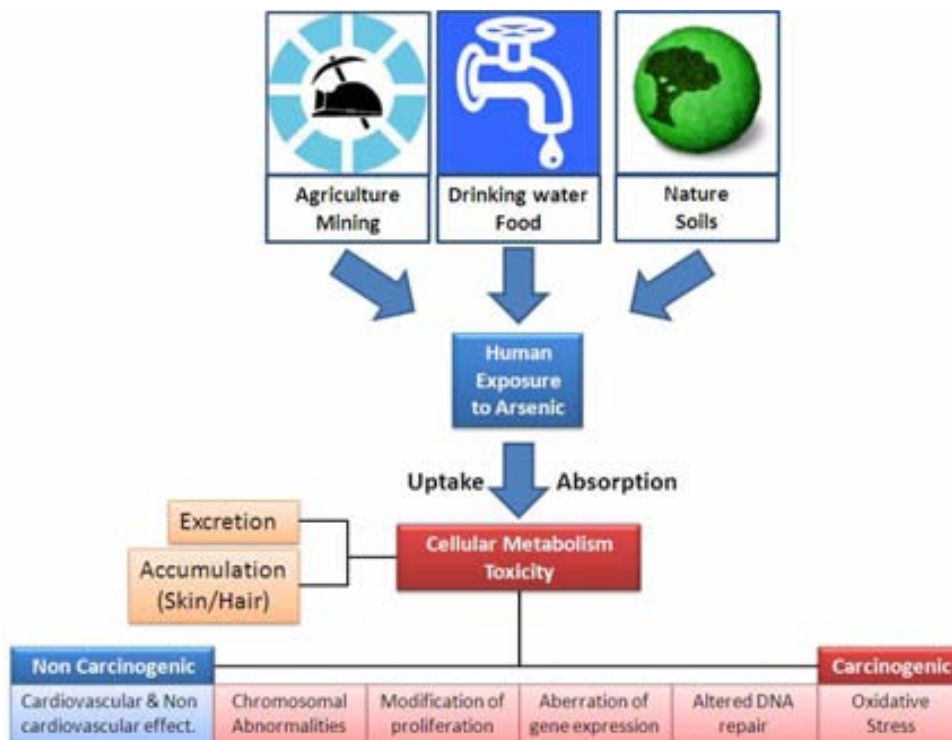
Figure 1.5. Sources of human exposure to arsenic and resulted toxicity.

The USEPA through the use of epidemiological data tried to establish the maximum contaminant level (MCL), which minimizes the adverse effects of arsenic toxicity, as the Figure 1.6 shows. In many countries, cancer risks due to arsenic in water supplies are comparable to those from environmental tobacco smoke and radon in homes.[46] This has forced the EPA to consider lowering the current arsenic MCL in drinking water to as low as 10ppb.

Figure 1.6. Arsenic regulation decisions for drinking water.

Arsenic assimilation by humans is produced in to principal ways, inhalation and ingestion. The assimilated amount is variable in a range of 10 – 1000 mg/L depending on the air and water quality, fish consume or pesticide uses in food croops. Adsorbed arsenic is easily distributed on the body and, except the arsenic accumulation in nails or hair, routes through which arsenic is quickly eliminated.[47]

The most serious effects of arsenic poisoning by oral ingestion are: intense abdominal pain, , vomiting, diarrhea and coma. Other effects due to the ingestion or continuous inhalation in relatively low arsenic amounts are detailed in Table 1.4.

Table 1.4. Principal harmful arsenic effects in human health.

Affected area	Toxic effects
Skin	Hyperpigmentation, hyperkeratosis, gangrene, skin cancer
Lung	Lung cancer
Liver	Cirrhosis
Kidney	Readsorption problems
Bloodstream	Porphyrin biosynthesis inhibition, leukocytes affection.
Reproductive system	Miscarriage
Peripheral nervous system	Paralysis, hearing losses

The arsenic toxicity depends on the oxidation state and decreases following the order As(-III) >> As(III) >> As(V) >> organometallic arsenic > As(0).[48] Methylation occurs as natural defense for the human health against the arsenic intoxication, becoming such a process the generator of organometallic arsenic compounds that are quickly removed from human body.

Although arsenic can occur in the environment in several oxidation states, the chemical forms normally encountered are not particularly toxic to aquatic organisms.[49] Among the commonly encountered forms, inorganic trivalent arsenite is more mobile, more soluble, and some 50 times more toxic than pentavalent inorganic arsenic, and several hundred times more toxic than organic species.[50] The chemical form of arsenic depends on many geochemical and biochemical processes, and arsenic species in environmental media widely fluctuate depending on organism, media, and geographic location. [51,52,53] Because of this variability, arsenic toxicity towards humans is not accurately assessed when analyses are limited to total arsenic alone.[54,55,56,57]

1.2.4. Arsenic speciation

Different species of the same element may have different chemical and toxicological properties. Therefore, determination of the total concentration of an element may not provide information about the actual physico-chemical forms of the element, required for understanding its toxicity.[58] With respect to the elements, speciation analysis is focusing actually on the transition metals (such as Cr, Ni, Cu, Pt, Hg), metals (such as Al, Sn, Sb, Pb) and metalloids (such as As, Se). However in a broader sense, also nonmetals (such as P, S) and halogens (I, Br) are of interest. As can be seen in Figure 1.7, 50% of all papers are dealing with only 5 elements, namely arsenic (15%), selenium (10%), mercury (9%), chromium (8%) and tin (7%). Another 30% of papers are dealing with copper, zinc, lead, cadmium and iron. All other elements in total are in the focus of only 20% of the publications.[59]
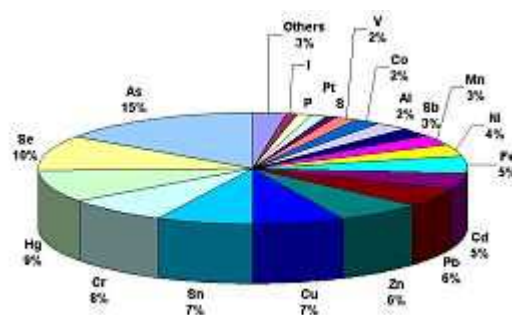
Figure 1.7. The distribution of elements in speciation studies published 2000-2005.[59]

The fundamental requirement in element speciation is the need to quantitatively determine each of the forms of a given element independently and without interference from the other forms. In this regard, an ideal element speciation method is the one that can provide the desired information without altering the original sample. In the absence of such a method, elemental speciation has relied on a combination of analytical techniques and methodologies, including spectroscopic, chromatographic, and electrochemical procedures. In many instances, physico-chemical approaches have been employed, whereby all forms of the element of interest are converted into one species and quantified.[50]

The majority of the methods developed for analytical indirect speciation include spectroscopic,[60] electrochemical, chromatographic[61] and hyphenated methods.[62] A scheme of the available technologies used for metal ion speciation is shown in Figure 1.8. Among these techniques and regarding arsenic speciation, methods based on HPLC-ICP-MS have been increasingly used to measure arsenic species, with more recent works being concentrated on determining inorganic As.[63] Arsenate is much easier determined by anion-exchange HPLC because it is well retained in contrast to arsenite, which elutes at or close to the void volume. This methodology includes an inherent problem related to the possibility of modifying the arsenic species during the analytical process.
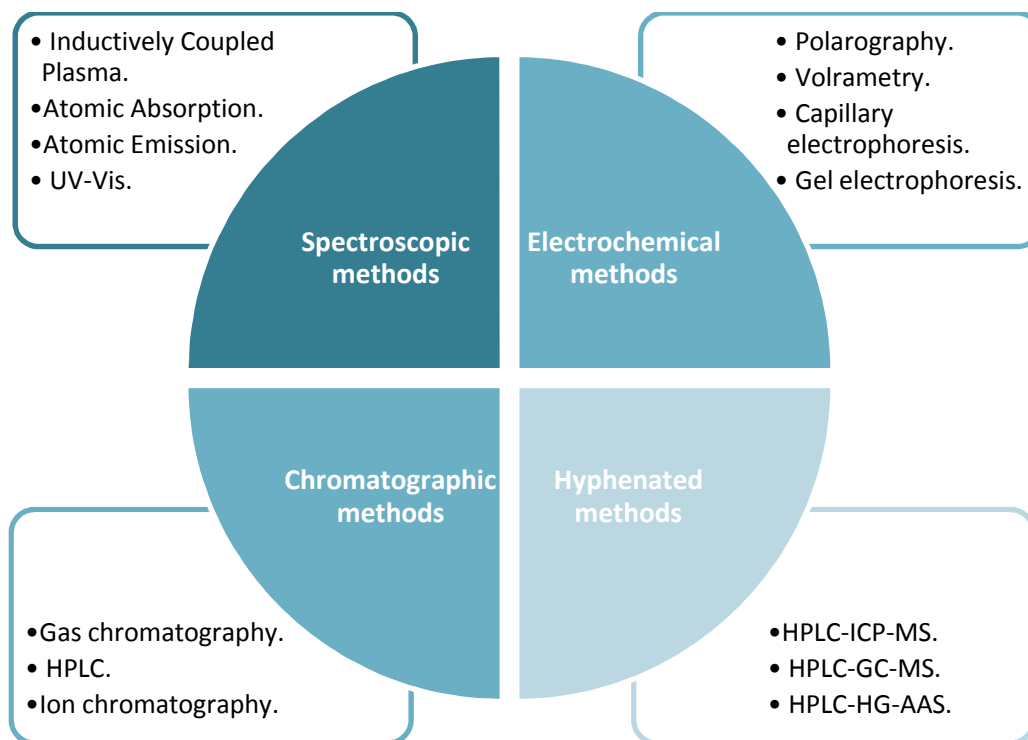
Figure 1.8. Different techniques for metal ion speciation.

These indirect speciation methods usually involve a number of steps, such as extraction, preconcentration, cleaning, derivatization, chromatographic separation and element specific detection. Such steps involve a potential modification of the existing species. Thereby, among other approaches that are used when dealing with arsenic speciation in water or in the adsorbent system, and which are able to keep the speciation of the system, it is noteworthy to highlight the **direct speciation approach**.[64]

Direct speciation intends to determine "in-situ" the species of a given element in the original matrix, without accounting for any pre-treatment step. Nevertheless, only a few direct speciation techniques exist for solid samples where species are found in complexes matrices. Some physical methods have been applied relying on the interaction between the sample and incident beam of either X-Rays or electrons (see Table 1.5).

Table 1.5. Direct speciation techniques for solid samples.

Radiation	Technique	Analysis Objective
X- Radiation	**XRD**: X-ray Diffraction	Identification of crystalline structures. Determination by comparison with reference compounds.
	SEM-EDS: Scanning Electron Microscopy – Energy Dispersive Spectroscopy	Excitation of elements by X-rays. Species identification by elemental associations.
e- beam	**SEM:** Scanning Electron Microscopy	Excitation of elements by X-rays. Species identification by elemental associations.
	TEM-SAED: Transmission Electron Microscopy – Selected Area Electron Diffraction.	Identification of crystalline structures. Determination by comparison with reference compounds.

Recently, the use of synchrotron radiation sources instead of the classical X-ray tubes allowed a significant improvement of the direct speciation approach applied to environmental samples. These techniques take advantage of the highly brilliant X-rays radiation generated in the synchrotron facility, which allows the improvement of already existing techniques (fluorescence, diffraction…), as well as the development of new techniques, such as XANES (X-ray Absorption Near Edge Structure) and EXAFS (Extended X-ray Absorption Fine Structure).[65]

1.3. Arsenic removal technologies from contaminated water

This section provides an overview for the most commonly used arsenic removal methods and presents some basic criteria to consider these methods.

Available literature on arsenic removal methods includes conservative treatment processes, co-precipitation, membrane processes, ion exchange and adsorption processes. Although many of these technologies are well developed, they are often considered expensive and consequently, new cost effective technologies applicable at small scales remain in demand.

When choosing a removal method, it is necessary to consider the final desired concentration as well as the associated costs and the feasibility of monitoring this goal. The natural distribution of inorganic arsenic species (arsenite and arsenate) in water influences both the treatment strategy and the removal efficiency.[66] The anionic characteristics of arsenate promote its removal, whereas the neutral characteristics of

arsenite limit its removal efficiency in conventionally applied physicochemical treatment methods at near neutral pH values.[67, 68]

Figure 1.9[69] proposes some requirements that should be fulfilled for an appropriate arsenic removal technique.

Water Quality	Economy	Operation & Maintenance	Safety & Reliability
• Method must be effective enough. • Method must perform well in the combined presence of potentially competing ions. • Method itself must not be an unwanted contaminants source.	• Affordable set-up, operation and maintenance.	• Simple operational and maintenance requirements • Minimal energy requirements. • Optimum pH range for the removal	• Operation process should be safe, reliable and robust. • Effective in removing both arsenite and arsenate species. • Occupational health should be considered

Figure 1.9. Requirements for an adequate arsenic removal technique.

In the following sections the main arsenic removal methods and their process characteristics are reported.

A great variety of water treatment methodologies are used for significant reduction or remove the environmental problems that harmful or toxic substances generate and all of these methodologies are summarized in Table 1.6.[70]

Table 1.6. Water treatment and metal ions removal methodologies.

Conventional recovery		
Methodology	**Fundaments**	**Ref.**
Precipitation	A soluble substance is transformed in an insoluble substance by a chemical reaction or by changing in the solvent composition that decrease the solubility of the substance of interest. It can be performed in different ways: direct, secondary or selective.	**5,71 72,73**
Oxidation	A process where is involved an increase in positive valence or removal of electrons to generate a change in the oxidation state. Chlorine, ozone, potassium permanganate, manganese oxides and hydrogen peroxide can be used to accelerate oxidation	**74,75**
Traditional recovery		
Methodology	**Fundaments**	**Ref.**
Evaporation	Volume reduction is generated in the contaminated solution by water evaporation.	**76**
Liquid-Liquid extraction	Separation of the dissolved compounds un a liquid solution by contact with another immiscible liquid where the compounds are more soluble. For metal ions, metal ions are dissolved in an aqueous phase and they contact with an organic phase with extractant specie which provides selectivity in the separation process by selective interactions.	**77**
Membrane separation	Semipermeable membranes which produce a separation of two liquid phases, avoiding the liquid pass through the membranes There are different ways: ultrafiltration, reverse osmosis or electrodialysis.	**78,79 80,81**
Ion Exchange	Macromolecular tridimensional nets with a fixed electrostatic charge and with an opposite mobile charge. These nets can form ions in solution and exchange other ions with same charge to the solution in equimolar proportions.	**82,83 84**
Emergent recovery		
Methodology	**Fundaments**	**Ref.**
Adsorption	Phenomenon that consist in a superficial retention over a solid of one or more solutes inside of a liquid or gaseous phase. Between the molecules in liquid or gaseous phase and the adsorbent molecules, different types of attraction forces are produced: Physisorption, Chemisorption or electrostatic adsorption.	**85,86 87,88 89**
Nanofiltration	Nanofiltration (NF) is a cross-flow filtration technology. The nominal pore size of the membrane is typically about 1 nanometre and nanofilter membranes are typically rated by molecular weight cut-off (MWCO) rather than nominal pore size.	**90**
Osmosis Reverse	RO membranes are effectively non-porous and, therefore, exclude particles and even many low molar mass species such as salt ions, organics	**91,92**

Conventional methodologies have their utility as non-selective treatment for the volume reduction of contaminant by concentration of toxic part and the separation of the non-toxic part. But these methodologies do not let the reuse of the waste with a beneficial aim. In the other hand, separation techniques main aim is the selective metal recovery and subsequently, to make use for different applications.

Therefore, separation methodologies can get the volume reduction of the generated solid wastes and, at the same time, the partial or completely recycle of the recovered fraction of the clean solution.

Regarding shortcomings of most of these methods, it must be highlighted the high investment and maintenance costs, secondary pollution (generation of toxic wastes, etc.) and complicated procedure involved in the treatment. Conversely adsorption processes do not add undesirable by-products and have been found to be superior to other techniques for wastewater treatment in terms of simplicity of design and operation, process speed and insensitivity to toxic substances.[93]

A wide variety of adsorbent systems for adsorption processes, described in the Table above, have been used: organic compounds such as activated carbon, biological materials, mineral oxides, polymeric resins… Most of these compounds are designed or modified with the aim to get a high degree of selectivity and a higher adsorption capacity. The properties of an ideal absorbent are described in the following scheme, Figure 1.10.

Ideal adsorbent systems

- High surface area.
- High distribution coeficients for the species of interes in a wide pH range.
- Quick adsorption kinetic.
- High mecanic resistance and chemical stability.
- Capacity to perform eluation processes.
- Capacity to work in complexes matrix.
- Selective to the element of interest.
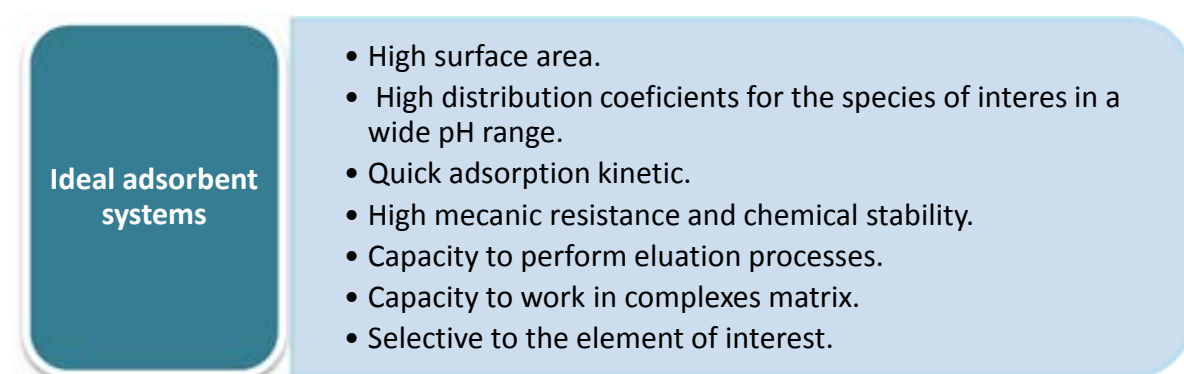
Figure 1.10. Properties for an ideal adsorbent system.

Regarding to arsenic adsorption in aqueous solutions, among the several types of adsorbents that have been used, many of them take advantage of Fe(III) compounds affinity towards inorganic arsenic. Metal oxides have been studied extensively in the last years for their potential to remove arsenic from water through adsorption. Manganese and activated

alumina, aluminosilicates, as well as iron oxides, such as goethite (either natural or synthetic), ferrihydrite, or hematite (Table 1.7) have all been tested and found to effectively remove arsenic from drinking water. Zero-valent iron has also been found to remove arsenic from drinking water, although its performance largely depends on the rate of iron oxidation or rusting of the metal as arsenic adsorbs to the iron oxide produced by this reaction.[94] In addition, different Fe(III) supported materials such as Fe(III)-loaded zeolites[95] or resins[96] have been successfully employed for arsenic removal.[97]

Table 1.7. References for the studied metal oxides for arsenic removal from water.

Metal Oxides for arsenic removal	Reference
➢ Manganese and Activated alumina	98
➢ Aluminosilicates	99
➢ Iron Oxides	100,101,102
❖ Goethite	103,104
❖ Ferrihydrite	105,106
❖ Hematite	107,108

1.3.1. Iron Oxides

Iron oxide is characterized by a low solubility of Fe(III), possible replacement of Fe with other cations, catalytic activity, and high energy of crystallization. Iron oxides form very small crystals both in nature and anthropogenically modified. Therefore, they can have high specific surface areas (SSA), such as > 100 m^2/g, making them effective sorbents for many dissolved ions, molecules and gases.[109]

Point of zero charge is another important parameter that gives information about the total charge of the Fe oxide surface. It has several components as show the Equation 1.1:

$$\sigma_{tot} = \sigma_{H+} + \sigma_{1S} + \sigma_{0s} \qquad (1.1)$$

where σH+ represents the charge due to the adsorbed potential determining ions (net proton change) and σ1s, σ0s refer to the charge due to inner and outer sphere adsorbing ions.

The point of zero charge is the pH at which net adsorption of potential determining ions on the oxide is zero and it is related to the intrinsic acidity. It provides an estimate of the acidity of the oxide surface. In general, iron oxides have pzc in the pH range 6-10. They are less acidic than SiO_2 and MnO_2 (pzc < 3) and similar to the Al oxides (pzc around 9). The

pzc of goethite is close to the upper end of the range, whereas those magnetite and maghemite are at the lower end.

It is important to realize that negative, positive and neutral functional groups can coexist on the oxide surface. At pH < pzc, the $FeOH_2^+$ groups predominate over the FeO^- groups. At the pzc, the number of $FeOH_2^+$ groups equals the number of FeO^- and as the pH increases, the number of FeO^- increases.[110]

Goethite (α-FeOOH),[109] ferrihydrite (HFO),[109] hematite (α-Fe$_2$O$_3$)[109] and magnetite (Fe$_3$O$_4$) [111] are common iron oxides employed as sorbents and the principal characteristics are described below (**Figure 1.11**).

Goethite: α-FeOOH

Goethite is an Fe(III) oxide with a structure based on hexagonal close-packed (hcp). Each iron atom is surrounded by three oxygen atoms and one hydroxide ion to give octahedral coordination. The length of the crystal can range from nanometer size to microns depending on the precipitation method. It is the most thermodynamically stable iron oxide. Therefore, it is the last in many transformation processes. Goethite surface area can range from 8-200 m^2/g in both natural and synthetic forms. At room temperature, goethite is antiferromagnetically ordered because of its low anisotropy constant and particle size. The point of zero charge (pzc) range from 7.5 to 9.4

Ferrihydrite: $(Fe^{3+})_2O_3 \bullet 0.5H_2O$

Ferrihydrite is a Fe(II) oxide prevalent in surface environments. It forms as a nanocrystal with a spherical shape and unless stabilized, transforms into other iron oxide. Ferrihydrite is poorly crystalline with an hcp structure. The small spherical particles often pack together to form aggregates. It has surface area ranging from 100 to 700 m^2/g. The magnetic properties of ferrihydrite can vary over a range of temperatures but at room temperature is superparamagnetic. The point of zero charge is 7.8.

Hematite: $α-Fe_2O_3$

Hematite is a Fe(III) oxide, the oldest known iron oxide. It has an hcp structure, each Fe atom is surrounded by six oxygen atoms but to provide charge balance, oxygen may be partially replaces by hydroxides. Hematite has a wide range of surface areas (<5-200 m^2/g). The magnetism of hematite is weakly ferromagnetic at room temperature with a point of zero charge of about 7.6.

Magnetite: $Fe^{2+}Fe^{3+}_2O_4$

Magnetite is a mixed oxide of Fe(II) and Fe(III) atoms with an inverse spinel structure (as **Figure 1.12** shows). Eight tetrahedral sites are distributed between Fe(III) and Fe(III) with Fe(III) occupying both tetrahedral and octahedral sites giving an octahedral crystal shape. Magnetite is frequently non-stoichiometric where it has a cation deficient Fe(III) sublatice. It is ferromagmetic which gives rocks their magnetic properties and is formed in various organisms by biological processes. Magnetite has a surface area ranging from 4-100 m^2/g with a point of zero charge ranging from 6.4 to 7.2.

Figure 1.11. Most common iron oxides employed as arsenic sorbents.
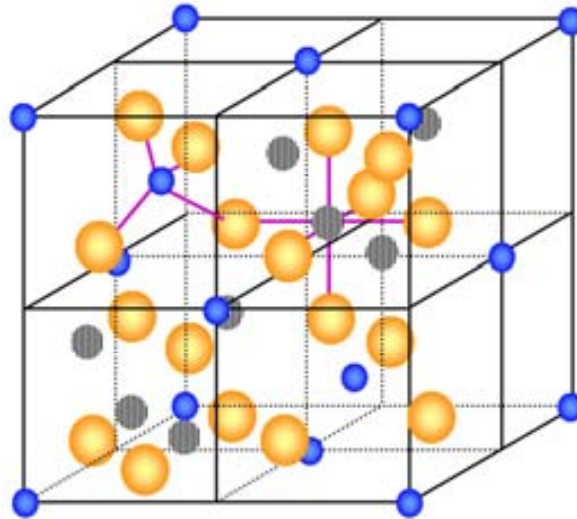
Figure 1.12. Crystal structure of magnetite. Blue atoms are tetrahedrally coordinated Fe^{3+}; black/white atoms are octahedrally coordinated, 50/50 Fe^{2+}/Fe^{3+}; orange atoms are oxygen.

However, such materials adsorption capacity can be further increased. In this sense, during the last decade, the investigations with several types of iron oxide nanomaterials (IONMs) have increased, mainly suggesting these materials as efficient, cost-effective and environmental friendly alternative to existing treatment materials, from both a resource conservation and an environmental remediation point of view.[112,113,114]

1.4. Nanotechnology: an overview

Nanotechnology holds out the promise of immense improvements in manufacturing technologies, electronics, telecommunications, health and even environmental remediation.[115,116,117] It involves the production and utilization of a diverse array of nanomaterials (NMs), which include structures and devices with a size ranging from 1 to 100 nm and displays unique properties not found in bulk-sized materials, as shows the Figure 1.13. [118,119]
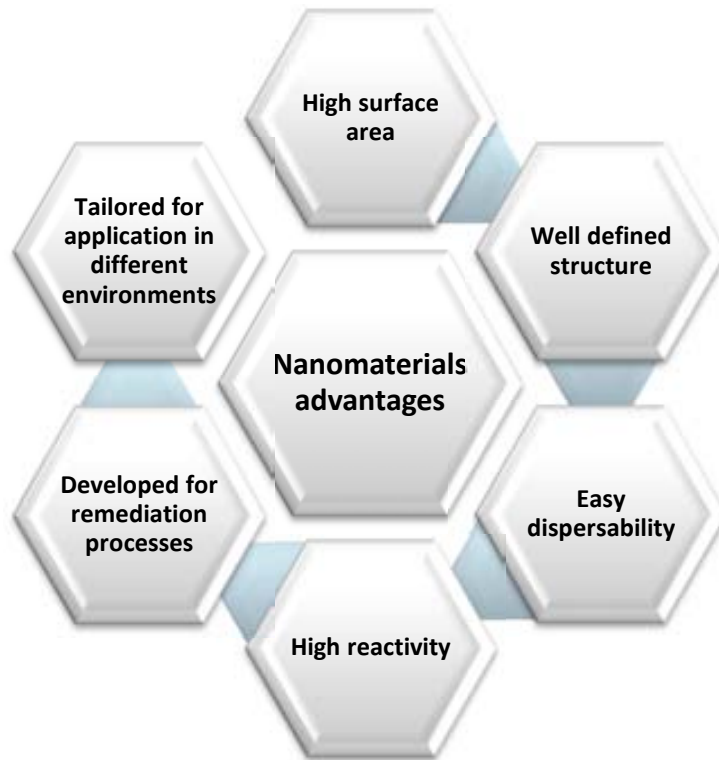
Figure 1.13. Nanomaterials unique properties and advantages not found in bulk-sized materials

Nanotechnology, now considered as one of the most important advancements in science and technology, is related to the study of the material control at atomic and molecular scale. The essence of nanoscience and nanotechnology involves the development and the engineering of materials, structures and systems, which combine the desired properties and functionalities to be achieved. At this length scale, materials exhibit new properties for novel applications.[120] Thus, nanotechnology involves the production of a diverse array of nanomaterials, including nanoparticles. The most commonly accepted definition for a nanomaterial refers to any material which has at least one dimension less than 100 nanometers (nm) in size, whereas nanoparticles are defined as objects with their three dimensions of less than 100nm.[121]

Nanotechnology combines cognitions and terms of many different kinds of sciences like physics, chemistry, biology and engineering which complement each other, as the Figure 1.14 shows. Therefore, nanotechnology has to be seen as one of the most important future technologies.[122]
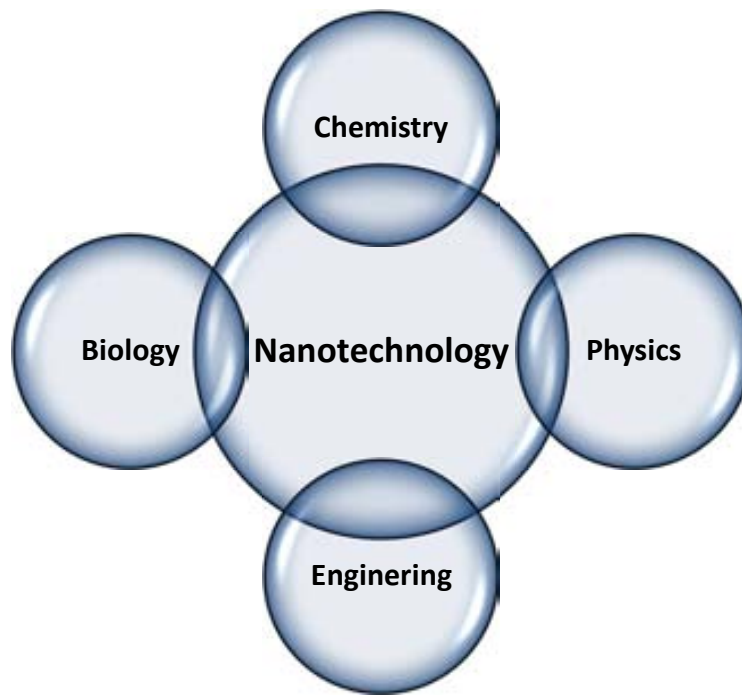
Figure 1.14. Multi-disciplinarity of nanotechnology

Chemistry and physics are fundamental scientific disciplines for the development of nanoscience and nanotechnology. Among the different fields involved in those disciplines, surface chemistry is especially of great importance concerning the properties of nanomaterials and nanoparticles in particular. The reason is that decreasing nanoparticles size causes their surface effects to become more significant due to an increase of surface atoms ration in the volume fraction.[104,123]

Nanoparticles are important building blocks in the fabrication of nanomaterials. As it was introduced, the novel properties of nanoparticles are size dependent (e.g. electrical, magnetic, optical…). The small size often results in higher reactivity since surface atoms make a large contribution to the thermodynamic characteristics of solids. Such small size gives nanoparticles a high surface area-to-volume ratio; surface tailorability and multifunctionality open to multitude of new possibilities for a wide variety of application in different fields of the science and technology.[124] In addition, chemical reactivity is enhanced by the large surface area, since large surface area might mean a high concentration of surface defects which facilitates interaction with several kinds of chemical species, both gaseous and aqueous. Hence, the properties and functions of nanomaterials often differ drastically from their bulk counterparts.

The ambition of nanotechnology is to influence and to manipulate nanostructures in a specific way so that special properties can be used to create new materials and to make surfaces more resistant against damages like scratches or solar irradiation by imitation of nature (Figure 1.15).
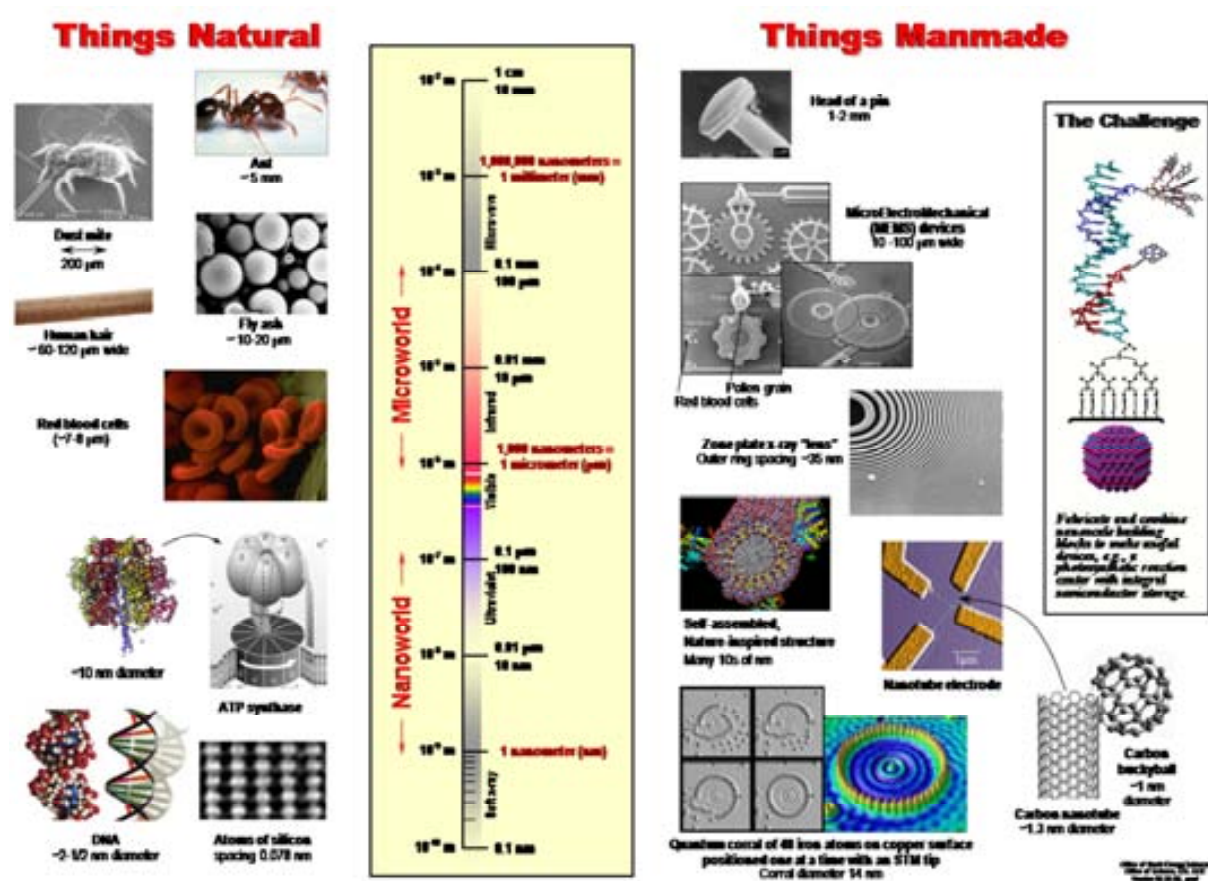
Figure 1.15. Graphical summary comparing the scale of the materials constitution.[125]

1.4.1. Nanotechnology applications

Nanoscale science holds extraordinary promises to impact the current crucial issues, such as improved medical diagnosis and treatment, renewable energy, more efficient information technology, and environmental protection as Figure 1.16 shows. From the basic science perspective, nanotechnology research designs new nanoscale building blocks, study their fundamental physical and chemical properties and develop ways to organize them into complex assemblies with new functionalities.
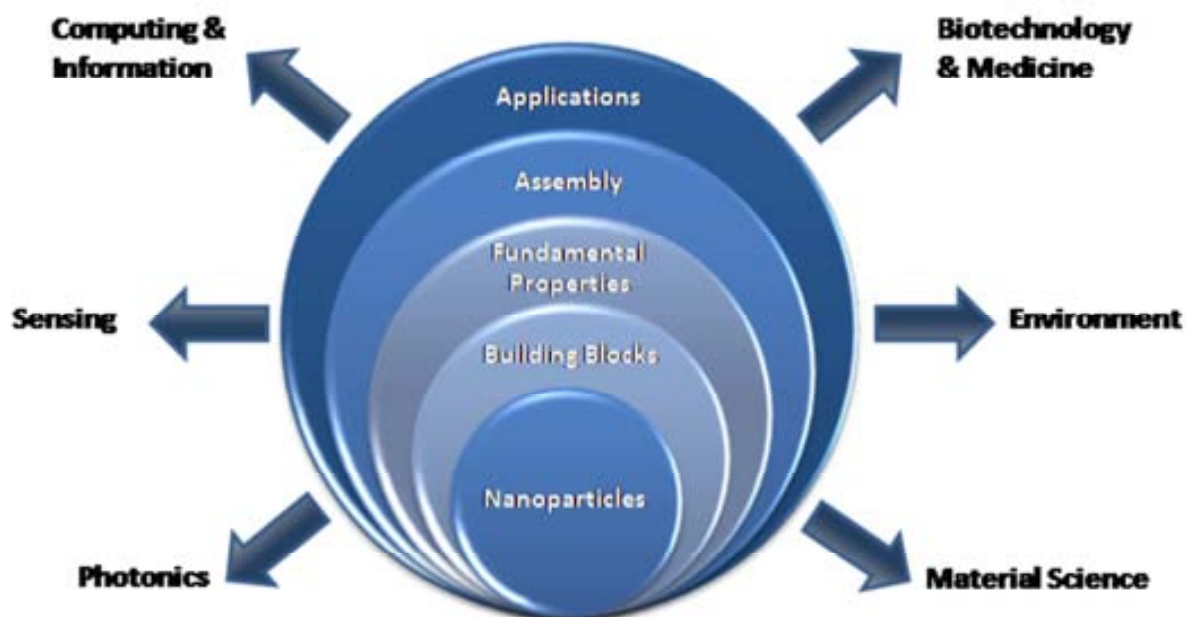
Figure 1.16. Nanoscience applications.

Regarding this PhD thesis, the investigation is centered in the development and study of new adsorbent systems properties based in iron oxide nanoparticles which fundamental application is the water treatment and purification.

1.4.2. Iron oxide nanoparticles

Iron oxides nanoparticles are compounds than are easily made in laboratories. Therefore, this fact makes iron oxides nanoparticles a subject of interest in many fields of science addressing arsenic removal. As Figure 1.17 shows, iron oxides nanoparticles have a multi-disciplinary nature in research.[126]

Figure 1.17. Iron oxide uses in multiple science fields.

Many research studies have been developed by using iron oxides nanoparticles to adsorb arsenic. Magnetite (Fe_3O_4), maghemite (γ-Fe_2O_3), hematite (α-Fe_2O_3) and goethite (FeOOH) are the most common forms.[127] In recent years, the synthesis and utilization of iron oxide nanomaterials with novel properties and functions have been widely studied, due to their size within the nano-range, high surface area to volume ratios and *superparamagnetism*.[128,129,130]

Particularly, an easy synthesis, coating or modification possibilities and the ability to control or manipulate material on an atomic scale provide unparalleled versatility.[131,132] Additionally, iron oxide nanomaterials poses low toxicity, chemical inertness and biocompatibility, showing a tremendous potential in combination with biotechnology.[133,134,135] The unique properties, which account for the application of iron oxide nanomaterials as well as the considerable differences among iron oxide bulk materials are presented in Figure 1.18. [136]
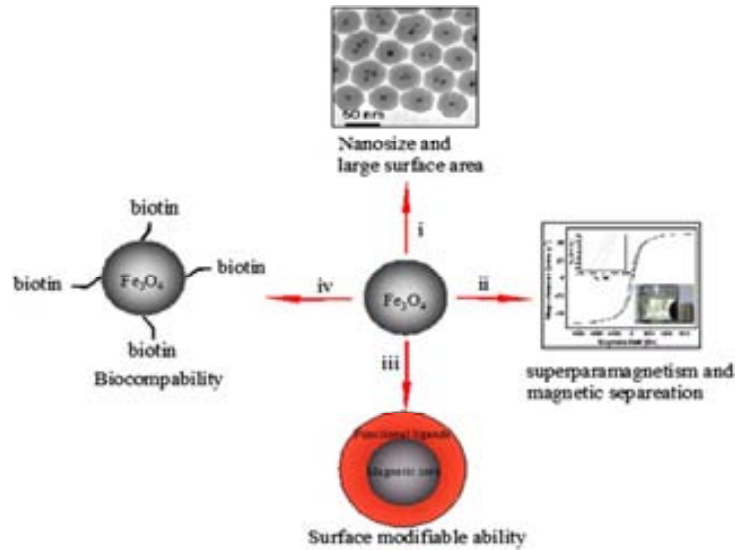
Figure 1.18. Important properties of iron oxide magnetic nanoparticles for water treatment applications. [137]

Advances in NMs synthesis enable the precise control of surface active sites.[138] Future studies should aim to address different challenges to provide new efficient and specific iron oxide NMs. In addition, the development of iron oxide NMs into a field scale may provide a productive area of research requiring the exploration and potential application of these novel NMs.

Generally, NMs should be stable to avoid aggregation and with a low deposition rate, in order to assure their reactivity and mobility. [139,140] However, it is reported that NMs tend to aggregate in solution.[141] One attractive potential approach is the modification of NMs, based on the fact that iron oxide NMs could react with different functional groups. The use of stabilizers, electrostatic surfactants, and steric polymers has been widely proposed for facilitating NMs with non-specific moieties, group specific or highly specific ligands. [142,143,144,145]

Regarding wastewater treatment, selection of the best method and material for wastewater treatment is a highly complex task, which should consider a number of factors, such as the quality standards to be met, the efficiency as well as the cost.[146,147] Therefore, the following scheme (Figure 1.19) shows four key issues that must be considered in the decision on wastewater treatment adsorption technologies: [147,148]
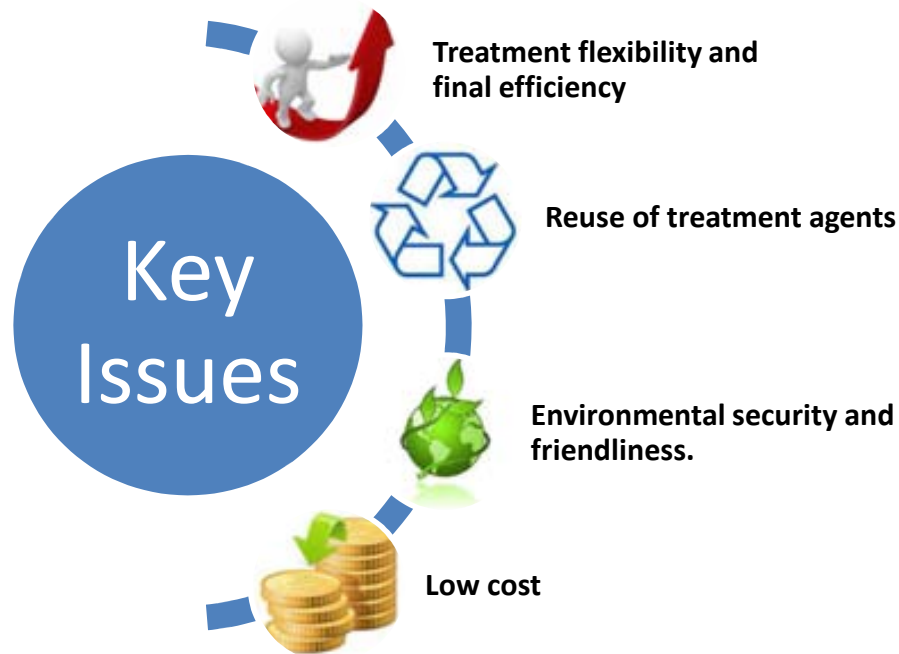
Figure 1.19. Key issues for the wastewater treatment adsorption technologies.

Iron oxide NMs are a promising material for industrial scale wastewater treatment, due to their low cost, strong adsorption capacity, easy separation and enhanced stability.[149,150,151] Current applications of iron oxide NMs in contaminated water treatment can be divided into two groups, as the Figure 1.20 shows.
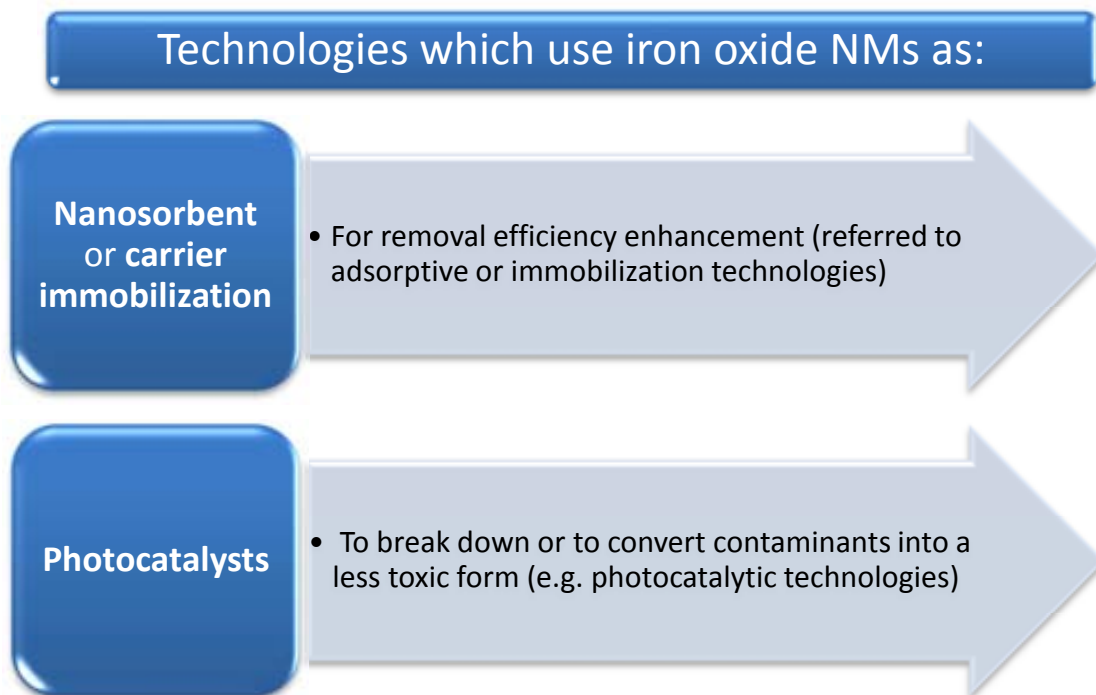
Figure 1.20. Current applications of iron oxide NMs in contaminated water treatment.

1.4.3. Superparamagnetic Iron Oxide Nanoparticles, SPION

The three main important published routes for the synthesis of superparamagnetism iron oxide nanoparticles (SPIONs) are summarized in Figure 1.21. Chemical routes are the most used in environmental applications due to these methods has shown to be an economic and versatile technique used to synthesize large amounts of material and with high yield.[152] In front of chemical routes, there are physical and biological routes that exhibit great disadvantages in controlling parameters such as particle size, particle size distribution, crystallinity degree and phase purity.[153]
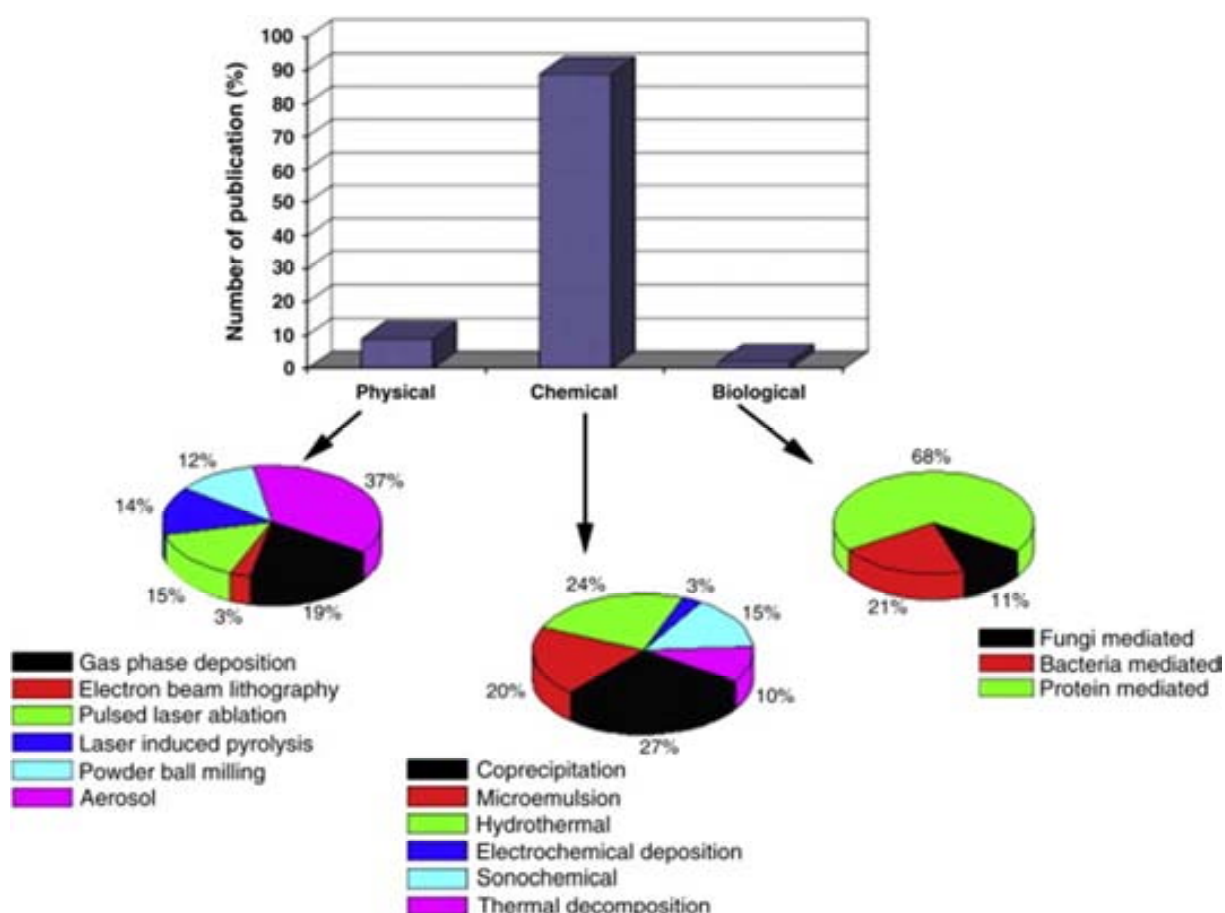
Figure 1.21. A comparison of published work (up to date) on the synthesis of SPIONs by three different routes.

Several methods for SPION *chemical synthesis* have been described. Those most commonly used are summarized in Table 1.8. Amongst these methods, co-precipitation of Fe^{2+} and Fe^{3+} ions in a basic aqueous media (e.g. NaOH or NH_4OH solutions) is the simplest way, but usually nanoparticles are polydispersed and poorly crystallized.[154] To avoid these

disadvantages, thermal decomposition methods have been employed to produce monodisperse SPION, uniform crystalline.[155][Error! Marcador no definido.]

Table 1.8. Main chemical methods for SPION preparation

Synthesis method	Advantages	Disadvantages	Ref.
Co-precipitation	Quick synthesis with high yield	Problem of oxidation and aggregation	156, 154.
Hydrothermal reactions	Narrow size distribution and good control, scalable	Long reaction times	157, 158.
High temperature decomposition	Good control of size and shape, high yield	Furthers steps needed to obtain water stable suspension	155, 159, 160.
Microemulsion	Control of particle size	Poor yield and large amounts of solvents required , excess of surfactant to eliminate	161, 162, 163.

1.4.3.1. Co-precititation synthesis

SPION can be formed by the addition of an alkali solution to an aqueous solution containing Fe^{3+} and Fe^{2+} in a molar ratio of 2, which leads to the formation of complexes with formula, $Fe^{2+}Fe^{3+}O_x(OH)^{2+}_{2(3-x)}\cdot xH_2O$, from which SPION precipitates. Also, it has been suggested that the formation of SPION involves the interaction of Fe^{2+} with precipitated ferrihydrite. In all cases, the solubility product of SPION has to be exceeded to be able to precipitate.

The hydrolysis of Fe^{3+} species proceeds through the formation of low molecular weight species (Equation 1.2) and above OH/Fe~1, these species interact to produce polynuclear species (Equation 1.3).

$$Fe^{3+} + H_2O \leftrightarrow FeOH^{2+} + H^+ \qquad (1.2)$$

$$FeOH^{2+} + H_2O \leftrightarrow Fe(OH)^+_2 + H^+ \qquad (1.3)$$
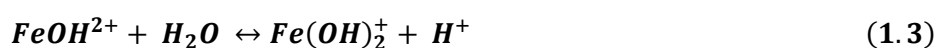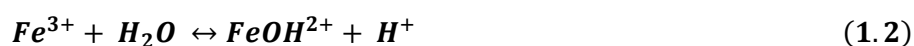
The formation of the dimer is a fast reaction whereas the dissolution is very slow in the absence of protons, which suggest that further polymerization may be very fast. In the particular case of the spinel ferrites, the formation of SPION, for instance, can be considered to proceed according to the overall reaction expressed by the Equation 1.4.

$$Fe^{2+} + 2Fe^{3+} + 8OH^- \leftrightarrow Fe_3O_4 + 4H_2O \qquad (1.4)$$
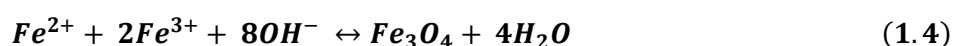
From Equation 1.4, it is clearly seen that in order to obtain SPION, the spontaneous oxidation of Fe^{2+} to Fe^{3+} has to be prevented.[109]

1.4.3.2.   Magnetism

Magnetism is a unique physical property that independently helps in water purification by influencing the physical properties of contaminants in water due to by applying a magnetic field, in function of the electron distribution in the valence band, the metal ion can change to ferromagnetic and interact with the nanoparticles by magnetic interaction. [164] Adsorption processes combined with magnetic separation has therefore been used extensively in water treatment and for environmental purposes.[165] The main advantage of this technology is that it can clean out a mass of wastewater in a very short period of time and produce no contaminants.[166]

There are various forms of magnetism that arise depending on how the dipoles interact with each other. Figure 1.22 shows a schematic representation of the different types of arrangements of magnetic dipoles.
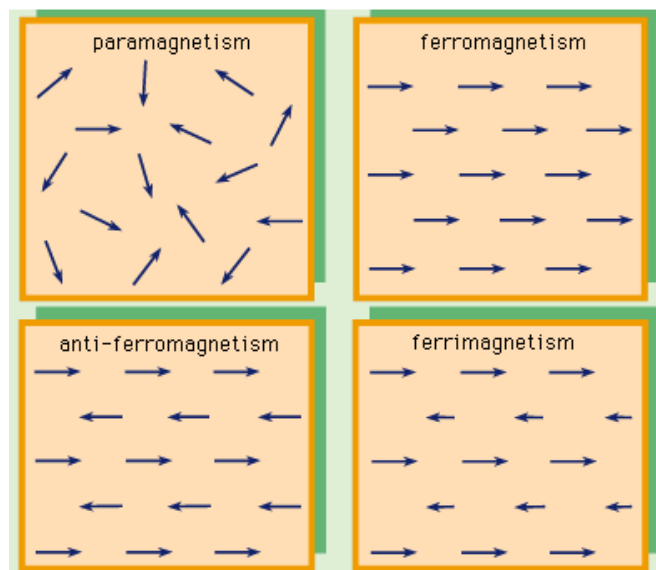
Figure 1.22. Different orientations of magnetic dipoles.

Magnetism arises from the intrinsic spin property of electrons as well as an orbital magnetic moment due to the movement of the electron orbitals. Materials can be classified in diamagnetic, paramagnetic and ferromagnetic[167]/antiferromagnetic[109] materials upon their magnetic properties as the Figure 1.23 shows.

Diamagnetism

- Diamagnetic materials are those materials that oppose an applied magnetic field, and therefore, are repelled by this field.

Paramagnetism

- Paramagnetic materials are only attracted in the presence of an externally applied magnetic field. They possess unpaired electrons that are randomly oriented throughout the sample. Application of a magnetic field causes the magnetic moments to align in the direction of that field. These materials are slightly attracted by a magnetic field and the material does not retain the magnetic properties when the external field is removed.

Ferromagnetism and antiferromagnetism

- Ferromagnetic and antiferromagnetic materials experience a stronger interaction in a magnetic field. There is sufficient energy exchange between neighbouring dipoles that let to interact, and may spontaneously align or anti-align and form magnetic domains, resulting in ferromagnetism (permanent magnets) or antiferromagnetism, respectively.

Figure 1.23. Classification of the magnetic behavior of materials.

For ferromagnetic materials, the point at which all of the domains are parallel to each other is defined as *magnetic saturation*. The graphical representation of a material's magnetization against the strength of an applied magnetic field provides the magnetization curve with a characteristic sigmoidal shape, where the magnetic saturation is reached if the applied magnetic field is large enough as the Figure 1.24 shows.
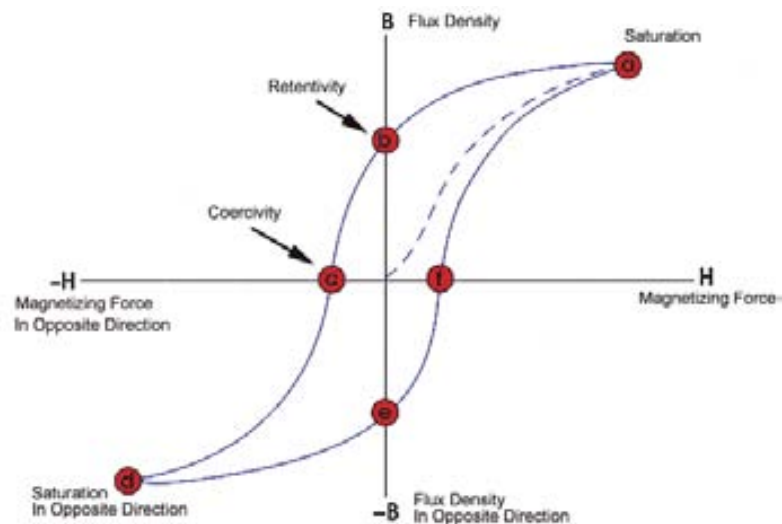
Figure 1.24. Magnetization curve displaying hysteresis loop.

For some magnetic particles, particularly for magnetic iron oxides, the shape of the magnetization curve is often dependent on the nanoparticle size. If particles are of large size (1µm), hysteresis is observed, while for nanoparticles, no hysteresis is observed due to a phenomenon called *superparamagnetism*.[168,169] Superparamagnetic materials are those which behave as ferromagnets in bulk state, but below sizes of 100nm, they consist of individual magnetic domains. When a ferromagnet is sufficiently small, it acts like a single magnet spin that is subject to Brownian motion.[170] In the absence of an external magnetic field, their magnetization appears to be in average zero: such materials are said to be in the superparamagnetic state. In this state, an external magnetic field is able to magnetize the NPs, similarly to a paramagnet but with a higher stability.[171] If enough energy is supplied, magnetism can be reversed along this axis, therefore no hysteresis is observed.[172]

1.4.4. Surface modification of SPION

Surface coating is of great importance in determining the nanoparticles stability under physiological, biological, environmental, etc… conditions as well as to improve their properties for a determined application. Due to the strong magnetic dipole-dipole interactions, the SPION tend to be aggregated without a hydrophilic coating layer. For those reasons, during the synthesis of SPION by co-precipitation in water using hydrophilic polymer as the capping agents, agglomeration might be a minor issue. Once produced, a surface modification step, it is necessary to render the SPION particles water insoluble,

biocompatible or functionalizable. Various methods have been developed, which can be roughly divided into three categories: ligand exchange, ligand addition and inorganic coating as illustrated in Figure 1.25. [173]
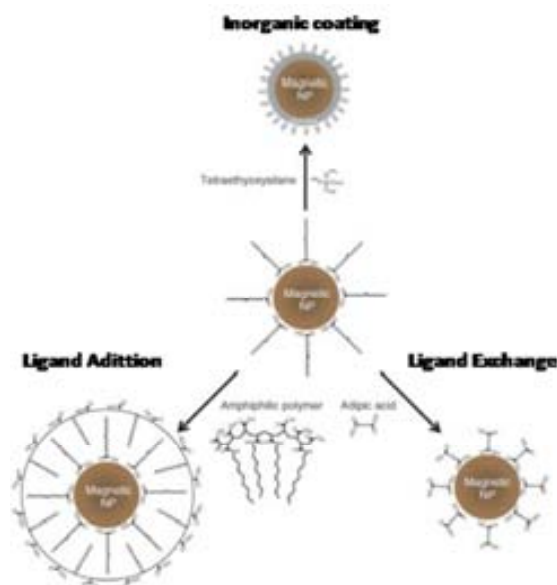
Figure 1.25. Different types of surface modification or functionalization.

Regarding this PhD thesis, ligand additions have been selected. The newly added ligand needs to be amphiphilic, with one end being hydrophobic and interacting with the inner hydrophobic SPION core, while sticking the hydrophilic tail into aqueous solution, offering the nanoparticles hydrophilicity and stability.

1.4.5. Supporting Materials for SPION

1.4.5.1. Forager® Sponge

Forager® sponge is a high porosity and economic ion exchange material with selective affinity for dissolved heavy metals in both cationic and anionic states. Such material is able to promote high rates of adsorption and flexibility which enables their compressibility into an extremely small volume to facilitate disposal once the capacity of the material has been exhausted.[174] Forager is an open celled cellulose sponge which contains a water insoluble polyamide chelating polymer formed by the reaction of polyethyleneimine and nitrilotriacetic acid. This material is claimed to contain free available ethyleneamine and iminodiacetate groups to interact with heavy metals ions by chelation and ion exchange.

Forager® sponge and other adsorbent sponges have been successfully employed in the treatment of heavy metals solutions.[175,176]

Among different advantages, given in the Figure 1.26, it is important to highlight that, in contrast to typical ion exchange systems for treating specific priority pollutant metals in naturally occurring groundwater, where some ions can interfere the effectiveness of the process, Forager® Sponge does not exhibit such interference.

Forager® Sponge is able to generate chelation with transition metal cations by cation exchange processes in the following sequence: $Cd^{2+}>Cu^{2+}>Hg^{2+}>Pb^{2+}>Au^{3+}>Zn^{2+}>Fe^{3+}>Ni^{2+}>Co^{2+}>Al^{3+}$. The Forager® Sponge polymer also contains tertiary amine salt groups that can bind anionic contaminants, such as the chromate, arsenic, and uranium oxide species. It can be designed for site specific needs to contain a cation that forms a highly insoluble solid with the anion of interest.

Forager® Sponge   **Highlight of advantages**

- Its open celled nature allows relatively high flow rate.
- Effectiveness cost.
- Material's low affinity for sodium, potassium and calcium become important issues.
- A simple treatment system could be designed and installed similar to a typical carbon adsorption system.
- Its high porosity and flexibility allows its compressibility into an extremely small volume to facilitate disposal.

Figure 1.26. Advantages of the Forager® sponge material.

The selective affinity of the polymer enables the Forager® Sponge to bind toxic heavy metals over monovalent and divalent cations such as calcium, magnesium, potassium and sodium. In addition, prior studies have shown that the sponge material is effective over a wide range of pH.[174]

1.4.5.2. Electrospun polymeric nanofibers

Electrospinning is a versatile method based on an electrohydrodynamic process for forming continuous thin fibers ranging from several nanometers to tens of micrometers. This method can be used for the one-step forming of thin fibrous membranes.[177,178,179,180,181] A wide variety of materials, such as polymer-solvent systems and polymerless sol-gel systems can be electrospun.[182] Electrospun nanofibers with high surface areas have drawn significant attention for their practical applications, such as high-performance filter media, protective clothes, composites, drug delivery systems, scaffolds for tissue engineering, sensors, and electronic devices, as the Figure 1.27 shows.[180]
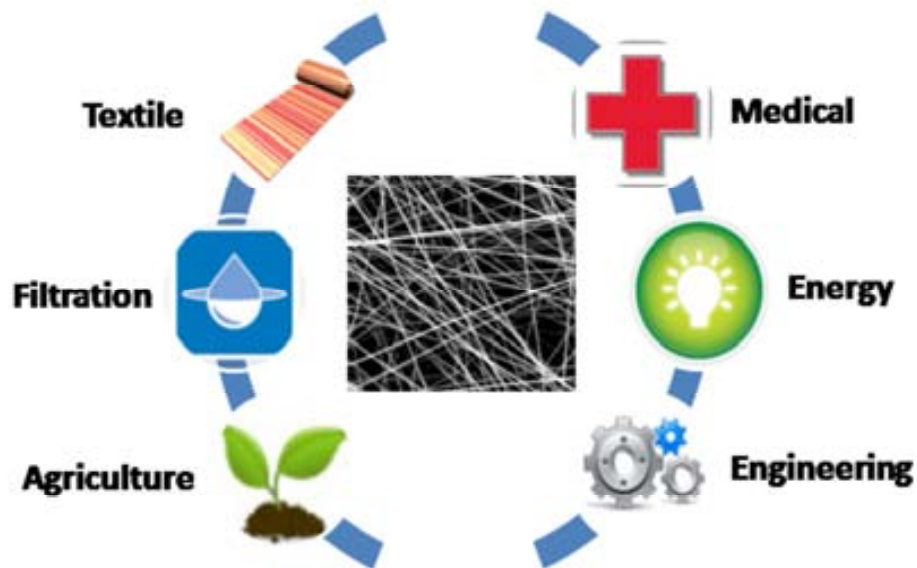
Figure 1.27. Broad spectrum of electrospun nanofibers applications in various fields.

The functionalities of the nanofibers are based on their nanoscaled-size, high specific surface area, and high molecular orientation, and the fact of being possible to control their fiber diameter, surface chemistry and topology, and internal structure of the nanofibers. In addition, processing innovations to improve not only the control of morphologies but also the production capacity of electrospun nanofibers are in progress. In particular, the high-throughput electrospinning systems are ongoing developments (e.g., multi-needle and needleless processes).[183]

Nanofibers are a unique nanomaterial because of the nanoscaled dimensions in the cross-sectional direction and the macroscopic length of the fiber axis (see Figure 1.28).

Therefore, nanofibers have both the advantages of functionality (due to their nanoscaled structure) and the ease of manipulation (due to their macroscopic length). Furthermore, three-dimensional nanofiber network assemblies provide good mechanical properties and good handling characteristics.
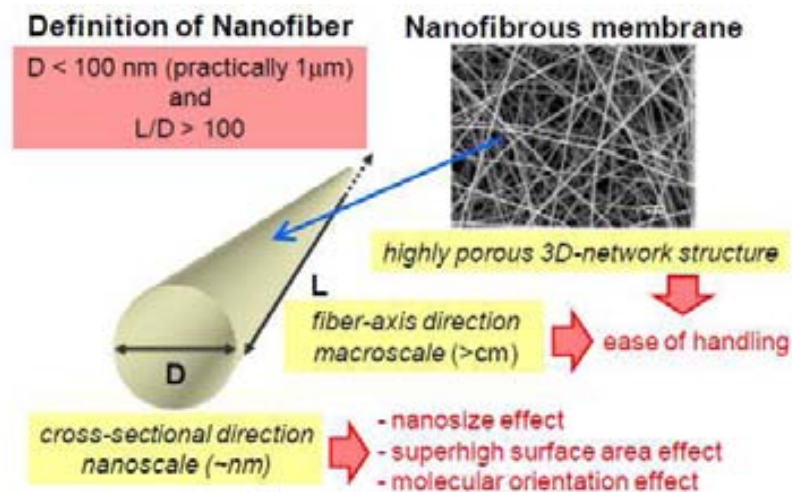
Figure 1.28. Characteristics of nanofibers.

The electrospinning process is governed by many parameters, classified broadly into solution parameters, process parameters, and ambient parameters. [184] Each of these parameters significantly affect the fibers morphology obtained as a result of electrospinning, and by proper manipulation of these parameters we can get nanofibers of desired morphology and diameters. [185] Such parameters and their effects on fiber morphology are shown in the Table 1.9.

Table 1.9. Electrospinning parameters (solution, processing and ambient) and their effects on fiber morphology

Parameters	Effect on nanofiber morphology	Ref.
Solution Parameters		
Viscosity	Low-beads generation, high-increase in fiber diameter, disappearance of beads	**186, 187, 188, 189.**
Polymer concentration	Increase in fiber diameter with increase of concentration	**190, 191, 192.**
Molecular weight of polymer	Reduction in the number of beads and droplets with increase of molecular weight.	**193, 194, 195.**
Conductivity	Decrease in fiber diameter with increase in conductivity	**186, 192, 196.**
Surface tension	No conclusive link with fiber morphology, high surface tension results in instability of jets	**189,197, 198, 199.**
Processing parameters		
Applied voltage	Decrease in fiber diameter with increase in voltage	**190, 192, 194.**
Distance between tip and collector	Generation of beads with too small and too large distance, minimum distance required for uniform fibers.	**188, 200, 201, 202.**
Feed rate/Flow rate	Decrease in fiber diameter with decrease in flow rate, generation of beads with too high flow rate.	**189, 198, 203.**
Ambient parameters		
Humidity	High humidity results in circular pores on the fibers	**199, 204, 205.**
Temperature	Increase in temperature results in decrease in fiber diameter.	**199, 203.**

The electrospun nanofibers possesses attractive properties such as high porosities, interconnected open pore structure, pore sizes ranging from sub-micron to several micrometers, high permeability for gases,[206,207] and a large surface area per unit volume. Through electrospinning a variety of morphologies can be obtained such as porous fibers, hollow fibers, beaded fibers, etc… which can be used for specific applications.[208] In addition to this, the thickness of the overall nanofiber membrane can be controlled. Some of these attributes make electrospun nanofibers highly attractive in separation technology. However, the use of electrospun nanofiber membranes (ENMs) in liquid separation is limited and still in its early stages. [209,210,211] The open porous structure of the ENM will be the key parameter that will influence the separation characteristics of particles. Nowadays, it is known reality that a highly efficient fibrous membrane for liquid separation can be produced through electrospinning.[212]

1.4.5.3. Environmental applications of electrospun polymeric nanofibers

, As an additional solution beyond those conventional remediation technologies, electrospun nanofibers have great potential in collecting metal ions from a solution because of their high specific surface area, high porosity and controllable surface functionality.

Two approaches have been used to improve the adsorption of metal ions on electrospun nanofibers: introducing functional materials on fiber surface using surface chemistry or coating techniques and increasing surface area to improve adsorption capability.[213]

1.5. Objectives

The main purpose of the work presented in this PhD thesis is focused on the synthesis of adsorbent systems based in SPION (in suspension, superficially modified or supported) for wastewater treatment application, specifically for arsenic removal and speciation. There are several considerations in the preparation of SPION such as the SPION suspension stability, ensuring prevention of the SPION oxidation and the inhibition of the degradation during the adsorption processes in water treatment application.

Taking into account these considerations, two main aims are proposed in this PhD thesis: the synthesis, optimization and characterization of the adsorbent systems and the determination of the principal arsenic adsorption parameters in the adsorption processes.

In overall, the major scientific and technical objectives of the PhD thesis involve:

➢ To optimize the synthesis of the Superparamagnetic Iron Oxide Nanoparticles by co-precipitation method with some modifications to avoid the partial oxidation of Fe^{2+} and a low reaction yield or a fractionated cleaning process.

➢ To perform the surface functionalization based in the wet impregnation of SPION with 3-mercaptopropionic acid due to the functional groups presents in the extractant can play the role to decrease the SPION aggregation and improve the adsorption capacity.

➢ To develop a procedure to support the SPION over Forager® Sponge to take advantage of its porosity to decrease the SPION aggregation and to get better adsorption capacity by increasing the specific surface area. In addition, the optimization of the SPION loaded over the Forager® Sponge.

➢ To develop and optimize the synthesis of CA and PAN nanofibers by electrospinning methods and the SPION loading over the nanofiber surface.

➢ To fully characterize the SPION and the new adsorbent systems using several instrumental techniques such as electron microscopy, X-ray diffraction, magnetization techniques, thermogravimetric analysis and synchrotron radiation techniques.

➢ To determine the optimum parameters in the adsorption processes such as contact time, pH effect, concentration effect, for adsorption of the different inorganic arsenic species: arsenite, arsenate and arsenite/arsenate mixture in order to obtain the SPION maximum loading capacity for the different adsorbent systems.

➢ To study the selectivity of the different adsorbent systems against metal ions such as Zn^{2+}, Ni^{2+} and Cu^{2+} or against most common interfering anions such as chloride, nitrate, sulphate and phosphate in a wide pH range.

➢ To study, for the nanofibrous system, the behaviour of the adsorption process in continuous mode and to compare, in terms of adsorption capacity, with the results in batch mode. Among the experiments in continuous mode, the flow effect (gravity flow vs. counterflow) will be taken into account.

➢ To develop a sensitive indirect speciation method, using HPLC-ICP-MS technique, to identify and quantify the chemical species of arsenic present in the liquid phases after the adsorption processes for the arsenic speciation study.

➢ To use synchrotron radiation sources, mainly X-ray Adsorption Near Edge Spectroscopy (XANES), to determine the arsenic chemical form directly in the solid phase of the adsorbent system. Additionally, the iron speciation will be studied by XANES in order to check the stability of the SPION structure during the adsorption process.

References

1. Gulledge, J.H. and O'Conner, J.T. Removal of Arsenic (V) from Water by Adsorption on Aluminum and Ferric Hydroxides. *Jour. AWWA*, **1973**, *65 (8)*, 548-552.

2. National Research Council (NRC). Arsenic in drinking Water. National Academy Press, Washington, D.C., **1999.**

3. USEPA United States Environmental Protection Agency. Technologies and Costs for Removal of Arsenic from Drinking Water, EPA 815-R-00-028, **2000**.

4. USEPA United States Environmental Protection Agency. *Arsenic in drinking water,* **2006**. http://www.epa.gov/safewater/arsenic/. Consulted on 29th August, **2013**.

5. Bothe, J.V., Brown, P.W., Arsenic immobilization by calcium arsenate formation. *Environmental Science and* Technology, **1999**, *33*, 3806-3811.

6. Matschullat, J. Arsenic in the geosphere. *The Science of the Total Environment*, **2000**, *249*, 297-312.

7. Berg, M., Tran, H.C., Nguyen, T.C., Pham, H.V., Schertenleib, R., Giger, W. Arsenic contamination of groundwater and drinking water in Vietnam: A human health threat. *Environmental Science and Technology*, **2001**, *35 (13)*, 2621-2626.

8. Bissen, M., Frimmel, F.H. Arsenic a review. Part I: Occurrence, toxicity, speciation, mobility, *Acta Hydrochimica Hydrobiology*, **2003**, *31 (2)*, 9-18.

9. Council Directive 98/83/EC. On the quality of water intended for human consumption. *Official Journal of the European. Communities,* **1998**, *330*, 32-54.

10. USEPA United States Environmental Protection Agency. National Primary Drinking Water Regulations; Arsenic and Clarifications to Compliance and New Source Contaminants Monitoring, **2001**.

11. Yuan, T., Luo, Q.-F., Hu, J.-Y., Ong, S.-L., Ng, W.-J. A study on arsenic removal from household drinking water. *Journal of Environment of Science Health*, **2003**, *38A*, 1731-1744.

12. Kumar, P.R., Chaudhari, S., Khilar, K.C., Mahajan, S.P. Removal of arsenic from water by electrocoagulation. *Chemosphere*, **2004**, *55*, 1245-1252.

13. Kim, J., Benjamin, M.M. Modeling a novel ion exchange process for arsenic and nitrate removal. *Water Research*, **2004**, *38*, 2053-2062.

14. Manning, B.A., Goldberg, S. Adsorption and stability of arsenic(III) at the clay mineral-water interface. *Environmental Science and Tehcnology*, **1997**, *31*, 2005-2011.

15. Lin, T.-F., Wu, J.-K. Adsorption of arsenite and arsenate within activated alumina grains: equilibrium and kinetics. *Water Research*, **2001**, *35*, 2049-2057.

16. Ning, R.Y. Arsenic removal by reverse osmosis. *Desalination*, **2002**, *143*, 237–241

17. Kim, Y., Kim, C., Choi, I., Rengaraj, S., Yi, J. Arsenic removal using mesoporous alumina prepared via a templating method. *Environmental Science and Technology*, **2004**, *38*, 924-931.

18. Gu, Z., Fang, J., Deng, B. Preparation and evaluation of GAC-based iron-containing adsorbents for arsenic removal. *Environmental Science and Technology*, **2005**, *39*, 3833-3843.

19. Rau, I., Gonzalo, A., Valiente, M. Arsenic(V) removal from aqueous solutions by iron(III) loaded chelating resin, *Journal of Radioanalytical and Nuclear Chemistry*, **2000**, *246*, 597-600.

20. Goldberg, S., Johnston, C.T. Mechanisms of arsenic adsorption on amorphous oxides evaluated using macroscopic measurements, vibrational spectroscopy, and surface complexation modelling. *Journal of Colloid and Interface Science*, **2001**, *234*, 204-216.

21. Smedley, P.L., Kinniburgh, D.G., A review of the source, behaviour and distribution of arsenic in natural waters. *Applied Geochemistry*, **2002**, *17*, 517-568.

22. Apak, R., Tütem, E., Hügül, M.; Hizal, J. Heavy metal cation retention by unconventional sorbents. *Water Research*, **1998**, *32 (2*), 430-440.

23. Welch, A.H., West John, D.B., Helsel, D.R., and Wanty, R.B. Arsenic in ground water of the United States, occurrence and geochemistry. *Ground Water*, **2000**, *38(4)*, 589-604.

24. International Groundwater Resources Assessment Centre (http://igrac.nitg.tno.nl/). Consulted on 29th August, 2012.

25. Azcue, J.M., Nriagu, J.O. *Arsenic in the environment. Part I: Cycling and Characterization*, J.O. Nriagu (Ed), John Wiley & Sons, New Cork; **1994**.

26. Clifford, D. and. Lin, C.C. Ion Exchange, Activated Alumina, and Membrane Processes for Arsenic Removal from Groundwater, Proceedings of the 45th Annual Environmental Engineering Conference, University of Kansas, February **1995**.

27. Ferguson, J.F., Gavis, J. A review of the arsenic cycle in natural waters. *Water Research*, **1972**, *6 (11)*, 1259-1274.

28. Gupta, S. K., Chen, K.Y. Arsenic removal by adsorption. *Journal Water Pollution Control Federation*, **1978**, *50*, 493-506.

29. Edwards, M. Chemistry of arsenic removal during coagulation and Fe-Mn oxidation. *Journal of American Water Works Association*, **1994**, *86 (9)*, 64-78.

30. Karcher, S., Caceres, L., Jekel, M., Contreras, R. Arsenic removal from water supplies in Northern Chile using ferric chloride coagulation. *Journal of the Chartered Institution of Water and Environmental Management*, **1999**, *13 (3*), 164-169.

31. Francesconi, K.A., Kuehnelt, D. Arsenic compounds in the environment. In: Environmental chemistry of arsenic, (Ed: Frankenberger, W. T., Jr.), p 56. Marcel Dekker, Inc., New York. **2002**.

32. Drever, J.I. The geochemistry of natural waters-Surface and groundwater environments. p. 82, 193. Prentice-Hall, Inc, New Jersey, **1997**.

33. Brookins, D.G. *Eh-pH Diagrams for Geochemistry*. Springer-Verlag Berlin, New York, **1988**.

34. Hering, J.G. and Chiu, V.Q. The Chemistry of Arsenic: Treatment and Implications of Arsenic Speciation and Occurrence. *AWWA Inorganic Contaminants Workshop*, San Antonio, TX, February 23-24, **1998**.

35. Košutić, K., Furač, L., Sipos, L., Kunst, B. Removal of arsenic and pesticides from drinking water by nanofiltration membranes. *Separation and Purification Technology*, **2005**, *42 (2)*, 137-144.

36. Smedley, P.L., D.G. Kinniburgh. A review of the source, behaviour and distribution of arsenic in natural waters. *Applied Geochemistry*, **2002**, *17*, 517-568.

37. Frankenberger, W.T., Environmental chemistry of arsenic. New York, **2002**.

38. Clesceri, L.S., Greenberg, A.E., Trussell, R.R., Franson, M.A. Standard methods for the examination of water and wastewater, 19th ed., American Public Health Association, Washington DC., **1992.**

39. Roy, P., Saha, A., Metabolism and toxicity of arsenic: A human carcinogen, *Current Science*, **2002**, *82*, 38-45.

40. Kipling M.D. Arsenic, the chemical environment. Ed. Lenihan J, Fletcher W.W. pp 93-120, **1977**.

41. WHO. *Environmental Health Criteria* 8. *Arsenic.* World Health Organization, Geneva: 174 pages, **1981**.

42. Pershagen, G. The epidemiology of human arsenic exposure. Biological and Environmental Effects of Arsenic, pp. 199-232, Elsevier/North-Holland Biomedical Press, Amsterdam, **1983**.

43. Lu F.J. Review of fluorescent humic substances and blackfoot disease in Taiwan. *Applied Organometallic Chemistry*, **1990**, *4*, 191-195.

44. Lu F. J. Blackfoot disease: arsenic in humic acid. *The Lancet*, **1990**, *336*, 115-116.

45. Csanady M. and Straub I. Health damage due to pollution in Hungary. In Proceedings of the Rome Symposium, September, **1994**.

46. Smith, A.H., C. Hopenhayn-Rich, M.N. Bates, H.M. Goeden, I. Hertz-Picciotto, H.M. Duggan, R. Wood, M.J. Kosnett and M.T. Smith. Cancer risks from arsenic in drinking water. *Environmental Health Perspective*, **1992**, *97*, 259-267.

47. J.E. Fergusson, *The heavy elements: chemistry, environmental impact and health effects,* J.E. Fergusson, Pergamon Press: Oxford (1990). Part IV. p.45

48. Penrose W.R, Rev. Arsenic in the marine and aquatic environment. Analysism, occurrence and significance. *Environmental Control*, **1974**, *4*, 465-482.

49. Moore, J.W., 1991. Inorganic Contaminants in Surface Waters. Research and Monitoring Priorities. Springer-Verlag, New York.

50. Jain, C.K., Ali, I. Arsenic: occurrence, toxicity and speciation techniques. *Water Research*, **2000**, *34(17)*, 4304-4312.

51. Cullen, W.R., Reimer, K.J. Arsenic speciation in the environment. *Chemical Rev*iews, **1989**, *89*, 713-764.

52. Matschullat, J. Arsenic in the geosphere: a review. *Science of the Total Environment*, **2000**, *249*, 297-312.

53. Mandal, B.D., Suzuki, K.T. Arsenic round the world: a review. *Talanta*, **2002**, *58*, 201-235.

54. ATSDR, Agency for Toxic Substances and Disease Registry, US Department of Health and Human Services. Toxicological Profile for Arsenic, **2000**.

55. Greene, R., Crecelius, E.A. Total and inorganic arsenic in midAtlantic marine fish and shellfish and implications for fish advisories. *Integrated Environmental Assessment and Management.*, **2006**, *2*, 344-354.

56. USEPA US Environmental Protection Agency. Guidance for Assessing Chemical Contaminant Data for Use in Fish Advisories: vol 1. Fish sampling and analysis. EPA-823-B-00-007, **2000**.

57. Yokel, R.A., Lasley, S.M., Dorman, D.C. The speciation of metals in mammals influences their toxicokinetics and toxicodynamics and therefore human health risk assessments. J*ournal of Toxicology and Environmental Health B*, **2006**, *9*, 63–85.

58. Peshut, P.J., Morrison, R.J., Brooks, B.A. Arsenic speciation in marine fish and shellfish from American Samoa. *Chemosphere*, **2008**, *71 (3)*, 484-492.

59. EVISA (European Virtual Institute for Speciation Analysis) website, [online resource], http://www.speciation.net/Public/Document/2003/09/11/502.html, Consulted on 8th September, **2013**.

60. Ebdon L., Steve H., Walton A. P. and Ward R. W. Coupled chromatography-atomic spectrometry for arsenic speciation - a comparative study. *Analyst*, **1988**, *113*, 1159-1165.

61. Hagege A., Niemczyk S. and Leroy M. J. F. Separation of selenium compounds using HPLC-ICP/AES. *Analysis*, **1995**, *23*, 476-481.

62. Raber, G., Stock, N., Hanel, P., Murko, M., Navratilova, J., Francesconi. K.A. An improved HPLC–ICPMS method for determining inorganic arsenic in food: Application to rice, wheat and tuna fish. *Food Chemistry*, **2012**, *134 (1)*, 524–532.

63. de la Calle, M. B., Emteborg, H., Linsinger, T. P. J., Montoro, R., Sloth, J. J., Rubio, R. Does the determination of inorganic arsenic in rice depend on the method? *Trends in Analytical Chemistry*, **2011**, *30 (4)*, 641–651.

64. Sanz-Medel, A. Trace element analytical speciation in biological systems: importance challenges and trends. S*pectrochimica Acta B*, **1998**, *53*,197-211

65. Suqin Liu, Chuanyong Jing, Xiaoguang Meng. Arsenic re-mobilization in water treatment adsorbents under reducing conditions: Part II. XAS and modeling study. *Science of the total environment*, **2008**, *392*, 137-144.

66. Gallagher, P.A., Schewegel, C.A., Wei, X., Creed, J.T. Speciation and preservation of inorganic arsenic in drinking water sources using EDTA with IC separation and ICP-MS detection. *Journal of Environmental Monitoring*, **2001**, *3*, 371-376.

67. McNeill, L.S., Edwards, M. Arsenic removal during precipitate softening. *Journal of American Water Works Association*, **1997**, *89 (1)*, 75-86.

68. Genç-Fuhrman, H., Tjell, J.C., McConchie, D. Adsorption of arsenic from water using activated neutralised red mud. *Environmental Science and* Technology, **2004**, *38*, 2428-2434.

69. Ruhland, A., Jekel, M. Concept for an integrated evaluation of arsenic removal technologies: demonstrated in a case study. *Water Science and Technology: Water Supply*, **2002**, *2 (2)*, 267-174.

70. Patterson, J.W., Passino, R. *Metals speciation. Separation and recovery,* Lewis Publishers Inc.: Chelsea, p 63, **1987**.

71. Chung, N.K. *Standard Handbook of Hazardous Waste Treatment and Disposal,* McGraw Hill Book Company: New York, p 7.21, **1999**.

72. Gregor, J. Arsenic removal during conventional aluminum-based drinking-water treatment. *Water Research*, **2001**, *35 (7*), 1659-1664*.

73. Holm, T.R. Effects of CO_3/bicarbonate, Si, and PO_4 on arsenic sorption to HFO. *Journal of American Water Works Association*, **2002**, *94 (4)*, 174-181.

74. Kartinen, E.O., Martin, C.J. An overview of arsenic removal processes. *Desalination*, **1995**, *103*, 79-88.

75. Driehaus, W., Seith, R., Jekel, M. Oxidation of arsenic(III) with manganese oxides in water treatment. *Water Research*, **1995**, *29 (1*), 297-305.

76. Manchan, S.R. *Hazardous Waste Chemistry, Toxicology and treatment,* Lewis Publishers, p. 280, **1990**.

77. Lo, T.C., Baird, M.H.I., *Hanson,* C. *Handbook of Solvent Extraction*, John Wiley & Sons: New York, **1983**.

78. McNeil, J.M., McCoy, D.E. *Standard Handbook of Hazardous Waste Treatment and Disposal,* McGraw Hill Book Company, New York, p.6.91, **1999**.

79. Brandhuber, P., Amy, G. Alternative methods for membrane filtration of arsenic from drinking water. *Desalination*, **2001**, *140*, 1-14.

80. Vrijenhoek, E.M., Waypa, J.J. Arsenic removal from drinking water by a "loose" nanofiltration membrane. *Desalination*, **2000**, *130*, 256-277.

81. Sato, Y., Kang, M., Kamei, T., Magara, Y. Performance of nanofiltration for arsenic removal. *Water Research*, **2002**, *36(13)*, 3371-3377.

82. M. Valcarcel, A. Gomez, Técnicas Analíticas de Separación, Reverté S.A., Barcelona, **1990**.

83. Korngold, E., Belayev, N., Aronov, L. Removal of arsenic from water by anion exchangers. *Desalination*, **2001**, *141*, 81-84.

84. Johnston, R., Heijnen, H. Safe water technology for arsenic removal. Technologies for arsenic removal from drinking water. Bangladesh University of Engineering and Technology, Dhaka, Bangladesh, **2001**.

85. McNeil, J.M., McCoy, D.E. Standard Handbook of Hazardous Waste Treatment and Disposal, McGraw Hill Book Company, New York, p.6.3, **1999**.

86. Thirunavukkarasu, O.S., Viraraghavan, T., Subramanian, K.S. Arsenic removal from drinking water using granular ferric hydroxide. *Water SA*, **2003**, *29 (2)*, 161-170.

87. Xu, Y., Nakajima, T., Ohki, A. Adsorption and removal of arsenic(V) from drinking water by aluminum-loaded Shirasu-zeolite. *Journal of Hazardous Materials*, **2002**, *B92*, 275-287.

88. Thirunavukkarasu, O.S., Viraraghavan, T., Subramanian, K.S., Tanjore, S. Organic arsenic removal from drinking water. *Urban Water*, **2002**, *4*, 415-421.

89. Xu, Y., Ohki, A., Maeda, S. Adsorption of As(V) by use of aluminum-loaded shirasu-zeolites. *Chemistry Letters*, **1998**, *10*, 1015-1016.

90. Baker, R.W. Membrane Technology and Applications, 2nd ed.; John Wiley & Sons, Ltd.: Chichester, **2004**.

91. Perry, R.H., Green, D.W. Chemical Engineers' Handbook, 7th ed.; McGrawHill, New York, **1997**.

92. Loeb, S., Sourirajan, S. Seawater demineralization by means of an osmotic membrane. *Advances in Chemistry Series*, **1993**, *38*, 117-132

93. Kaykioglu, G., Lofrano, B. Emerging Compounds Removal from Wastewater, Springer Briefs in Green Chemistry for Sustainability. Chapter 2: Removal of Emerging Contaminants from Water and Wastewater by Adsorption Process, **2012**.

94. Farrell, J., Wang, J., O'Day, P., Conkin, M. Electrochemical and spectroscopic study of arsenate removal from water using zero-valent iron media. *Environmental Science & Technology*, **2001**, *35 (10)*, 2026-2032.

95. Li, Z., Jean, J.S., Jiang, W.T., Chang, P.H., Chen, C.J. Removal of arsenic from water using Fe loaded natural zeolite. *Journal of Hazardous Materials*, **2011**, *187 (13)*, 318-323.

96. Rau, I., Gonzalo, A., Valiente, M. Arsenic(V) adsorption by immobilized iron mediation. Modeling of the adsorption process and influence of interfering anions. *Reactive and Functional Polymers*, **2003**, *54*, 85-94.

97. Mohan, D., Pittman Jr., C.U. Arsenic removal from water/wastewater using adsorbents. A critical review. *Journal of Hazardous Materials*, **2007**, *142*, 1-53.

98. Kunzru, S., Chaudhuri, M. Manganese amended activated alumina for adsorption-oxidation of arsenic. *Journal of Environmental Engineering*, **2005**, *131 (9)*, 1350-1353.

99. Dousova, B., Grygar, T., Martaus, A., Fuitova, L., Kolousek, D., Machovic, V. Sorption of As(V) on aluminosilicates treated with Fe(II) nanoparticles. *Journal of Colloid and Interface Science*, **2006**, *302*, 424-431.

100. Driehaus, W., Jekel, M., Hildebrandt, U. Granular ferric hydroxide-a new adsorbent for the removal of arsenic from natural water. *Journal of Water SRT-Aqua*, **1998**, *47 (1)*, 30-35.

101. Joshi, A. and Chaudhuri, M. Removal of arsenic from ground water by iron oxide-coated sand. *Journal of Environmental Engineering*, **1996**, *122 (8)*, 769-771.

102. Westerhoff, P., Highfield, D., Badruzzaman, M., Yoon, Y. Rapid small-scale columnt tests for arsenate removal in iron oxide packed bed columns. *Journal of Environmental Engineering*, **2005**, *131 (2)*, 262-271.

103. Fendorf, S., Eick, M.J., Grossl, P., Sparks, D.L. Arsenate and chromate retention mechanisms on goethite: I. Surface structure. *Environmental Science & Technology*, **1997**, *31*, 315-320.

104. Sherman, D.M., Randall, S.R. Surface complexation of arsenic(V) to iron(III) (hydr)oxides: Structural mechanism from ab initio molecular geometries and EXAFS spectroscopy. *Geochimica et Cosmochimica Acta*, **2003**, *67*, 4223-4230.

105. Waychunas, G.A., Rea, B.A., Fuller, C.C., Davis, J.A. Surface chemistry of ferrihydrite: Part 1. EXAFS studies of the geometry of coprecipitated and absorbed absorbed arsenate. *Geochimica et Cosmochimica Acta*, **1993**, *57*, 2251-2269.

106. Jessen, S., Larsen, F., Koch, C.B., Arvin, E. Sorption and desorption of arsenic to ferrihydrite in a sand filter. *Environmental Science & Technology*, **2005**, *39*, 8045-8051.

107. Singh, D.B., Prasad, G., Rupainwar, D.C. Adsorption technique for the treatment of As(V) rich effluents. *Colloids and Surface A*, **1996**, *1*, 49-56.

108. Gimenez, J., Martinez, M., Pablo, J., Rovira, M., Duro, L. Arsenic sorption onto natural hematite, magnetite and goethite. *Journal of Hazardous Materials*, **2007**, *141*, 575-580.

109. Cornell, R.M., Schwertmann, U. The iron oxide: Structure, properties, reactions, occurrence and uses. VCH, Ed., Germany, **2003**, p. 9.

110. Cornell, R.M., Schwertmann, U. The iron oxide: Structure, properties, reactions, occurrence and uses. VCH, Ed., Germany, **2003**, p. 236.

111. Yu, B.Y., Kwak, S.Y. Assembly of magnetite nanocrystals into spherical mesoporous aggregates with a 3-D wormhole-like pore structure. *Journal of Material Chemistry*, **2010**, *20*, 8320-8328.

112. Friedrich KA, Henglein F, Stimming U, Unkauf W. Investigation of Pt particles on gold substrates by IR spectroscopy - particle structure and catalytic activity. *Colloids and Surfaces A*, **1998**, *134 (1–2)*, 193-206.

113. Dimitrov D. Interactions of antibody-conjugated nanoparticles with biological surfaces. *Colloids and Surfaces A*, **2006**, *282-283*, 8-10.

114. Dastjerdi, R., Montazer, M., A review on the application of inorganic nano-structured materials in the modification of textiles: focus on anti-microbial properties. *Colloids and Surfaces B*, **2010**, *79 (1)*, 5-18.

115. Gross, M. Travels to the nanoworld: miniature machinery in nature and technology. New York: Plenum Trade; **2001**.

116. Kim, D., El-Shall, H., Dennis, D., Morey, T. Interaction of PLGA nanoparticles with human blood constituents. *Colloids and Surfaces B*, **2005**, *40 (2)*, 83–91.

117. Moore, M.N. Do nanoparticles present ecotoxicological risks for the health of the aquatic environment?. *Environment International*, **2006**, *32 (8)*, 967-976.

118. Stone, V., Nowack, B., Baun, A., van den Brink, N., von der Kammer, F., Dusinska, M. Handy, R., Hankin, S., Hassellöv, M., Joner, M., Fernandes, T.F. Nanomaterials for

environmental studies: classification, reference material issues, and strategies for physico-chemical characterisation. Science of total environment, **2010**, *408 (7)*, 1745-1754.

119. Wang, L.B., Ma, W., Xu, L.G., Chen, W., Zhu, Y.Y., Xu, C.L. Nanoparticle-based environmental sensors. *Materials Science and Engineering:R,* **2010**, *70(3-6)*, 265-274.

120. Uheida, A., Salazar-Alvarez, G., Björkman, E., Yu, Z., Muhammed, M. Fe_3O_4 and γ -Fe_2O_3 nanoparticles for the adsorption of Co^{2+} from aqueous solution. *Journal of Colloid and Interface Science*, **2006** , *298*, 501-507.

121. Siegel, R.W., Hu, E., Roco, M.C. Nanostructure Science and Technology, A Worldwide Study, WTEC, Loyola College Kluwer Academic, Baltimore, MD, **1999**.

122. Haverkamp, R.G. A decade of nanoparticle research in Australia and New Zealand. *Particulate science and technology*, **2010**, *28(1)*, 1-40.

123. Klabunde, K.J., Richards, R.M. *Nanoscale materials in chemisty*, **2009**, 121-167.

124. Whitesides, G.M.The "right" size in nanobiotechnology. *Nature biotechnology*, **2003**, *21(10)*, 1161-1165.

125. US Department of Energy. Office of Science. http://science.energy.gov/bes/news-and-resources/scale-of-things-chart/. Consulted on 9th September, 2013.

126. Shipley, H.J., Yean, S., Kan, A.T., Tomson, M.B. Adsorption of arsenic to magnetite nanoparticles: Effect of particle concentration, pH, ionic strength, and temperature. *Environmental Toxicology and Chemistry*, **2009**, *28(3)*, 509-515.

127. Chan, H.B.S., Ellis, B.L. Carbon-encapsulated radioactive 99mTc nanoparticles. *Advanced Materials*, **2004**, *16*, 144-149.

128. Afkhami, A., Saber-Tehrani, M., Bagheri, H. Modified maghemite nanoparticles as an efficient adsorbent for removing some cationic dyes from aqueous solution. *Desalination*, **2010**, *263(1–3)*, 240-248.

129. McHenry, M.E., Laughlin, D.E. Nano-scale materials development for future magnetic applications. *Acta Materials*, **2000**, *48(1)*, 223-238.

130. Pan, B.J., Qiu, H., Pan, B.C., Nie, G.Z., Xiao, L.L., Lv, L., Zhang, W., Zhang, Q., Zheng, S. Highly efficient removal of heavy metals by polymer-supported nanosized hydrated Fe(III) oxides: behavior and XPS study. *Water Research*, **2010**, *44(3)*, 815-824.

131. Dias, A.M.G.C., Hussain, A., Marcos, A.S., Roque, A.C.A. A biotechnological perspective on the application of iron oxide magnetic colloids modified with polysaccharides. *Biotechnology Advances,* **2011**, *29(1)*, 142-155.

132. Boyer, C., Whittaker, M.R., Bulmus, V., Liu, J.Q., Davis, T.P. The design and utility of polymerstabilized iron-oxide nanoparticles for nanomedicine applications. *NPG Asia Materials*, **2010**, *2*, 23-30.

133. Gupta, A.K., Gupta, M. Synthesis and surface engineering of iron oxide nanoparticles for biomedical applications. *Biomaterials*, **2005**, *26(18)*, 3995-4021.

134. Roco, M.C. Nanotechnology: convergence with modern biology and medicine. *Current Opinion in Biotechnology,* **2003**, *14(3)*, 337-346.

135. Huang, S.H., Liao, M.H., Chen, D.H. Direct binding and characterization of lipase onto magnetic nanoparticles. *Biotechnology Progress*, **2003**, *19(3)*, 1095-1100.

136. Selvan, S.T., Tan, T.T.Y., Yi, D.K., Jana, N.R. Functional and multifunctional nanoparticles for bioimaging and biosensing. *Langmuir*, **2010**, *26(14)*, 11631-11641.

137. Bystrzejewski, M., Pyrzyńska, K., Huczko, A., Lange, H. Carbon-encapsulated magnetic nanoparticles as separable and mobile sorbents of heavy metal ions from aqueous solutions. *Carbon*, **2009**, *47(4)*, 1201-1204.

138. Li, Y., Somorjai, G.A. Nanoscale advances in catalysis and energy applications. *Nano Letter*, **2010**, *10(7)*, 2289-2295.

139. Kanel, S.R., Nepal, D., Manning, B., Choi, H. Transport of surface-modified iron nanoparticle in porous media and application to arsenic(III) remediation. *Journal of Nanoparticles Research*, **2007**, *9(5)*, 725-735.

140. Tiraferri, A., Chen, K.L., Sethi, R., Elimelech, M. Reduced aggregation and sedimentation of zero-valent iron nanoparticles in the presence of guar gum. *Journal of Colloid Interface Science*, **2008**, *324(1–2)*, 71-79.

141. Lin, C.L., Lee, C.F., Chiu, W.Y. Preparation and properties of poly (acrylic acid) oligomer stabilized superparamagnetic ferrofluid. *Journal of Colloid Interface Science*, **2005**, *291(2)*, 411-420.

142. Harris, L., Goff, J., Carmichael, A., Riffle, J., Harburn, J., Pierre, T.G.S. Magnetite nanoparticle dispersions stabilized with triblock copolymers. *Chemistry Materials*, **2003**, *15(6)*, 1367-1377.

143. Batalha, I.L., Hussain, A., Roque, A. Gum arabic coated magnetic nanoparticles with affinity ligands specific for antibodies. *Journal of Molecular Recognition*, **2010**, *23(5)*, 462-471.

144. Sung, Y.K., Ahn, B.W., Kang, T.J. Magnetic nanofibers with core (Fe_3O_4 nanoparticle suspension)/sheath (poly ethylene terephthalate) structure fabricated by coaxial electrospinning. *Journal of Magnetism and Magnetic Materials*, **2012**, *324(6),* 916-922.

145. Hyeon, T., Lee, S.S., Park, J., Chung, Y., Na, H.B. Synthesis of highly crystalline and monodisperse maghemite nanocrystallites without a size-selection process. *Journal of American Chemistry Society*, **2001**, 123(51), 12798-12801.

146. Huang, D.L., Zeng, G.M., Feng, C.L., Hu, S., Jiang, X.Y., Tang, L., Su, F.F., Zhang, Y., Zeng, W., Liu, H.L. Degradation of lead contaminated lignocellulosic waste by Phanerochaete chrysosporium and the reduction of lead toxicity. *Environmental Science & Technology*, **2008**, *42(13)*, 4946-4951.

147. Oller, I., Malato, S., Sánchez-Pérez, J.A. Combination of advanced oxidation processes and biological treatments for wastewater decontamination: a review. *Science of Total Environment,* **2011**, *409(20)*, 4141-4166.

148. Zhang, L.D., Fang, M. Nanomaterials in pollution trace detection and environmental improvement. *Nano Today*, **2010**, *5(2)*, 128-142.

149. Fan, F.L., Qin, Z., Bai, J., Rong, W.D., Fan, F.Y., Tian, W., Wu, X.L., Wang, Y., Zhao, L. Rapid removal of uranium from aqueous solutions using magnetic Fe_3O_4–SiO_2 composite particles. *Journal of Environmental Radioactivity*, **2012**, *106*, 40-46.

150. Carabante, I., Grahn, M., Holmgren, A., Kumpiene, J., Hedlund, J. Adsorption of As (V) on iron oxide nanoparticle films studied by in situ ATR–FTIR spectroscopy. *Colloids and Surface A*, **2009**, *346(1–3)*, 106-113.

151. Hu, J., Chen, G., Lo, I. Removal and recovery of Cr (VI) from wastewater by maghemite nanoparticles. *Water Research*, **2005**, *39(18)*, 4528-4536.

152. Mahmoudi, M., Sant, S., Wang, B., Laurent, S., Sen, T. Superparamagnetic iron oxide nanoparticles (SPIONs): development, surface modification and applications in chemotherapy. *Advanced Drug Delivery Reviews*, **2011**, *63*, 24-46.

153. Qiao, R., Yang, C., Gao, M. Superparamagnetic iron oxide nanoparticles: from preparations to in vivo MRI applications. *Journal of Material Chemistry*, **2009**, *19*, 6274-6293.

154. Mahmoudi, M., Simchi, A., Imani, M., Milani, A.S., Stroeve, P. Optimal design and characterization of superparamagnetic iron oxide nanoparticles coated with polyvinyl alcohol for targeted delivery and imaging. *Journal of Physical Chemistry B*, **2008**, *112*, 14470-14481.

155. Park, J., An, K., Hwang, Y., Park, J.G., Noh, H.J., Kim, J.Y., Park, J.H., Hwang, N.M., Hyeon, T. Ultra-largescale syntheses of monodisperse nanocrystals. *Nature Materials*, **2004**, *3*, 891-895.

156. Mahmoudi, M., Milani, A.S., Stroeve, P. Synthesis surface architecture and biological response of superparamagnetic iron oxide nanoparticles for application in drug delivery: a review. *International Journal of Biomedical Nanoscience and Nanotechnology*, **2010**, *1*, 164-201.

157. Wang, X., Zhuang, J., Peng, Q., Li, Y. A general strategy for nanocrystal synthesis. *Nature*, **2005**, *437*, 121-124.

158. Khan, Y., Durrani, S.K., Siddique, M., Mehmood, M. Hydrothermal synthesis of α-Fe_2O_3 nanoparticles capped by Tween-80. *Materials Letters*, **2011**, *65*, 2224-2227.

159. Sun, S., Zeng, H., Robinson, D.B., Raoux, S., Rice, P.M., Wang, S.X., Li, G. Monodisperse MFe_2O_4 (M = Fe, Co, Mn) nanoparticles. *Journal of the American Chemical Society*, **2004**, *14*, 273-279.

160. Chikate, R.C., Jun, K.W., Rode, C.V. Nonaqueous synthesis and characterization of capped Fe_2O_3 nanoparticles from iron(III) hydroxyoleate precursor. *Polyhedron*, **2008**, *27*, 933-938.

161. Mahmoudi, M., Simchi, A., Imani, M. Recent advances in surface engineering of Superparamagnetic iron oxide nanoparticles for biomedical applications. *Journal of the Iranian Chemical Society*, **2010**, *7*, 1-27.

162. Dresco, P.A., Zaitsev, V.S., Gambino, R.J., Chu, B. Preparation and properties of magnetite and polymer magnetite nanoparticles. *Langmuir*, **1999**, *15*, 1945-1951.

163. Narita, A., Naka, K., Chujo, Y. Facile control of silica shell layer thickness on hydrophilic iron oxide nanoparticles via reverse micelle method. *Colloids and Surfaces A: Physicochemical and Engineering Aspects*, **2009**, *336*, 46-56.

164. Ambashta, R.D., Sillanpää, M. Water purification using magnetic assistance: a review. *Journal of Hazardous Materials*, **2010**, *180(1–3)*, 38-49.

165. Mahdavian, A.R., Mirrahimi, M.A.S. Efficient separation of heavy metal cations by anchoring polyacrylic acid on superparamagnetic magnetite nanoparticles through surface modification. *Chemical Engineering Journal*, **2010**, *159(1–3)*, 264-71.

166. Feng, Y., Gong, J-L., Zeng, G-M., Niu, Q-Y., Zhang, H-Y., Niu, C-G., Deng, J-H., Yan, M. Adsorption of Cd(II) and Zn(II) from aqueous solutions using magnetic hydroxyapatite nanoparticles as adsorbents. *Chemical Engineering Journal*, **2010**, *162*, 487-494.

167. Kittel C. *Introduction to solid state physics*, Wiley: New York, **1996**.

168. Lu, A-H., Salabas, E.L., Schüth, F. Magnetic Nanoparticles: Synthesis, Protection, Functionalization, and Application. *Angewandte Chemie. International Edition*, **2007**, *46*, 1222-1244.

169. Elliot, S. R. *The Physics and Chemistry of Solids.* New York:Wiley, **1998**.

170. Mishima, N., Petrosky, T.Y., Minowa, H., Goto, S. Model experiment of two-dimensional Brownian motion by microcomputer. *American Journal of Physics*, **1980**, *48(12)*, 1050-1055.

171. Shen, T., Weissleder, R., Papisov, M., Bogdanov Jr., A., Brady, T.J. Monocrystalline iron oxide nanocompounds (MION): Physicochemical properties. *Magnetic Resonance in Medicine*, **1993**, *29*, 599-604.

172. Gittleman, J.I., Abeles, B., Bozowshi, S. Superparamagnetism and relaxation effects in granular Ni-SiO_2 and Ni-Al_2O_3 films. *Physical review B*, **1974**, *9*, 3891-2897.

173. Hultman, K.L.; Raffo, A.J.; Grzenda, A.L.; Harris, P.E.; Brown, T.R.; O'Brien, S., *Acs Nano,* **2008**, *2*, (3), 477-484.

174. EPA U.S. Environmental Protection Agency, Superfund Innovative Technology Evaluation. Demonstration Bulletin: Forager® Sponge technology, EPA/540/MR 94/522. **1994**.

175. Baghai, A., Bowen, H.J.M. Separation of rhodium and iridium using silicone rubber foam treated with tri-n-octalymine. *Analyst*, **1976**, *101*, 661-665.

176. Al Bazi, S.J., Chow, A. Mechanism of the extraction of palladium(II) thiocyanate complex by polyether foam. *Talanta*, **1983**, *30*, 487-492.

177. Matsumoto, H. Nanofibrous membranes - Preparation and application of electrospun membranes. *Maku,* **2010**, *35*, 113-118.

178. Yoon, K., Hsiao, B.S., Chu, B. Functional nanofibers for environmental applications. *Journal of Material Chemitry,* **2008**, *18*, 5326-5334.

179. Greiner, A., Wendorff, J.H. Electrospinning: A fascinating method for the preparation of ultrathin fibers. *Angewandte Chemie International Edition,* **2007**, *46*, 5670-5703.

180. Li, D., Xia, Y. Electrospinning of nanofibers: Reinventing the wheel? *Advanced Materials,* **2004**, *16*, 1151-1170.

181. Doshi, J., Reneker, D.H. Electrospinning process and applications of electrospun fibers. *Journal of Electrostics,* **1995**, *35*, 151-160.

182. Son, W.K., Cho, D., Park, W.H. Direct electrospinning of ultrafine titania fibers in the absence of polymer additives and formation of pure anatase titania fibers at low temperature. *Nanotechnology* **2006**, *17*, 439-443.

183. Zhou, F.L., Gong, R.H., Porat, I. Mass production of nanofiber assemblies by electrostatic spinning. *Polymer International,* **2009**, *58*, 331-342.

184. Chong, E.J., Phan, T.T., Lim, I.J., Zhang, Y.Z., Bay, BH., Ramakrishna, S. Evaluation of electrospun PCL/gelatin nanofibrous scaffold for wound healing and layered dermal reconstitution. *Acta Materialia,* **2007**, *3*, 321-330.

185. Li, D., Xia, Y. Electrospinning of nanofibers: reinventing the wheel. *Advanced Materials*, **2004**, *16*, 1151-1170.

186. Jiang, H.L., Fang, D.F., Hsiao, B.S., Chu, B., Chen, W.L. Optimization and characterization of dextran membranes prepared by electrospinning. *Biomacromolecules*, **2004**, *5*, 326-333.

187. Huang, L., Nagapudi, K., Apkarian, R.P., Chaikof, E.L. Engineered collagen-PEO nanofibers and fabrics. *Journal of Biomaterials Science, Polymer Edition*, **2001**, *12*, 979-993.

188. Zhao, Z.Z., Li, J.Q., Yuan, X.Y., Li, X., Zhang, Y.Y., Sheng, J. Preparation and properties of electrospun poly (vinylidene fluoride) membranes. *Journal of Applied Polymer Science,* **2005**, *97*, 466-474.

189. Zhang, C., Yuan, X., Wu, L., Han, Y., Sheng, J. Study on morphology of electrospun poly (vinyl alcohol) mats. *European Polymer Journal*, **2005**, *41*, 423-432.

190. Kim, B., Park, H., Lee, S.H., Sigmund, W.M. Poly (acrylic acid) nanofibers by electrospinning. *Material Letter*, **2005**, *59*, 829-832.

191. Son, W.K., Youk, J.H., Lee, T.S., Park,W.H. The effects of solution properties and polyelectrolyte on electrospinning of ultrafine poly (ethylene oxide) fibers. *Polymer*, **2004**, *45*, 2959-2966.

192. Jun, Z., Hou, H., Schaper, A., Wendorff, J.H., Greiner, A. Poly-L-lactide nanofibers by electrospinning, influence of solution viscosity and electrical conductivity on fiber diameter and fiber morphology. *e-Polymer*, **2003**, *9*, 1-9.

193. Chen, V.J., Ma, P.X. Nano-fibrous poly (L -lactic acid) scaffolds with interconnected spherical macropores. *Biomaterials*, **2004**, *25,* 2065–2073.

194. Demir, M.M., Yilgor, I., Yilgor, E., Erman, B. Electrospinning of polyurethane fibers. *Polymer*, **2002**, *43*, 3303-3309.

195. Gupta, P., Elkins, C., Long, T.E., Wilkes, G.L. Electrospinning of linear homopolymers of poly (methylmethacrylate): exploring relationships between fiber formation, viscosity, molecular weight and concentration in a good solvent. *Polymer*, **2005**, *46*, 4799-4810.

196. Koski, A., Yim, K., Shivkumar, S. Effect of molecular weight on fibrous PVA produced by electrospinning. *Material Letter*, **2004**, *58*, 493-497.

197. Hohman, M.M., Shin, M., Rutledge, G., Brenner, M.P. Electrospinning and electrically forced jets. II. Applications. *Physics of fluids*, **2001**, *13*, 2221-2236.

198. Zuo, W.W., Zhu, M.F., Yang, W., Yu, H., Chen, Y.M., Zhang, Y. Experimental study on relationship between jet instability and formation of beaded fibers during electrospinning. *Polymer Engineering Science*, **2005**, *45*, 704-709.

199. Mit-uppatham, C., Nithitanakul, M., Supaphol, P. Ultrafine electrospun polyamide-6 fibers: effect of solution conditions on morphology and average fiber diameter. *Macromolecular Chemistry and Physics*, **2004**, *205*, 2327–2338.

200. Ki, C.S., Baek, D.H., Gang, K.D., Lee, K.H., Um, I.C., Park, Y.H. Characterization of gelatin nanofiber prepared from gelatin-formic acid solution. *Polymer*, **2005**, *46*, 5094–5102.

201. Geng, X., Kwon, O.H., Jang, J. Electrospinning of chitosan dissolved in concentrated acetic acid solution. *Biomaterials*, **2005**, *26*, 5427–5432.

202. Buchko, C.J., Chen, L.C., Shen, Y., Martin, D.C. Processing and microstructural characterization of porous biocompatible protein polymer thin films. *Polymer*, **1999**, *40*, 7397–7407.

203. Sill, T.J., Recum, H.A.V. Electrospinning: applications in drug delivery and tissue engineering. *Biomaterials,* **2008**, *29*, 1989–2006.

204. Casper, C.L., Stephens, J.S., Tassi, N.G., Chase, D.B., Rabolt, J.F. Controlling surface morphology of electrospun polystyrene fibers: effect of humidity and molecular weight in the electrospinning process. *Macromolecules*, **2004**, *37*, 573–578.

205. Li, D., Xia, Y. Electrospinning of nanofibers: reinventing the wheel. *Advanced Materials*, **2004**, *16*, 1151–1170.

206. Miwa, M., Nakajima, A., Fujishima, A., Hashimoto, K., Watanabe, T. Effects of the surface roughness on sliding angles of water droplets on superhydrophobic surfaces. *Langmuir*, **2000**, *16*, 5754.

207. Ma, M., Hill, R.M., Lowery, J.L., Fridrikh, S.V., Rutledge, G.C. Electrospun poly(styrene-block-dimethylsiloxane) block copolymer fibers exhibiting superhydrophobicity. *Langmuir*, **2005**, *21*, 5549.

208. Seeram, R., Fujihara, K., Teo, W.E., Lim, T.C., Ma, Z. *An introduction to electrospinning and nanofibers World scientific publishing*, Singapore, **2005**.

209. Wang, X., Fang, D., Yoon, K., Hsiao, B.S., Chu, B. High performance ultrafiltration composite membranes based on poly(vinyl alcohol) hydrogel coating on crosslinked nanofibrous poly(vinyl alcohol) scaffold. *Journal of Membrane Science*, **2006**, *278*, 261.

210. Zuwei, M., Wei, H., Thomas, Y., Seeram, R. Grafting of Gelatin on electrospun poly9caprolactone) nanofibers to improve endothelial cell spreading and proliferation and to control cell orientation. *Tissue Engineering*, **2005**, *11*, 1149.

211. Gopal, R., Kaur, S., Ma, Z., Ramakrishna, S., Matsuura, T. *Electrospun nanofibrous filtration membrane.* Journal of Membrane Science, **2006**, *281*, 581.

212. Feng, C., khulbe, K.C., Matsuura, T., Tabe, S., Ismail, A.F. Preparation and characterization of electrospun nanofiber membranes and their possible application in water treatment. *Separation and Purification Technology*, **2013**, *102*, 118-135.

213. Fang, J., Wang, X., Lin, T. Nanofibers – Production, properties and functional applications, Chapter 14: Functional Applications of Electrospun Nanofibers. InTech, Ed., Croatia, **2011**, p. 298.

2

Methodology

2. METHODOLOGY

2.1. Characterization techniques

The detailed characterization of the different adsorbent systems based in SPION (non-supported SPION or supported SPION systems) is essential for the appropriate development of such new materials. It allows a better understanding of the main features of their synthesis, explaining their properties, and determining areas for their potential application. Several widely used techniques are applicable to the characterization of nanomaterials[1,2] and the main parameters that usually characterize them include composition, size and distribution of nanoparticles, nanomaterials morphology, and special properties (i.e., magnetism).

Additionally, liquid phases containing the target compounds to be removed must be characterized to determine the main parameters providing the adsorption capacity of the new materials that are being tested.

The techniques indicated below have been used in this work for the characterization purposes.

2.1.1. Inductively Coupled Plasma Optical Emission Spectrometry, ICP-OES

ICP-OES technique was employed to analyze the metal content in the liquid phases of several adsorption parameters. These parameters include arsenite and arsenate as the target species under the adsorption process study and other metal ions (i.e, copper, zinc and nickel) in experiments where the adsorption selectivity was evaluated. Also, iron content was determined to control the stability of SPION in the experimental media during the adsorption experiments. Equipment description is specified in Table 2.1.

Table 2.1. ICP-OES equipment employed in the determinations.

Equipment	ICP-OES
Models	Iris Intrepid II XSP and iCAP 6000 Series
Company and Country	Thermo Scientifics, UK
Laboratory of analysis	• *Centre Grup de Tècniques de Separació en Química*, GTS (UAB, Barcelona, Spain) • *Division of Functional Materials*, FNM (KTH, Stockholm, Sweden)
Images	

Corresponding wavelengths of higher sensitivity without interference were selected to determine arsenic and iron concentration. The instrumental average uncertainty of metal ions determination was in all cases lower than 2%. [3,4,5,6]

Table 2.2 shows the selected emission lines for As and Fe to perform the analysis and also, their detection limits, possible interferences, solution flow and working pressure.

Table 2.2. Summary of spectroscopic parameters of the performed analysis.

Parameters	Arsenic, As	Iron, Fe
Emission Lines (nm)	193.759	259.940
Detection limit (ppm)	0.076	0.0062
Main interferences	Al, V	Mn, Ti
Solution flow (mL/min)	1.0	
Nebulizer pressure (psi)	30	

2.1.2. Inductively Coupled Plasma Mass Spectrometry, ICP-MS

When the arsenic and metal ions concentrations were very low (about ppb level), ICP-MS was employed after a previous treatment of the sample by following the same procedure as described for ICP-OES. Additionally, iron content was determined to control the stability of SPION in the experimental media during the adsorption experiments and the results reveal an iron content below the detection limit of the equipment (1 ppb). This content confirms the SPION stability in all the performed experiments. The instrumental

average uncertainly of metal ions determination was in all cases lower than 2%.[7,8] Equipment description is specified in Table 2.3.

Table 2.3. ICP-MS equipment employed in the determinations.

Equipment	ICP-MS
Models	VG Plasma Quad ExCell and XSeries 2
Company and Country	Thermo Scientifics, UK
Laboratory of analysis	*Centre Grup de Tècniques de Separació en Química*, GTS (UAB, Barcelona, Spain)
Image	

Moreover, ICP-MS was used when coupling to HPLC to develop the arsenic speciation as described below.

2.1.3. High Pressure Liquid Chromatography hyphenated to Inductively Coupled Plasma Mass Spectrometer, HPLC-ICP-MS

To analyze the different inorganic arsenic species (As(III) and As(V)) in the liquid phases for the adsorption experiments, a method using liquid chromatography hyphenated to an inductively coupled plasma mass spectrometer (HPLC-ICP-MS) was employed. Equipment description is specified in Table 2.4.

Table 2.4. HPLC and ICP-MS employed in hyphenated determinations.

Equipment	HPLC- ICP-MS
Models	Shimadzu LC-10AT vp and XSeries 2 ICP-MS
Company and Country	Shimadzu Scientific Instruments, Inc., Japan and Thermo Scientifics, UK
Laboratory of analysis	*Centre Grup de Tècniques de Separació en Química*, GTS (UAB, Barcelona, Spain)
Image	

The method allowed separation, identification and quantification of arsenite and arsenate (arsenic oxoanions in solution) due to the use of appropriate anionic HPLC column (HAMILTON PRPX-100; 10 µm anion exchange resin) and mobile phase (Figure 2.1). [9,10]
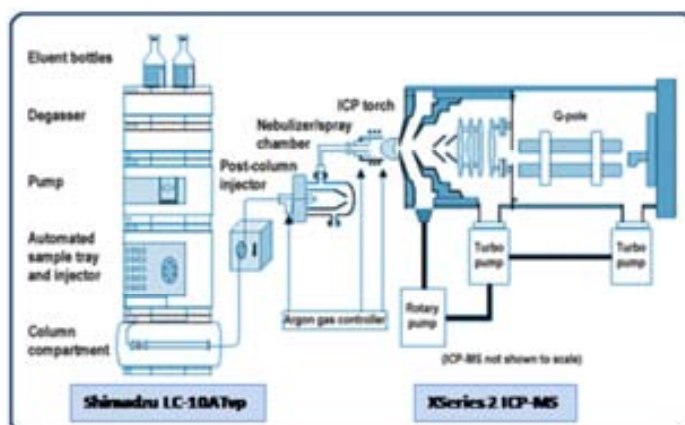
Figure 2.1. Experimental setup for HPLC-ICP-MS analysis.

2.1.3.1. Analysis procedure

40 mM $(NH_4)H_2PO_4$ mobile phase was prepared by dissolving $(NH_4)H_2PO_4$ in miliQ water with 1% MeOH. The pH is adjusted to 5.8. After the solution preparation, filtration is needed to remove any particle in suspension by 0.22 µm filter. Solution pH is controlled before and after the filtration using an aliquot of the prepared solution.

Reference solutions containing known amounts of As(III)/As(V) mixtures within a range of 1-500 ppb were prepared in order to perform calibration curves. Experimental samples were also processed by direct ICP-MS analysis samples to verify the correspondence of both total arsenic and the arsenic species content.

The obtained results were presented as a chromatographic spectrum, as show the Figure 2.2, where the different arsenic species which are present in the sample are detected at different times and represented as peaks that must be well defined and separated.[11]
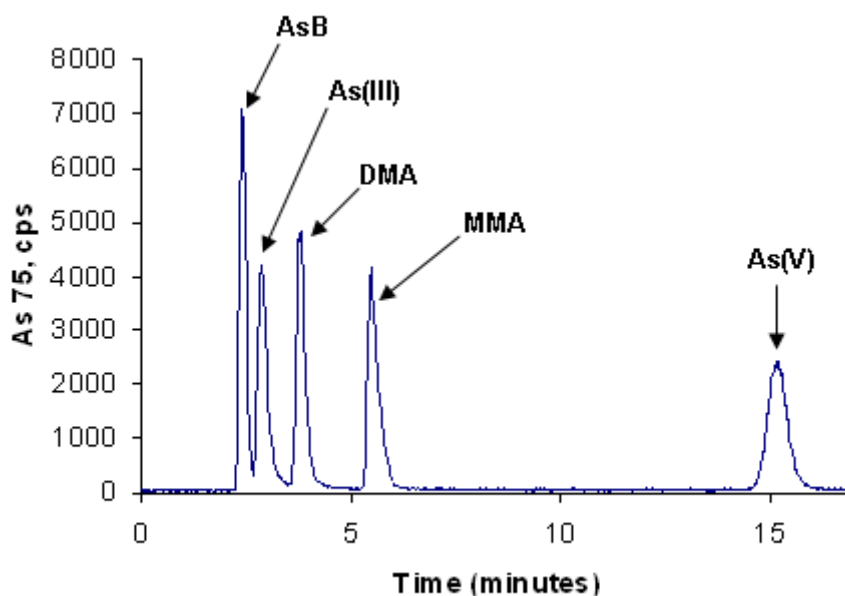
Figure 2.2. Typical HPLC-ICP-MS chromatogram of an As multi-analyte reference sample.

2.1.3.2. Experimental conditions

Optimized experimental conditions for both HPLC arsenic species separation and ICP-MS arsenic quantification are given in Table 2.5.

Table 2.5. Summary of experimental parameters for the HPLC and ICP-MS analysis.

HPLC experimental conditions	
Parameters	Conditions
Mobile Phase Composition	40mM $(NH_4)H_2PO_4$ and 1% MeOH at pH 5.8
Mobile Phase Flow Rate	1.5 mL min^{-1}
Column Dimensions	250 × 4.1-mm i.d.
Stationary Phase Composition	10-µm anion-exchange resin HAMILTON PRPX-100
Column Temperature	Ambient
Sample Injection Volume	100 µL
Pressure	25 MPa
ICP-MS experimental conditions	
Parameters	Conditions
Nebulizer Gas Flow	0.9 mL min^{-1}
ICP-MS configuration	Collision Cell ICP-MS (CCT)
Forward Plasma Power	1400 W
Data Acquisition	Mode transient Time Resolved Acquisition (TRA)
Monitored Masses	^{75}As
Dwell Times (mass specific)	150 ms
Run Duration	10 min
Detection Limit	300 ppt

2.1.4. X-ray Absorption Near Edge Structure, XANES

XAS experiments were carried out in two different Synchrotron facilities. While XAS experiments for arsenic speciation on Forager® Sponge loaded with SPION were developed at ESRF (Grenoble, France), experiments for iron speciation were performed at DESY-HASYLAB (Hamburg, Germany).

The experimental beamlines and the specific conditions for each beamline setup are specified in Table 2.6.

Table 2.6. Beamline setup for each synchrotron radiation source facilities.

	Synchrotron facilities	
	ESRF	**DESY-HASYLAB**
Synchrotron Image		
Beamline	BM25 – 16 bunch mode	A1 – 16 bunch mode
Insertion devices	Ondulator	Bending Magnets
Energy Source	5-45 keV	5-43 keV
Maximum Current	90 mA	140 mA
Monochromator crystals	Si (111)	2 Si (111)
Resolution (ΔE/E)	10^{-4}	10^{-4}
Photon flow	10^{13} photons/s	10^{10} photons/s
Spot size at the sample	1.5x1.0 mm	5.0x0.8 mm
Detectors	3 Ionization chambers (Transmittance) and Si(Li) 13 elements (Fluorescence)	3 Ionization chambers (Transmittance) and Si(Li) 7 elements (Fluorescence)
Beam-sample angle	45°	45°
Temperature	Room temperature	Room temperature

2.1.4.1. Sample preparation

For arsenic and iron XAS analysis, Forager® sponge samples were dried, homogenized, milled to a fine powder in a mortar and mixed with polyethylene powder (Sigma Aldrich, USA) which is transparent to X-rays. Samples of this mixed powder were converted into pellets by hydraulic pressure (hydraulic press 25t RIIC, London) to be analyzed at the experimental station of the synchrotron facility. The obtained pellets were encapsulated in Kapton® foils in order to avoid direct contact with the atmosphere and conserve the sample properties (Figure 2.3). Kapton® is a high temperature polyimide and it is used in the sample preparative for synchrotron analysis due to its excellent physico-chemical properties such as high temperature resistance, being chemically inert and a high resistance to ionizing radiation performance.

Figure 2.3. Example of pellet samples encapsulated in Kapton® foils for the synchrotron experiments.

The reference samples for individual arsenic and iron species consist of a homogenized mixture of reference samples with polyethylene to dilute and give consistence to the pellet. Later, the samples were homogenized, milled to a fine powder and converted into pellets by hydraulic pressure like the target samples.

Compounds that were employed in the SPION synthesis or in the arsenic adsorption process were used as reference compounds. Thus, $NaAsO_2$ and Na_2HAsO_4 were the compounds employed to prepare the reference samples for arsenic. For iron, chloride salts which were used in the SPION synthesis and SPION reference were the principal references to determine if any structural change is produced in the adsorption process.

Each pellet has a total weight of 100 mg, 20 mg of reference compound and 80 mg of polyethylene.

Sample holders and their placement on the beamline setup at ESRF and HASYLAB beamlines are shown in Figure 2.4. While in HASYLAB, sample holder holds 6 samples simultaneously and it is moved vertically in the beam source path, in ESRF two sample holders can be charged with 3 samples each one and it is moved in the XYZ space to locate the samples in the right position.
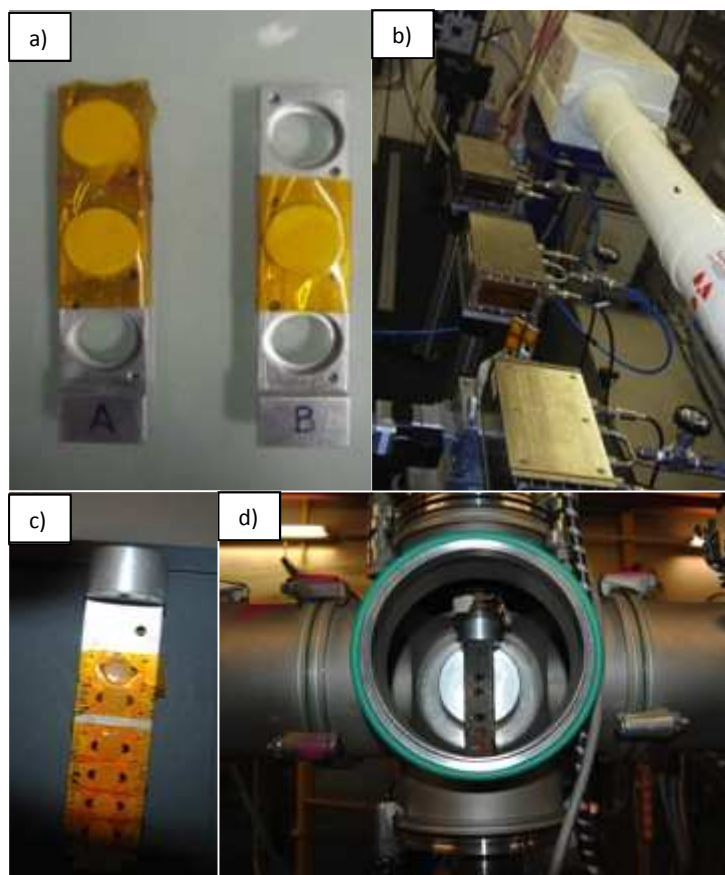
Figure 2.4. Sample holder and its position in XAS setup for ESRF BM25 beamline (a,b) and HASYLAB A1 beamline (c,d).

2.1.4.2. XAS measurements

XAS experiments for the arsenic and iron speciation studies were carried out at both BM25 and A1 beamlines described in the previous section. As can be observed in Figure 2.5, a common experimental setup is composed of 3 ionization chambers aligned with the sample position and a fluorescence detector perpendicular to the sample position.
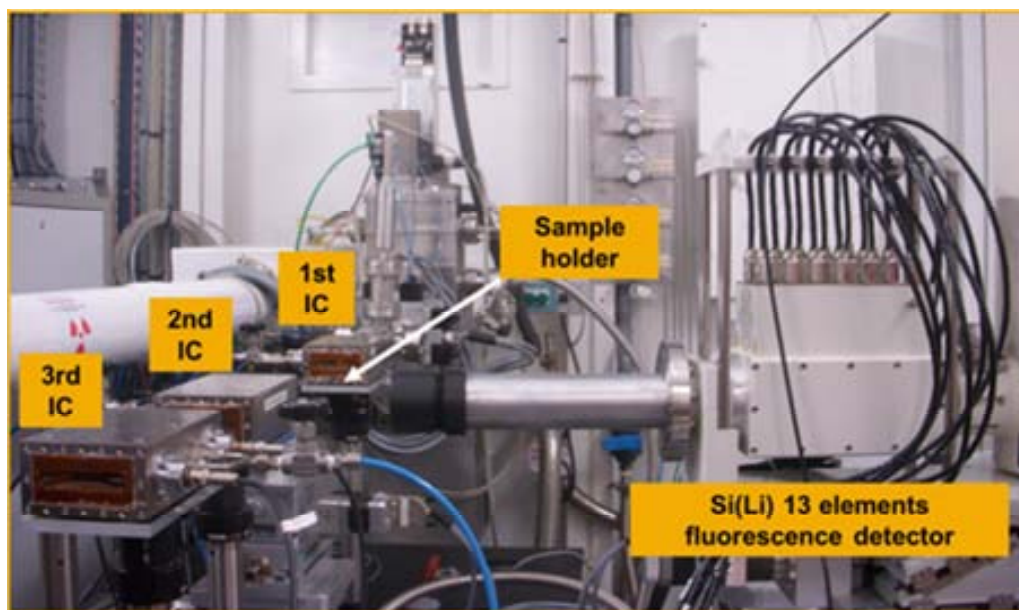
Figure 2.5. Experimental setup for XAS analysis in ESRF BM25 beamline in Grenoble

Arsenic absorption was recorded at the edge energy for its K line at 11867 eV and its fluorescence $K_{\alpha 1}$ at 10543.4 eV and $K_{\beta 1}$ at 11725.8 eV. In the same way, iron absorption was recorded at the edge energy for its K line at 7112 eV and its fluorescence $K_{\alpha 1}$ at 6405.2 eV and $K_{\beta 1}$ at 7059.3 eV.

Three main spectral regions can be observed in the typical XAS absorption spectra. Such regions contain related, but slightly different, information about an element's local coordination and oxidation state as the Figure 2.6 shows:[12]
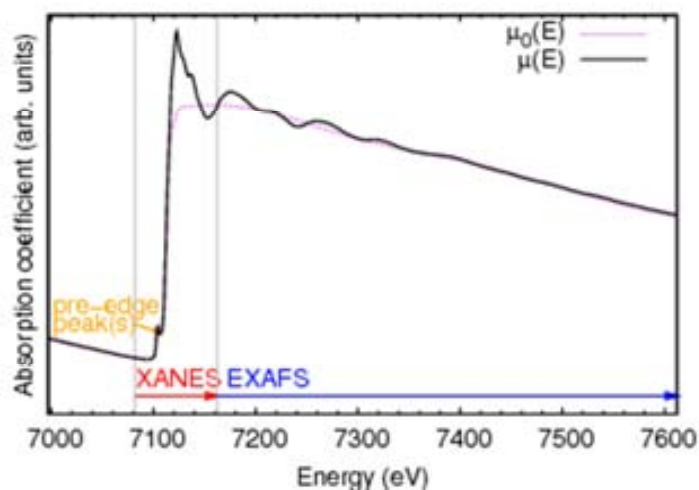
Figure 2.6. Typical X-ray adsorption spectrum

a) **Pre-edge** (E<E$_0$): About 2-50 eV below the main adsorption edge. In this region where no significant adsorption phenomena occurs, only electronic transitions from the core level to the higher unfilled or half-filled orbitals.

b) **XANES**: In the region between 2 eV below up to 50 eV above the adsorption edge. In this region, transitions of core electrons to non-bound levels with close energy occur. Because of the high probability of such transition, a sudden raise of adsorption is observed.

c) **EXAFS**: The region starts approximately from 50 eV and continues up to 1000 eV above the edge. In this region, the photoelectrons have high kinetic energy and single scattering by the nearest neighbouring atoms normally dominates

Before starting the XAS analysis, a X-ray adsorption experiment must be recorded over the sample to determine the actual adsorption peak for the element of interest (intensity vs wavelength) under the established conditions. Once the possible interferences are determined and removed, the optimum spot size is selected. A fluorescence spectra is performed (fluorescence intensity vs energy) which is scanned by energy steps according to the region of interest. In this sense, pre-edge and edge region are needed to be thoroughly studied, being the steps number in these region higher than in the rest of the spectra and subsequently, the resolution of the XAS spectra is higher.

Both fluorescence and transmittance intensities are registered by using different detectors. The selection of the detection mode depends upon the sample concentration and the matrix background.[13] Transmission mode measures sample absorption and is typically used for high concentrations of absorber (>2 wt%). The absorption by a sample of thickness x and adsorption coefficient μ is related to the ratio I_0 and I as show the following equation.

$$\boldsymbol{\mu x = ln(I/I_0)} \tag{2.1}$$

Consequently, the right thickness for transmission measurements requires a uniform sample, free of pinholes. Fluorescence detection follows the fluorescent X-Ray yield from the front-face of the sample. Fluorescence detection is used for samples with lower absorber concentrations (<2 wt%), with high matrix absorption or for very small samples, and therefore I_f/I_0 is proportional to μ. Hence, due to a higher signal-to-noise ratio, the

fluorescence yield is 10 to 100 times more sensitive than absorption coefficients measured in transmittance mode.[14],[15]

Therefore, reference compounds were analyzed by transmittance mode. Due to these standards are pure samples with high concentration, the spectra are very sharp and less replicates are needed. The unknown samples were analyzed by fluorescence detection mode (multi-element solid state detector) as they present more noise when the concentration is lower. Then, more replicated and more analysis time are needed to obtain a sharp spectra.

2.1.4.3. XAS data treatment

The XAS spectra were analyzed with XAS data analysis software IFEFFIT (developed by Matt Newville at CARS, Consortium for Advanced Radiation Sources, at The University of Chicago) and the data analysis is focused in XANES region which inform about the oxidation state for the arsenic adsorbed in Forager® Sponge loaded with SPION. Samples were analyzed after the Arsenic adsorption.

Averages of spectra replicates for each reference and unknown sample were made, the energy is calibrated and background correction and edge normalization were performed.

Arsenic quantitative speciation is performed in two main steps:

➢ **Principal Components Analysis (PCA):** it consists on a mathematical decomposition of a set of data files into the minimum number of components needed to describe the variance in the data. These principal components are mathematically sufficient to reconstruct each of the experimental spectra by any linear combination. The main outcome of this procedure is the determination of the number and type of reference compounds needed to describe the set of data files within the experimental error.[16],[17]

➢ **Least squares fitting:** this is the second step regarding speciation analysis, which consists on the fitting of reference compounds to the already corrected experimental data. The fingerprint adjustments are normally achieved by the minimization of the least squares fitting between the sample spectra and a combination of reference spectra.

IFEFFIT is the data treatment software used to perform the speciation analysis. That program produces, in a first step, the iterative PCA adjustments until no more significant components

are identified and, in a second one, the linear combination of all components spectra by least squares fitting to get a 100 % fit (a ±10% error is allowed).[18]

The relative quality of the fit was quantified by the residual value, a measure of how close the fit (x_{fit}) is to the data (x_{data}) based on a sum of square differences. Determination of the fractional misfit is defined as follows (Equation 2.2):

In summary, the complete process since the sample preparation until data treatment analysis is compiled in the following diagram (Figure 2.7):
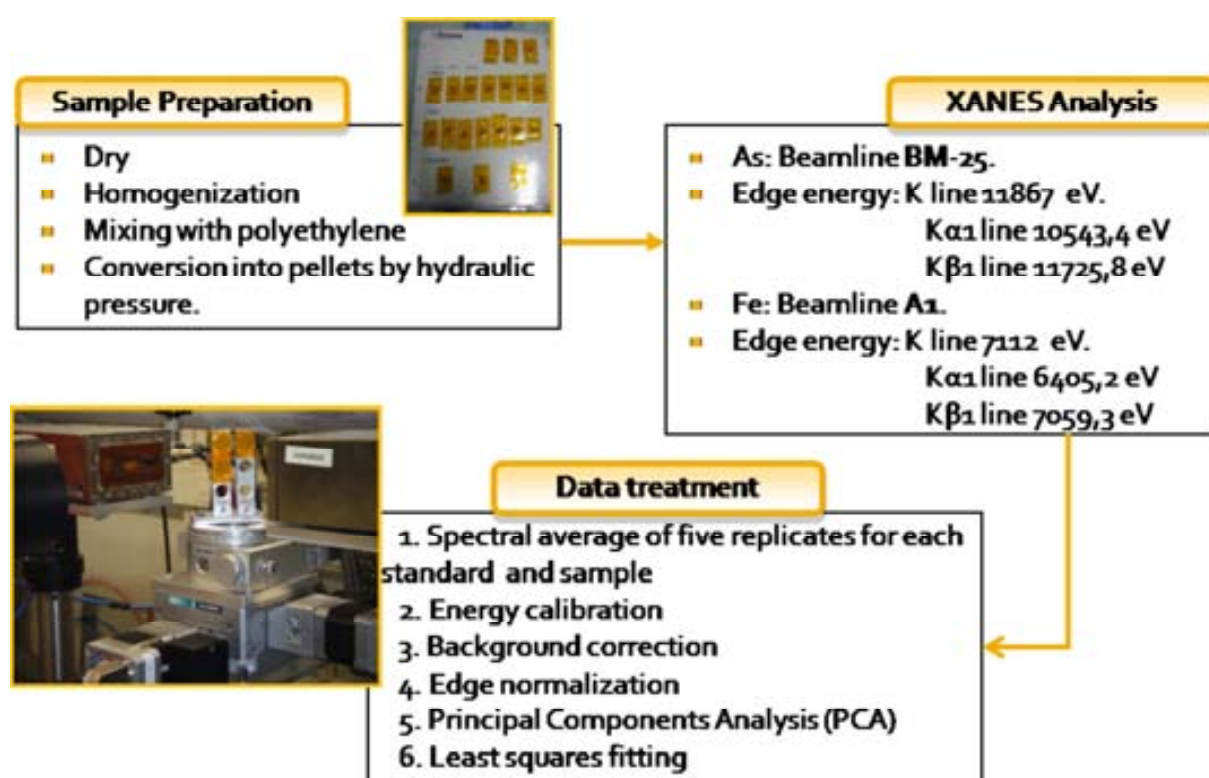
Figure 2.7. Scheme of the complete process for XAS experiments

2.1.5. Transmission Electron Microscopy, TEM

TEM technique was employed to characterize the morphology of the SPION and their particle size distribution. For dispersible PAN and CA nanofibers, their dispersion in organic

media (i.e., DMF or Ethanol) and solvent evaporation on the Cu-grid was carried out. Equipment description is specified in   Table 2.7.

Table 2.7. TEM equipment used in present studies.

Equipment	TEM
Models	JEOL FEG-TEM 2100F, JEM-1400 and JEOL JEM-2011 HRTEM
Company and Country	Jeol Ltd., Japan
Laboratory of analysis	• *Servei de microscopía* (UAB, Barcelona, Spain) • *Division of Functional Materials*, FNM (KTH, Stockholm, Sweden)
Image	

For non-soluble nanocomposites (Forager® Sponge), samples were embedded in an epoxy resin and cross-sectioned with a Leica EM UC6 ultramicrotome using a 35° diamond knife form Diatome.

By the digital treatment of TEM images, it is possible to produce size histograms from the sample data. The measurement of the diameter of a representative number of NPs is needed, and was obtained by a measuring tool of Gatan Digital Micrograph 3.4 soft package and the related histograms were represented by Microsoft Excel. The frequency (in %) of the NP size is generally described by corresponding Gaussian equation of 3 parameters (Equation 2.3), where a is the height of the curve`s peak, μ is the center peak position (corresponding to the most frequent diameter) and s is the standard deviation:[19,20]

$$y = a \cdot e^{\left[-0.5\left(d-\mu/s\right)^2\right]}$$

(2.3)

2.1.6. Scanning Electron Microscopy, SEM

SEM technique was employed to study the morphology of the adsorbent systems surface in the case of Forager Sponge loaded SPION, CA-SPION nanofibers and SPION loaded H-PAN nanofibers. Equipment description is specified in   Table 2.8.

Table 2.8. SEM equipment used in present studies.

Equipment	SEM
Models	Zeiss EVA MA 10, Zeiss MERLIN FE, ZEISS FEG-SEM Ultra-55 and Hitachi S-570
Company and Country	Carl Zeiss Microscopy, LLC., Germany and Hitachi High-Tec, Japan
Laboratory of analysis	• *Servei de microscopía* (UAB, Barcelona, Spain). • *Division of Functional Materials*, FNM (KTH, Stockholm, Sweden)
Image	

2.1.7. Energy Dispersive X-ray Spectrometer, EDS or EDX

Coupled to SEM or TEM microscopes, EDS/EDX provides the elemental chemical composition of the samples based on the X-Rays emitted by specific atoms which have been interacted with a particular electron beam. Each atom has a unique X-Ray spectrum, thus the elemental composition can be obtained by detected radiation. These microscopes are also equipped for X-Ray diffraction techniques that allow characterizing the crystalline structure of the SPION nanoparticles by diffraction patterns.

2.1.8. X-Ray Diffraction, XRD

The determination of SPION crystallographic phase was also undertaken by X-ray powder diffraction (XRD). In a diffraction pattern, the location of the peaks on the 2Θ scale can be compared to reference peaks. For the analysis, samples in powder form were deposited in glass sample holders. Diffraction patterns were collected by a monochromatized X-ray beam with nickel-filtered Cu(Kα) radiation with a wavelength of 0,154021 nm in similar conditions that already reported in the literature. [21]

Equipment description is specified in   Table 2.9.

Table 2.9. XRD equipment employed in present studies.

Equipment	XRD
Models	X'Pert-MPD X-ray Diffraction System
Company and Country	Philips, Netherlands
Laboratory of analysis	*Servei Difracció Raigs X* (UAB, Barcelona, Spain)
Image	

In Table 2.10, experimental conditions during the XRD spectra acquisition are described. These conditions were applied to detect the representative SPION peaks.

Table 2.10. Experimental conditions during XRD spectra acquisition

Parameter	Conditions
Monochromatic Beam	Cu Kα
Wavelength (nm)	0.154021
2θ (º)	10 – 70
Step size (º)	0.04
Time of step (s)	4.0

2.1.9. Superconducting Quantum Interference Device, SQUID

Magnetic susceptibility of SPION and Forager Sponge loaded SPION was characterized by SQUID. It was made in a magnetic field range from -7 to 7 T, to measure extremely weak magnetic fields based on superconducting loops. The knowledge of the magnetic susceptibility will mark the required magnetic field to easily remove the SPION from the treated solution. Equipment description is specified in Table 2.11.

Table 2.11. SQUID equipment used in present studies.

Equipment	SQUID
Models	SQUID MPMS-XL7
Company and Country	Quantum design Inc., USA
Laboratory of analysis	*Institut Català de Nanotecnologia*, ICN (UAB, Barcelona, Spain)
Image	

A 5 mg of sample was accurately introduced in suitable test tubs and the magnetization was analyzed at 300K. The magnetic properties of the nanocomposites were represented by plotting the magnetic moment (normalized by the amount of magnetic component in the sample) versus the applied magnetizing field (H), emu/gCO vs Oesterds (Oe) in cgs units (Table 2.12). [22,23,24]

Table 2.12. Table of quantities and units used in magnetism

Quantity	Symbol	SI unit	Cgs unit
Length		10^{-2} m	1 cm
Mass	m	10^{-3} kg	1 g
Force	F	10^{-5} N	1 dyne
Energy	E	10^{-7} J	1 erg
Magnetic induction	B	10^{-4} T	1 G
Magnetic Field Strength	H	$10^{3}/4\pi$ Am^{-1}	1 Oe
Magnetic moment	μ	10^{-3} JT^{-1} or A m^{2}	1 erg G^{-1} or emu
Magnetization	M	103 Am^{-1} or JT^{-1}m^{-3}	1 Oe or emu cm^{-3}
Magnetic susceptibility	χ	$4\,\pi$	1 emu cm^{-3} or emu cm^{-3}Oe^{-1}
Molar susceptibility	χ_m	$4\pi \times 10^{-6}$ m^{3} mol^{-1}	1 emu mol^{-1} or emu mol^{-1} Oe^{-1}
Mass susceptibility	χ_g	$4\,\pi \times 10^{-3}$ m^{3}kg^{-1}	1 emu g^{-1} or emu g^{-1} Oe^{-1}
Magnetic flux	ϕ	10^{-8} Tm^{2} or Wb	1 G cm^{2} or Mx
Demagnetization factor	N	$0<N<1$	$0<N< 4\pi$

2.1.10. Attenuated total reflectance – Fourier Transform Infrared, ATR-FTIR

FT-IR was used to check whether the reagent was bound to the surface of the functionalized SPION (3-MPA coated SPION) and to check the surface modification of the PAN nanofibers when the hydrolysis and the modification with EDA were produced. Equipment description is specified in Table 2.13.

Table 2.13. ATR-FTIR employed in the study.

Equipment	ATR-FTIR
Models	Nicolet I Avatar-100 with ATR diamond at 303 K and Shimadzu IRAffinity-1 with ATR 8000A
Company and Country	Shimadzu Scientific Instruments, Inc., Japan
Laboratory of analysis	• *Division of Functional Materials*, FNM (KTH, Stockholm, Sweden) • *Leitat Technological Center* (Terrassa, Spain)
Image	

The analysis is carried out at 4000-500 cm^{-1} wavelength range, with percentage of transmittance as measurement mode, 32 scans per sample with a resolution of 4.0 cm^{-1}. [25,26]

2.1.11. Termogravimetric Analysis, TGA

Thermograms were carried out to determine the polymer degradation temperatures in composite materials and quantify the functionalization degree of the 3-MPA coated SPION. The process was accomplished by heating the samples with a heating rate of 10°C/min until 900°C under N_2 atmosphere. The weight loss percentage versus temperature was represented. [27,28] Equipment description is specified in Table 2.14.

Table 2.14. TGA equipment employed in present study.

Equipment	ATR-FTIR
Models	Q-500
Company and Country	TA Instruments, USA
Laboratory of analysis	*Division of Functional Materials*, FNM (KTH, Stockholm, Sweden).
Image	

2.1.12. Field Portable X-Ray Fluorescence, FP-XRF

For the direct determination of the total arsenic and iron concentration in the samples prior to synchrotron experiments, FP-XRF technique was used. The analysis is carried out over the pellets that are encapsulated in Kapton® foil. Equipment description is specified in Table 2.15.

Table 2.15. FP-XRF equipment employed in XRF analysis.

Equipment	FP-XRF
Models	FP-XRF ALPHA 6500R
Company and Country	Innov-X Systems, USA
Laboratory of analysis	*Centre Grup de Tècniques de Separació en Química*, GTS (UAB, Barcelona, Spain)
Image	

The analyzing time for each sample was set to 120s for the heavy elements and 90s for the light elements. This time period is established as the best tradeoff between accuracy and speed of analysis. For accuracy, an instrument blank and calibration verification check (NIST 2710) were done each working day before and after analyses. Such controls are conducted once every twenty samples following EPA Method 6200.[29]

A blank is used to verify the absence of contamination in both the spectrometer and the probe window. In our case, silicon dioxide samples were employed as a blank following the one used in EPA Method 6200 described before, although there are other alternatives as polytetraflurorethylene (PTFE) block, a quartz block, "clean" sand, or lithium carbonate. An instrument blank should also be analyzed whenever contamination is suspected by the analyst.

A calibration verification check sample is used to examine the accuracy of the instrument and to assess the stability and consistency of the analysis for the target analytes.

2.2. Superparamagnetic Iron Oxide Nanoparticles synthesis, SPION.

The synthesis of 10 nm SPION (Equation 2.4) is performed as described elsewhere [30,31] with some modifications such as:

✓ The direct addition of Fe^{2+} as salt powder and not in a mixture solution with Fe^{3+} to avoid the partial oxidation of Fe^{2+} to Fe^{3+} and a low reaction yield.

✓ A fractionated cleaning process, where the SPION synthesized is divided in different aliquots to get better cleaning.

$$FeCl_3 \xrightarrow[\text{30 min, 70 ºC}]{NH_4OH} Fe(OH)_3 + NH_4Cl + NH_4OH \xrightarrow[\text{45 min, 70 ºC}]{FeCl_2} Fe_3O_4 + NH_4Cl \quad (2.4)$$
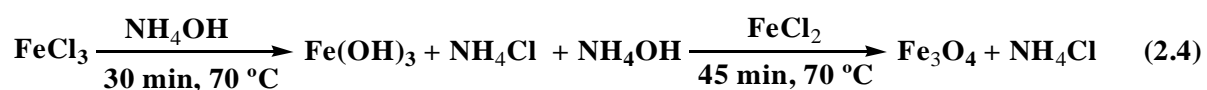
The synthesis requires a constant bubbling of nitrogen to prevent oxidation of Fe^{2+} to Fe^{3+} and therefore, the generation of other iron oxides such as maghemite or ferrihydrite. A stock solution of Fe^{3+} in a chloride medium is prepared by dissolving $FeCl_3.6H_2O$ in a deoxygenated HCl 0.2 M solution. A stock solution of NH_4OH 0.7 M is deoxygenated under nitrogen atmosphere and heated to 70º C. Later on, Fe^{3+} solution is added to the deoxygenated NH_4OH solution. The reaction cause a colour change in the solution and it takes brown colour. A suspension is formed (Figure 2.8a). After few minutes, anhydrous $FeCl_2$ was added, in a ratio 1:2 of Fe^{2+}/Fe^{3+}, generating an immediate colour change. In this case, the suspension turns black (characteristic SPION colour, Figure 2.8b). Then, the solution is kept 45 minutes under mechanical stirring and nitrogen bubbling for the ageing of nanoparticles. After sample cooling in a water bath, the resulting suspension was centrifuged at 2000 rpm, separating the nanoparticles by a magnet and washing with deoxygenated water several times. A subsequent redispersion step of the SPION is realized. A deoxygenated aqueous solution of tetramethylammonium hydroxide (TMAOH) 0.01 M (pH≈12) let to obtain SPION in a stable suspension for 6-8 months under deoxygenated atmosphere.
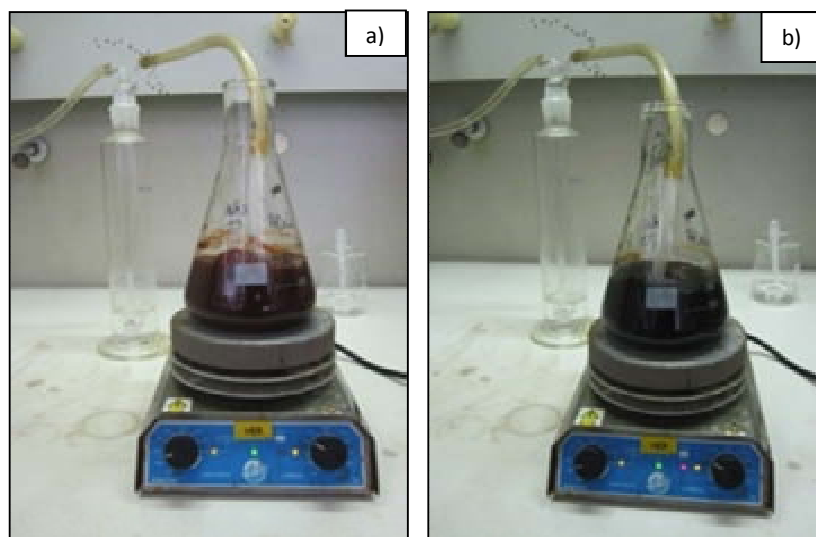
Figure 2.8. Stepwise synthesis of SPION: a) addition of $FeCl_3.6H_2O$ to the synthesis media and b) $FeCl_2.4H_2O$ powder addition to solution b)

2.3. 3-mercaptopropionic acid (3-MPA) coated SPION synthesis

After SPION synthesis, functionalization of SPION using 3-mercaptopropionic acid is performed. 3-MPA was coated on the surface of SPION by mixing a known amount of SPION with 150 mM solution of 3-MPA in toluene using rotary shaker for 24 hours. Different pHs are defined for the coating taking into account the point of zero charge of SPION due to the surface charge can affect to the coating process. The pHs of study are 2.0; 6.8 and 11.0 and are adjusted with HNO_3 1.0M or NaOH 1.0M. After phase separation using magnetic settlement, the nanocomposites are washed with toluene several times to remove the 3-MPA which is deposited and not coating the SPION surface. The nanocomposites are dried at room temperature (23 ˚C) overnight and then homogenized.

2.4. Forager® Sponge loaded SPION synthesis, Sponge loaded

SPION

Forager® Sponge is a quelatant synthetic polymer of cellulose and polyamide with amino tertiary and iminodiacetic groups which accomplish for selective affinity for metal and heavy metal ions, both cationic and anionic. Forager® Sponge is commercialized in 1.5x1.5 cm cubic form with an orange colour. A mechanical milling is made in order to obtain a small dust for a better handle as show the Figure 2.9. [32,33]

Figure 2.9. Forager® Sponge in cubic and dust form after milling

2.4.1. Forager® Sponge Surface treatment

After SPION synthesis, Forager® Sponge is loaded with SPION to develop a new adsorbent material. A pretreatment, by immersion in a hydrochloric acid for wiping their acidic form, is performed in order to activate the amino groups and to facilitate SPION immobilization.[34]

The sponge pretreatment consists in a preliminary cleaning with miliQ water and the conversion to acidic form by 1.0 M HCl treatment in batch mode with rotatory mixing. Once in protonic form, Forager® Sponge is rinsed again with miliQ water until pH 4.0 is reached. Later, Forager® Sponge is treated with a diluted HCl solution at pH 2.5 and it is rinsed slightly with miliQ water to remove the excess of acidic solution. Finally, the sponge is dried during 24h at 40 C in oven and introduced in a desiccator until their use.

2.4.2. Forager® Sponge loaded SPION

Having the SPION and the Forager® Sponge in acidic form, SPION load on the Forager® Sponge surface is performed as shows Figure 2.10. Such surface treatment is achieved using a pneumatic nebulizer that generates a homogeneous SPION dispersion, with the assistance of a peristaltic pump, under a 30 psi nitrogen stream (maximum nebulizer pressure).
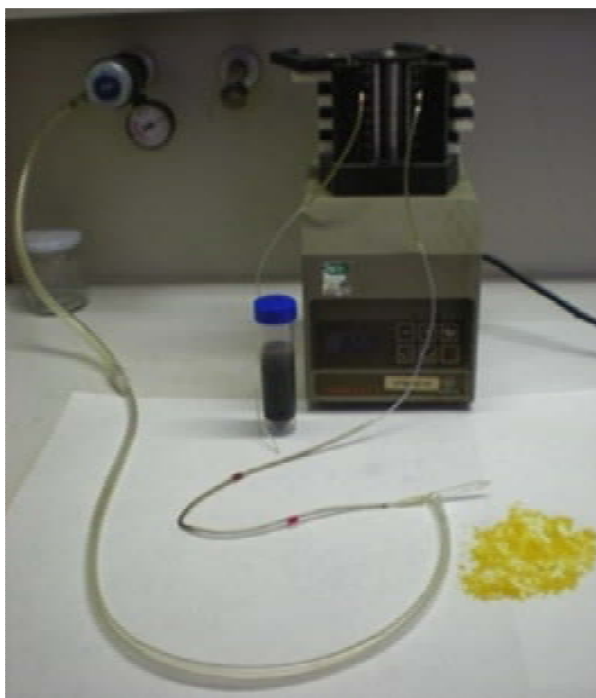
Figure 2.10. Experimental set-up for the SPION fixation over the Forager® Sponge surface

Variation on the number of SPION impregnations and also the impregnation time produced different adsorbent materials. The Forager® Sponge appearance change completely and a colour change from orange-yellow to black after the SPION impregnation, was observed, see Figure 2.11. Finally, a cleaning process is needed with nitrogen saturated water in order to remove the SPION excess that is not attached over the sponge surface. SPION loaded sponge is dried during 24 hours at 40 C in oven and is kept in a desiccator until their use. The amount of SPION deposited was calculated by difference between the initial sponge acidic form weight and the weight of the loaded sponge, being verified by the analysis of the Fe present in Forager® Sponge loaded SPION using microwave digestion and determining Fe by ICP-OES.

Figure 2.11. Forager® Sponge before and after the SPION fixation

2.5. Nanofiber synthesis by Electrospinning

Electrospinning process of polymer nanofibers is shown schematically in Figure 2.12. This technique is based on three main components: a high voltage supply, a syringe connected to a needle of small diameter and a metallic collecting plate. In this process, to make an electrically charged jet of polymer solution or melt out of the needle, a high voltage is applied between two electrodes connected to the spinning solution and to the collector which is normally grounded, respectively. The electric field is subjected to the tip of the needle containing a droplet of the polymer solution. The surface of the droplet is electrified. Increasing the intensity of the electric field changes the hemispherical surface of the fluid at the tip of the needle to a conical shape known as the Taylor cone. After a special intensity of the electric field (this intensity is the optimum intensity to generate the nanofiber and it depends of several parameters such as, conductivity and viscosity of electrospinning solution, distance tip-collector, solution flux, collector rotation, needle size,…), the repulsive electrostatic force dominates the surface tension and a charged jet of the polymer solution/melt is ejected from the tip of the Taylor cone. Due to the mutually repulsive forces of the electric charges of the jets, the polymer solution jet undergoes an instability (bending instability) and is elongated. The bending instability makes the jet very long and thin. Evaporation of the solvent while occurrence of bending instability results in formation of a charged polymer fiber which is deposited as an interconnected web on the collector. [35,36]
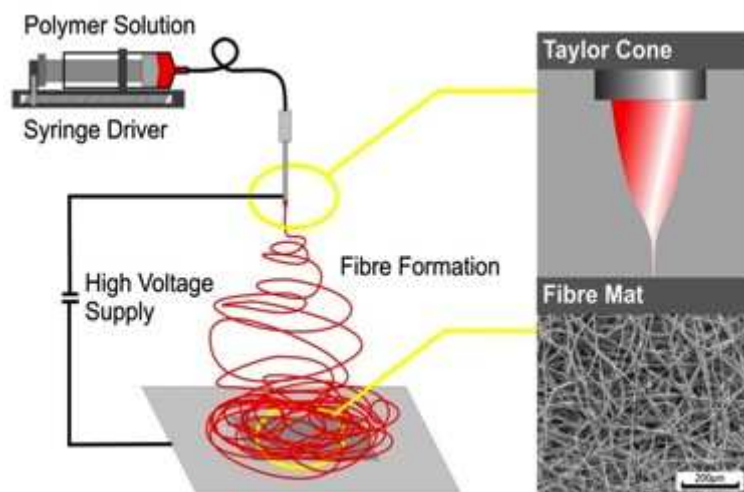
Figure 2.12. A schematic diagram for electrospinning processing of polymer nanofibers.

As described in *Section 1.4.5.2.*, the polymer solution jet is subject to three opposing forces including electrostatic and viscoelastic forces and surface tension. Similar to mechanical drawing in conventional fiber spinning, as stretching force, an increase of electrostatic repulsion of the charges in the jet increases its surface area by reduction of the fiber diameter. Gradually evaporation of the solvent intensifies this effect. On the other hand, the surface tension of the polymer solution tries to lower the total surface of the jet through an instability called "Rayleigh instability" by breaking up the jet into spherical droplets.[37]

In the polymer solution being electrospun, entanglement of polymer chains results in a viscoelastic force that resists against the stretching of the jet by electrical force. Also, viscoelastic force stands any rapid change in shape of the jet by surface tension. The nature and mechanical properties of the polymer solution including its viscosity and surface tension are determining factors for predominance of one of these forces to the other one.[38]

2.5.1. Cellulose Acetate – SPION nanofiber composites synthesis, CA-SPION NFCs

In this case, the electrospinning solutions varied cellulose acetate concentration between 10-20 % (w/v), being acetone and dimethylacetamide (DMAc) in 2/1 (v/v) the solvents for the CA solutions. Experiments were performed to determine the optimal CA

concentration providing most stable jet and to synthesize homogeneous electrospun CA nanofibers.

2.5.1.1. Electrospinning experimental conditions

The electrospinning solution is placed in a 10 mL syringe with a metal needle of 0.016 mm in diameter. A power supply is used to provide a voltage of 9-12 kV to the syringe needle tip and a metal collector. The electrospun fibers are collected on an aluminium foil of 10 cm of diameter, as show the Figure 2.13a. It is used a tip-to collector distance of 5 cm and a solution flow rate of 0.5 mL/h (Figure 2.13b). All of the electrospinning procedures are carried out at room temperature (25 ^{o}C) with a relative humidity of 50 %. The obtained electrospun nanofibers are dried in a vacuum oven for 24 h at 60 °C for characterizations and adsorption experiments.

Figure 2.13. Electrospun CA nanofiber (a) and electrospinning equipment for the synthesis of CA nanofibers (b)

Once the electrospun CA nanofibers are synthesized, two different procedures are used for SPION fixation in CA nanofibers. The first one involves the synthesis of CA nanofibers with the presence of SPION in the electrospinning solution in order to generate CA nanofibers with SPION inclusions. The second one requires dipping electrospun CA nanofibers in a SPION suspension in order to fix SPION on the nanofiber surface.

Table 2.16 shows the different electrospinning conditions for the different used CA concentrations. The different conditions depend on the different parameters such as the CA concentration, the solution viscosity and conductivity.

Table 2.16. Experimental conditions for the different electrospun CA nanofibers.

Polymer	Electrospinning solution	Viscosity (cP)	Conductivity (μS/cm)	Experimental conditions
CA	10.0 (w/v)% in DMAc/Acetone	1954	8,29	Voltage: 8.0 kV, Distance: 50 mm, Flux: 0.5 mL/h, Needle: GA 22*.
CA	15.0 (w/v)% in DMAc/Acetone	3439	7,81	Voltage: 8.0 kV, Distance: 50 mm, Flux: 0.5 mL/h, Needle: GA 22*.
CA	20.0 (w/v)% in DMAc/Acetone	4173	7,43	Voltage: 9.0 kV, Distance: 50 mm, Flux: 0.5 mL/h, Needle: GA 22*.

* GA 22: 12,7mm tips with 0.33mm inner diameter.

2.5.1.2. Electrospun CA-SPION nanofibers

Following the process indicated above, d15 % (w/v) CA solutions were prepared with different SPION concentration (0.3 and 3.0 % w/v). Firstly, CA dissolution and SPION dispersion were prepared separately. Both dissolution and dispersion are mixed and sonicated in order to obtain the electrospinning solution, shaking at room temperature to avoid sedimentation of SPION. . The obtained CA-SPION nanofibers are dried in a vacuum oven for 24 h at 60 °C for characterizations and adsorption experiments.

Table 2.17 shows the different electrospinning conditions for the different used SPION concentrations. The different conditions depend on the different parameters such as the SPION concentration, the solution viscosity and conductivity.

Table 2.17. Experimental conditions for the different electrospun CA-SPION nanofibers.

Polymer	Electrospinning solution	Viscosity (cP)	Conductivity (μS/cm)	Experimental conditions
CA	15.0 wt% + 0.3 % SPION in DMAc/Acetone	3139	8,23	Voltage: 12.0 kV, Distance: 50 mm, Flux: 0.5 mL/h, Needle: GA 22*
CA	15.0 wt% + 3.0 % SPION in DMAc/Acetone	3858	16,97	Voltage: 12.0 kV, Distance: 50 mm, Flux: 0.5 mL/h, Needle: GA 22*

* GA 22: 12,7mm tips with 0.33mm inner diameter.

2.5.1.3. CA-SPION nanofibers by dipping

The second procedure requires the CA nanofiber dipping into the SPION suspension of the 15 % (w/v) CA nanofiber at different pH (3, 6.8, 11) with a fixed SPION concentration of 0.3 % (w/v) during two hours under oscillatory shaking, generating SPION fixation over the surface of the CA nanofibers. The pHs were selected regarding the point zero charge of

SPION (pzc 6.8)[39] and under those conditions the SPION surface have different charge properties (positive, neutral or negative). Afterwards, the obtained CA-SPION nanofibers are rinsed with deoxygenated water in order to remove the SPION excess that is not attached over the nanofiber surface and dried in a vacuum oven for 24 h at 60 °C.

2.5.2. SPION loaded Hydrolyzed PAN nanofiber synthesis, HPAN-SPION NFs

2.5.2.1. PAN nanofibers synthesis

Electrospinning solutions are prepared by 7-15 wt% PAN solutions in DMF. Magnetic stirring is applied for 3 h at 60 °C in order to obtain homogeneous PAN solutions. The electrospinning solution is placed in a 10 mL syringe with metal needles of different diameters. A power supply is used to provide a high voltage of 20-30 kV to the syringe needle tip and a metal collector in continuous and constant rotatory movement (200 rpm). The electrospun fibers are collected on an aluminium foil obtaining a textile material of 60x20 cm size, as shows Figure 2.14a. A tip-to collector distance between 10-30 cm and a solution flow rate between 0.1 to 2.0 mL/h were employed (Figure 2.14b). All of the electrospinning procedures are carried out at room temperature (25 °C) with a controlled 50% relative humidity. The obtained nanofibers are dried in a vacuum oven for 24 h at 60 °C for characterizations and adsorption experiments.

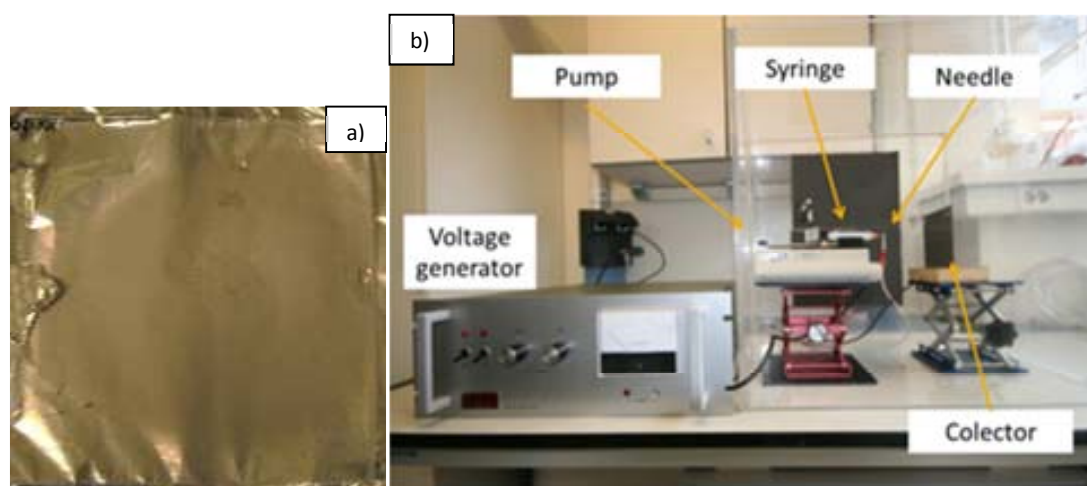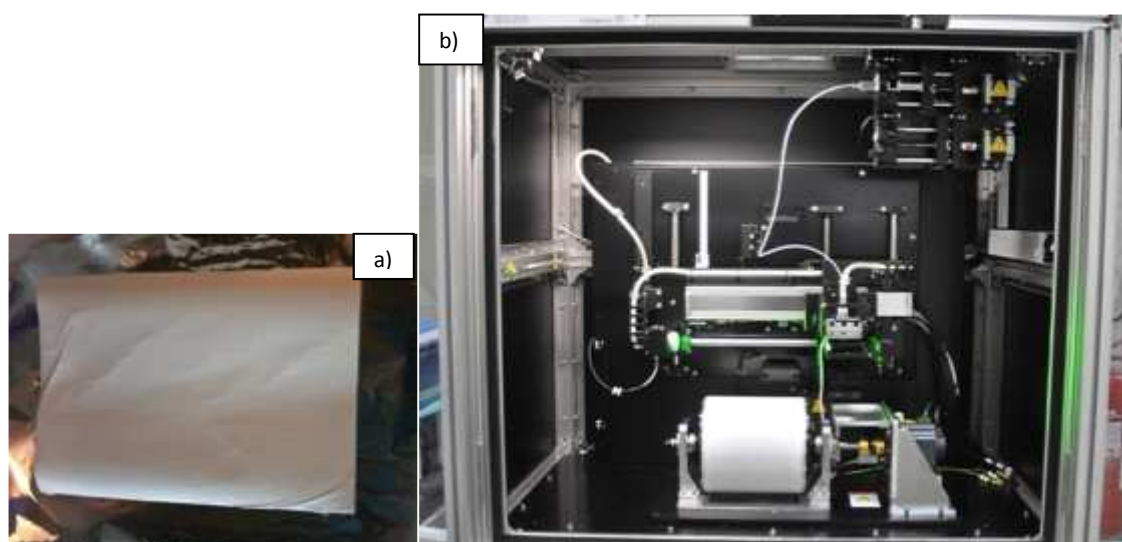**Figure 2.14.** Electrospun PAN nanofiber (a) and electrospinning equipment for the synthesis of PAN nanofibers (b)

Table 2.18 shows the different electrospinning conditions for the different used PAN concentrations. The different conditions depend on the different parameters such as the PAN concentration, the solution viscosity and conductivity.

Table 2.18. Experimental conditions for the different electrospun PAN nanofibers.

Polymer	Electrospinning solution	Viscosity (cP)	Conductivity (µS/cm)	Experimental conditions
PAN	15.0 wt% in DMF	5936	127.1	Voltage: 18.0 kV, Distance: 150 mm, Flux: 1.5 mL/h, Needle: GA 22*.
PAN	10.0 wt% in DMF	848	110.9	Voltage: 25.0 kV, Distance: 150 mm, Flux: 1.8 mL/h, Needle: GA 23**.
PAN	8.5 wt% in DMF	381	96.6	Voltage: 27.5 kV, Distance: 200 mm, Flux: 1.5 mL/h, Needle: GA 23**.
PAN	7.0 wt% in DMF	196	86.2	Voltage: 27.5 kV, Distance: 150 mm, Flux: 1.2 mL/h, Needle: GA 23**.

* GA 22: 12,7mm tips with 0.33mm inner diameter.
** GA 23: 12,7mm tips with 0.41mm inner diameter.

2.5.2.2. Modified surface PAN nanofibers

Electrospun PAN nanofibers with 200 cm^2 surface area are immersed in 100 mL 15% NaOH for 60 min at 50 °C, similarly to the process in the following **equation**. Then, the nanofiber is washed with distilled water and placed in 1.0 M HCl at room temperature for 120 min. The colour of the hydrolysed yellowish PAN nanofibers (HPAN) turned into white (the initial one). After that, the nanofiber is immersed in 100 mL 10% solution of ethylenediamine (EDA) for 60 min at room temperature (HPAN-EDA).

$$(2.5)$$
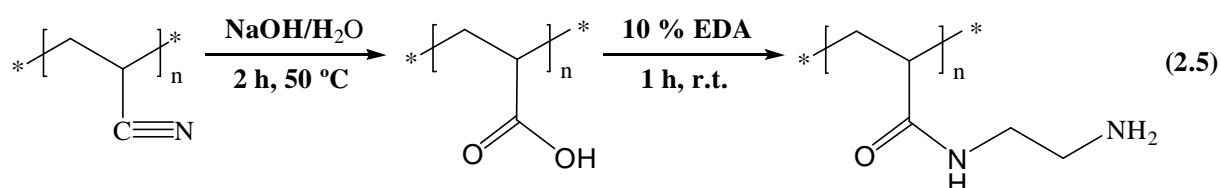
2.5.2.3. SPION loaded HPAN and HPAN-EDA nanofibers

Finally, the HPAN and HPAN-EDA nanofibers are immersed in 100 mL of SPION suspension in 0.01 M TMAOH media with different amounts of SPION for 3 hours at room temperature. The SPION is added from a suspension with known concentration by addition of the corresponding volume, as shows the Table 2.19. Afterwards, the obtained SPION

loaded HPAN and SPION loaded HPAN-EDA nanofibers are rinsed with deoxygenated water in order to remove the SPION excess that is not properly fixed on the nanofiber surface and kept in deoxygenated water for adsorption analysis. For characterization experiments, nanofibers are dried in a vacuum oven for 24 h at 60 °C.

Table 2.19. Pipetted volume and the corresponding SPION amount.

SPION suspension 28.82 mg/mL	
SPION suspension (µL)	**SPION (mg)**
500	14.41
250	7.20
125	3.60
60	1.73
30	0.86
20	0.58
10	0.29

2.6. Adsorption-desorption procedure

The experiments were performed at 1-1000 ppm As(III), As(V) or As(III)/As(V) mixtures. These studies were performed in a wide range of concentrations. Performing experiments until 1000 ppm, push the adsorbent systems to the limit in order to observe its maximum adsorption capacity. Two different modes were studied:

➤ **Batch adsorption experiments** were performed to optimize the principal experimental parameters such as the contact time, optimum pH, maximum loading capacity or the selectivity in presence of metal ions or interfering anion.

➤ **Continuous mode experiments** were performed to obtain a most appropriate contact between adsorbent material and contaminated water for higher efficiency, as well as to approach real conditions.

2.6.1. Batch adsorption experiments

The adsorption experiments were performed in batch mode by mixing aqueous solution of As(v), As(III)or As(III)/As(V) mixture in 0.2M Acetic/Acetate media (in presence or not of metal ions and interfering anions) at room temperature with constant amounts of the different adsorbent systems (Table 2.20) using a rotatory shaker (Figure 2.15). The pH of the solutions was controlled using 1.0M HNO$_3$ or 1.0M NaOH standardized solutions and confirmed with pH measurements (pH meter, Crison).
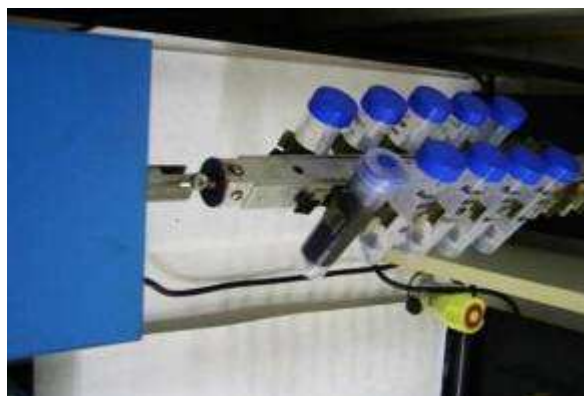
Figure 2.15. Experimental setup for batch experiments.

Table 2.20. Different adsorbent systems and corresponding quantities used in batch experiments.

Adsorbent System	Quantity (mg)
SPION	50
3-MPA coated SPION	10
Forager Sponge loaded SPION	50
SPION loaded HPAN nanofibers	100

After mixing, the solid phase was removed from the supernatant by decantation with magnet and filtration with cellulose acetate Milipore filters of 0.22 μm. Arsenic content in the obtained supernatant is determined by ICP-OES or ICP-MS and the dissolution of SPION is monitored by determining the concentration of iron in aqueous solutions, the final pH was measured as the pH value of the experiment and this value was used as pH value in all the adsorption experiments.

The adsorption capacity (q_{As}, mmol/g) is determined measuring the initial (C_{Asin}, mmol As/l) and final (C_{Asfin}, mmol As/l) arsenic concentration for each experiment and applying the following equation:

$$q_{As} = \frac{V_{ads} \cdot (C_{As\,ini} - C_{As\,fin})}{m_{ads}} \qquad (2.6)$$

where V_{ads} is the volume of reaction (l) and m_{ads} is the adsorbent quantity (g).

Through the following sections, specific experimental conditions are going to be described for the evaluation of each parameter in order to optimize the adsorption procedure.

2.6.1.1. Effect of the contact time in the adsorption process

In this experimental section, the effect of contact time on the adsorption is described. The experiments were carried out by mixing 50 mL of 100 ppm of either As(III), As(V) or 200 ppm As(III)/As(V) mixtures (100 ppm As(V) and 100 ppm As(III)) with a constant amount of the adsorbent system (described in section 6.1.), working at room temperature (23±1 ºC) and pH 3.6-4.0 (after the adsorption process) with the contact time varying in the period of 1-360 min.

2.6.1.2. pH effect in the adsorption process

These experiments were carried out by mixing 50 mL of 100 ppm of either As(III), As(V) or 200 ppm As(III)/As(V) mixtures (100 ppm As(V) and 100 ppm As(III)) with a constant amount of the adsorbent system at room temperature (23±1 ºC) during 120 min. A pH range 2.0-11.0 (pH values after the adsorption process) was studied in order to identify the optimum adsorption pH.

2.6.1.3. Effect of the Arsenic concentration in the maximum adsorption capacity of the

adsorbent system

These experiments were performed to evaluate the effect of the initial arsenic concentration on the sorption of As(III), As(V) or As(III)/As(V) mixtures and estimate the maximum loading capacity of the different adsorbent systems. The initial arsenic concentration was in the range of 1 ppm and 1000 ppm (double concentration is applied in case of mixtures as explained above) at optimum pH (pH 3.8-4.0). 50 mL solution was mixed with each adsorbent system at room temperature (23±1 ºC) during 120 minutes.

2.6.1.4.   Selectivity against the presence of metal ions

To evaluate the adsorbent system separation capacity for As(III) or As(V) from a mixture containing other metals, such as Cu^{2+}, Zn^{2+} and Ni^{2+}, the selective sorption of As(III) or As(V) in presence of metal ions was investigated.

The experiments were performed with 100 ppm solutions of As(III), As(V) or 200 ppm As(III)/As(V) mixtures (100 ppm As(V) and 100 ppm As(III)) containing Cu^{2+}, Zn^{2+} and Ni^{2+} metal ions in molar ratios 1:1 and 1:2 (As : metal ions). Experiments were performed as indicated before by mixing a known amount of adsorbent system with 50 mL target solution containing both Arsenic species and indicated metal ions, at room temperature (23±1 ºC) during 120 minutes.

2.6.1.5.   Selectivity with the presence of interfering anions

Finally, selective sorption of As(III) or As(V) in the presence of interfering anions was investigated in order to examine the selectivity performance of the adsorbent system in mixtures containing anions, such as Cl^-, NO_3^-, SO_4^{2-} or PO_4^{3-}.

100 ppm solutions of As(III), As(V) or 200 ppm As(III)/As(V) mixtures (100 ppm As(V) and 100 ppm As(III)) containing 0.25 M of interfering anions (ratio 200:1 respect of total arsenic in solution) were treated to observe the behaviour of the adsorbent system in presence of interfering anions in a pH range 2-11. The experiments were performed as indicated before by mixing a known amount of adsorbent systems with 50 mL of solution at room temperature (23±1 °C) during 120 minutes.

2.6.1.6.   Desorption process

Desorption experiments were performed by 10 mL of the elution solution (HNO_3, H_3PO_4, NaOH or NaCl) that was added to an accurate quantity of adsorbent system already loaded with arsenic. After 60 minutes of contact at room temperature (23±1 °C), the aqueous and the solid phases were separated by centrifugation and the concentration of arsenic in the supernatant was measured by ICP-MS.

2.6.2. Continuous adsorption-desorption experiments

Adsorption experiments in continuous mode were performed to observe the behaviour of the adsorbent system under more practical working conditions in order to assess a future application of these systems. For this reason, different column sizes are employed.

Experiments in continuous mode were performed for As(V) adsorption studies with the nanofibrous systems, CA-SPION nanofibers and SPION loaded HPAN nanofibers. 100 mg of corresponding nanofibers were introduced in two different column sizes: 10x1.0 cm and 20x1.5 cm (only for SPION loaded HPAN) and 2l of 100ppm As(V) solution were pumped through the column with a certain flow rate during 24 hours and eluted solution was sampled periodically. The selected sampling times were 0, 1, 2, 3, 4, 5, 10, 15, 20, 30, 60, 90, 120, 150, 180, 210, 240, 270, 300, 330, 360, 1320 y 1440 minutes.

Willing to observe the behaviour of these adsorbent systems under continuous water flow, two different column sizes were selected Taking into account the swelling properties, different columns were used to define the best dimensions to carry out the experiments under real waste water.

2.6.2.1. As(V) adsorption with small size columns, 10x1.0 cm for CA-SPION nanofibers and SPION loaded HPAN nanofibers

The adsorption experiments with small columns were performed with a 1 mL/min flow rate during 24 hours in all cases. During the experiment, different aliquots were periodically collected in order to determine the behaviour and the adsorption capacity of the adsorbent systems. Each aliquot was centrifuged and clarified with external magnet previous decantation. Arsenic and iron content in the obtained supernatant was determined by ICP-OES (in the case of CA-SPION nanofibers) and ICP-MS (when using SPION loaded HPAN nanofibers).

In the Figure 2.16, the experimental set-up for three adsorption experiments in continuous mode by gravity is shown with SPION loaded HPAN nanofibers with different amounts of SPION (14.41 mg of SPION on the left; 0.29 mg in the middle and a blank HPAN on the right).

93

Figure 2.16. Experimental set-up of As(V) adsorption in continuous mode by gravity with 10x1.0 cm columns

2.6.2.2. As(V) adsorption-desorption with big size columns, 20x1.5 cm

The adsorption experiments with bigger columns were performed with a 2 mL/min flow rate during 24 hours with two different modes, by gravity and counterflow (Figure 2.17). After the experiment, the aliquot was centrifuged and decantation with external magnet. Arsenic and iron content in the obtained supernatant were determined by ICP-MS.

Figure 2.17. Experimental set-up of As(V) adsorption in continuous mode by gravity (a) and counterflow (b) for SPION loaded HPAN nanofibers with 20x1.5 cm columns

Desorption experiments were performed by pumping a desorbent solution (1.0 M HNO$_3$ or 0.5M H$_3$PO$_4$) through the column by counterflow with a 2.0 mL/min flow rate during

1.5 hours. The samples were taken every 5 minutes. As and Fe content in the obtained supernatant were determined by ICP-MS.

2.6.2.3. As(V) adsorption-desorption of wastewater real sample

Water from a dumping lixiviation at Bailin (Huesca, Spain) was used to perform these experiments. This water (solution at pH 4 with high content in K, Na, Mg, Ca and Cl⁻) with no detectable As(V) is doped with 5 ppm As(V) due to both the impossibility to get a real wastewater contaminated with arsenic and its matrix with lithogenic compounds usually presents in mine wastewaters.[40,41] In addition, the dumping lixiviation water present high content in chloride that is present in practically all of the wastewaters. This fact can give information about the adsorption capacity in presence of a possible interfering anion. The experimental conditions were the same than in the continuous mode by counterflow with a 20x1.5 cm column size.

Adsorption and desorption experiments were performed in order to study the behaviour of the system treating industrial samples (Figure 2.18) and to compare if the adsorbent system is useful for this application when industrially contaminated water samples are treated.

Figure 2.18. Experimental set-up of As(V) adsorption (a) and desorption (b) in continuous mode by counterflow with 20x1.5 cm columns

References

1. Joshi M., Bhattacharyya, A., Ali, W. Characterization techniques for nanotechnology applications in textiles. *Indian Journal of Fibre and Textile Research,* **2008**, *33*, 304-317.

2. Richman, E., Hutchison J. The nanomaterial characterization bottleneck. *ACS Nano*, **2009**, *3(9)*, 2441-2449.

3. Skoog, D.A., Leary, J.J. Principios de Análisis Instrumental, Ed. McGraw-Hill (5ª edición), **2000**.

4. Edbon, l., Evans, E.H., Fisher, A., Hill, S.J. An Introduction to Analytical Atomic Spectroscopy; John Wiley & Sons; New York, **1998**.

5. Boumans, P.W.J.M. Inductively Coupled Plasma Emission Spectroscopy Part 1, P.W.J.M. Boumans (Ed); John Wiley & Sons; New York, **1987**.

6. Winge, R.K., Fassel, V.A., Peterson, V.J., Floyd, M.A. Inductively Coupled Plasma-Atomic Emission Spectroscopy. An Atlas of Spectral Information, Elsevier, Amsterdam, **1985**.

7. Rajaković, L.V., Marković, D.D., Rajaković-Ognjanović, V.N., Antanasijević, D.Z. Review: The Approaches for Estimation of Limit of Detection for ICP-MS Trace Analysis of Arsenic. *Talanta*, In Press, Accepted Manuscript, Available online 21 August **2012.**

8. Gómez-Ariza, J.L., Sánchez-Rodas, D., Giráldez, I., Morales, E. A comparison between ICP-MS and AFS detection for arsenic speciation in environmental samples. *Talanta*, **2000**, *51 (2)*, 257-268.

9. Chatterjee, A. Determination of total cationic and total anionic arsenic species in oyster tissue using microwave-assisted extraction followed by HPLC–ICP-MS. *Talanta*, **2000**, *51 (2)*, 303-314.

10. Ronkart, S.N., Laurent, V., Carbonnelle, P., Mabon, N., Copin, A., Barthélemy, J-P. Speciation of five arsenic species (arsenite, arsenate, MMAAV, DMAAV and AsBet) in different kind of water by HPLC-ICP-MS. *Chemosphere*, **2007**, *66 (4)*, 738-745.

11. Sleikovec, Z., Falnoga, I., Goessler, W., van Elteren, J. T., Raml, R., Podgornik, H., Cernelc, P. Analytical Artefacts in the Speciation of Arsenic in Clinical Samples. *Analitical Chimica Acta*., **2008**, *607*, 83-91.

12. Hippert, F., Geissler, E., Hodeau, J.L., Lelièvre-Berna, E., Regnard, J.R. Neutron and X-ray Spectroscopy. Ed. Springer, **2006**.

13. Koningsberger, D.C., Prins, R. X-ray absorption. Wiley, New York, **1988**.

14. Brown Jr., G.E., calas, C., Waychunas, G.A., Patiau, J. X-Ray adsorption spectroscopy and its applications in Mineralogy and Geochemistry. *Reviews in Mineralogy*, **1988**, *18 (11)*, 431-512.

15. Castro, G.R. XAS – X-Ray absorption Spectroscopy. SpLine, Spanish CRG BM25 at ESRF (Grenoble, France). **2013**. (*Personal Contribution*).

16. Beauchemin, S., Hesterberg, D., Beauchemin, M. Principal Component Analysis Approach for Modeling Sulfur K-XANES Spectra of Humic Acids. *Soil Science Society of America Journal*, **2003**, *66*, 83-91.

17. Struis, R.P., Ludwig, C., Lutz, H., Scheidegger, A.M. Speciation of zinc in municipal solid waste incineration fly ash after heat treatment: an X-ray absorption spectroscopy study. *Environmental Science and Technology*, **2004**, *38 (13)*, 3760-3767.

18. Kim, C.S., Bloom, N.S., Rytuba, J.J., Brown, G.E. Jr. Mercury speciation by X-ray adsorption fine structure spectroscopy and sequential chemical extractions: A comparison of speciation methods. *Environmental Science and Technology*, **2003**, *37*, 5102-5108.

19. Zhu, Y., Jiang, F.Y., Chen, K., Kang, F., Tang, Z.K. Size-controlled synthesis of monodisperse superparamagnetic iron oxide nanoparticles. *Journal of Alloys and Compounds*, **2011**, *509*, 8549– 8553.

20. Maleki, H., Simchi, A., Imani, M., Costa, B.F.O. Size-controlled synthesis of superparamagnetic iron oxide nanoparticles and their surface coating by gold for biomedical applications. *Journal of magnetism and magnetic materials*, *In Press,* **2012**.

21. Cullity, B.D., Stock, S.R. *Elements of X-Ray Diffraction* (3rd Edition), Prentice Hall, **2001**.

22. Adolphi, N.L. et al. Characterization of magnetite nanoparticles for SQUID-relaxometry and magnetic needle biopsy. *Journal of Magnetism and Magnetic Materials*, **2009**, *321*, 1459-1464.

23. Garza, M., Hinojosa, M., Gonzalez, V. Desarrollo de nanocomposites superparamagneticos de matríz biopolimérica. *CIENCIA UANL*, **Abril-Junio 2009**, *Vol XII.*

24. Kim, K.H., Kim, M.J., Choa, Y.H., Kim, D.H., Yu, J.H. Synthesis and Magnetic properties of surface coated Magnetite superparamagnetic nanoparticles. *IEEE Transitions on Magnetics*, **2008**, *44* (11), 2940-2943.

25. Gupta, A.K., Gupta, M. Cytotoxicity suppression and cellular uptake enhancement of surface modified magnetic nanoparticles. *Biomaterials*, **2005**, *26 (13)*, 1565–1573.

26. Uzun, K., Çevik, E., Senel, M., Sözeri, H., Baykal, A., Abasiyanik, M.F., Toprak, M.S. Covalent immobilization of invertase on PAMAM dendrimer modified superparamagnetic iron oxide nanoparticles. *Journal of Nanoparticle Research*, **2010**, 12 (8), 3057-3067.

27. Xie, X., Zhang, C. Controllable Assembly of Hydrophobic Superparamagnetic iron oxide nanoparticles with mPEG-PLA Copolymer and its effect on MR transverse Relaxation Rate. *Journal of Nanomaterials*, **2011**, Article ID 152524, 7 pages.

28. Mahmoudi, M., Simchi, A., Milani, A.S., Stroeve, P. Cell toxicity of superparamagnetic iron oxide nanoparticles. *Journal of Colloid and Interface Science*, **2009**, *336*, 510–518.

29. Method 6200. Field Portable X-Ray Fluorescence Spectrometry for the determination of elemental concentrations in soil and sediment. http://www.epa.gov/osw/hazard/testmethods/sw846/pdfs/6200. Consulted on September 2013.

30. Uheida, A.; Salazar-Alvarez, G.; Björkman, E.;Zhang, Y; Muhammed, M. Sorption of palladium(II), rhodium(III) and platinum(IV) on Fe_3O_4 nanoparticles. *J. Colloid Interface Sci.*, **2006**, *301*, 402-408.

31. Uheida, A., Salazar-Alvarez, G., Björkman, E., Zhang, Y., Muhammed, M. Fe_3O_4 and γ-Fe_2O_3 nanoparticles for the adsorption of Co^{2+} from aqueous solution. *Journal of Colloid Interface Science*, **2006**, *298*, 501-507.

32. Rainer, N.B. *Product for the adsorption of metal ions,* US PATENT 5,002,984, **1991**.

33. Rainer, N.B. *Polymer product for the selective absorption of dissolved ions,* US PATENT 5,096,946, **1992**.

34. Muñoz, J.A., Gonzalo, A., Valiente, M. Arsenic adsorption by Fe(III)-loaded Open-Celled Cellulose Sponge. Thermodynamic and Selective Aspects. *Environmental Science and Technology,* **2002**, *36*, 3405-3411.

35. Bhardwaj, N., Kundu, S.C. Electrospinning: A fascinating fiber fabrication technique. *Biotechnology Advances*, **2010**, *28*, 325–347.

36. Teo, W.E., Ramakrishna, S. A review on electrospinning design and nanofibre assemblies. *Nanotechnology*, **2006**, *17*, 89–106.

37. Ramakrishna, S., Fujiharac, K., Teo, W.E., Yong, T., Ma, Z., Ramaseshana, R. Electrospun nanofibers: solving global issues. *Materials Today*, **2006**, *9 (3)*, 40-50.

38. Ramakrishna, S. An introduction to Electrospinning and Nanofibres. *World Scientific Publishing Co. Pte. Ltd. 381*, **2005**.

39. Yean, S., Cong, L., Yavuz, C.T., Mayo, J.T. Yu, W.W., Kan, A.T., Colvin, V.L., Tomson, M.B. Effect of magnetite particles size on adsorption and desorption of arsenite and arsenate. *Journal of Materials Research*, **2005**, *20 (12)*, 3255-3264.

40. Esbri, J.M., Bernaus, A., Avila, M., Kocman, D., García, E.M., Guerrero, B., Gaona, X., Álvarez, R., Perez, G., Valiente, M., Higueras, P., Horvat, M., Loredo, J. XANES speciation of mercury in three mining districts – Almadén, Asturias (Spain), Idria (Slovenia). *Journal of Synchrotron Radiation*, **2010**, *17(2)*, 179-186.

41. Avila, M., Perez, G., Esshaimi, M., Mandi, L., Ouazzani, N., Brianso, J.L., Valiente, M. Heavy metal contamination and mobility at the mine area of Draa Lasfar (Morocco). *The Open Environmental Pollution & Toxicology Journal*, **2012**, *3(1-M2)*, 2-12.

3

Results and Discussion

3. RESULTS AND DISCUSSION

The current chapter describes the results obtained from the studies carried out in the present thesis including the characterization of all adsorbent system materials (non-supported nanostructured systems: SPION in suspension or functionalized SPION as well as new supported nanostructured systems: SPION loaded Forager® Sponge or CA and PAN nanofibers). Such characterization is complemented with adsorption studies when applying the developed systems to treat polluted solutions containing both arsenite and arsenate.

Accordingly, results are presented in two main sections for each target system: Characterization and adsorption studies. Chart below indicates the full content scheme.

Non-supported Nanostructured Systems

The current section describes the results obtained for the adsorption studies with non-supported nanoparticles, both SPION and functionalized SPION in suspension, including complete characterization of the adsorbent system. Such characterization is complemented with the optimization of adsorption parameters and the determination of selectivity towards inorganic arsenic species that is basic for applications to polluted waters containing both arsenite and arsenate.

3.1. Ligand-Exchange Mechanism for Arsenic Species adsorption

The mechanism here described is basic to explain the obtained results on the studied arsenic adsorption processes.

As(V) and As(III) are bound to iron (hydr)oxides by an inner-sphere ligand-exchange mechanism, in which the arsenic oxyanion competes with and exchanges with surface ≡Fe-OH or ≡Fe-OH$_2^+$ groups at the iron (hydr)oxide surface. An inner sphere complex is one in which the adsorbed ligand coordinates directly with the surface structural cation. [1,2]

Extended X-ray absorption fine structure (EXAFS)[3,4,5] and FTIR spectroscopy[6] have shown As(V) and As(III) to form monodentate[3] and bidentate[4,5,6] inner sphere surface complexes with iron (hydr)oxide sites in co-precipitated and adsorbent solids. A bidentate ligand-exchange mechanism based on the Fe:As stoichiometry 2:1 can be proposed for the adsorption of arsenic species on the SPION, as it has been considered for other iron oxide-based materials. [7,8,9] The corresponding reactions can be written as follows:

$$\equiv Fe - OH + AsO_4^{3-} + xH^+ \rightarrow\ \equiv FeH_{x-1}AsO_4^{x-3} + H_2O \qquad (3.1)$$

$$\equiv Fe - OH + AsO_3^{3-} + xH^+ \rightarrow\ \equiv FeH_{x-1}AsO_3^{x-3} + H_2O \qquad (3.2)$$
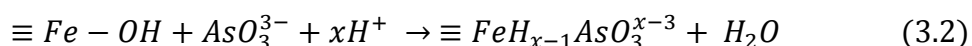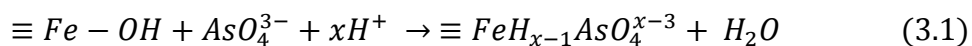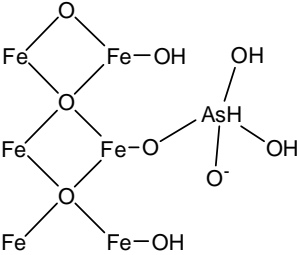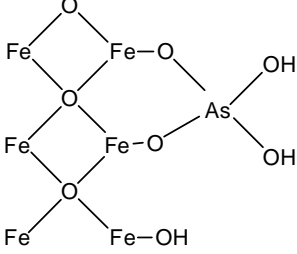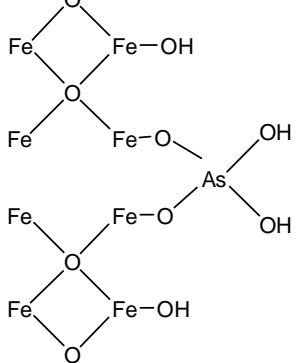
with an equilibrium constant

$$K = \frac{\overline{[As]}}{\overline{[Fe]}[H^+]^x[As]} \qquad (3.3)$$

where $\overline{[As]}$ indicates the amount of arsenic species adsorbed on the SPION (mmol/g), $\overline{[Fe]}$ indicates the amount of iron in the SPION and not complexed with As (mmol/g), $[H^+]$ indicates the concentration of free protons in solution (mmol/g), and [As] indicates the free concentrations of either the corresponding AsO_3^{3-} or AsO_4^{3-} ions in solution (mmol/g) which have been calculated from the experimental values of total arsenic concentration and pH of the solution.[10]

In the case of As(V), the possible chemical structures which arsenate may form on the iron oxide surface upon chemical adsorption are different as present the Table 3.1. [11]

Table 3.1. Schematic representation of different chemical complexes that arsenate may form on the iron oxide surface.

Type of Complex	Chemical Structure
Monodentate	
Bidentate mononuclear	
Bidentate binuclear	

The conclusions in the literature are, however, contradictory regarding the formation of monodentate complexes. In recent publication,[12] based on EXAFS and FTIR measurements, it was concluded that the only complex formed on the goethite surface was

the *monodentate species*. On the other hand, in other studies it has been concluded that the formation of monodentate species only occurred at low surface coverage, whereas *bidentate binuclear complexes* formed at higher surface coverage.[3,5,13] Moreover, in another study it was concluded that the peak assigned to monodentate complex was instead due to the formation of a *bidentate mononuclear complex*.[13] In yet another publication,[3] the conclusion was that the formation of monodentate and bidentate mononuclear complexes was not very likely since they are thermodynamically unstable and that the peak previously assigned to a bidentate mononuclear complex should be assigned to the As-O-O-As structure.[14]

Despite the many studies aiming at elucidating the structure of arsenate complexes adsorbed on iron oxide, the reported results are contradictory and there is still no consensus regarding the structure of the complex being bidentate binuclear complexes, as shows the Equation 3.4, which have traditionally been reported as the most thermodynamically stable complex formed and thus the most probable.[15]

The formation of the bidentate binuclear complex has also been studied by Fourier Transform Infrared Spectroscopy (FTIR) on dry samples and it was demonstrated that the arsenic complexes were formed via the hydroxyl groups at the iron oxide surface.[16,17] This is a very tight bond, and once the bond is formed, removal of the arsenic is difficult.

$$+ \quad H_2AsO_4^- \quad \longrightarrow \quad + \quad H_2O \qquad (3.4)$$
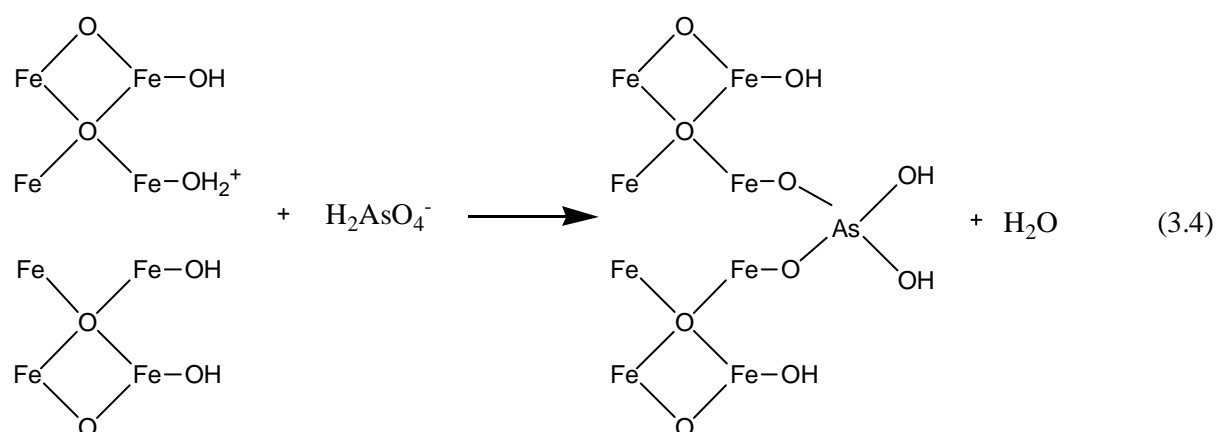
In the case of As(III) adsorption by iron (hydr)oxides, both bidentate binuclear-bridging complexes and monodentate complexes have been observed. A monodentate complex is one in which a single oxygen atom from the arsenite oxyanion coordinates a single structural Fe^{3+} at the iron (hydr)oxide surface, as shown below the Equation 3.5.[18]

$$+ \quad H_2AsO_3 \quad \longrightarrow \qquad\qquad\qquad\qquad\qquad + \quad H_2O \qquad (3.5)$$
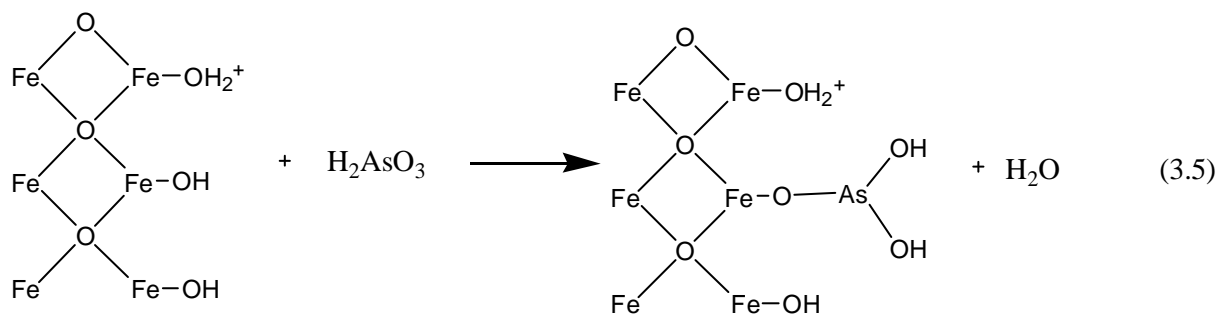
3.1.1. Influence of pH on adsorption process

The adsorption of As(III) and As(V) by Fe oxides is influenced by pH. The adsorption of As(V) by most iron (hydr)oxides (including goethite, lepidocrocite ferrihydrite and magnetite), is maximum at low pH. However, the adsorption of As(III) is usually higher at high pH. In most cases the maximum adsorption of As(III) occurs between pH 8 and pH 10. [19]

When Equation 3.1 and Equation 3.2 are expressed as a function of the adsorbed species, the stability of the complexes can be accurately evaluated:

$$\equiv Fe - OH + H_2AsO_4^- \rightarrow\, \equiv FeHAsO_4^- + H_2O \quad \log K = 2.5 \pm 0.3 \qquad (3.6)$$

$$\equiv Fe - OH + H_3AsO_3 \rightarrow\, \equiv FeH_2AsO_2 + H_2O \quad \log K = 0.53 \pm 0.07 \qquad (3.7)$$
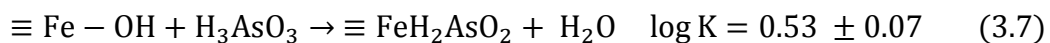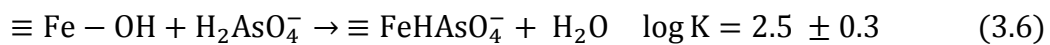
The adsorption of arsenate on iron oxides involves interactions between the adsorbate and the hydroxyl group of the iron oxide. The surface chemistry of the iron oxides has a pH-dependent charge. At low pH, the hydroxyl groups at the surface of the iron oxide are doubly protonated ($\equiv FeOH_2^+$) and the surface charge of the iron oxide is thus positive. At a certain pH, the hydroxyl group is protonated with only one proton ($\equiv FeOH$) and thus the (net) surface charge of the iron oxide is neutral. This pH is called the point of zero charge (PZC) and for iron oxides the point of zero charge (PZC) ranges between 5.5 and 9 8 (in case of SPION pzc is 6.8). At pH values above the PZC, the hydroxyl group is deprotonated ($\equiv FeO^-$), and consequently the iron oxide surface bears a negative charge. Then As(III) and As(V) can be adsorbed to both positively and negatively charged surfaces. That is, the negatively charged As(V) species can be adsorbed to the negatively charged Fe oxide surface. This behavior is a characteristic of many inner-sphere adsorption complexes.[20]

3.2. Non-supported Superparamagnetic Iron Oxide Nanoparticles

Appropriate information obtained concerning characterization parameters and its physical-chemical properties will lead to best understanding the behavior of the target adsorbent material (SPION). On the other hand, the results focused in the optimization of the adsorption parameter are outlined in the following sections.

3.2.1. SPION Characterization

The main characterization processes for SPION are outlined in this section. Thus, the present results include particle morphology and size by Transmission Electron Microscopy (TEM) as well as a size distribution histogram, qualitative identification of the SPION by X-Ray Diffraction (XRD) and magnetic susceptibility measurements were carried out on a superconducting quantum interference device (SQUID) at room temperature. Corresponding results are described and discussed below.

3.2.1.1. Transmission Electron Microscopy (TEM)

The characterization of nanoparticles morphology, mainly its size that determines their adsorption capacity, requires from TEM measurements. A review of the actual existing literature highlights an optimal particle size range between 8-10 nm for adsorption applications.[21,22,23] From the TEM micrographs (Figure 3.1) a main spherical nanoparticles morphology can be observed, being partially aggregated when SPION are in suspension.
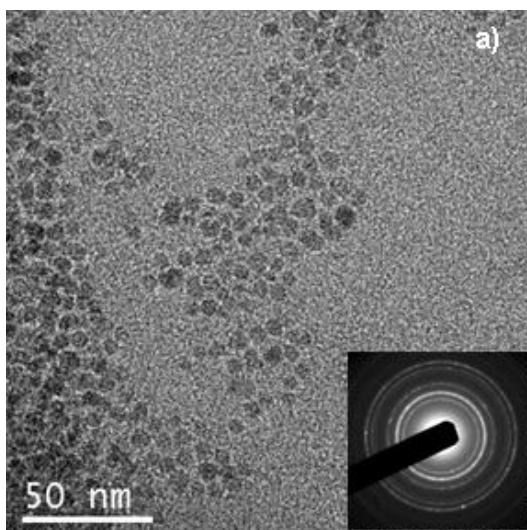
Figure 3.1. TEM micrograph of synthesized SPION with its diffractogram (a) and TEM micrograph at high resolution (b).

The main nanoparticle size obtained by using the described synthesis method has an average size of 10.2 nm (see the histogram given in Figure 3.2). Such particle size agrees with reported values on the literature and it is the optimal particle size for adsorption application.[21,23] These results were reproduced in the successive preparations of SPION by the indicated synthesis.
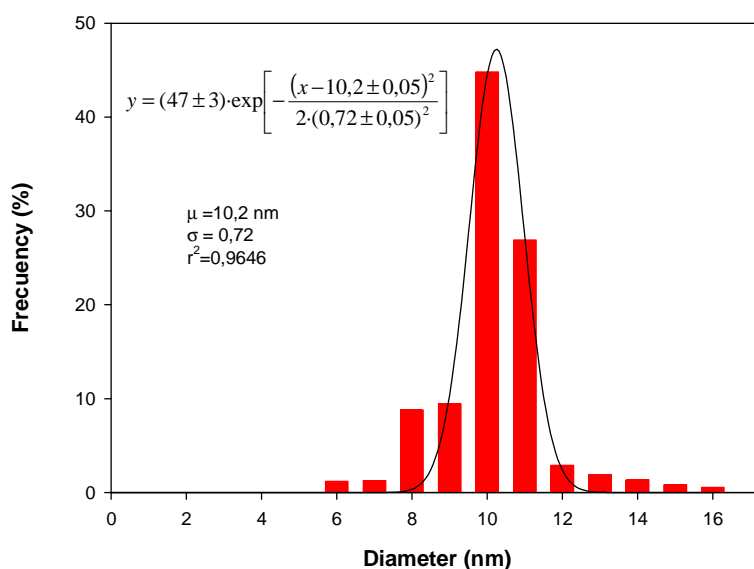
Figure 3.2. Histogram of distribution SPION size.

3.2.1.2. X-Ray Diffraction (XRD)

Additional information regarding SPION crystalline structure is obtained when analyzing by X-Ray diffraction. The SPION diffractogram given in Figure 3.3 indicates the presence of a single phase corresponding to SPION (Fe_3O_4) as compared to a Fe_3O_4 standard found in the database.[24]
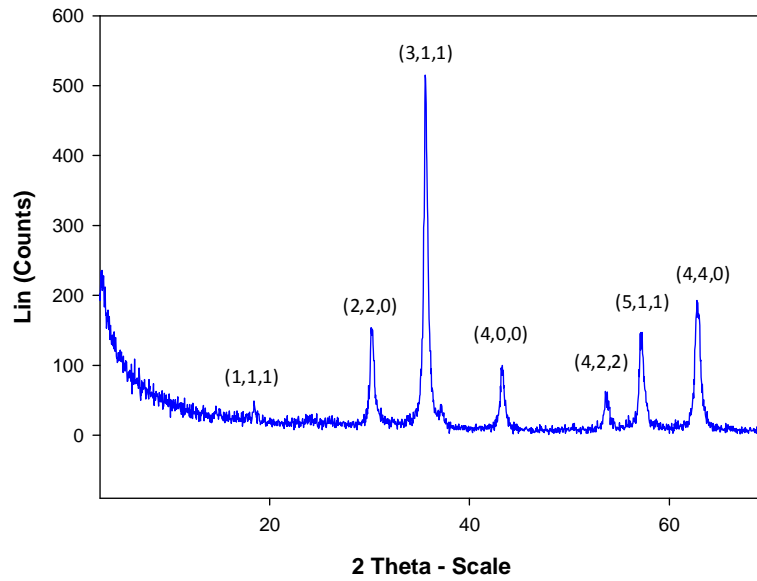
Figure 3.3. X-Ray diffraction spectra which shows the characteristic picks of the SPION and its crystallographic planes.

3.2.1.3. Superconducting Quantum Interference Device (SQUID)

SPION magnetic properties were visually confirmed by direct retention when using low-field magnet, as shown in Figure 3.4 where the SPION was highly pulled by the magnet.

Figure 3.4. SPION suspension in TMAOH (a) and SPION separation from the solution under an external magnetic field (b).

Superparamagnetic materials have no permanent magnetic moment and, hence, no hysteresis loop. To test the magnetic susceptibility, the temperature was held constant at

113

300 K for hysteresis measurements at the applied field ±7 T, see
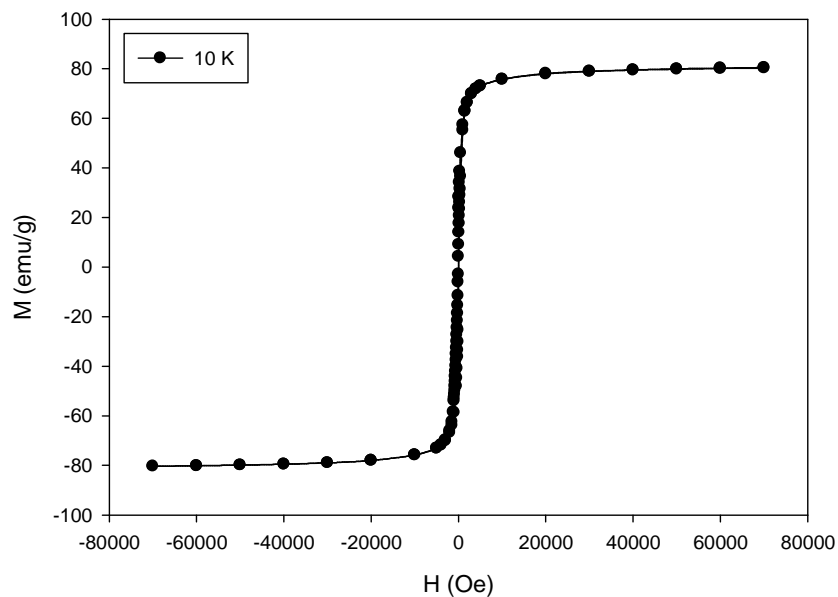
Figure 3.5. The evaluation of the magnetic hysteresis represents the corresponding magnetization as a function of magnetic field applied to SPION powder. The shape of the hysteresis curve for the sample was normal and tight with no hysteresis losses, typical behavior of a superparamagnet. Under low applied field, a high magnetization (M) value was observed. The saturation magnetization (M_s) and the coercivity (H_c) of the SPION are about 80 emu/g and 143 Oe respectively, values close to bulk Fe_3O_4 (85-100 emu/g and 115-150 Oe, correspondingly).[25,26] Accordingly to the observed remaining magnetic capacity, together with the high specific surface areas and strong magnetic properties, SPION appears as an excellent adsorbent candidate for environmental applications.[27]
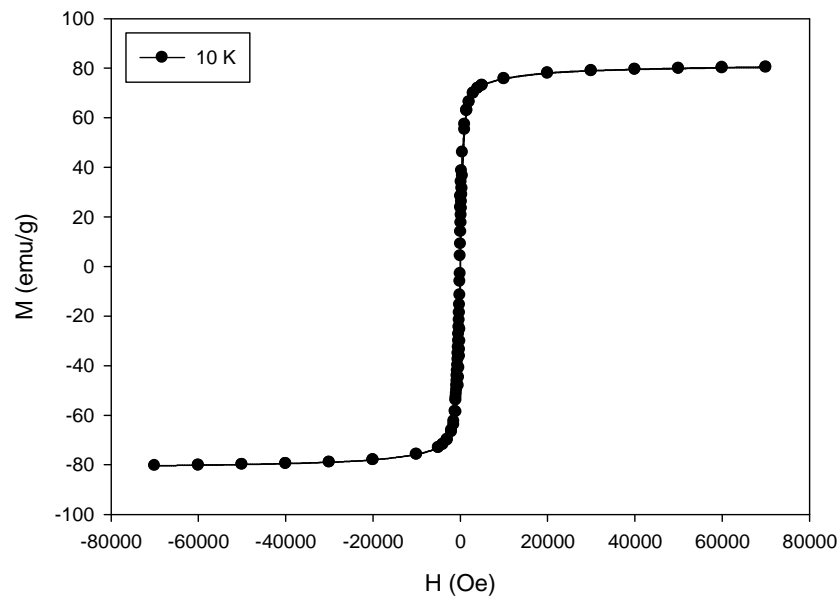
Figure 3.5. Magnetic hysteresis loop of the SPION.

3.2.2. Characterization of Arsenite and Arsenate adsorption on SPION

Results on the adsorption of aqueous As(III) and As(V) on SPION will be presented in this section. An appropriate characterization of the adsorbent material includes the determination of adsorption kinetics for both As(V), As(III) and their mixture solutions, as well as the effect of the pH in the adsorption process by determining the adsorption capacity. In addition, evaluation of selectivity includes both interfering metal ions and anions, using arsenite and arsenate mixtures to mimic real situations.

3.2.2.1. Effect of the contact time in the adsorption process

Adsorption kinetics for arsenite, arsenate and corresponding mixtures will be described along this section.

In the case of arsenate, the variation of its adsorption with time, independently of pH effect, is relatively fast, as seen in Figure 3.6a, where longer contact time provide no significant variations in the adsorption capacity of the SPION. The results of the interaction between the arsenate solutions and the SPION suspension at different pHs show that arsenate adsorption is highly pH dependent. The increase of deprotonated arsenic species by increasing the pH in the range of 2.8 to 3.8 is the reason of the observed increase on the adsorption capacity in this range of pH. At higher pH values, the competition of OH$^-$ ions

against arsenate to complex Fe(III) lead to a decrease of the arsenate adsorption . For this reason, pH effect must be studied in more detail.

On the other hand, in the case of Arsenite, the dynamics of the adsorption process is observed to be relatively fast in a similar way of arsenate. However, in this case, the adsorption is independent of pH (see Figure 3.6b) what corresponds to the less acidic properties of arsenious vs Arsenic acid and, consequently, to a decrease of deprotonated arsenite species within the studied range. This leads to the observed almost constant arsenite adsorption capacity with pH.
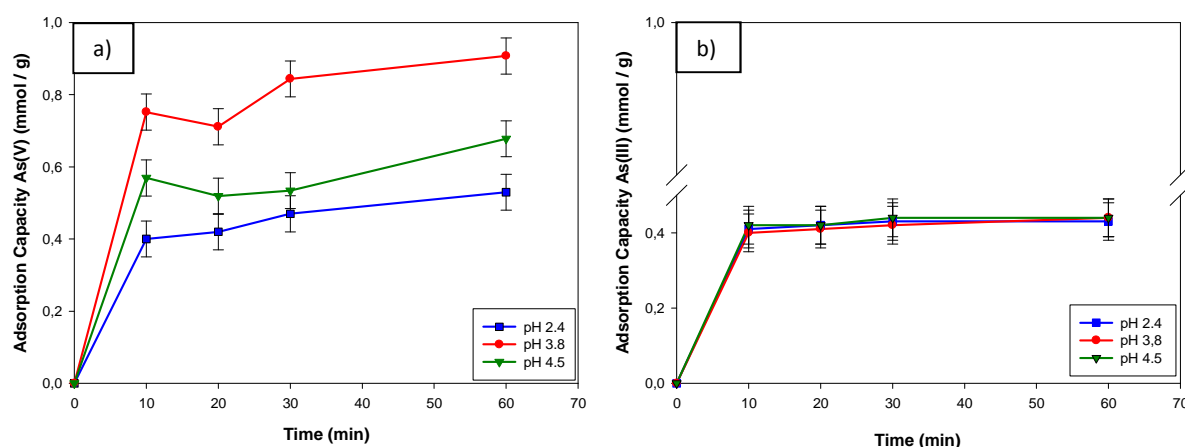
Figure 3.6. SPION kinetic adsorption capacity at different pH: As(V) (a), As(III) (b)

When using monocomponent solutions, the maximum adsorption capacity values obtained at stationary state, were found to be 0.91 mmol As(V) / g SPION and 0.43 mmol As(III) / g SPION, respectively. These values were obtained around pH 3.8.

To characterize the adsorption processes in presence of both arsenic species, separate experiments using mixtures of both species were performed. The results given in Figure 3.7 reveal a competition between both species. This competition explains the adsorption values closer to As(V) behavior (expected from its better interaction with SPION). The observed decrease in the adsorption is due to the less concentration of As(V) in the target solutions.
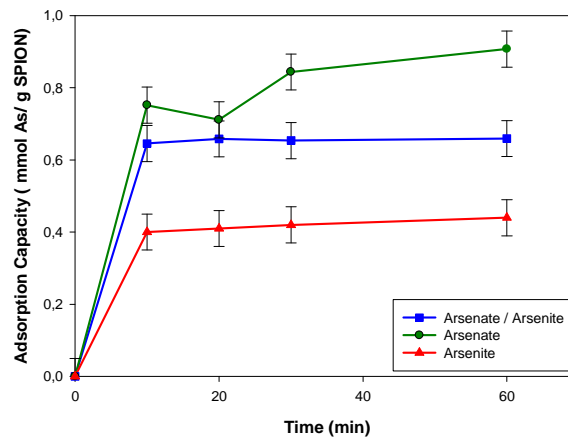
Figure 3.7. SPION kinetic adsorption for As(III)/As(V) mixtures at pH 3.8.

The achieved adsorption capacity at the stationary state was 0.66 mmol As / g SPION revealing the lower concentration of As(V) in the target mixture solution against the monocomponent As(V) solution.

3.2.2.2. pH effect in the adsorption process

Taking into account the adsorption mechanism explained above in *Section 3.1* and in order to have a most clear observation of acid-base properties of Arsenic systems, the pH distribution diagrams for both arsenite and arsenate forms are shown in Figure 3.8 and Figure 3.9.[28]

Figure 3.8. Distribution diagram of the different species of As(III) as a function of pH.

Figure 3.9. Distribution diagram of the different species of As(V) as a function of pH.

Arsenite and arsenate SPION adsorption capacity varies according to the experimental pH (range 2.0 - 8.0), as illustrated in Figure 3.10. Arsenate adsorption is strongly influenced by the pH, especially at low pH values where the acidity of arsenate species (pK_{a1} = 2.2) produce deprotonated species, is responsible of the observed relatively high adsorption capacity in the pH range 2.0-3.8. With the increase of pH above the indicated range, competition between OH^- and As(III) ions for Fe(III) centers increases and it leads to that the observed decrease on the adsorption of arsenate.

For arsenite, the situation is completely different. Less acidity of arsenite species ($pKa1$ = 9.2) as well as the reduced presence of deprotonated arsenite species in the pH range of study produces a non-significant pH effect.[29]
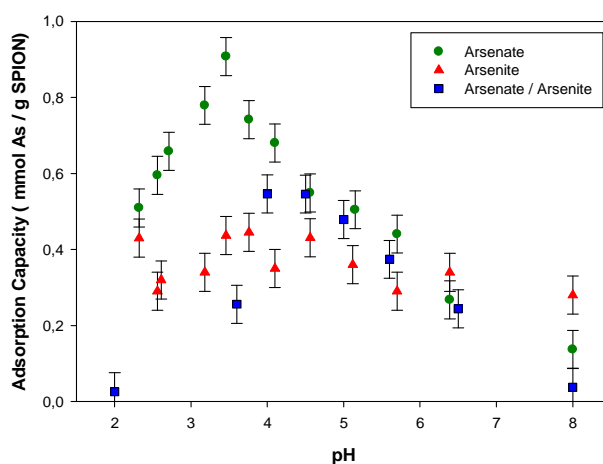
Figure 3.10. pH effect for As(V) and As(III) adsorption on SPION suspensions.

When analyzing As(III)/As(V) mixtures, the shape of the figure presents competitiveness between both arsenite and arsenate. This competitiveness shows certain pH dependency due to the arsenate adsorption. Arsenate is more acid than arsenite (there is a unique specie at the studied pH range, H_3AsO_4) thus adsorption capacity of mixtures changes in the same way than arsenate solutions. These results suggest that, taking into account the related results for the individual species, arsenite is also adsorbed but in much less proportion than arsenate. Then, a decrease in the total arsenic adsorption is generated respect the adsorption capacity reached with only arsenate present.

3.2.2.3. Maximum SPION adsorption capacity

These experiments are planned to assess the effect of the initial arsenite or arsenate concentration on the sorption process and estimate the maximum SPION adsorption capacity for both species, verifying if further optimization of maximum adsorption capacity can be achieved. Initial arsenic concentration in the range of 1.3×10^{-5} mol/L (1ppm) and 1.3×10^{-2} mol/L (1000ppm) were tested. The relationship between the equilibrium aqueous concentration and the equilibrium adsorption capacity for arsenite and arsenate, shown in Figure 3.11, fits Langmuir adsorption model, as follows (Equation 3.8):

$$q_e = \frac{q_{max} k_L C_e}{1 + k_L C_e}$$

(3.8)

that can be written as (Equation 3.9):

$$\frac{C_e}{q_e} = \frac{1}{q_{max} k_L} + \frac{C_e}{q_{max}}$$

(3.9)

where q_e is th equilibrium adsorption capacity (mmol/g), C_e is the equilibrium metal concentration in the aqueous phase (mmol/ L), q_{max} is the maximum loading capacity (mmol/g) corresponding to a monolayer coverage, and k_L is Langmuir constant (L/mol).
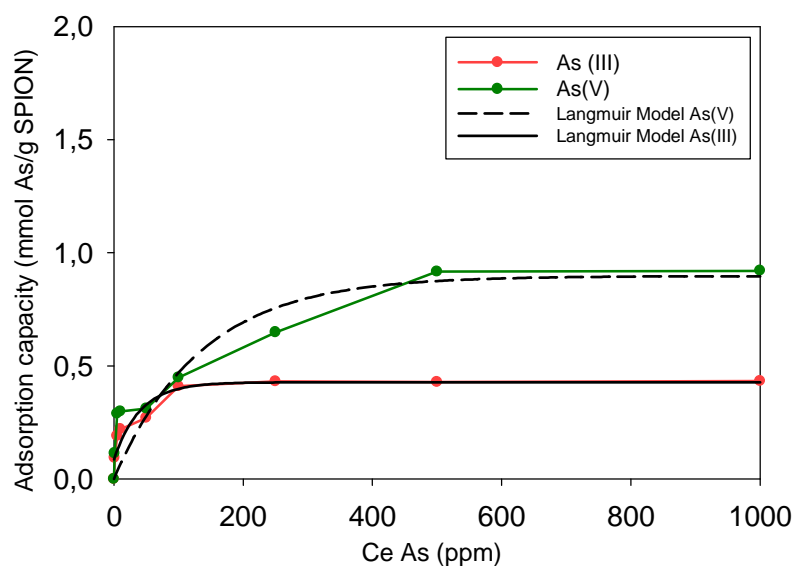
Figure 3.11. Effect of initial As(V) and As(III) concentration.

For both arsenite and arsenate, the adsorption capacity increases with the initial concentration due to the saturation effect. For Arsenate, optimal adsorbent working conditions are reached at pH 3.6, providing a saturation of arsenate adsorption capacity near 0.91mmol As(V)/g SPION. The minimum arsenate concentration needed for the saturation is 500 ppm, representing the extreme working conditions, in terms of concentration, that can face the adsorbent. The SPION works similarly in the case of arsenite but reaching a maximum adsorption capacity of 0.43 mmol As(III)/g SPION being 100 ppm of arsenite needed to saturate the system. The experimental model fits Langmuir model as indicated in the figure. Langmuir constant values are determined as shown in Figure 3.12, being 8.52 L/mol and 1.57 L/mol for arsenite and arsenate, respectively.
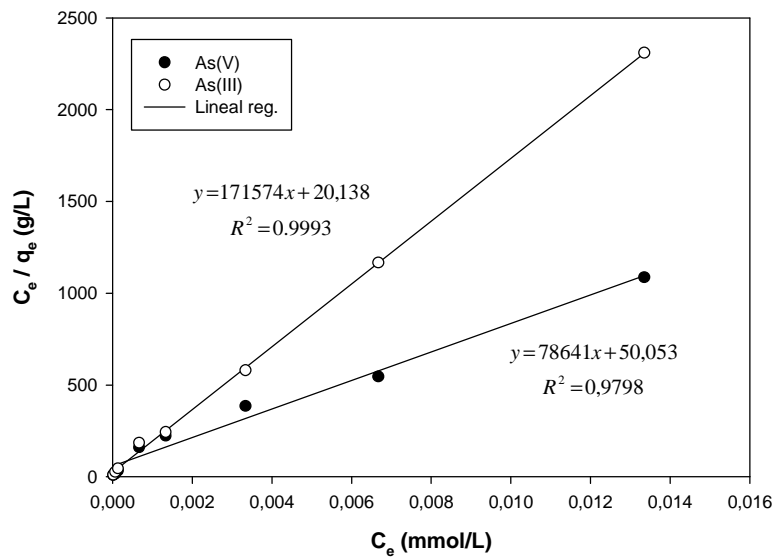
Figure 3.12. Fitting experimental data for the Langmuir model.

Then, the study of the maximum adsorption capacity in the As(III)/As(V) mixtures shows in Figure 3.13 that the saturation in the adsorption capacity for As(III)/As(V) mixtures is reached when the maximum adsorption capacity is about 0.86 mmol As/g SPION. This fact, as it was explained above, reveals the preference for As(V) since the obtained value is very similar to that obtained for As(V) monocomponent. At the same time that both arsenite and arsenate concentration increase, the media provides more probabilities to interact with arsenate and react by ligand exchange to the system. In this way, increasing the concentration of both species, As(V) has better interaction with SPION and increase its adsorption while the adsorption of As(III) decrease providing a low competitiveness between both species with the Fe(III) centers the SPION.

Comparing the independent maximum adsorption capacities for arsenite (0.43 mmol/g) and arsenate (0.92 mmol/g) with the mixture of inorganic arsenic species (0.86 mmol/g), the arsenate must be most adsorbed due to its acidity and the proportion of deprotonated species presents in the media at the pH of study which provides major contribution in the adsorption capacity. This fact could confirm that the maximum adsorption capacity with the mixture of species is similar to the maximum adsorption capacity for arsenate.
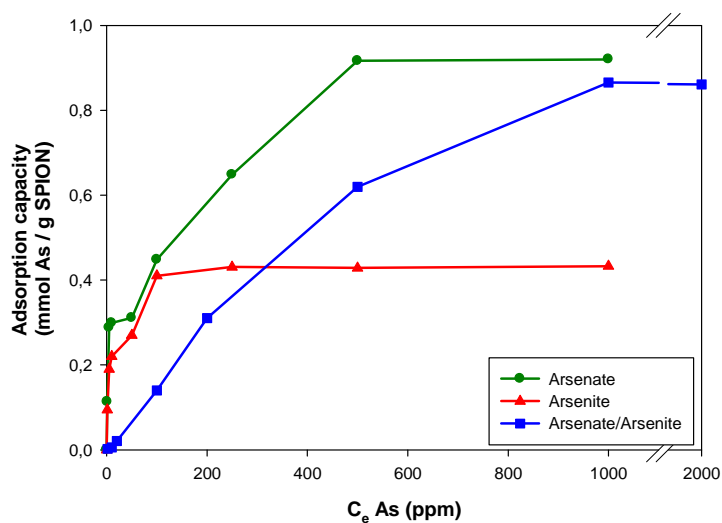
Figure 3.13. Effect of initial As concentration on its adsorption.

After considering the achieved results, bearing in mind the observed nanoparticles aggregation throughout the characterization studies, there is a need to improve this adsorbent system. Thus, new systems based in SPION and minimizing the indicated aggregation are needed. In addition, to assure that SPION can be a potential adsorbent for polluted solutions (either industrial or from nature), it is necessary to understand the selectivity of the adsorbent system. Then, As(III)/As(V) mixtures were used during selectivity studies against metal ions or anionic interferes.

3.2.3. Selectivity

The evaluation of SPION selectivity was carried out using mixtures of As(III)/As(V), in the presence of other metal ions such as Cu(II), Ni(II) or Zn (II) (using 1:1 and 1:2 molar ratios) as well as in presence of other interfering anions such as chloride, nitrate, sulphate and phosphate (using 1:200 molar ratios). Such experiments let us the better understanding of the behavior of our adsorbent system in possible application to treat polluted waters.

3.2.3.1. Metal Ions interference on SPION arsenic adsorption

In order to examine the separation capacity of arsenic from a mixture containing metals, the selective sorption of As(III)/As(V) mixtures from a solution containing a mixture of Cu(II), Zn(II), and Ni(II) (typical metals in hydrometallurgy industrial waters) was studied.

The results obtained are graphically displayed in Figure 3.14, indicating that SPION can be used to extract arsenic selectively from aqueous solutions under the employed experimental conditions.
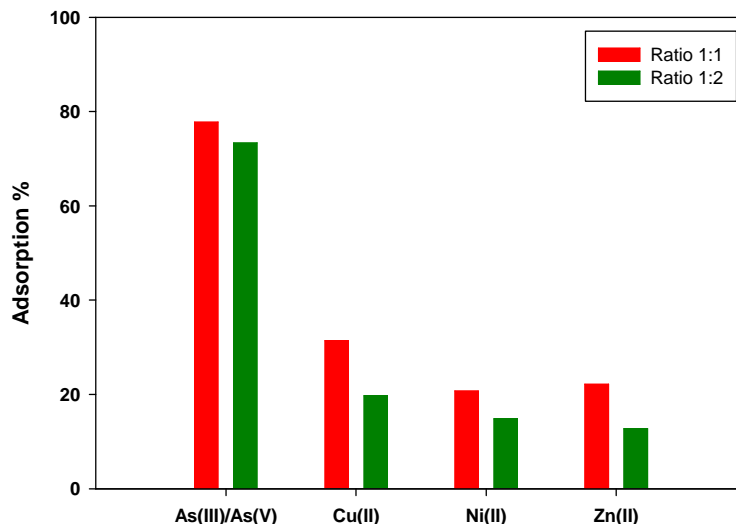
Figure 3.14. Selective adsorption of arsenic from a mixture of base metals.

SPION selectivity and specificity against metal ions were studied. Up to twofold arsenic adsorption percentages (molar ratio is 1:1) are obtained when comparing to those achieved for the other metal ions such as Cu^{2+}, see Table 3.2. Such differences reach up to 4 times when using a higher molar ratio, 1:2, for all interfering metal ions. It is noteworthy to reflect that, at the pH of study (3.6) the hydroxyl groups at the surface of the SPION are doubly protonated ($\equiv FeOH_2^+$) and the surface charge is thus positive. This fact favors the interaction with arsenic species due to the anionic forms that both arsenate and arsenite can produce.

By other side, increasing the molar concentration of Cu^{2+}, Ni^{2+} and Zn^{2+} entails a constant arsenic adsorption percentage while for the other metal ions it is observed a decrease. Then, the active centers for the adsorption process continue playing their interaction by ligand exchange mechanism with arsenic. For the other metal ions, the adsorbed amount is practically the same than with molar ratio 1:1 but the percentage of adsorption decreases due to the increase of the total concentration present in the media for each metal ion. These values confirm the high selectivity of SPION for arsenic.

Table 3.2. Selective adsorption of arsenic mixture against some metals.

Metal Ions	Sorption (%)	
	Molar ratio 1:1	Molar ratio 1:2
As(V)/As(III)	77.8	73.4
Cu(II)	31.4	19.8
Ni(II)	20.8	14.9
Zn(II)	22.2	12.7

3.2.3.2. Anions interference on SPION selectivity

Anions commonly present in wastewaters such as chloride, nitrate, sulphate or phosphate, potentially interfere the arsenic adsorption, being such interference very significant leading to a reduction of the arsenic adsorption capacity. The general trend previously observed for arsenic adsorption is varying the adsorption capacity with the pH, being similar when different anions are present. While an increase of the adsorption capacity is observed when the pH increases until 4.5 or 5.0, a continuous decrease until pH 11.0 is detected as shown in Figure 3.15.

When anions are present in the arsenic solution, the adsorption of arsenic on SPION has remarkable decrease. The adsorption capacity at low and high studied pHs increases due to the presence of interfering anions favor the anionic environment on the anion exchange centers leading to an easier anion exchange process. At the maximum adsorption pH, the presence of different anions in high quantity, especially phosphate, produce an efficient competition with arsenic in the ligand exchange centers of the SPION. This fact is consequence of the similar affinity for phosphate and arsenate. For the other anions, spite the competition with Arsenate is less intensive, the maximum of adsorption disappear in all cases and a plateau is reached by decreasing the adsorption capacity by three fold.
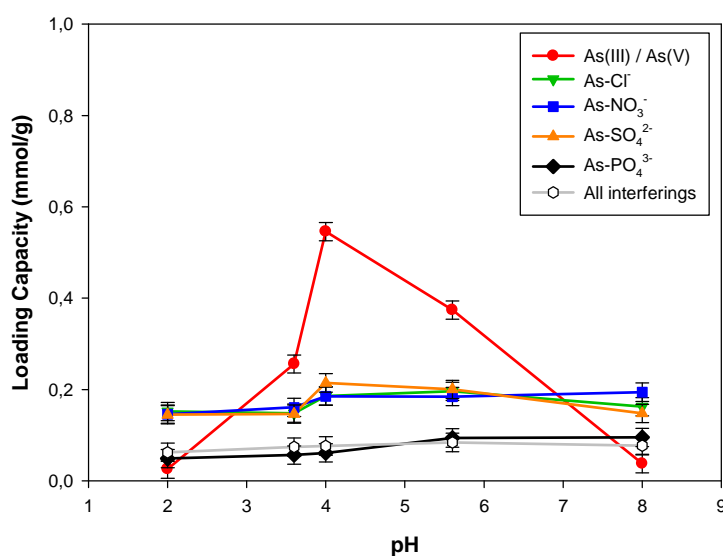
Figure 3.15. Effect of the presence of interfering anions on the arsenic adsorption on SPION in a pH range of 2.0 to 8.0.

The decrease of adsorption capacity is used to quantify the interfering effect of the different anions at pH 4.0 (conditions for the higher adsorption capacity values).[30] The obtained values are given in **Table 3.3**.

Table 3.3. Interfering effect of different anions on arsenic adsorption capacity at pH 4.0 with a molar ratio 1:200 of Arsenic vs anions.

Sample	Adsorption Capacity (mmol/g)	Decrease of Adsorption Capacity (%)
Without Interference	0.55	-
Chloride	0.19	65.9
Nitrate	0.19	66.1
Sulphate	0.22	60.5
Phosphate	0.06	88.8
All interfering anions	0.08	85.9

The observed interference level decreases as follows, phosphate >> sulphate ~ nitrate ~ chloride. Therefore, the results show that the adsorption capacity is similar in the presence of all interfering anions except phosphate, which presents a more pronounced interfering effect. The high interference effect shown by phosphate in all pH range is due to both the effective competition for Fe(III) centers of the SPION, according to the similar affinity of phosphate and arsenate for Fe(III) and the higher concentration of phosphate versus arsenate.[31]

The adsorption capacity in presence of interfering anions is less reduced when sulphate is present as interfering anions than when phosphate is the interfering due to the ligand exchange process in the system presents higher affinity when the anion has higher ionic charge.

The adsorption process increase when nitrate and chloride are present as interfering anions due to these anions have less interference in the ligand exchange process.

Finally, the effect of the phosphate in the remarkable decrease of the adsorption capacity of arsenic can be explained by the efficient competition with arsenic in the ligand exchange centers of the SPION for the complete pH range of study. This fact is consequence of the similar affinity of the phosphate and arsenate for Fe(III) centers[31] and due to the higher phosphate concentration in relation with the arsenic concentration.

When comparing the maximum adsorption capacity achieved when using SPION for arsenic adsorption against other previously employed adsorbent materials, it is clearly observed an important increase, see Table 3.4. The reason for such increase of SPION adsorption capacity lies on the size of the SPION (10 nm) which specific surface area is much higher than bulk Fe_3O_4 and it generates a high amount of accessible centers for the arsenic ions (arsenite and arsenate), making SPION more reactive.

Table 3.4. Comparison of adsorbent materials adsorption capacity.

Adsorbent Material	As(V)		As(III)		Ref.
	mmol / g SPION	mmol / g Fe	mmol / g SPION	mmol / g Fe	
SPION	0.91	1.2	0.43	0.71	
Ferrihydrite	0.25 – 0.38				**32**
Fe(III) loaded Forager® Sponge	0.49		0.24		**33**
Fe(III) loaded resin	0.45		---		**34**
Goethite	0.29		0.05		**35**

Nevertheless, the partial aggregation of SPION in suspension reduces their potential adsorption capacity, being required new adsorbent systems designs based on SPION able to avoid such aggregation. To this purpose, the next section includes the functionalization of SPION with an organic extractant that can favor the dispersion of SPION, increase the contact surface and help arsenite and arsenate adsorption through the affinity of thiol groups to the arsenic and iron species. 3-mercaptopropionic acid (3-MPA) was selected as extractant due to two main reasons: 3-MPA has not yet been used for water treatment

applications and can produce a new nanocomposite as a novel adsorbent system. In other hand, carboxylic and thiol groups can play the expected role to decrease the SPION aggregation and increase the adsorption capacity.

3.3. Functionalized non-supported SPION

In the next section, 3-mercaptoproponic acid (3-MPA) coated SPION were synthesized, characterized by different techniques and their feasibility for the removal of inorganic arsenic species from dilute aqueous solutions was demonstrated. Separation efficiency of the coated nanoparticles and the equilibrium isotherm of arsenite and arsenate adsorption were investigated too.

3.3.1. 3-MPA coated SPION Synthesis and Characterization

The synthesized 3-MPA coated SPION, following the procedure described in *Section 2.3* of Methodology, was characterized using Transmission Electron Microscopy (TEM), Thermogravimetric Analysis (TGA), Fourier Transform Infra-Red Spectrometry (FT-IR). Finally, a mechanism of the functionalization process was proposed. Such characterization techniques were employed to understand the way the organic extractant is fixed on the SPION surface, the efficiency of this functionalization and the amount of 3-MPA coating the SPION surface. Three different modifications were performed at different selected pHs by considering the PZC of the SPION: at pH 2.0, 6.8 and 11.0 and The characterization results that are outlined below are related with the developed modification at pH 2.0.

3.3.1.1. Thermogravimetric Analysis (TGA)

The amount of 3-MPA coated on the surface of SPION was determined from the percentage weight loss measured by the thermogravimetric analysis (TGA). As shown in **Figure 3.16**, the TGA curve for SPION shows an 8% weight loss over 100–350 $^{\circ}$C. This is most likely due to the loss of adsorbed water and dehydration of internal OH groups. However, for 3-MPA coated SPION, the TGA curve shows two weight loss steps. The first weight loss step over 100–180 $^{\circ}$C might be due to the loss of residual water adsorbed physically in the sample. The second weight loss over 200–800 $^{\circ}$C was due to the decomposition of 3-MPA. Based on the TGA data, the amount of 3-MPA coated on the surface of SPION is determined to be 3.7 mmol/g.
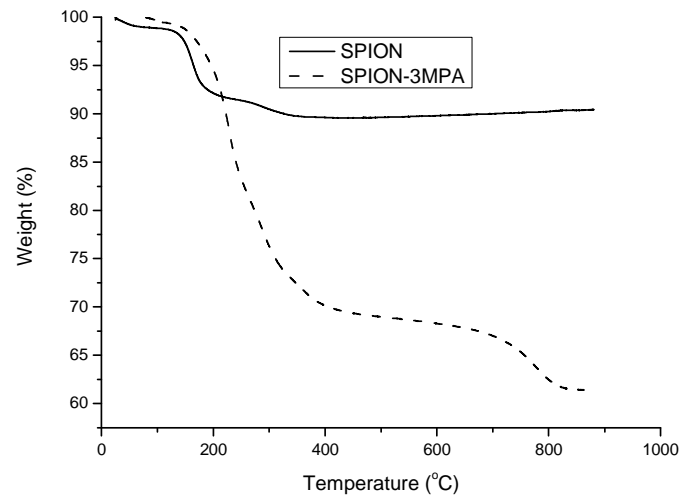
Figure 3.16. TGA curves of SPION (pristine nanoparticles) and 3-MPA-coated SPION.

3.3.1.2. Transmission Electron Microscopy – Energy Dispersive X-Ray spectroscopy (TEM-EDX)

The TEM image of 3-MPA coated SPION is shown in Figure 3.17a. Energy Dispersive X-ray (EDX) analysis (Figure 3.17b) show the main elements in the sample to be Fe, O, (JCPDS File No. 19-629) and S. The presence of sulphur in the sample, confirms the coating process.[21,22,23,26,29]

(a)   (b)
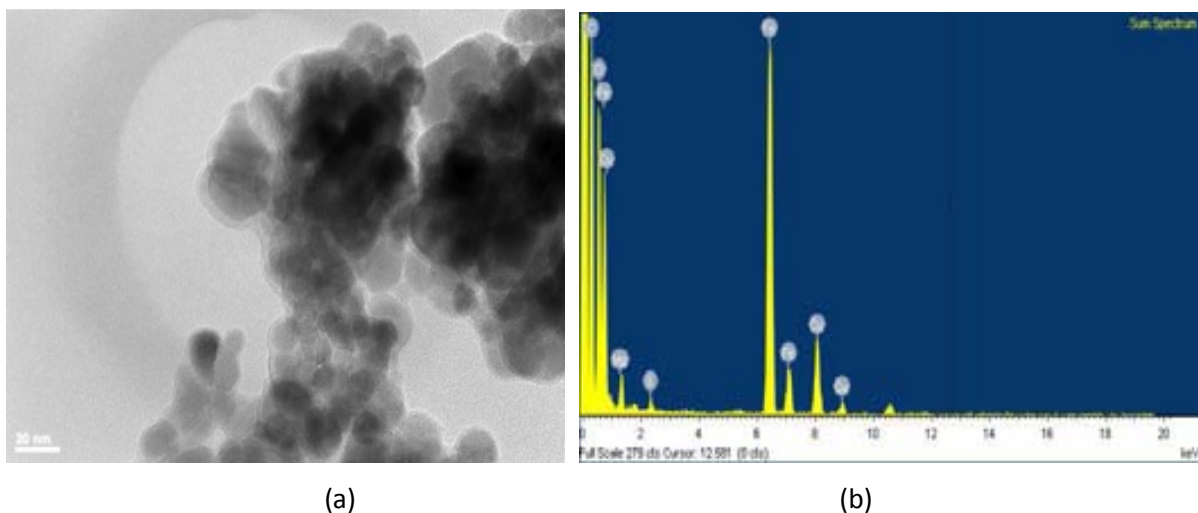
Figure 3.17. (a) TEM image of the SPION synthesized with co-precipitation method and surface coated with 3-MPA; (b) EDX analysis of the coated SPION.

3.3.1.3. Fourier Transformed – Infrared spectroscopy (FT-IR)

In order to confirm the coating of the SPION surface with 3-MPA, FT-IR spectra of SPION, 3-MPA coated SPION, and 3-MPA were obtained. As seen in Figure 3.18, new bands were observed in the spectrum of 3-MPA coated SPION. However, their frequencies are shifted to lower values than in free 3-MPA, indicating strong bonding of S. The reagent (3-MPA) has two important functional groups: thiol (-SH) and carboxylic (-COOH). The vibration of –SH group is at 2400 cm^{-1} and it was observed in all samples. The –COOH group has stretching vibration C=O at 1760-1690 cm^{-1} and the stretching vibration C-O at 1320-1210 cm^{-1}. The bending vibration O-H was not observed at 1440 and 950 cm^{-1}. A reasonable conclusion would therefore be that the reagent is bonded to the surface of SPION primarily through the carboxylic group. In addition, at low wavenumber, 700-600 cm^{-1} the stretching vibration Fe-O was observed. These findings suggest that the SPION keeps the structure and the link with the 3-MPA is produced by the carboxylic group. [36,37,38]
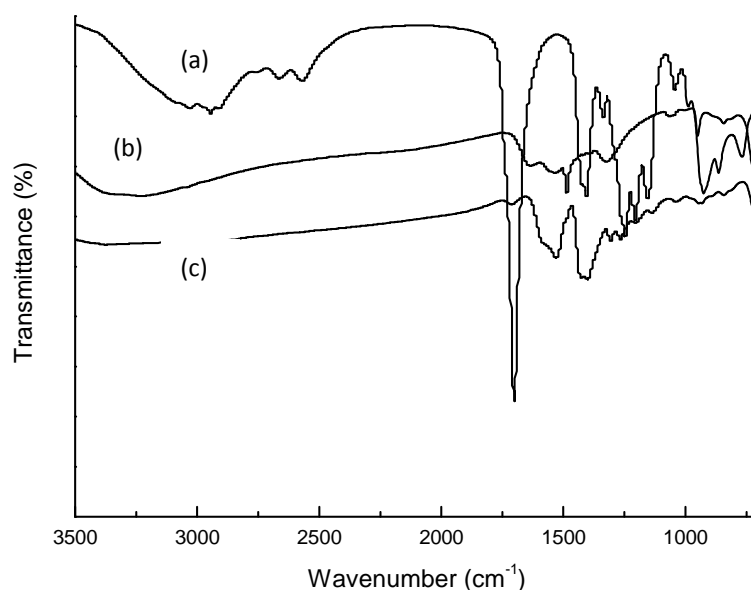
Figure 3.18. FT-IR spectra of (a) 3-MPA, (b) SPION, (c) 3-MPA-coated SPION.

3.3.1.4. Proposed mechanism for 3-MPA and SPION interaction

Taking into account the results obtained from the TGA and FT-IR analysis, a proposed mechanism for 3MPA coated SPION generation at acidic pH can be illustrated as follows:[39]

$$\equiv Fe \longrightarrow OH_2^+ \ + \ \text{[carboxylic acid with SH group]} \ \longrightarrow \ \text{[Fe-coordinated complex with SH group]} \ + \ H_3O^+ \qquad (3.10)$$
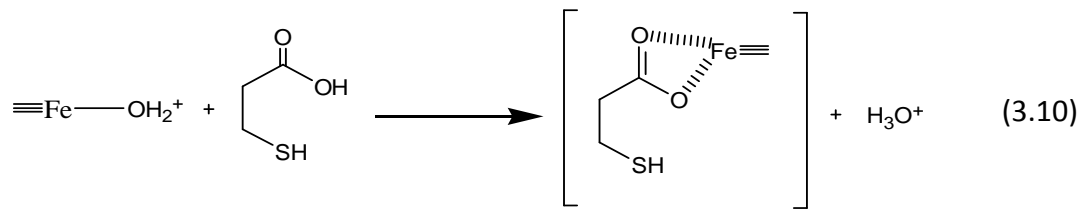
where Fe≡ represent the SPION.

The presence of a good leaving group such as OH_2^+ on the SPION surface when producing the functionalization appears as a key factor to this reaction leading to increase the extension of functionalization over the SPION surface (this fact will be corroborated with the adsorption experiments that will be outlined below). In this sense, while TGA results corroborate the high degradation of organic compounds between 200-800 °C, TEM-EDX results showed qualitatively corresponding sulphur concentrations.

3.3.2. Arsenite and arsenate adsorption parameters

This section includes a compilation of different parameters affecting the adsorption process as well as its selectivity against most common interfering ions, i.e., contact time, pH or concentration.

3.3.2.1. Effect of the contact time in the adsorption process

The coating process of 3-MPA on the SPION surface was made at two different pH values to observe the effect on the Arsenic adsorption process. The obtained results are presented in Figure 3.19 where the observed high adsorption kinetics for As(V) and As(III)on the 3-MPA coated SPION synthesized at low pH (pH 2.0) against the one synthesized at high pH (pH 11.0) corroborates that the modification process is most efficient at low pH since more active centers of 3-MPA are located for the arsenic adsorption, being this 3-MPA coated SPION selected for the adsorption experiments.

The 50% of the equilibrium sorption (t1/2) is reached in less than 10 minutes in both cases. However, to ensure equilibrium, 1 hour contact time was maintained during the extraction studies.

The preliminary adsorption capacities of arsenite and arsenate are 0.62 mmol As/g coated SPION and 0.17 mmol As/g coated SPION, respectively.
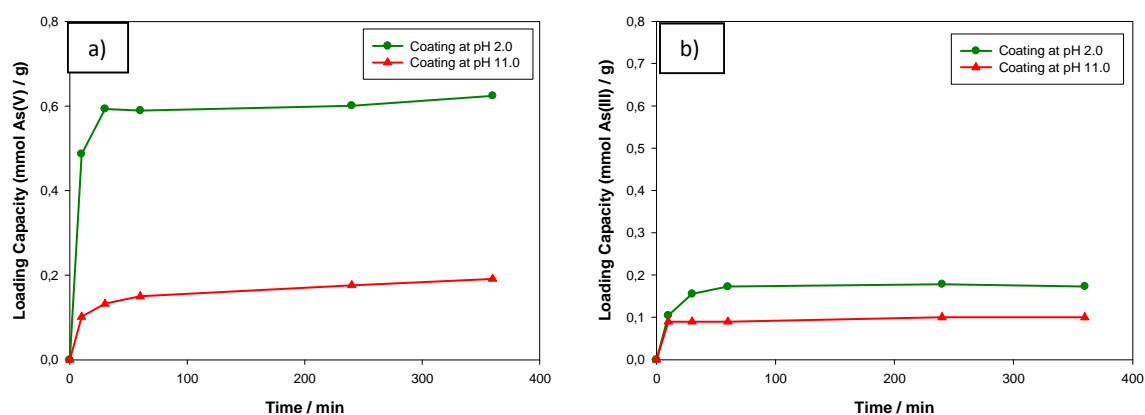
Figure 3.19. Effect of contact time on the removal of arsenic with 3-MPA coated SPION at pH 2.0 and 11.0 for a) As(V) and b) As(III).

An experiment to study the effect of contact time in arsenite and arsenate mixtures was performed. The results in the Figure 3.20 show that the contact time keeps the equilibrium at 60 min as in the case of single inorganic arsenic species solutions. The results reflect the high competition between both arsenic species to have better interaction with the two reactive centers (SPION and thiol group) in the adsorbent system. While, the Fe(III) forming the SPION has better affinity for the most acidic specie, which is the As(V), the presence of As(III), entails that not all As(V) that is able to interact with SPION, can be fixed due to this competition. When 3-MPA takes place in the adsorption process, a non-selective interaction with both arsenite and arsenate through the thiol group can be carried out without any special affinity.

The maximum adsorption capacity is 0.26 mmol As/g SPION. This value is intermediate between the maximum adsorption capacity of arsenite and arsenate for individual solutions and reveals that both species are interacting with the 3-MPA coated SPION.
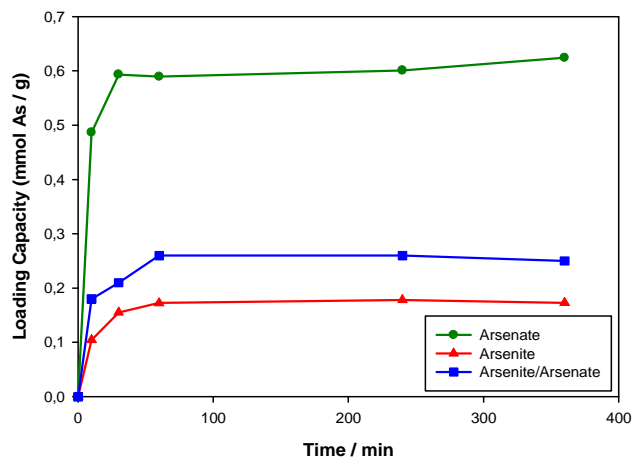
Figure 3.20. Effect of contact time on the removal of arsenic with 3-MPA coated SPION at pH 2.0 for a mixture of As(V) and As(III).

3.3.2.2. pH effect in the adsorption process

The obtained results (Figure 3.21) revealed that for this adsorbent system the adsorption of As(V) and As(III) by 3-MPA coated SPION is pH dependent. This is in agreement with the results obtained from solvent extraction studies using 3-MPA as extractant.[40] For As(V), this can be explained by the dependence of pH on the various As(V) species present in the aqueous solution.
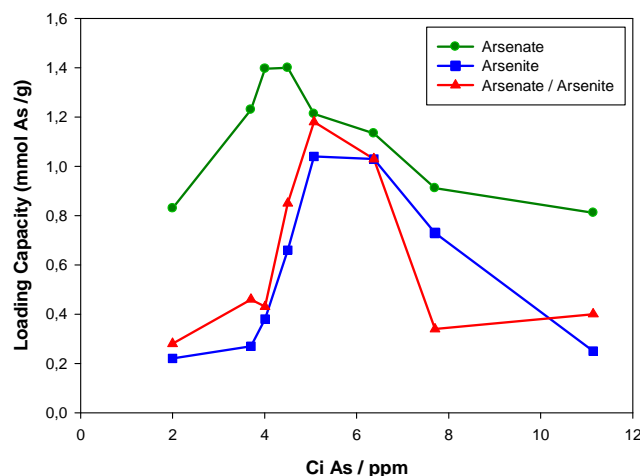
Figure 3.21. Effect of pH on the removal of As(V), As(III) or mixtures using 3-MPA coated SPION.

A comparison of the observed pH effect with those obtained on previous As(V) adsorbent studies, i.e. SPION alone, revealed similar behaviour with an adsorption maximum at pH 3.8. This similarity supports that arsenic species responsible of the adsorption are the

133

same. It is noteworthy that the thiol groups are able to interact with arsenate to scavenge the As(V) as shows the Figure 3.22. Arsenic centres are distributed all around the sample although in the zones where Sulphur is most concentred, Arsenic has less presence. Then, there is a strongest interaction between Fe(III) from SPION and As(V) than with the thiol group.[41]

Figure 3.22. SEM micrograph of SPION coated 3MPA after As(V) adsorption a). SEM-mapping of Arsenic b), Sulphur c) and Iron d).

In the case of As(III), 3-MPA coated SPION present a pH dependent adsorption which is not visible when the adsorbent system is SPION alone. In this situation, the presence of thiol groups in the SPION surface is the responsible of this main adsorption effect due to there is only one specie at all pHs, H_3AsO_4, and it presents low adsorption by using SPION alone. Then, the adsorption capacity reached is around 1.1 mmol As(III)/g SPION at a pH range between 4.6 and 6.5. This value is too close to the obtained for As(V) (1.4 mmol/g) which demonstrate that the presence of thiol groups let recover arsenite under same conditions than for arsenate.

For mixtures, the shape of the figure presents competitiveness between both arsenite and arsenate as in the case of SPION alone but keeping a similar adsorption capacity like both species individually. These results could suggest that, exist a pH dependency in the competitiveness due to the arsenate adsorption on the SPION and the interaction of both arsenite and arsenate on the thiol groups are optimal at different pHs. Then, being arsenate

more acid than arsenite, tend to interact with Fe(III) centers in SPION more efficiently while As(III) has strong interaction with the thiol groups of 3MPA.

3.3.2.3. Maximum adsorption capacity of SPION

The relationship between the adsorbed Arsenic and the Arsenic remaining in the aqueous solution at the equilibrium for the different experiments in relation with the analyzed species is shown in Figure 3.23.
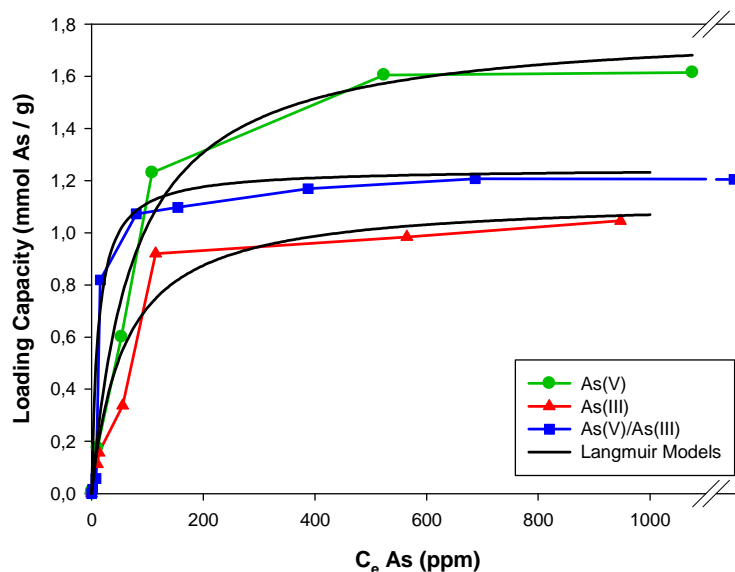
Figure 3.23. Effect of equilibrium concentration of As(V), As(III) or mixture of species at pH of highest As adsorption.

The observed behaviour is similar to that of non-coated SPION when increasing the aqueous Arsenic concentration. However and in the case of As(V), the observed higher adsorption capacity can be attributed to the increase of surface area due to the nanoparticles partial disaggregation produced in presence of 3MPA. The results show that at optimal pH conditions, the saturation in the adsorption capacity for arsenate is reached when the maximum adsorption capacity is about 1.6 mmol As(V) / g adsorbent.. The 3-MPA coated SPION works in the same way for arsenite arriving to the maximum adsorption capacity at 1.03 mmol As(III)/g adsorbent with 100 ppm of arsenite. The Langmuir model is adjusted to the experimental model as can be observed in the Figure 3.23 and the predicted value corresponds with the experimental ones. The maximum adsorption capacity of As(V) corresponded to 54% (molar basis) of the total binding sites (3.7 mmol 3-MPA/g SPION) and

for As(III) corresponded to 43%. Then, the major part of the reagent is likely to be accessible to As(V) ions.

For the mixtures, the maximum adsorption capacity is about 1.2 mmol As/g adsorbent, an intermediate value between the maximum adsorption capacity of As(V) and As(III) and this means that, as for non-coated SPION, both species are contributing in the adsorption capacity. Then, this fact reveals high competitiveness between both species with the Fe(III) centers the SPION and As(V) is the most acidic specie which has better interaction with SPION. In presence of As(III), not all As(V) that is able to interact with SPION can be fixed due to this competition

Similarly to the studies using non supported nanostructured systems such as SPION, the experimental agrees with the Langmuir adsorption model and the values of the Langmuir constant, extracted from the fitting results, for arsenite, arsenate and the mixture of arsenic species are 0.95 L/mmol, 1.29 L/mmol and 10.30 L/mmol, respectively, see Figure 3.24.
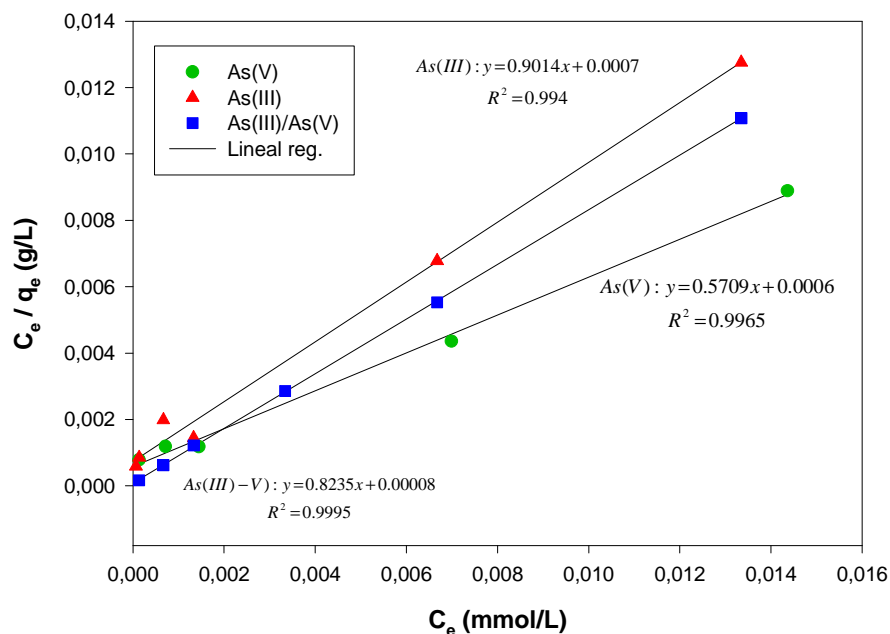
Figure 3.24. Fitting of the experimental data for the Langmuir constant

With all parameters optimized, adsorption mechanisms can be described at pH 4.0, where the predominant species are $H_2AsO_4^-$ for As(V) and H_3AsO_3 for As(III).[28,33]

> **_For As(III):_**

$$+ \ 2 \ H_2O \quad (3.11)$$

> **_For As(V):_**

$$+ \ H_2O \ + \ OH^- \quad (3.12)$$
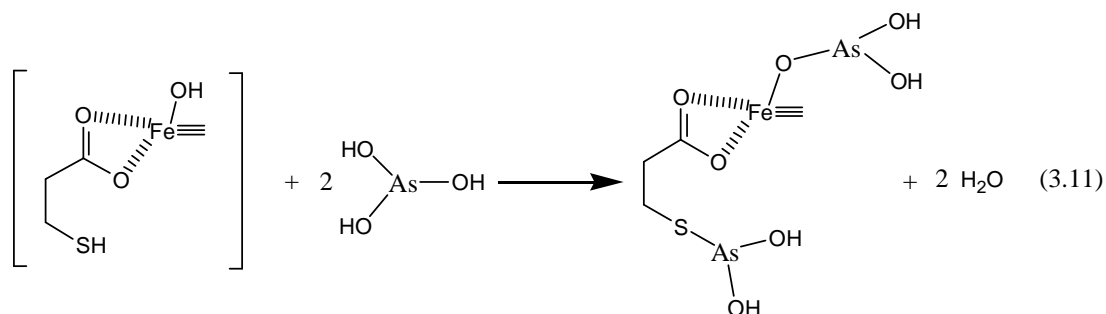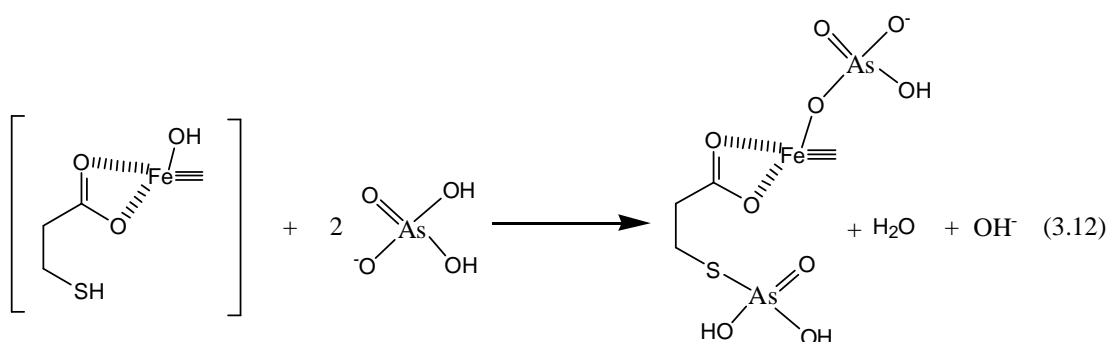
For As(V), the observed increase of the solution pH supports the appropriateness of the proposed adsorption mechanism.

3.3.3. Selectivity

To evaluate the adsorption selectivity of arsenic species in a mixture containing interfering metal ions and interfering anions (chloride, nitrate, sulfate and phosphate), separate experiments were carried out following those in the previous section for non-coated SPION.

3.3.3.1. Metal Ions interference on 3-MPA coated SPION

The obtained results are shown in Table 3.5 and they are in agreement with those already reported for solvent extraction studies.[19] This fact indicates that 3-MPA coated SPION can be used to remove As(V) selectively from aqueous solutions under the studied experimental conditions.

Table 3.5. Selective adsorption of As(V), As(III) and both species from a mixture of metals.

Metal ions	As(III) Sorption (%)		As(V) Sorption (%)		As(III-V) Sorption (%)	
	Molar ratio 1:1	Molar ratio 1:2	Molar ratio 1:1	Molar ratio 1:2	Molar ratio 1:1	Molar ratio 1:2
As	13.5	8.0	95.0	96.0	35.9	28.5
Cu(II)	12.0	7.0	2.3	0.1	10.3	3.4
Ni(II)	15.6	12.6	0.5	1.6	8.92	1.1
Zn(II)	25.1	6.2	0.5	3.0	8.7	2.8

It is noteworthy that in one hand, at optimal pH (3.6), both the hydroxyl groups at the surface of the SPION and thiol groups of 3-MPA are doubly protonated ($\equiv FeOH_2^+$ and $-SH_2^+$ respectively)[20,42] and the surface charge of the adsorbent is thus positive. This fact favors considerably the interaction with arsenate due to its negative charge and works against for the interaction with arsenite due to its neutral charge.

On the other hand, by increasing the molar concentration of Cu^{2+}, Ni^{2+} and Zn^{2+} the arsenic adsorption percentage keeps constant while for the other metal ions, decrease. Then, the active centers for the adsorption process continue playing their interaction by ligand exchange mechanism with arsenic. For the other metal ions, the adsorbed amount is practically the same than with molar ratio 1:1 but the percentage of adsorption decreases due to the increase of the total concentration present in the media for each metal ion. These values confirm their high selectivity of SPION..

For As(III), a reduced selectivity is observed due to the low adsorption capacity the 3MPA coated SPION presents (1.03 mmol As(III)/g). This fact reveals a low adsorption percentage and favors the interaction of the adsorbent system with the metal ions presents in the media.

However, on a mixture including As(III), the selectivity against As(V) is greatly reduced due to the As(III) interfering role as happened in previous studies (determination of the maximum adsorption capacity) where in presence of As(III) and due to the competitiveness between both, not all As(V) that is able to interact with SPION can be fixed.

3.3.3.2. Anion interference on the Arsenic adsorption on 3MPA coated SPION

As it is presented in the literature,[35,43] when comparing the adsorption results between synthetic solution and industrial water, a greater efficiency of the adsorbent

system for the metal ions removal from synthetic solution is observed. This can be attributed to the matrix effect of ~~real~~ industrial water samples which increase the ionic strength of the solution as well as the ions competition by the adsorption sites. In our case, using the interfering anions, we could mimic the ionic strength of industrial waters.

The Figure 3.25 shows the effect of the pH in the adsorption of As(III) (Figure 3.25a), As(V) (Figure 3.25b) and As(III)/As(V) mixture (Figure 3.25c) in the pH range 2-11 for the 3-MPA coated SPION when using solutions in presence or absence of anions commonly presents in waste waters which can potentially interfere the arsenic adsorption such as chloride, nitrate, sulphate or phosphate. It can be emphasized that the interfering effect of these anions is very significant, since the arsenic adsorption capacity, in the presence of one of these anions is always lower than its absence. However, the general trend of varying the adsorption capacity with the pH is similar for all interfering anions, with an increase of the adsorption capacity when the pH increases until 4.5 or 6.0 and stabilization until pH 11.0.
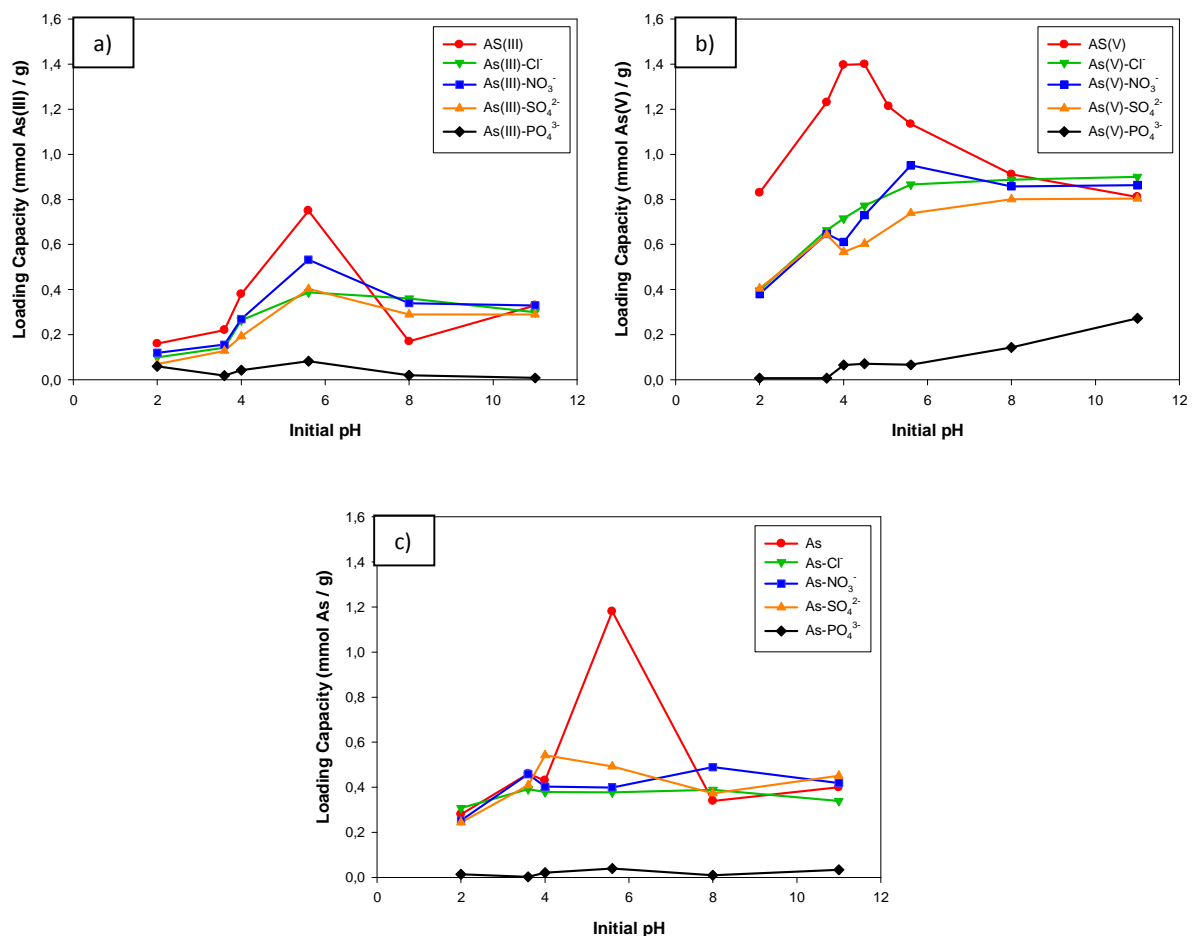
Figure 3.25. Effect of the presence of interfering anions on the removal of a) As(V), b) As(III) or c) As(III)-As(V) mixture with 3 MPA coated SPION.

These values collected in Table 3.6 present a general decrease of Arsenic adsorption when is in presence of any of the target anions.

Table 3.6. Interfering effect of different anions in the adsorption capacity of As(III), As(V) and As(III)/As(V) mixture with a molar ratio 1:200 of Arsenic vs anions.

Sample	As(III)		As(V)		As(III-V)	
	Adsorption Capacity (mmol/g)	Decrease %	Adsorption Capacity (mmol/g)	Decrease %	Adsorption Capacity (mmol/g)	Decrease %
As	0.75		1.40		1.18	
As-Chloride	0.39	48.0	0.77	44.8	0.38	66.9
As-Nitrate	0.53	29.3	0.73	56.9	0.40	66.1
As-Sulphate	0.40	46.7	0.60	86.6	0.49	58.5
As-Phosphate	0.08	89.3	0.07	94.9	0.04	96.6

The selectivity decreases in order phosphate >> sulphate ~ nitrate ~ chloride. Therefore, the results show that the adsorption capacity is similar in the presence of all interfering anions except phosphate, which present a more pronounced interfering effect, similarly to the case with non-functionalized SPION. The high interfering effect of phosphate in the adsorption capacity of both arsenic species in all pH range is due to the effective competence for the Fe(III) centers of the SPION according with the similar affinity of phosphate and arsenate for Fe(III) as well as the major concentration of phosphate present in test solutions.[31]

3.3.4. Desorption processes

In general, to get an effective desorption process, it's necessary to develop the experiment with a high concentration of the stripping specie and this specie must be more strongly retained than the adsorbate. In case that the stripping specie would lower affinity for the adsorbent than target ions (Arsenic in this case), the required concentration of the stripping agent will be relatively high.

Different eluting solutions such as HNO_3 and NaCl were employed for the recovery of arsenic species from the loaded 3-MPA coated SPION. Corresponding results of the desorption process show (Table 3.7) a 97 % of recovery when using 1.0 M HNO_3 and 5 % for

1.0 M NaCl in the case of As(V). For As(III), a 89 % of recovery when using 1.0 M HNO_3 is achieved while a 8 % for 1.0 M NaCl. Adsorbed Arsenic in mixtures provides a 92 % of recovery when using 1.0 M HNO_3 and 16 % for 1.0 M NaCl. These results agree with the described pH effect on the adsorption process.

From these results, desorption process by using chloride ions indicates the known interaction between chloride ions and Fe(III) ions from the coated SPION is not enough to desorb both arsenite and arsenate. Otherwise, by using nitric acid the proton (H$^+$) favours the desorption of the adsorbed arsenic species, due to H$^+$ compete efficiently with Fe(III) from SPION.

Table 3.7. Effect of stripping solution on the recovery of different arsenic species.

Striping Solution	As(III) Recovery (%)	As(V) Recovery (%)	As(III-V) Recovery (%)
NaCl 1.0M	8	5	16
HNO$_3$ 1.0M	89	97	92

In addition, NaCl and HNO_3 eluting solutions, entails in the absence of iron in the aqueous phase, that means no degradation of 3-MPA coated SPION is produced in the striping process.

Other tested desorbing reagents such as NaOH (1.0 M and 0.1 M) and H_3PO_4 (0.5 M) become a problem for the adsorbent system due to the degradation of SPION to Fe(II) and Fe(III) species that were found in the respective solutions. Such degrading phenomenon was confirmed by analysing the remaining iron content at the striping solution that revealed a 26% loss of the initially SPION in the adsorbent system.

Several 3-MPA coated SPION samples have been observed by SEM after the desorption process and all of them keep their structure with presence of Sulphur that means that mercaptopropionic agent remains on the SPION surface. In other words, by using 1.0 M HNO_3, the absorbent material is stable after the treatment and it is ready to be used for adsorption-desorption cycles.

The possibility of combining the superparamagnetic properties of SPION with the selectivity of the reagent (3-MPA) could result in the development of a more effective

sorbent for the selective recovery of As(V) from dilute solutions. In addition, the resulting increase of 3-MPA coated SPION adsorption capacity for As(V) almost double the adsorption capacity of SPION under the same conditions, which is attributed to the increase of active adsorption sites and to 3MPA effect on decreasing the SPION aggregation.

143

3.4. Comparison between non-supported SPION systems

Developed non-supported adsorbent systems have been compared, in terms of the optimum conditions as well as the adsorption capacities under these optimized conditions (Table 3.8). Significant differences between adsorbents are observed, mainly 3-MPA coated SPION provide greater capacity for adsorption of As(III) and As(V), around two fold the obtained with non-coated SPION.

Table 3.8. Adsorption capacity variation for As(V) and As(III) depending on the used non-supported SPION nanostructured system.

Parameters	As(III)		As(V)	
	SPION	Coated SPION	SPION	Coated SPION
Contact Time (min)	30	10	30	10
Optimum pH	-*	4.5	3.76	3.8
Maximum adsorption capacity (mmol/g)	0.43	1.03	0,91	1.60

* As(III) adsorption is pH independent.

Other significant difference is the minimum contact time needed to get the equilibrium. While the non-coated SPION needs 30 min, 3-MPA coated SPION needs 10 min. This fact shows that 3-MPA decreases both the SPION aggregation and the resistance for the penetration of arsenic species in the SPION environment that potentiate the adsorption capacity of SPION with a faster dynamic.

At this point it is observed the difficulties to minimize the aggregation of the SPION despite the fact that the functionalization helps to increase the adsorption capacity. In view of this situation and with the minimization of the aggregation as the principal aim, the use of supporting materials was undertaken to face this problem. Several supports, such as ion exchange resins, zeolites or clays, have been studied but Forager® Sponge was selected as the support for the SPION. It was observed in previous studies in our laboratory, this sponge was used in the fixation of Fe(III) for arsenic removal.[33] Then, taking into account this knowledge, the study was performed. The porosity of this support will decrease the SPION aggregation and this fact may increase the adsorption capacity of the system due to the increase the specific surface area.

145

SPION supported Nanostructured Systems

The current section describes the results obtained for the adsorption studies with the three developed new SPION supported nanostructured systems, Forager® Sponge loaded SPION and electrospun Cellulose acetate (CA) or Polyacrylonitrile (PAN) nanofibers loaded SPION, including the characterization of the adsorbent system materials, complemented with arsenic adsorption studies in order to determine the influence of process adsorption parameters including the arsenic selectivity when applying the developed systems to treat polluted solutions containing both arsenite and arsenate.

3.5. Forager® Sponge loaded SPION

In the next section, Forager® Sponge, as it`s described in the *Section 1.4.5.1* is used as specific support for SPION to develop an improved adsorbent system that helps to decrease the SPION aggregation. SPION loaded Forager® Sponge were prepared, characterized by different techniques and their feasibility for the adsorption of inorganic arsenic species from dilute aqueous solutions was evaluated by determining the separation efficiency of the supported SPION and related equilibrium isotherms of arsenite and arsenate adsorption were performed.

3.5.1. Forager® Sponge loaded SPION Characterization

The prepared SPION loaded Forager® Sponge was characterized using Transmission Electron Microscopy (TEM), Scanning Electron Microscopy (SEM) and Superconducting Quantum Interference Device (SQUID). Such characterization techniques were employed to understand the way the SPION is fixed on the sponge surface, the efficiency of this fixation and the amount of SPION layers formed in the sponge surface. The characterization results are outlined below.

3.5.1.1. Transmission Electron Microscopy (TEM)

The SPION dispersed over the Sponge surface was characterized using the same characterization techniques as described in the *Section 3.2.1*. The result was that the particle size is around 10 nm. The Figure 3.26 shows the TEM micrographs of SPION loaded Forager® Sponge and indicate that a greater specific surface is achieved with an adequate optimization of the SPION dispersion process, and therefore, greater adsorption capacity could be obtained in SPION loaded Forager® Sponge due to the high dispersion of SPION.

Figure 3.26. TEM micrograph of SPION loaded Sponge. Loading by dipping during 24h (a). Low (b), intermediate (c) and high load (d) of SPION over the sponge surface.

In order to characterize the SPION distribution on the sponge, different deposition ways were developed, such as Forager® Sponge impregnation by dipping for 24 hours in SPION suspension or spray this suspension by pneumatic nebulizer. These tests reveal that longer dipping processes (Figure **3.26**a) produce a higher aggregation of SPION than using a pneumatic nebulizer (Figure 3.26 b, c, d). Thus, with a low loading (20 mg SPION/g Sponge), a homogeneous and uniform SPION distribution on the Forager® Sponge surface was observed, not achievable at a high loading (140 mg SPION/g Sponge).

These loading properties will result of key importance for the As(III) and As(V) adsorption process efficiency on SPION. Theoretically, the decrease of SPION aggregation generates an increase of the specific surface area and therefore an increment in the reactive centers on the adsorbent material for the adsorption process of As(III) and As(V).

3.5.1.2. Scanning Electron Microscopy (SEM)

SEM was employed to characterize the SPION distribution on the sponge. To this purpose, micrographs and Fe-mapping were performed, see Figure 3.27.
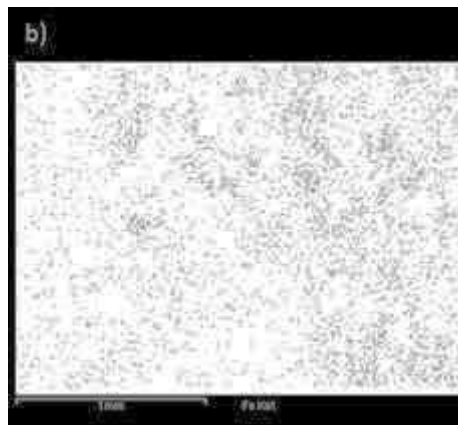
Figure 3.27. SEM micrograph of SPION loaded Sponge (a). SEM-mapping of Iron (b).

The Fe-mapping shows that SPION distribution is homogenous over all sponge surfaces and confirms the TEM results. In addition, the SEM analysis revealed the impregnation to penetrate inside of the sponge pores providing a complete SPION layer on the sponge surface.

3.5.1.3. Superconducting Quantum Interference Device (SQUID)

The evaluation of the magnetic hysteresis of the SPION loaded Forager® Sponge, Figure 3.28, was performed to determine their magnetization and to compare the magnetization with the SPION powder. As it was indicated for SPION, superparamagnetic materials have no permanent magnetic moment and, hence, no hysteresis loop. The evaluation of the magnetic hysteresis represents the corresponding magnetization as a function of magnetic field applied to Forager® Sponge loaded with SPION under the the optimized   conditions providing 20 mg SPION/g Forager® Sponge. The shape of the hysteresis curve for the sample was normal and tight with no hysteresis losses, as expected for a superparamagnet. Under low applied field, a high magnetization (M) value was observed. The saturation magnetization (M_s) and the coercivity (H_c) of the SPION loaded Forager® Sponge are about 30 emu/g (80 emu/g for SPION powder) and 48 Oe (143 Oe for SPION powder) respectively. Taking into account that 2mg of sample were needed for the experiment and the SPION loaded Forager® Sponge has a concentration of 20 mg SPION/g

Forager® Sponge, the obtained values reflected that despite the lower amount of SPION over the sponge surface if compared with the SPION powder, the SPION still retained their magnetization. Thus, reveal a remaining magnetic capacity of interest in order to recover the product when treating contaminated solutions.
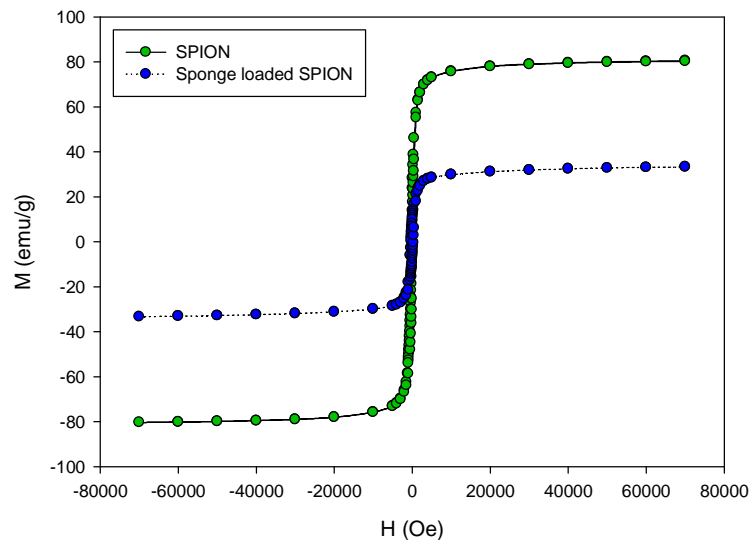
Figure 3.28. The M vs H dependence for SPION and SPION loaded Forager® Sponge at 300K.

3.5.2. Arsenite and arsenate adsorption parameters

This section includes results of different parameters affecting the adsorption process as well as its selectivity against most common interfering ions and the desorption process, such as pH and SPION load. At this point, contact time was assumed as a constant parameter at 60 min, being selected for the shake of comparison with the previous systems.

3.5.2.1. pH effect in the adsorption process

The adsorption of the different arsenic species using SPION loaded Forager® Sponge was investigated by varying the solution pH in the range 2-7 taking into account that for the previous studied materials, pH values higher than 7 does not affect the adsorption process. The obtained results (Figure 3.29a) revealed that the adsorption of As(V) is pH dependent and As(III) is pH independent. Such behavior can be explained by the presence of different As(III) and As(V) forms in the aqueous solution at different pHs. Additionally, Forager® Sponge presents a very small arsenite and arsenate adsorption which is important to

determine the adsorption capacity of SPION loaded in the system. In this case, Forager®
Sponge is just a support without interference in the adsorption process.
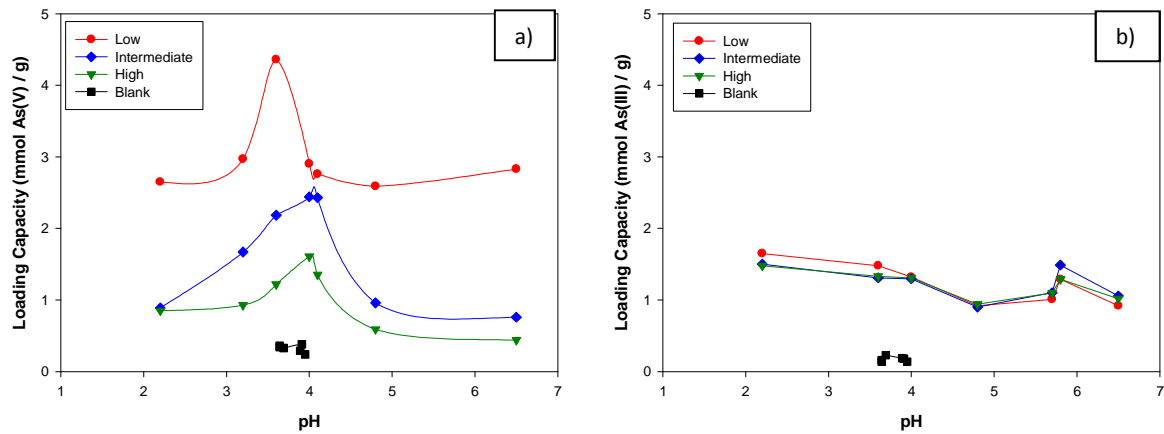
Figure 3.29. pH effect over As(V), a) and As(III), b) SPION loaded Forager® Sponge adsorption capacity.

A comparison of the observed pH effect with that obtained on previous As(V)
adsorbents, non-supported SPION alone and 3MPA coated SPION, revealed similar behavior
with an adsorption maximum at pH 3.8. In addition, the amount of SPION loaded on the
Forager® Sponge was considered. In this case, three different SPION loadings were
generated by pneumatic nebulization over the Sponge, low (44.5 mg SPION/g Forager®
Sponge), intermediate (84.2 mg SPION / g Forager® Sponge) and high loading (146.7 mg
SPION/g Forager® Sponge). In all these situations the pH influence is similar, achieving a pH
of maximum adsorption capacity at 3.6-3.8.

The observed higher adsorption capacity for the low loading SPION is due to the
higher dispersion of SPION on the sponge, what provides higher specific surface area that
will increase the adsorption rate of arsenite in SPION.

For arsenite, SPION loaded Forager® Sponge presents a completely different situation
(Figure 3.29b) due to the absence of adsorption capacity variation within the target pH range.
Such behavior follows the observed for non-supported SPION. As in that case, the less acidity
of arsenite species (pK_{a1} = 9.2) is the reason for such non-significant pH effect.

In this sense, the ion exchange and the adsorption of both forms of Arsenic is
possible at any pH range, with a maximum of 0.3 mmol As(V) / g sponge within the pH range

(3-5). Moreover, only in basic solutions, As(III) may dominate. Under the working pH conditions, the operational capacity of the sponge is very small (0.15 mmol As(III) / g sponge), being the adsorption of As(III) on sponge very low in all the pH range.

3.5.2.2. SPION load effect

The effect of the of SPION amount loaded on the Forager® Sponge on the adsorption capacity of As(V) and As(III), was studied with the optimized time conditions (60 minutes) and in a wide pH range to evaluate the behavior in the target pH range 3.8 – 4.0. In all cases, as shows the Figure 3.30.
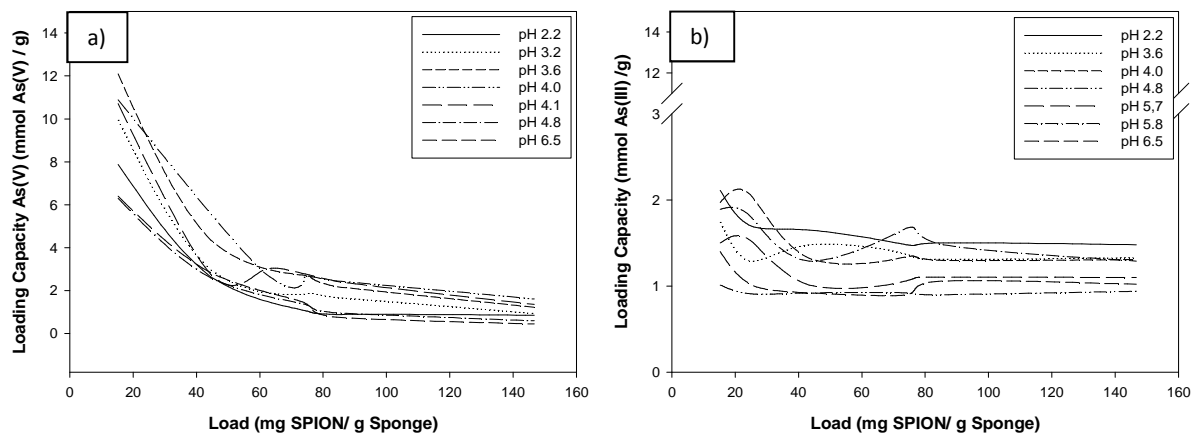
Figure 3.30. Adsorption capacity for SPION loaded sponge with different loads: As(V), a). As(III), b).

The observed behaviour can be interpreted based on two differentiated types of interactions. In one hand, an anion exchange of arsenic species corresponding to the protonated amine groups present in the matrix of the Sponge.[44] However, there is a second process where a ligand exchange, provided by the Fe(III) ions immobilized in the SPION is promoted:

a) The first interaction, as show Equation 3.13, involves an anion exchange of arsenic species corresponding to the protonated amine groups present in the matrix of the sponge. This interaction will be dependent of the equilibrium pH of the aqueous solution, where Y is the species of arsenic exchanged by the counter ion (X).

$$(3.13)$$
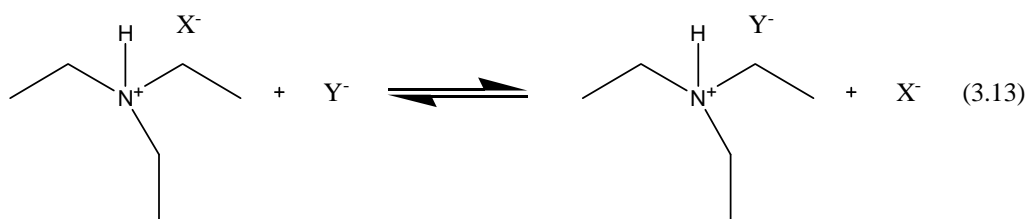
b) There is a second process where an exchange of ligands provided by the Fe(III) ions of the SPION immobilized in the supporting material, Forager® Sponge, is promoted. This can be expressed by the general equation:

$$R - Fe(III) - OH + X \leftrightarrow (R - Fe)X + Z \qquad (3.14)$$
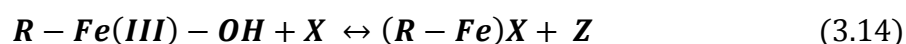
where R is the matrix of the SPION, X is the chemical species of arsenic ($H_2AsO_4^-$ and H_3AsO_3 at the optimal pH) and Z is the exchanged ligand, OH^- ions in the case of As(V) and H_2O for As(III). The affinity of arsenic oxoanions for the iron on SPION is higher for the Fe(III) ions than Fe(II) ions. This provides a higher activity of the Fe(III) ions with OH- than Fe(II) ions.

As mentioned above, the differential behaviour of both arsenic species is related to the different acidity of their respective oxoanions. While H_3AsO_4 is a strong acid ($pKa_1 = 2.24$, $pKa_2 = 6.76$ y $pKa_3 = 11.60$), H_3AsO_3 is a very weak one ($pKa_1 = 9.23$, $pKa_2 = 12.10$ y $pKa_3 = 13.41$)[45]. This generates the existence of an As(V) oxoanions in solution , which will be adsorbed on the sponge by the protonated amine groups from a relatively acidic pH to basic pH values. Moreover, the difference in adsorption between the blank sponge and the SPION loaded Forager® Sponge it is attributed to the presence of Fe(III) ions in the nanoparticles, which provide exchange adsorption centres for arsenic species. In this sense, the processes occurring during the arsenite and arsenate adsorption, at the studied pH, on SPION loaded Forager® Sponge, could be explained by these equations: [28]

$$R - Fe - OH + H_2AsO_4^- \leftrightarrow (R - Fe)HAsO_4^- + H_2O \qquad \log K = 3.51 \qquad (3.15)$$
$$R - Fe - OH + H_3AsO_3 \leftrightarrow (R - Fe)H_2AsO_3 + H_2O \qquad \log K = 0.92 \qquad (3.16)$$
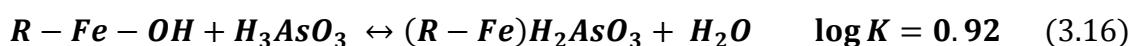
With these calculated data, that follow the tendency of similar adsorption reactions,[33] and if we assume the ligand exchange model expressed before, the adsorption of As(V) on the SPION loaded Forager® Sponge is favoured over the adsorption of As(III),

similarly to the adsorption observed over other iron oxides.[33,22] Finally, adsorption affinity follows solubility parameters; the anion being more prone to be adsorbed is the one able to form the more insoluble compound with the cation.[24]

The presence of SPION immobilized in the sponge enhances the adsorption capacity of both arsenic species with respect to the non-supported SPION, so that the maximum adsorption of the sponge is 12.09 mmol As (V)/ g SPION at initial pH 3.6 and 2.11 mmol As (III)/ g SPION at pH 4.0. This range confirms the optimum pH for maximum adsorption obtained for arsenic adsorption on SPION suspension. This fact, coupled with the reduced adsorption of As(III) throughout the studied pH range, shows the possibility of separating both arsenic species .

In conclusion, the different adsorption of As(V) and As(III) by SPION supported on sponge can be interpreted as a dual process consisting of an ion exchange of ammonium groups and an exchange of ligands on Fe(III) cores of the nanoparticles immobilized in the sponge. The use of supported SPION significantly improved both the adsorption capacity and selectivity of the As(V) adsorption process compared to the use of Forager® Sponge non loaded with SPION. Losses of SPION are not significant within the studied pH range, becoming promising for a potential application to remove As(V) from contaminated effluents. Increasing the number of impregnations of SPION over the sponge reduces the adsorption capacity of the supported SPION due to an increased aggregation.

3.5.3. Selectivity

The interference of the metal ions and interfering anions (chloride, nitrate, sulfate and phosphate) was studied following the procedure employed in the previous section.

3.5.3.1. Selectivity with the presence of Metal Ions

The obtained results are listed in Table 3.9 and they are in agreement with the previous result obtained with the previously described SPION adsorbent systems. This fact indicates that SPION loaded Forager® Sponge can be used to selectively extraction of As(V)

and As(III) when these species are present in solution under the studied experimental conditions.

Table 3.9. Selective adsorption of As(V), As(III) and both species from a mixture of metals.

Metal ions	As(III) Sorption (%)		As(V) Sorption (%)		As(III-V) Sorption (%)	
	Molar ratio 1:1	Molar ratio 1:2	Molar ratio 1:1	Molar ratio 1:2	Molar ratio 1:1	Molar ratio 1:2
As	77.5	81.0	99.0	98.0	94.3	97.8
Cu(II)	23.0	4.0	0.33	0.13	6.1	2.6
Ni(II)	16.1	4.8	0.14	0.19	5.7	1.4
Zn(II)	15.7	6.2	0.48	0.18	5.7	1.1

It is noteworthy that in one hand, at optimum pH (3.6), the hydroxyl groups at the surface of the SPION are doubly protonated ($\equiv FeOH_2^+$) and the surface charge of the adsorbent is thus positive. This fact favors considerably the interaction with arsenate due to its negative charge and works against for the interaction with arsenite due to its neutral charge reducing the interaction and lowering the selectivity.

On the other hand and as occurs in case of the non-supported SPION adsorbent systems, by increasing the molar concentration of Cu^{2+}, Ni^{2+} and Zn^{2+} the arsenic adsorption percentage keeps constant while for the other metal ions decreases. Then, the active centers for the adsorption process continue playing their interaction by ligand exchange mechanism with arsenic and for the other metal ions, the percentage of adsorption decreases due to the increase of the total concentration present in the media for each metal ion. These values confirm that SPION keeps their high arsenic selectivity when the nanoparticles are supported over the Forager® Sponge.

On the other hand, by using higher molar ratio the arsenic adsorption percentage keeps constant while for the other metal ions decreases.

In presence of As(III)/As(V) mixtures adsorption on SPION loaded Forager® Sponge shows selectivity for Arsenic against other metal ions. In this process, the SPION dispersion on the sponge surface provides relatively higher number of active centers for the arsenic than non-supported SPION. However, additional tests including speciation would be necessary to determine the selectivity between As(III) and As(V).

3.5.3.2.   Selectivity with the presence of Interfering Anions

The pH effect on the adsorption of As(III) (Figure 3.31a), As(V) (Figure 3.31b) and As(III)/As(V) mixture (Figure 3.31c) on SPION loaded Forager® Sponge was studied within the pH range 2-11, both in presence and in absence of anions such as chloride, nitrate, sulphate or phosphate, following the previous studies for the non-supported SPION as adsorbent materials. It can be emphasized that the interfering effect of these anions is very significant, since the competition for the iron centers is very high and the general trend with the pH is similar to the non-supported system for all interfering anions. Thus, while, for As(V) a peak on the adsorption capacity is observed at pH 3.6 followed by stable lower values until pH 11.0. As(III) and As(III)/As(V) mixtures show a constant value for the adsorption capacity at the same pH range studied.
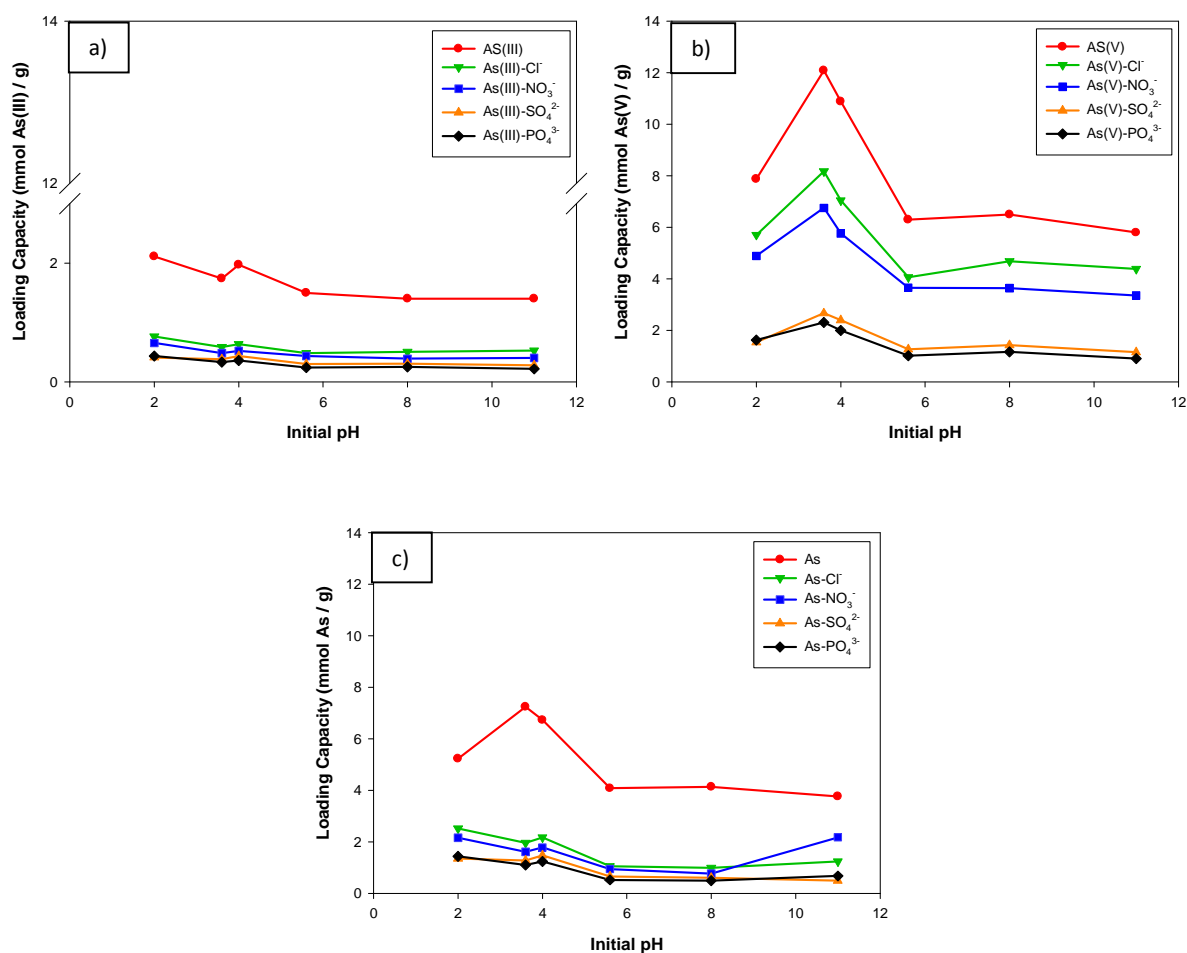
Figure 3.31. Effect of the presence of interfering anions on the removal of a) As(III), b) As(V) or c) As(III)/As(V) mixture with Forager® Sponge loaded SPION.

Corresponding quantitative values are collected in the Table 3.10 with the effect for each target anion.

Table 3.10. Interfering effect of different anions in the adsorption capacity of As(III), As(V) and As(III)-As(V) mixture with a molar ratio 1:200 of Arsenic vs anions.

Sample	As(III)		As(V)		As(III-V)	
	Adsorption Capacity (mmol/g)	Decrease %	Adsorption Capacity (mmol/g)	Decrease %	Adsorption Capacity (mmol/g)	Decrease %
As	2.11		12.1		7.24	
As-Chloride	0.761	64.0	8.18	32.3	1.95	73.1
As-Nitrate	0.653	69.2	6.76	44.1	1.62	77.6
As-Sulphate	0.412	80.5	2.67	77.9	1.27	82.5
As-Phosphate	0.444	79.1	2.31	80.9	1.11	84.7

The selectivity, as in the case of non-supported SPION adsorbent systems, decreases following the order phosphate >> sulphate ~ nitrate ~ chloride and the high interfering effect of phosphate continues been present as in the previous studied adsorbent systems.

The adsorption capacity in presence of interfering anions is reduced when sulphate is present as interfering anions, similarly to the effect in non-supported SPION therefore both exhibit similar affinities for the anionic exchange non selective centers (protonated amine groups of Forager® Sponge) but not for the ligand exchange centers of SPION where arsenate has a specific adsorption process.

In the cases of nitrate and chloride presence, the same behaviour than non-supported SPION is observed.

In comparison with the previously described adsorbent systems based on SPION, when As(III) and As(V) are present in the media the adsorption capacity of SPION loaded Forager® Sponge in presence of phosphate is 1.11 mmol As/g SPION while for 3MPA coated SPION and SPION alone are 0.04 and 0.08 mmol As/g SPION. Then, SPION loaded Forager® Sponge keeps its high arsenic adsorption capacity respect to non-supported SPION in spite of the anion interference.

3.5.4. Desorption process

Different desorbing species have been used for the desorption process and the desorption percentage was calculated between the desorbed amount of As(III), As(V) or

As(III)/As(V) mixture and the adsorbed amount in the previous adsorption process. The obtained results are shown in Table 3.11.

Table 3.11. Desorption percentage for different desorbing species.

Striping Solution	As(III) Recovery (%)	As(V) Recovery (%)	As(III-V) Recovery (%)
NaOH 1.0 M	49.0	48.6	42.8
NaOH 0.1 M	31.6	38.9	34.3
NaOH 0.05 M	12.7	25.3	19.7
NaCl 2.0 M	37.0	54.1	39.4
NaCl 1.0 M	56.1	67.5	61.5
H_3PO_4 0.5 M	89.8	91.3	90.5
HNO_3 1.0 M	99.3	98.2	97.2

Corresponding results of the desorption process show a 99.3 % of recovery when using 1.0 M HNO_3 and 89.8 % for 0.5 M H_3PO_4 in the case of As(III). For As(V), a 98.2 % of recovery when using 1.0 M HNO_3 is achieved while a 91.3 % for 0.5 M H_3PO_4. Mixtures reveal a 97.2 % of recovery when using 1.0 M HNO_3 and 90.5 % for 0.5 M H_3PO_4. In addition, some desorbing species such as NaOH (1.0 M and 0.1 M) and H_3PO_4 become a problem for the adsorbent system due to these desorbents remove the SPION of the Sponge surface and degrade the SPION to Fe(II) and Fe(III). Then, the adsorbent system loss the principal adsorbent compound and it cannot be used for new water treatments.

The desorption process by using chloride and hydroxide ions suggest that the interaction between the ions and the Fe(III) ions from the SPION is not enough strong to desorb both arsenite and arsenate. On the other hand, phosphoric acid, despite having the phosphate higher affinity to Fe(III) is not able to fully accomplish the desorption of Arsenic. Finally, in the case of nitric acid, is the proton (H^+) which compete efficiently with Fe(III) from SPION to desorb the adsorbed arsenic species. When comparing phosphoric and nitric acid, the later one is stronger and then, present more free H^+ to react (1.0 M in the case of HNO_3 and 0.0576 M for H_3PO_4).

Then, desorption of both arsenite and arsenate seems be effective by ionic exchange but not by ligand exchange. By ligand exchange the interaction is stronger due to the exchange is produced in the inner sphere of coordination.

Therefore, 1.0 M HNO_3 is the desorbing reagent that is most able to efficiently desorb without degrading the adsorbent system.

3.6. Non-supported systems and SPION loaded Forager® Sponge comparison

A comparison of the different adsorbent systems for arsenic species will be carried out, in terms of the optimum conditions, adsorption capacities under these optimized conditions and under the effect of interfering compounds present in the target solutions (Table 3.12). Significant differences between supports are observed, mainly SPION loaded Forager® Sponge provide greater capacity for adsorption of As(III) and As(V). Up to thirteen and four times higher capacity than the obtained with unsupported SPION were achieved respectively.

Table 3.12. Adsorption capacity for As(V) and As(III) on the different SPION adsorbent materials.

Parameters	As(III)			As(V)			As(III)/As(V)		
	SPION	Coated SPION	Sponge	SPION	Coated SPION	Sponge	SPION	Coated SPION	Sponge
Contact Time (min)	30	10	60*	30	10	60*	30	10	60*
Optimum pH	-**	4.5	-**	3.76	3.8	3.6	3.8	4.5	3.6
Maximum adsorption capacity (mmol/g)	0.43	1.03	2.11	0.92	1.60	12.09	0.86	1.2	7.24
Metal Ion Selectivity 1:2 (% Recovery)									
- As:Cu	n/a	8.0 : 7.0	81.0 : 4.6	n/a	96.0 : 0.1	98.0 : 0.1	73.4:19.8	28.5:3.4	97.8:2.6
- As:Ni	n/a	8.0 : 12.6	81.0 : 4.8	n/a	96.0 : 2.0	98.0 : 0.2	73.4:14.9	28.5:1.1	97.8:1.4
- As:Zn	n/a	8.0 : 6.2	81.0 : 6.2	n/a	96.0 : 3.0	98.0 : 0.2	73.4:12.7	28.5:2.8	97.8:1.1
Anionic Selectivity (% Decrease adsorption)									
- Chloride	n/a	48.0	64.0	n/a	44.8	32.3	65.9	66.9	73.1
- Nitrate	n/a	29.3	69,2	n/a	56.9	44.1	66.1	66.1	77.6
- Sulphate	n/a	46.7	80.5	n/a	86.6	77.9	60.5	58.5	82.5
- Phospate	n/a	89.3	79.1	n/a	94.9	80.9	88.9	96.6	84.7

* Contact time is assumed at 60 min by comparison with the previous systems.
** As(III) adsorption is pH independent.

Respect the 3-MPA coated SPION, SPION loaded Forager® Sponge present an improvement in the adsorption capacity of the SPION providing an increase from double in the adsorption capacity for As(III) and 7 times in the case of As(V)what is due to the dispersive effect of the sponge as support.

The impregnation by pneumatic nebulization of SPION over Forager® Sponge produces the nanoparticles dispersion and decreases the aggregation, improving the specific adsorption capacity of As(III) and As(V). The role of the sponge is to provide support for SPION on its surface, with a very weak contribution to the adsorption of As(V) species, 80 times smaller compared with the loaded sponge and 9 times smaller compared to SPION suspension.

3.6.1. Adsorption capacity comparison with similar adsorbent systems

Comparing the obtained results, as shown by Table 3.13, with similar studies employing the same type of Forager® Sponge loaded with Fe(III), a high difference adsorption is observed. To explain this behaviour, it must be taken into account that the SPION provide more accessible centres for the Arsenic adsorption respect the Fe(III). Forager® Sponge loaded SPION is 35 times more effective for As(V) and 16 times higher for As(III) than non-supported SPION. SPION dispersion over the sponge surface provides a more active adsorption sites accessible to both arsenite and arsenate. Something similar happen in the case of different types of resins loaded with iron(III), where the SPION loaded sponge improves As(V) adsorption 19 times, while doubles the adsorption capacity of As(III). The most important reason for the observed increase of is the decrease of SPION aggregation by a dispersion that leads to a higher availability of adsorption positions. [46,47,48,49]

Table 3.13. Comparison of adsorbent materials adsorption capacity.

Adsorbent Material	As(V)		As(III)		pH	Ref.
	mmol / g SPION	mmol / g Fe	mmol / g SPION	mmol / g Fe		
SPION	0.91	1.25	0.43	0.71	3.8	
Coated SPION	1.60	n/a	n/a	n/a	3.8	
Forager® Sponge loaded SPION	12.06	n/a	2.11	n/a	3.6	
Fe(III) loaded Forager® Sponge	n/a	0.5	n/a	0.2		32

Fe(III) loaded resin	n/a	**0.45**	n/a	n/a		33
Ferrihydrite	n/a	**0.25 - 0.38**	n/a	n/a		34
Goethite	**0.29**	n/a	0.05	n/a		35
Flower-like iron oxides	**0,07**	n/a	n/a	n/a	**4.0**	50
Hydrous iron oxide MNPs	**0,51**	n/a	n/a	n/a	**4.5**	51
Ascorbic acid-coated SPION	**0.22**	n/a	**0.65**	n/a	**7.0**	52
Magnetite-Maghemite nanoparticles	**0.05**	n/a	**0.05**	n/a	**2.0**	53
Fe$_3$O$_4$@CTAB	**0.31**	n/a	n/a	n/a	**3.0**	54

When the comparison is made with nanoparticles or nanocomposites, something similar happens. The three developed systems, non-supported, modified and Sponge loaded SPION present better adsorption capacity than the reported results in the literature.

3.7. Cellulose Acetate – SPION nanofiber composites for water purification

In this section we describe Cellulose acetate (CA) and cellulose acetate–SPION nanofiber composites synthesis, characterization by electron microscope techniques and their feasibility for the As(V) removal studied in continuous mode.

3.7.1. Synthesis and optimization of CA-SPION nanofiber composite

Cellulose acetate (CA) and cellulose acetate–SPION nanofiber composites were prepared by electrospinning technique. In this study, the preparation of nanocomposites was optimized by both CA nanofibers concentrations (10-20% w/v) and SPION concentrations (0.3% w/v and 3.0% w/v). Also the influence of SPION concentration on the size and morphology of the fibers was examined.

3.7.1.1. SPION Characterization

The characterization of nanoparticles morphology and the main particles size using the described method of synthesis is the same described in the *Section 3.2.1*. Mainly, its size that determines their adsorption capacity requires from TEM to be determined. In TEM micrographs (Figure 3.32), main spherical nanoparticles morphology can be observed, being partially aggregated when SPION are in suspension and the size of main portion of particles has an average of 10.5 nm.

Figure 3.32. TEM micrograph of synthesized SPION.

3.7.1.2. Nanofibrous structure of CA nanofibers

The electrospinning of the solutions was carried out by keeping a constant solution rate (0.5 ml/h), constant needle to target distance (5 cm) and by applying 9 kV voltage between the target and the needle due to this voltage was the only one able to perform CA nanofibers. The target was a drum covered with aluminum foil. The samples were observed by SEM and TEM.

SEM micrographs of CA-Nanofibers given in Figure 3.33 show the difference in diameter and the homogeneity of the nanofiber with the variation of concentration of the Cellulose Acetate in the electrospinning solution.[55]

165
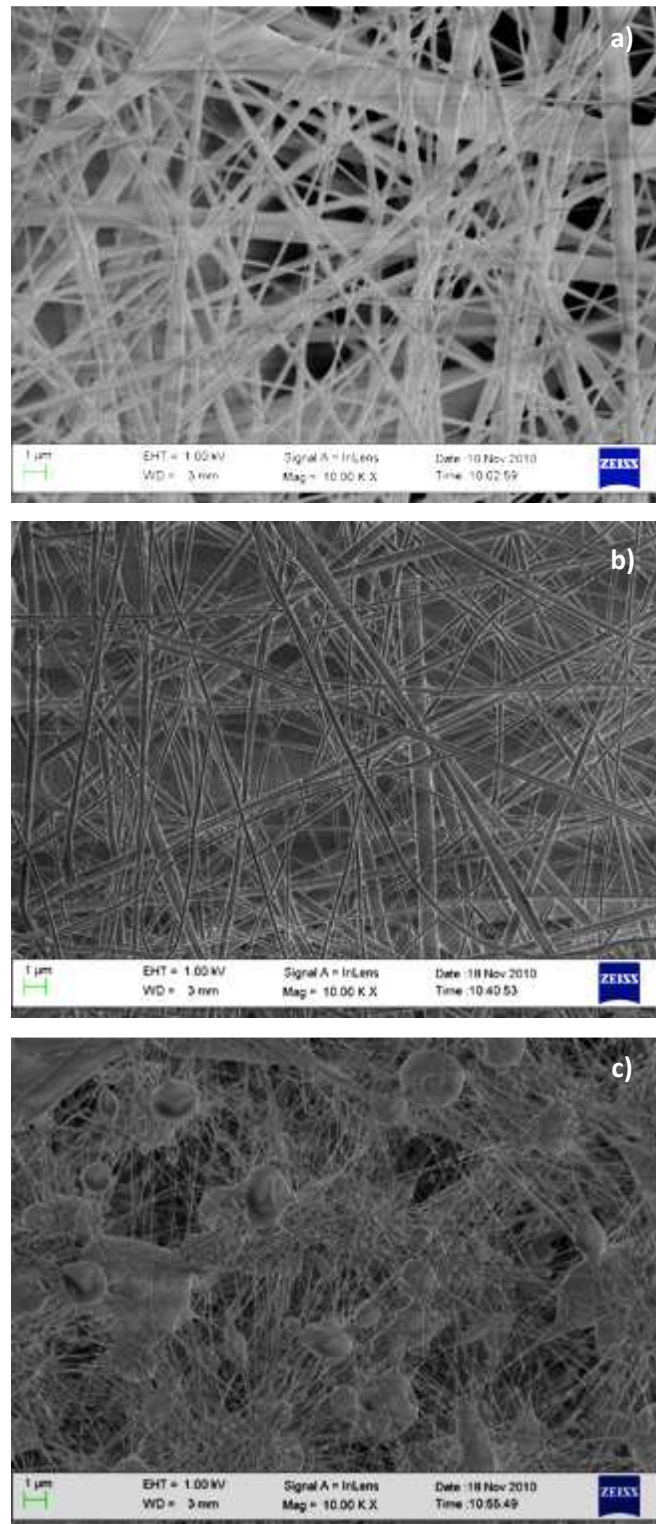
Figure 3.33. SEM micrograph of CA nanofiber at 20% (a), 15% (b) and 10% (c) CA concentration (w/v) at 9 kV.

SEM micrographs guided us to establish most appropriate CA concentration. At 10% w/v CA, a combination of smooth and beaded fibers was obtained (Figure 3.33c). The fibers are not homogeneous in diameter and beads defects appear suggesting an unstable electrospinning as well as the generation of non-homogenous or reproducible nanofibers. At

this low concentration, the low viscosity of the solution provides a low viscoelastic force not sufficient to counter the stretching forces from both the electrostatic and repulsion forces. Overstretching of the charged jet, as a result of these forces, resulted in partial breakup of the jet and, as a result of the surface tension, beads were formed on some of the fibers. It must be pointed out that the employed solvent mixture had a quite high boiling point and a reduced volatility (due to the addition of DMAc) in contrast to common volatile organic solvents. Also, less time is available for solvent evaporation as the production of the fibers becomes quicker. Subsequently, residual solvent remains in the fibers when they reach the target.

At 20% (w/v) CA, fiber of heterogeneous diameter ranging between 300 nm and 1 μm (Figure 3.33a) are produced. This fact shows that high CA concentrations involve higher jet instability, which creates random fibers and thus non-uniform structures.

Electrospinning of 15% w/v CA concentration (Figure 3.33b) resulted in the formation of smooth fibers, generating with constant and stable electrospinning jet that produces homogeneous CA nanofibers with an average diameter size of 250 nm. This fact demonstrates that the viscoelastic forces were sufficient to prevent partial breakup of the jet.

Once the nanofibers were synthesized, different solutions were prepared with different concentration of SPION. Two different procedures were applied for the impregnation with SPION to prepare nanocomposites. The first procedure uses Cellulose Acetate dissolution with SPION dispersion on the polymer solvents (acetone/DMAc mixture). The generated dissolution and dispersion were agitated by ultrasounds in order to obtain the electrospinning solution, shaking at room temperature to avoid sedimentation of the particles. Such procedure generates SPION particles inside CA nanofibers. The second procedure requires electrospun CA nanofiber to impregnate into the SPION suspension at different pH (3.0; 6.8; 11.0), for two hours under oscillatory shaking to produce SPION impregnated on SPION over the surface of the CA nanofibers. Afterwards, the obtained nanocomposites are rinsed with water and dried in a vacuum oven.

3.7.1.3. Fibrous structures of CA-SPION nanofiber composites by electrospinning

For the CA-SPION nanofiber composites, SEM and TEM were performed and the influence of SPION concentration on the fiber size can be analysed. Rather peculiar were the results considering the influence of SPION concentration on the fiber size. By adding only 0.3% w/v of SPION in dry powder, an increase in the average fiber diameter is observed (400nm), as seen in Figure 3.34. However, further increase of the SPION content helps to stabilize the electrospinning process but does not seem to have any major influence on the fiber size (Figure 3.34b). Usually, by increasing the concentration of the solution, the fiber size is also increased, due to increase in the viscosity of the electrospinning solution.[56]

Figure 3.34. SEM micrograph of CA-SPION Nanofiber composites at 15% of CA and different SPION concentration: 0.3% w/v (a), 3.0% w/v (b) at 9 kV.

It must be taken into account that the addition of the SPION into the polymer solution has a double effect. First viscosity should increase due to the increase of the total

dispersion concentration. However, the SPION powder hinders polymer chain interactions by increasing their distance. The second phenomenon prevails in the 3.0% SPION dispersion. While with further increase of SPION content, the first phenomenon becomes dominant and the expected increase of the viscosity is observed, it should be mentioned, that due to nanoscale effects a decrease in viscosity of polymer blend will be expected.[57]

TEM micrographs of the 0.3% w/v SPION nanofiber composite are presented in Figure 3.35(a,b). In this composite, the presence of SPION inside of the fibers can be observed revealing no aggregation and that the electrospinning technique is useful for the preparation of this adsorbent materials. The limitation with TEM technique is the difficulty to observe that inclusion of SPION inside the nanofiber.

Figure 3.35. TEM micrograph of CA-SPION nanofiber composites with 15% w/v of CA - 0.3% w/v of SPION (a) and 15% w/v of CA - 3.0% w/v of SPION (b) at 9 kV.

3.7.1.4. Fibrous structures of CA-SPION nanofiber composites by dipping

Representative SEM pictures of the composite materials are presented in **Figure 3.36**. Taking into account that the SPION pzc is 6.8, while for acidic (pH 3.0, **Figure 3.36a**) and basic (pH 11.0, **Figure 3.36c**) SPION media in the dipping process, SPION aggregates are hardly visible distributed over all electrospun CA nanofibers (in the case of pH 11.0) or localized in different points of the nanofibers surface (in the case of pH 3.0), for neutral SPION media (pH 6.8, **Figure 3.36b**) SPION aggregates can be seen upon the electrospun CA nanofibers with a high homogeneity over all nanofibers. As a result of the neutral charge of the SPION

surface at pH 6.8 a better interaction with the Cellulose acetate nanofiber surface is provided and a better SPION distribution is achieved.

CA can also undergo hydrolysis which involves the removal of acetyl groups from the polymer backbone. This leads to changes in the performance of the nanofibers because the concentration of acetyl groups in the polymer can influences the SPION retention on the nanofiber. The hydrolysis reaction is strongly dependant on pH and is faster under acidic or alkaline conditions being the optimal operating range between pH 4 and pH 8.[58] Then, due to this fact, at pH 6.8 the SPION interaction with the CA nanofiber surface is most efficient and provides a more homogeneous distribution than in acid and basic media.
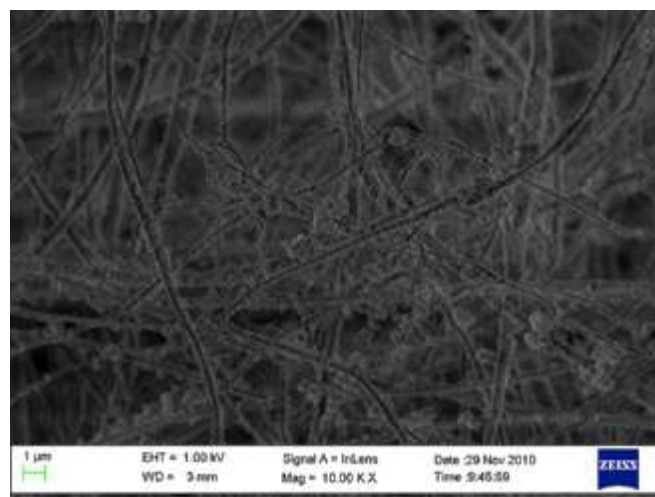
Figure 3.36. SEM micrograph of CA-SPION nanofiber composites by dipping at different pHs: 3.0 (a), 6.8 (b) and 11.0 (c) with 0.3% of SPION at 9 kV.

Finally it is worth mentioning that all of the prepared composite materials in similar way as in the SPION loaded Forager® Sponge, the adsorbent system could be magnetized. Thus, they could possibly be used in advanced separation processes inducing external magnetic field separation due to their pore structure as well as magnetism.

3.7.1.5. Characterization by Attenuated Total Reflection Fourier Transform Infrared

The IR spectrums of both electrospun CA and CA-SPION nanofibers are shown in **Figure 3.37**. Electrospun CA nanofibers showed two strong adsorption bands at 1752 cm^{-1} and 1236 cm^{-1}, which are attributed to the C=O stretching and the acetyl groups, respectively.[59,60] The adsorption band at 1635cm^{-1} was assigned to the water adsorption, and 1371 cm^{-1} and 1434 cm^{-1} were assigned to the symmetric and asymmetric vibrations of -CH$_3$.[61] Taking into account this information, it can be concluded that the electrospun nanofiber composition is cellulose acetate and no degradation is observed in presence of SPION.
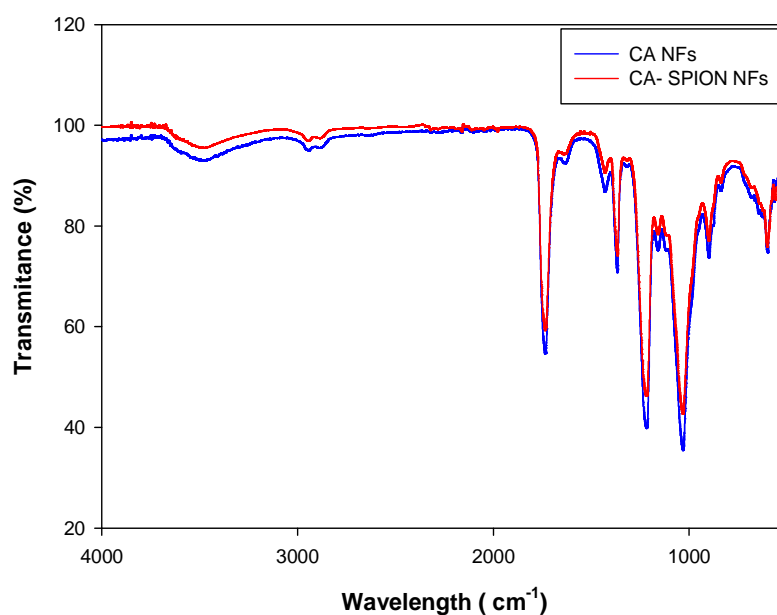
Figure 3.37. IR spectra of electrospun CA and CA-SPION nanofibers.

3.7.2. As(V) adsorption kinetic of CA-SPION nanofiber composites

Nanofiber composite of 0.3% w/v SPION and 15% w/v CA prepared both by electrospinning and by dipping at pH 6.8 with 0.3% w/v and 15% w/v electrospun CA nanofiber, were used for the As(V) adsorption in continuous mode. The equilibrium was acquired at 120 minutes of contact time in continuous mode as shows the Figure 3.38 and the adsorption capacity reaches 0.06 mmol As(V)/g SPION working with SPION loaded CA nanofibers by impregnation in comparison with 0.04 mmol As(V)/g SPION obtained with SPION loaded CA nanofibers by electrospinning. These results reveal higher accessibility of Arsenic to the electrospun CA nanofibers impregnated with SPION.
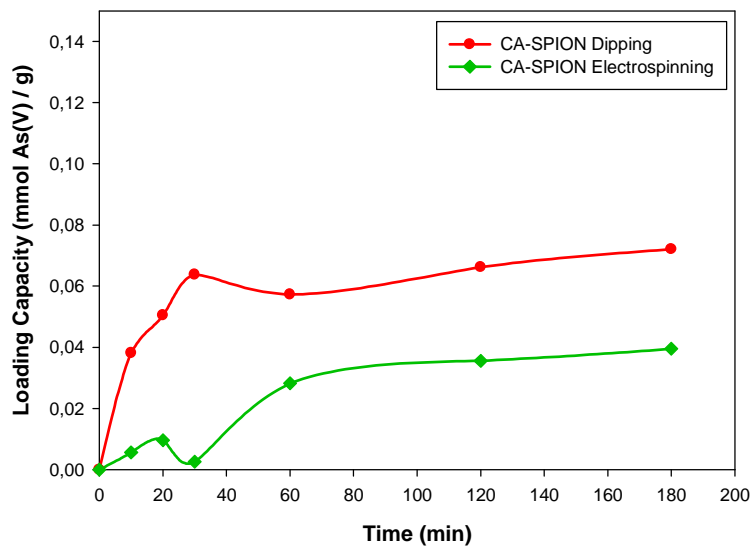
Figure 3.38. Equilibrium time study for the As(V) adsorption at pH 3.6 in electrospun and dipped CA-SPION nanofibers composites.

The present study demonstrates that CA-SPION nanoparticles composites can be potentially applied for the removal of As(V) in water treatment applications. However, considering the selected polymer (of similar chemical composition of that constituting the Forager® Sponge basic structure) and the nanometric size of CA nanofibers, higher values for the As(V) adsorption were expected due to the much higher surface area of the nanofiber composite.

On view of such poor results, another polymer was chosen in order to develop new nanofiber composites through electrospinning technique based in Polyacrylonitrile (PAN).

The selection of this polymer was based on similar advantages than those given by CA, such us the feasibility to perform this kind of nanofibers,[62] the multiple applications in the field of heavy metals removal[63,64,65,66,67,68,69,70,71,72,73] and the possibility to develop different surface modifications on produced nanofibers.[74,75,76,77,78,79,80,81,82,83,84,85,86,87]

3.8. SPION loaded HPAN nanofibers for arsenic adsorption

In this section, PAN nanofibers by electrospinning, modified PAN nanofibers (Hydrolyzed PAN (HPAN) and Ethylenediamine modified HPAN (HPAN-EDA)) and SPION loaded HPAN nanofiber were performed and characterized by different techniques. The feasibility for the As(V) removal was studied taking into account different conditions, such as the PAN concentration that affect the nanofiber size, SPION concentration, the adsorption mode (batch or continuous mode) being employed on continuous mode, in both gravity or counterflow alternatives

3.8.1. Characterization of PAN and SPION loaded modified Surface PAN nanofibers

Electrospun PAN nanofibers, modified surface PAN nanofibers and SPION loaded HPAN nanofibers were characterized using Transmission Electron Microscopy (TEM), Scanning Electron Microscopy (SEM) and Attenuated Total Reflected Fourier Transform Infrared (ATR-FTIR). Such characterization techniques were employed to understand the size of the nanofibers, to study the modification and the way the SPION is fixed on the HPAN surface as well as the efficiency of this fixation. The characterization results are outlined below.

3.8.1.1. PAN nanofibers characterization

Morphology of the electrospun PAN nanofiber performed with 10 wt% PAN solution was observed by SEM and the results are shown in Figure 3.39. The diameter of these nanofibers was rather uniform, with average values being 350 ±25 nm. The size of these fibers was comparable to those reported in the literature.[88]
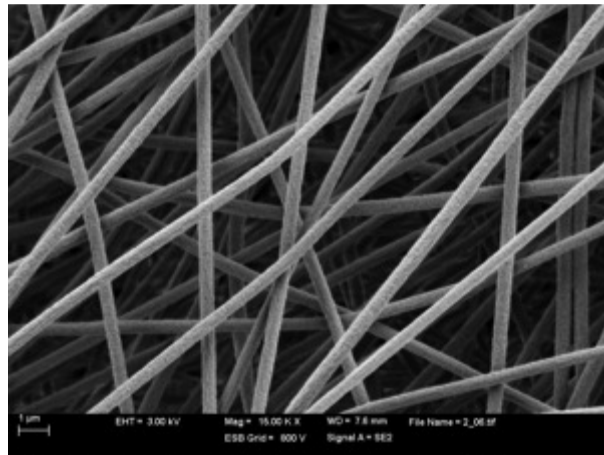
Figure 3.39. Representative SEM image of the electrospun 10 wt% PAN nanofiber mat.

Electrospun PAN nanofibers ATR-FTIR spectra is illustrated in Figure 3.40. For the electrospun PAN nanofibers, the peak at about 2918 cm^{-1} is assigned to the stretching vibration of methylene (-CH$_2$) group. The band at 2242 cm^{-1} is in correspondence with the nitrile (-CN) stretching mode. The peak at 1664 cm^{-1} corresponds with the C-C stretching mode and 1452 cm^{-1} is due to the bending vibration of methylene group.[73] In view of the principal absorption peak, electrospun PAN nanofibers present their characteristic peaks and these nanofibers can be used in the next steps of this study.
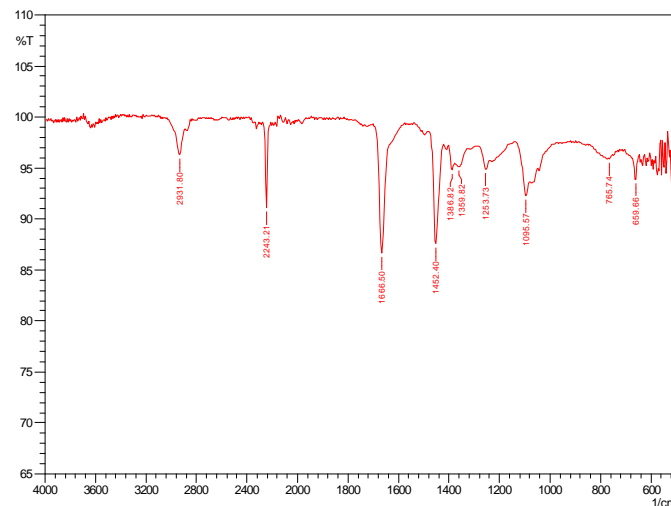
Figure 3.40. ATR-FTIR spectra of the electrospun 10 wt% PAN nanofiber mat.

3.8.1.2. Modified surface PAN nanofibers characterization

The PAN surface modification process schematized in the Equation 3.17 and described in the *Section 2.5.2.2*, was employed for the electrospun PAN modification in two

different steps in order to get different modifications. In the first step, Hydrolyzed PAN (HPAN) nanofibers are obtained and in the second step, HPAN-EDA to observe the SPION behaviour when a longer chain is introduced in the nanofiber surface.

$$(3.17)$$
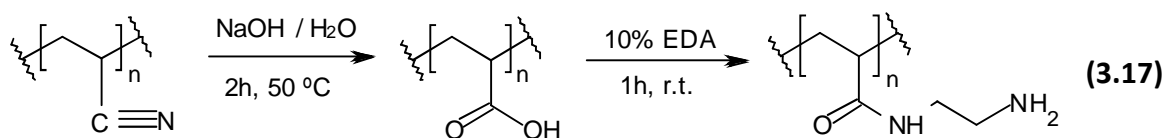
ATR-FTIR technique has been used to identify the principal groups of these two different electrospun PAN nanofiber modifications. Spectra of hydrolyzed PAN nanofibers and Surface modified EDA hydrolyzed PAN nanofibers are illustrated in Figure 3.41. [89,90,91,92]

For the HPAN nanofibers, the peak present at 3420 cm^{-1} can be due to the stretching mode of the free-hydroxyl groups. The peak at about 2933 cm^{-1} is assigned to the stretching vibration of methylene (-CH$_2$) group. The band at 2243 cm^{-1} is in correspondence with the nitrile (-CN) stretching mode due to the remaining nitrile groups after the synthesis. The region of 1780-1400 cm^{-1} in the FT-IR spectrum shows the carbonyl absorption bands with two strong peak at 1666 cm^{-1} and 1500 cm^{-1} that correspond to the stretching mode of C=O and C-O, respectively. In addition, a strong band at about 1452 cm^{-1} corresponding the bending mode of the hydroxyl (-O-H) and methylene (-CH$_2$) groups is observed.
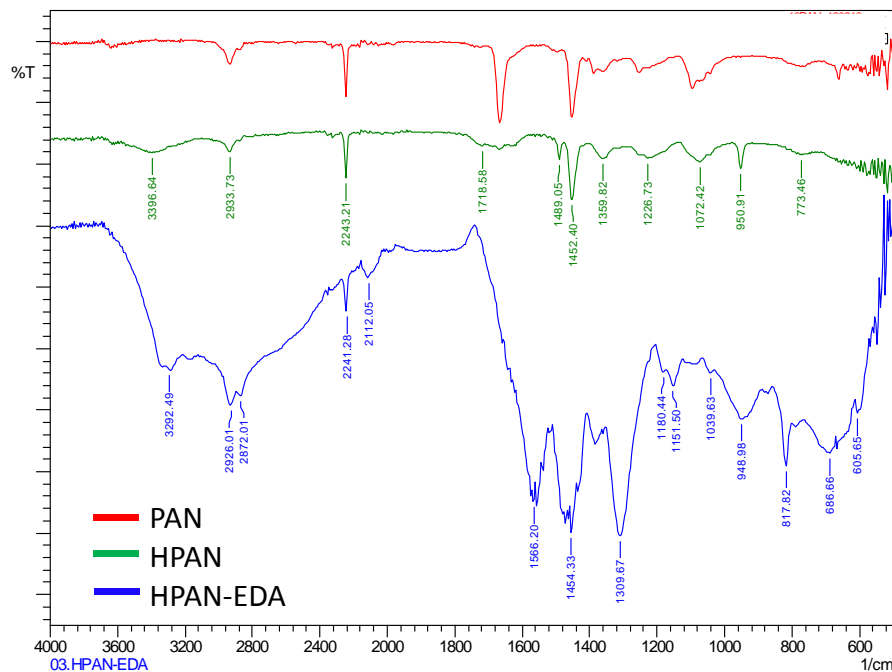
Figure 3.41. ATR-FTIR spectra of HPAN and HPAN-EDA nanofibers.

For the HPAN-EDA nanofibers, after the reaction of the PAN fiber with ethylenediamine, several bands of the amine arose widely. Amide II (N-C=O) group at 1566 cm^{-1}, amine (N-H) group bend at 1454 cm^{-1} and strong broad band in amine stretching vibrations at 3500-2000 cm^{-1}. It can be inferred that the CN groups (2241 cm^{-1}) still remain in HPAN-EDA. This result confirms that hydrolysis of the nitrile groups was not completed and nitrile groups did not participate in the amination process, only the carboxylic groups favor the amination. Spite of the nitrile peak did not totally disappear, it was significantly reduced.

Then, these types of nanofibers have been employed for the fixation of different amounts of SPION. The starting procedure of SPION fixation over the nanofibers was developed over the three types of electrospun nanofibers: PAN alone, HPAN and HPAN-EDA. This strategy was made in order to verify the previous reported results where the electrospun HPAN-EDA nanofibers show a more efficient SPION fixation due to the presence of the amide and amine groups.[74]

Through Figure 3.42 it can be observed that PAN and HPAN-EDA nanofibers present a lower fixation of SPION after 12 hours of contact with the suspension, while HPAN show a practically total fixation of the SPION when 0.03 wt% SPION suspension is used (maximum

177

quantity of SPION). This fact reveals that the presence of more carboxylic groups on the PAN nanofiber surface (HPAN) provide a corresponding ligand exchange mechanism with SPION and it produce an strong interaction that fix the SPION on HPAN nanofibers.

Figure 3.42. Electrospun PAN, HPAN and HPAN-EDA in contact with SPION suspension after 12 hours.

The fixed SPION over the electrospun PAN, HPAN and HPAN-EDA nanofiber surface using different amounts of SPION is quantified by ICP-MS after sample treatment by microwave digestion process. A comparison with the SPION initially employed assessed the effect of modification and impregnation procedure (see Table 3.14).

Table 3.14. SPION amount fixed over the nanofibers vs the initial amount (Calculated assuming that all iron is in SPION form).

Sample	Fe (mg)	SPION (mg)	Theoretical SPION (mg)
PAN –SPION	0.73	1,01	14,41
HPAN – SPION	10.12	13.98	14.41
	5.14	7.10	7.27
	2.49	3.45	3.63
	1.14	1.58	1.73
	0.53	0.73	0.86
HPAN-EDA – SPION	0.94	1.29	14.41
	0.32	0.45	7.27
	0.25	0.34	3.63
	0.12	0.16	1.73
	0.10	0.14	0.86
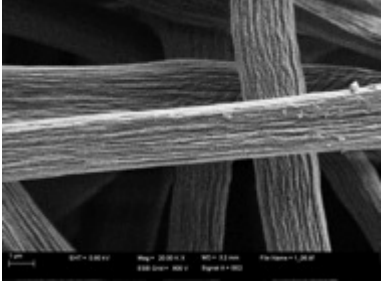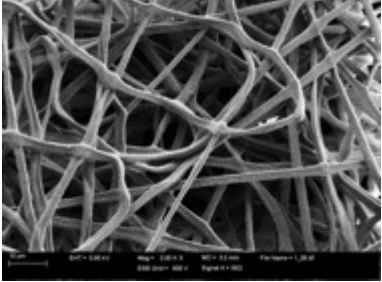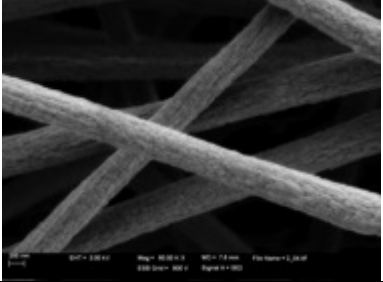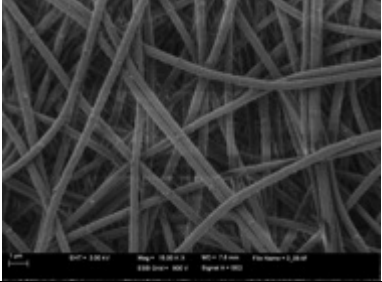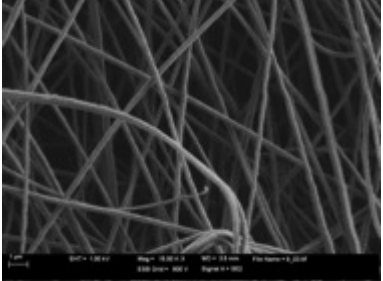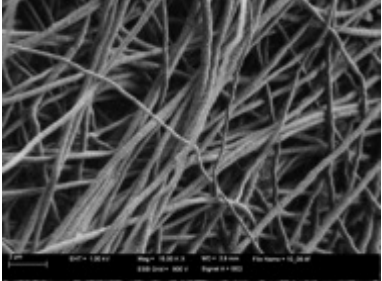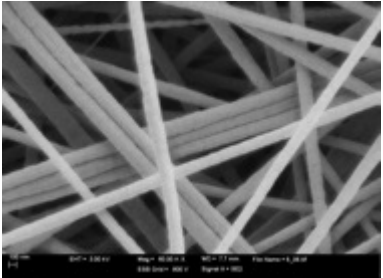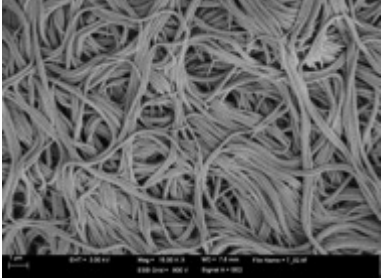
The results show that a 90-97% of the initial SPION amount is fixed over the HPAN nanofiber surface while a 6-9% is fixed over the HPAN-EDA nanofibers and a 7% in the case of the electrospun PAN nanofibers with the maximum amount of SPION. Then, similarly to 3MPA coated SPION, a strong interaction of the SPION with the HPAN carboxylic group is favor by ligand exchange process that let the fixation of the SPION over the nanofibers opposite than with primary amine groups which provides low interaction with SPION.

Therefore, hydrolysis was chosen as unique step of surface modification and HPAN nanofibers were employed for the SPION fixation to obtain the adsorbent system for water treatment applications.

>>Once the modification process is defined, different PAN concentrations were used to fabricate PAN nanofibers. By **Scanning Electron Microscope** (SEM), the optimum diameter size for the electrospun PAN nanofibers to perform the more useful nanofibers for this application was evaluated. This parameter is related with the PAN concentration in the electrospinning solution.

As the Table 3.15 shows, an increase in the PAN concentration of the electrospinning solution produces an increase in the nanofiber size, arriving to obtain microfibers when the PAN concentration is high (15 wt%). The fiber size decreases considerably when the concentration of the electrospinning solution is 10 wt% reaching up to 350 nm.

Table 3.15. Effect of PAN concentration in the nanofiber size and in the modification.

PAN wt%	PAN	HPAN	Nanofiber size
15			1.5 µm
10			350 nm
8,5			300 nm
7			200 nm

The comparison between the electrospun PAN and HPAN nanofibers shows that by decreasing the electrospun PAN nanofiber size, after the hydrolysis process, the HPAN nanofibers have a tendency to be more agglomerate, especially in the case of the 7 wt% electrospun PAN nanofibers. For this sample, SEM image shows that the nanofibers are attached all together that may results on a low water flow through the adsorbent system will be too low. The diameter size of 350 nm and the apparent porosity makes this adsorbent system more appropriate for water treatment applications.

3.8.1.3. Characterization of SPION loaded HPAN nanofibers

Transmission Electron Microscope (TEM) was used to observe the distribution of SPION on the HPAN nanofiber surface and as the Figure 3.43 shows, the SPION is distributed homogeneously over the HPAN surface but the SPION tend to be slightly aggregated limiting its adsorption capacity.
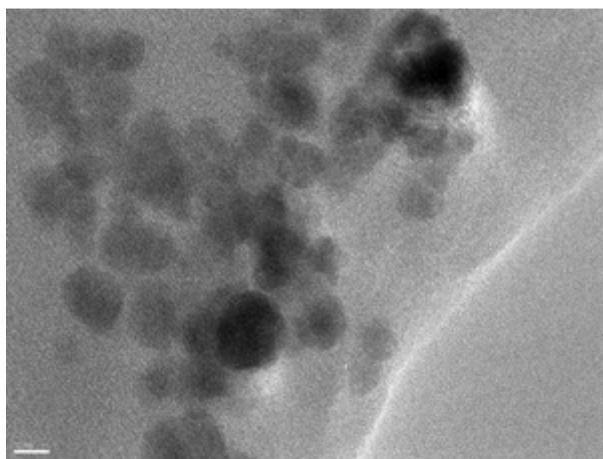
Figure 3.43. TEM image of the SPION loaded HPAN nanofibers.

3.8.2. Adsorption parameters in batch experiments

Different batch experiments were developed in order to test the adsorption capacity of the different adsorbent systems developed. The evaluation of the PAN and SPION respective concentrations on the adsorption capacity will determine the conditions for the most efficient performance. A comparison with Forager® Sponge loaded SPION and SPION suspension will show the differences in the adsorption capacity in front of previous developed adsorbent systems.

3.8.2.1. SPION effect in As(V) adsorption process

The Figure 3.44 presents the results of the As(V) adsorption capacity for the different SPION loaded HPAN nanofibers that have been prepared with different PAN concentrations in the electrospinning solution. In comparison with SPION in suspension and Forager® Sponge loaded SPION, the nanofiber based adsorbent systems reach similar or higher adsorption capacity except in the case of the SPION loaded HPAN nanofibers with nanofibers of 250nm size (HPAN 7 wt% and 7d wt%, where HPAN 7d wt% have double thickness due the

fragility of the normal one). In these cases, the low adsorption capacity can be interpreted by two additive effects, in one hand, the nanofibers agglomeration leads to a decrease in the water flow through the system and on the other hand, the SPION dispersion is lower than the obtained in the other systems.
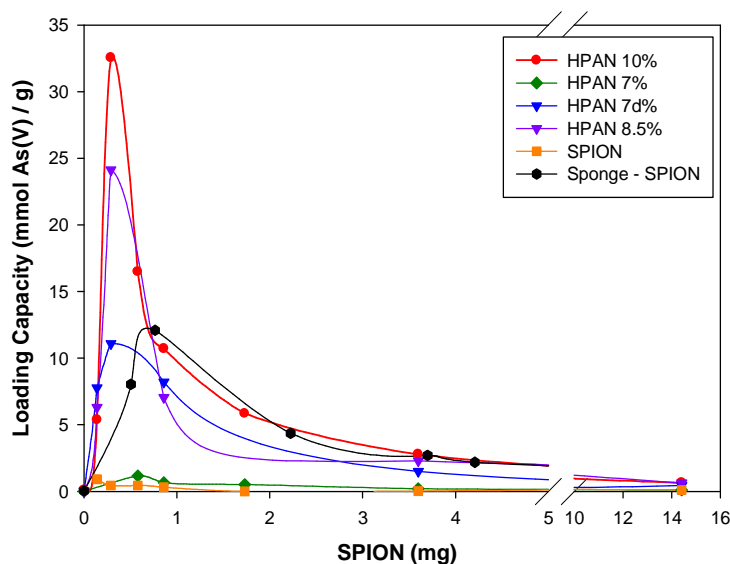
Figure 3.44. Adsorption capacity, expressed in mmol of As(V) per gram of SPION, for the different nanofiber based adsorbent systems, SPION and Forager® Sponge loaded SPION.

SPION loaded HPAN nanofibers presents a different adsorption profile if compared with that of the sponge. The new adsorbent material has a low adsorption capacity when the amount of SPION present in the HPAN nanofiber is high. Since the SPION is aggregated in the HPAN nanofiber surface and it does not let the SPION the high surface area to contact solution (increase in aggregation, decrease the specific surface area and decrease the adsorption capacity).

Additionally, when the amount of the SPION is within 0.5-4 mg per gram of HPAN nanofiber 10 wt%, the adsorption capacity increases to a very high level reaching a value of 32 mmol As(V)/g SPION, almost three times higher than the SPION loaded Forager® Sponge loaded.

3.8.2.2.   PAN effect in As(V) adsorption process

Comparing the synthesized nanofiber adsorbent systems, SPION loaded HPAN nanofibers with nanofibers of 350nm size (HPAN 10 wt%), the maximum adsorption capacity

and the optimum amount of SPION is about 2.9 mg of SPION/g of HPAN on the nanofiber surface. The lower adsorption capacity observed for nanofibers from lower HPAN concentration (Figure 3.45) is due to the nanofiber agglomeration that, as indicated before, decreases the surface contact area. When the concentration of HPAN increases above 10 wt%, then bigger size nanofibers are obtained leading to a decrease of the relative surface area that produces a decrease on the adsorption capacity.
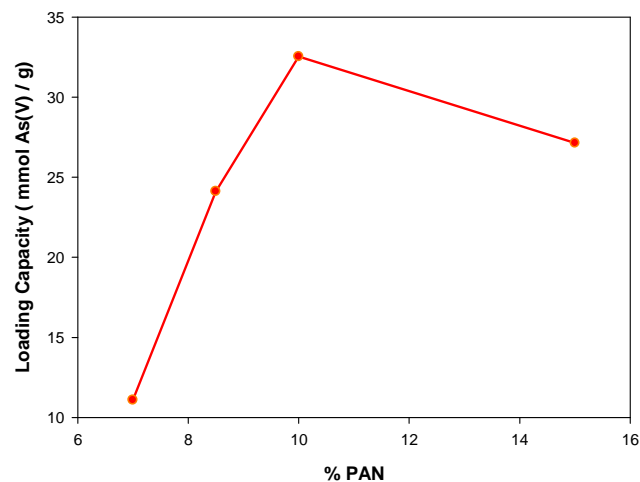
Figure 3.45. Adsorption capacity respects the PAN wt% in the electrospinning solution. SPION loading was kept at 2.9 mg SPION / g HPAN)

An interesting and important observation for the SPION loaded HPAN nanofibers with 350nm nanofiber size (HPAN 10 wt%), is their high swelling capacity, as seen in Figure 3.46, where 100 mg of SPION loaded HPAN nanofibers in contact with water solution can be absorb up to 500 ml of this solution). This behaviour reflects an important fact that can help to the adsorption process. The swelling capacity generates a higher contact surface area of the nanofibers improving their Arsenic adsorption capacity. As a consequence, a small nanofiber amount is needed for the adsorption process and it can be compressed afterwards generating a small solid waste that can be easily treated or stored.

Figure 3.46. SPION loaded HPAN nanofibers after the SPION impregnation (a) and SPION loaded HPAN nanofibers 2 hours later in a water solution.

3.8.3. Adsorption-desorption parameters in continuous mode

Once the optimum size and the maximum adsorption capacity were determined in batch mode, adsorption experiments in continuous mode were performed in order to observe the behaviour of the adsorbent system more close to conventional working conditions. For such purpose, different column sizes were employed.

3.8.3.1. As(V) adsorption in continuous mode with synthetic samples

3.8.3.1.1.   As(V) adsorption with small size columns, 10x1.0 cm

As the results show in Figure 3.47, while blank and SPION loaded HPAN nanofibers with high SPION content (144.1 mg/g HPAN) present a negligible adsorption capacity, SPION loaded HPAN nanofibers with 2.9 mg SPION/g HPAN presents an adsorption capacity of 52.6 mmol As(V) per gram of SPION, almost twice with the same sample in batch mode. In continuous mode, the efficiency of adsorption process is higher than in batch mode.
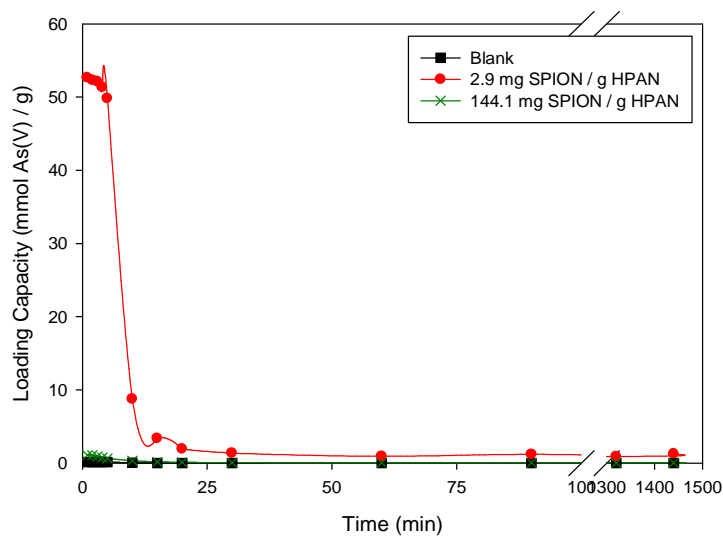
Figure 3.47. Adsorption kinetic for HPAN blank and SPION loaded HPAN.

A limitation in this adsorption procedure is due to the compression of the nanofiber composite during the adsorption process which is higher with the increase of SPION concentration and because of the fast As(V) adsorption. At 10 min, the SPION loaded HPAN nanofibers are saturated and the adsorption is finalized (Figure 3.48 shows that at 10 min the ratio between final and initial As(V) concentration is 1).
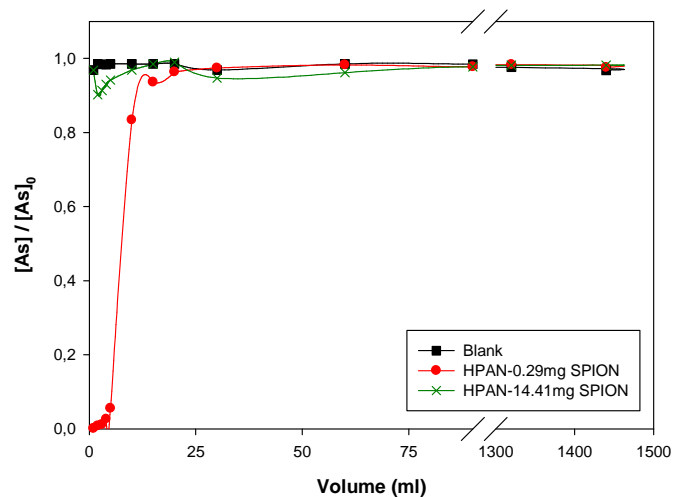
Figure 3.48. Saturation curve for As(V) adsorption with HPAN blank and SPION loaded HPAN nanofibers.

The results show that the column adsorptions are more effective than batch adsorptions. The adsorption capacity of the system is very high at the beginning showing a "flash adsorption" in a short period of time. To solve the observed compression effect, an increase

185

in the column size is carried out in order to keep the SPION loaded HPAN nanofibers swelled during all the adsorption experiment.

3.8.3.1.2. As(V) adsorption-desorption with higher size columns, 20x1.5 cm

As the results show in the Table 3.16, while the adsorption in gravity mode reach up to 20.25 mmol As(V)/g SPION, the adsorption in counterflow reaches an adsorption capacity about 63 mmol As(V)/g SPION. Then, the adsorption capacity for the system arrives to 850 mg of As(V)/g of adsorbent system. This value is expressed in form for reasons of comparison with other available adsorbent systems.

Table 3.16. Adsorption parameters in continuous mode by gravity and counterflow with 20x1.5 columns.

Parameters	Gravity	Counterflow 1	Counterflow 2
Contact time(min)	20	60	60
Adsorbed As(V) (mg)	28.4	83.9	86.1
Q max (mmol As / g SPION)	20.25	62.30	64.51
Q system (mg As / g HPAN-SPION)	317.7	830.1	851.7
Stripping solution	1.0 M HNO_3	1.0 M HNO_3	0.5 M H_3PO_4
Desorption time (min)	90	90	90
Desorbed As(V) (mg)	0.32	8.48	6.64

To highlight the dynamic behavior of the system

Figure 3.49 collects the different experiments in form of break-through curves. The counterflow experiments present a different profile than gravity experiments, producing higher efficiency for Arsenic adsorption.. It is also important to remark that HPAN-SPION nanofiber composite is not compressed during the counterflow experiment; this fact solves one problematic point in the adsorption process when smaller columns were used.
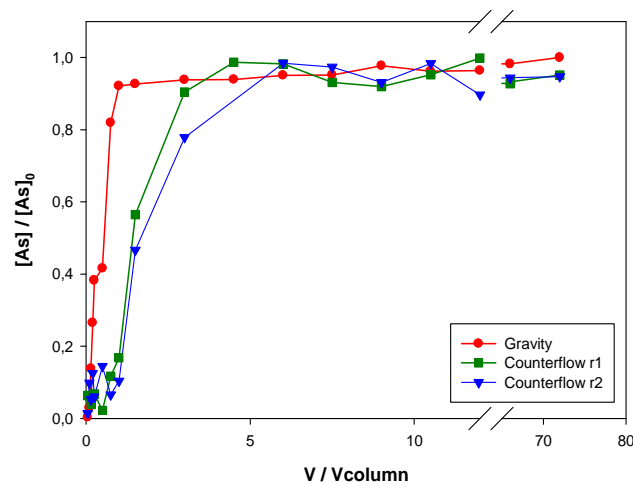
Figure 3.49. Break-through curves for As(V) adsorption by both gravity and counterflow with HPAN-SPION in 20x1.5cm columns.

3.8.3.2. As(V) adsorption-desorption in wastewater sample by counterflow mode

A comparison between an industrial wastewater sample and the synthetic solutions experiment using counterflow mode was performed to characterize the adsorbent system performance against the waste water matrix. As the Figure 3.50 shows, both experiments are similar showing small differences in the removed percentage due to the amount of potential interfering compounds that are presents in the matrix of the wastewater. During the first hour, all As(V) that is present in the wastewater and goes into the column is removed.
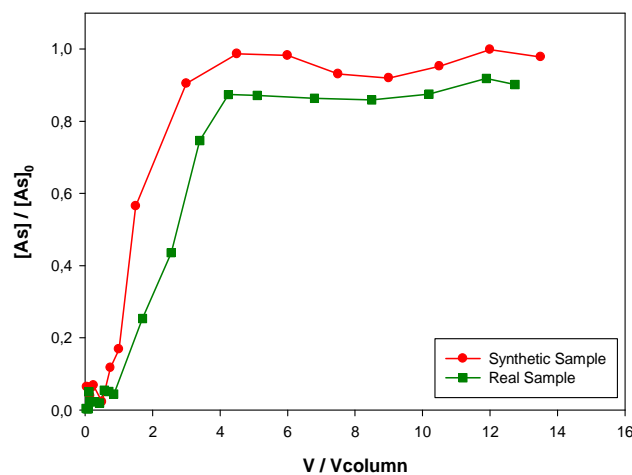
Figure 3.50. Break-through curves comparison of real and synthetic samples by counterflow in 20x1.5cm columns.

187

In the desorption step, by using 1.0 M HNO_3 and 0.5 M H_3PO_4, only 10% of the total adsorbed As(V) is desorbed. This fact suggest that the interaction between the ions from the stripping solutions and the Fe(III) ions from the SPION is not enough strong and effective to desorb the adsorbed arsenate. Surprisingly is the data of the desorption effect with phosphate ions, spite of the high affinity to Fe(III) observed on the selectivity experiments with previous adsorbent systems.

189

3.9. Summary

To sum up, five different adsorbent materials based in the presence of SPION, as the active material in the system, have been prepared, characterized and used for the study of arsenic adsorption on both non-supported nanostructured systems (SPION in suspension and 3-MPA coated SPION) and supported nanostructured systems (SPION loaded Forager® Sponge or SPION loaded CA and SPION loaded PAN nanofibers).

The results achieved show that SPION suspension, 3-MPA coated SPION and Forager® Sponge loaded SPION to present high selectivity for As(V) in presence of As(III), metal ions or interfering anions. To enhance the efficiency of As(V) adsorption Cellulose Acetate (CA) and Polyacrylonitrile (PAN) nanofibers were include.

The Table 3.17 sum up the results obtained for As(V) adsorption including the contact time and the adsorption capacity. The results let to conclude that SPION is a promising selective and fast adsorbent for As(V).

Table 3.17. Summary of the principal parameters for As(V) adsorption with all synthesized adsorbent systems.

Parameters	As(V)				
	SPION	Coated SPION	Sponge	CA	PAN
Contact Time (min)	30	10	60*	120	60
Optimum pH	3.76	3.8	3.6	3.6**	3.6**
Maximum adsorption capacity (mmol/g)	0.91	1.60	12.06	0.06	64.51

* It is assumed this contact time bear in mind the results for SPION and Coated SPION
** It is assumed this pH bear in mind the results for SPION and Coated SPION

Direct and Indirect Arsenic Speciation

Considering these results and taking into account that the adsorbent systems which have been developed are promising for arsenic removal applications, especially As(V), arsenic speciation is required to determine the selectivity level of these systems. Both direct and indirect speciation techniques through HPLC-ICP-MS and synchrotron radiation techniques respectively, were employed.

Among all adsorbent systems developed and employed to study their behaviour when treating arsenic contaminated solutions with As(III)/As(V) mixtures, 3-MPA coated SPION and SPION loaded Forager® Sponge were selected for the speciation studies. SPION suspension produce a high SPION aggregation and reduce the potential adsorption capacity of the system, therefore, SPION suspension was refused for this study. By other side, while indirect speciation studies were conducted over 3-MPA coated SPION samples, direct speciation studies were performed over SPION loaded Forager® Sponge samples. The reason to employ different separation materials was to accomplish the goal of speciation in each methodology by using the simplest material to perform corresponding techniques.

3.10. Indirect Arsenic Speciation for Functionalized SPION by HPLC-ICP-MS

In the *Section 3.3*, 3-MPA coated SPION was studied as an adsorbent system useful for water treatment applications but the principal observed problem concerns the generation of aggregates that do not let the adsorbent system to accomplish the adsorption activity in the optimum way. Anyway, and taking into account their important adsorption capacity for both arsenic species, arsenite and arsenate, speciation experiments were realized in order to determine the system feasibility to produce Arsenic species separation for their corresponding determination.

The section include results of arsenic speciation in the course of all the studied parameters in the arsenic adsorption over 3-MPA coated SPION, i.e., contact time, pH or concentration affecting the adsorption process as well as the arsenic selectivity against common interfering metal ions or anions in conditions of optimum pH.

3.10.1. Arsenic speciation and contribution for the different adsorption parameters

The starting study was developed in order to determine de retention times of each specie, arsenite and arsenate. Indirect Speciation was performed by a hyphenated system consisting of HPLC and ICP-MS and then, different reference samples were prepared in a concentration range 1-500 ppb of As(III)/As(V) mixture.

The experimental conditions were:

- An anionic chromatography Column HAMILTON PRP-X100 was used for the separation of the arsenic species in the HPLC chromatographic system.

- The mobile phase was $(NH_4)H_2PO_4$ 40 mM 1 % MeOH at pH 5.8 and a flow rate of 1.5 ml min^{-1}.

- 100μL injection volume, a maximum work pressure of 25 MPa and 10 minutes of total elution time. ICP-MS detection was performed with CCT-KED configuration, 0.90 ml min^{-1} nebulization flow.

In Figure 3.51a, it is observed that the analysis of synthetic As(III)/As(V) mixture reference samples, with known concentration in a similar matrix than the samples, produces correct results since two defined peaks can be observed for all analyzed standards, and only arsenite and arsenate are presents in the reference samples.

In order to confirm that these peaks are arsenite and arsenate, reference samples with one unique specie, arsenite or arsenate are analyzed with two objectives: determine the retention time of both species and detect which is the specie less retained in the chromatographic system. As shown by Figure 3.51b, while arsenite is the less retained specie with retention time about 3.0 min, arsenate is the more retained specie with retention time about 6.6 min. These results are in concordance with the literature.[93,94]
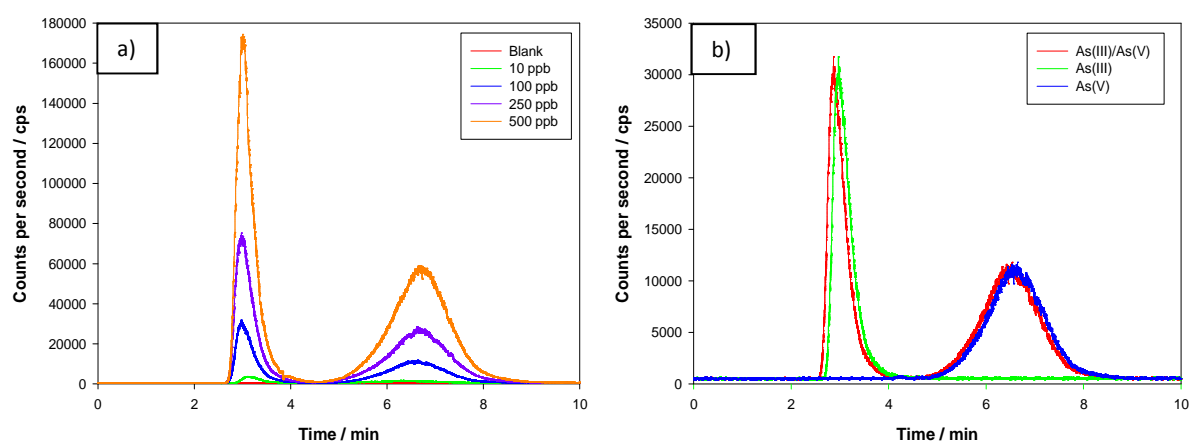
Figure 3.51. Chromatogram of 1-500 ppb references of As(III)/As(V) mixtures (a) and chromatogram of 100 ppb references of As(III), As(V) and As(III)/As(V) mixtures(b).

It is necessary to remark that chromatogram intensity depends of the optimization of ICP-MS parameters (*Methodology Chapter, Section 2.1.3.2*) which are controlled performing a calibration in each experiment but the retention times for arsenite and arsenate don't vary due to they are dependent of the chromatographic system .

Once the retention times are identified, the samples which were employed in *Section 3.3*, for the 3-MPA coated SPION with arsenite and arsenate mixtures, were here analyzed in order to study the speciation capacity of this adsorbent system.

3.10.1.1. Effect of the contact time in the adsorption process for arsenic speciation

The studied samples to determine the optimum contact time were analyzed for the speciation experiments. As shows the Figure 3.52, while arsenite specie is resolved at a retention time of 3.0 min, arsenate is resolved at 6.6 min. These values agree with those in the references chromatograms.
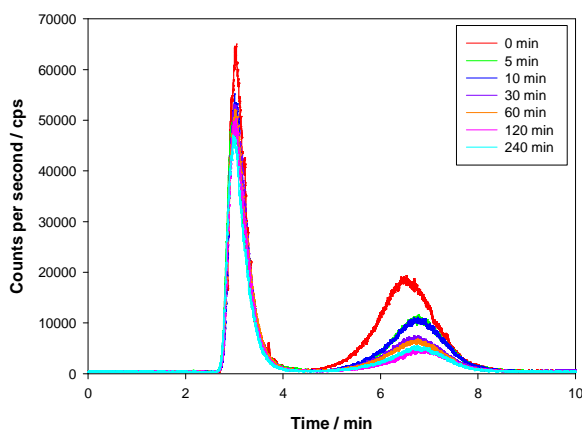
Figure 3.52. Arsenic speciation chromatograms for the contact time samples.

By the determination of the adsorbed arsenite and arsenate after the separation by HPLC, it was observed (

Figure **3.53**) that at short time (1-10 min), 32 % of adsorbed arsenic is arsenite and 68 % arsenate. At the equilibrium time (10 min), 27 % is arsenite and 73 % arsenate. Therefore, the 3-MPA coated SPION system helps to eliminate partially arsenate in presence of both arsenite and arsenate species.

Figure 3.53. Arsenite and arsenate adsorbed on the 3-MPA coated SPION at different contact time. The table shows the values of adsorption for each species in terms of concentration.

Table 3.18, illustrates satisfactory recoveries with values ranging from 93 % to 99 % achieved (Recoveries between 75 % and 125 % are admitted). Such recoveries are given by a ratio between the sum of the adsorption values for As(III) and As(V) obtained by HPLC-ICP-MS and the obtained results for the total adsorbed arsenic by ICP-MS:[95]

$$\% \textbf{ Recovery} = \frac{[\textbf{As(III)}]_{\textbf{HPCL-ICP-MS}} + [\textbf{As(V)}]_{\textbf{HPLC-ICP-MS}}}{[\textbf{As}]_{\textbf{ICP-MS}}} \times \textbf{100} \quad (\textbf{3.18})$$

Table 3.18. Correlation between total arsenic adsorbed by ICP-MS and combination of adsorbed arsenite and arsenate by HPLC-ICP-MS in the time effect experiments.

Sample	As(III) (ppb) HPLC-ICP-MS	As(V) (ppb) HPLC-ICP-MS	As(III) + As(V) HPLC-ICP-MS	As total (ppb) ICP-MS	Recovery %
initial	195.12	147.62	342.74	368.13	93
5 min	175.00	105.55	280.55	299.90	94
10 min	166.61	88.93	255.54	280.95	91
30 min	167.73	58.73	226.46	240.84	94
60 min	161.34	54.35	215.69	217.52	99
120 min	155.74	38.09	193.83	201.11	97
240 min	156.20	44.21	200.41	208.05	97

3.10.1.2. pH effect in the arsenic speciation

In this section, studied samples from experiments to test the pH effect were analyzed to determine the percentage of As(III) and As(V) that have been adsorbed for the 3-MPA coated SPION nanocomposites at the different pH values at the contact equilibrium time. Figure 3.54 shows that arsenite is resolved at a retention time about 3.0 min while arsenate is resolved at 6.6 min, similar to the references chromatograms. These values are obtained for both types of samples, before (Figure 3.54a) and after (Figure 3.54b) the arsenic adsorption process (contact time).
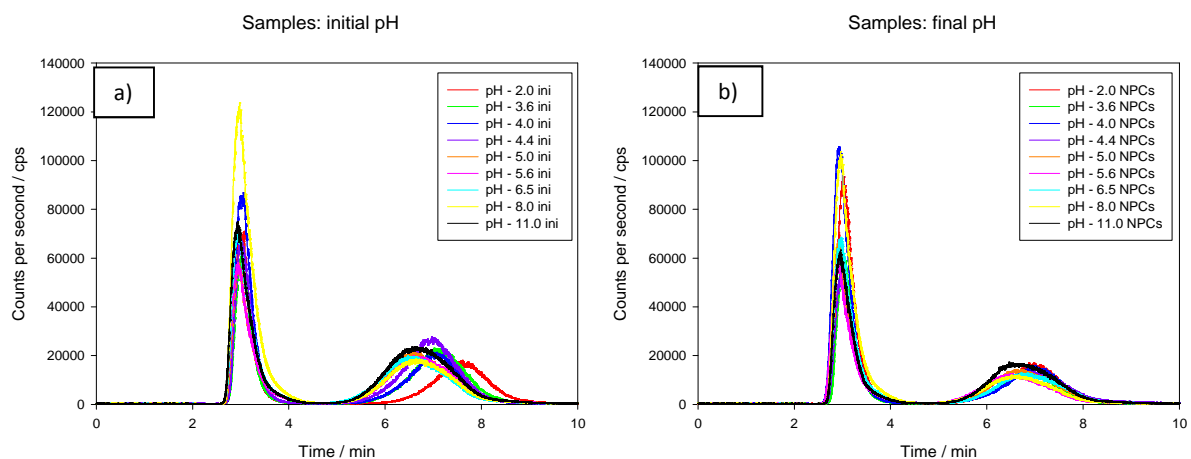
Figure 3.54. Arsenic speciation chromatograms of the initial (a) and final (equilibrium contact time) (b) samples in the pH effect experiments.

It was observed (Figure 3.55) that at extreme pHs (2.0 and 8.0-11.0 range), about 45 % of adsorbed arsenic is arsenite and 55% arsenate. These results are in concordance with previous results presented in *Section 3.3.2.2.*, which show that at extreme pH values, the adsorption capacity for As(V) is too low with a similar adsorption capacity than As(III). At pH range 3.6-6.5, adsorbed arsenic is arsenite in a percentage ranging 0-26 % and on an 84-100 % is arsenate. Therefore, the Coated SPION system helps the partial elimination of arsenate in arsenite and arsenate mixtures in the pH studied range of 3.6 to 6.5.

Figure 3.55. Arsenite and arsenate adsorbed on the 3-MPA coated SPION at different pH values.

The recoveries, as given by the Table 3.19, range 91 % to 107 %.

Table 3.19. Correlation between total arsenic adsorbed by ICP-MS and combination of adsorbed arsenite and arsenate by HPLC-ICP-MS at the pH effect experiments.

Sample	As(III) (ppb) HPLC-ICP-MS	As(V) (ppb) HPCL-ICP-MS	As(III) + As(V) HPLC-ICP-MS	As total (ppb) ICP-MS	Recovery %
pH - 2.0 initial	246.51	201.31	447.82	468.78	96
pH - 2.0 final	203.22	148.54	351.76	380.66	92
pH - 3.6 initial	204.96	228.68	433.64	435.72	100
pH - 3.6 final	201.05	142.16	343.21	348.65	98
pH - 4.0 initial	284.82	198.15	482.97	454.67	106
pH - 4.0 final	274.17	141.12	415.29	353.48	107
pH - 4.4 initial	228.67	274.43	503.10	472.30	106
pH - 4.4 final	212.95	166.85	379.80	419.35	91
pH - 5.0 initial	205.88	242.59	448.47	458.45	98
pH - 5.0 final	203.57	161.62	365.19	291.22	105
pH - 5.6 initial	218.48	221.52	440.00	420.80	105
pH - 5.6 final	218.19	136.35	354.53	345.90	102
pH - 6.5 initial	262.25	217.12	479.37	502.91	95
pH - 6.5 final	249.51	144.18	393.69	419.90	94
pH - 8.0 initial	466.40	207.54	673.94	652.30	103
pH - 8.0 final	368.59	136.04	504.63	519.50	97
pH - 11.0 initial	283.43	271.99	555.42	591.50	94
pH - 11.0 final	221.59	195.35	416.94	431.50	96

3.10.1.3. Maximum adsorption capacity effect in the arsenic speciation

The next step after arsenic maximum adsorption capacity study is the performance of speciation experiments in order to quantify arsenite and arsenate in the same samples. As shows the Figure 3.56, while arsenite is resolved at retention time about 3.0 min, arsenate is resolved in a range of 6.0 and 6.6 min. These results are verified by the references chromatograms and the spiked samples. These values are obtained for both types of samples, before (Figure 3.56a) and after (Figure 3.56b) the arsenic adsorption process.
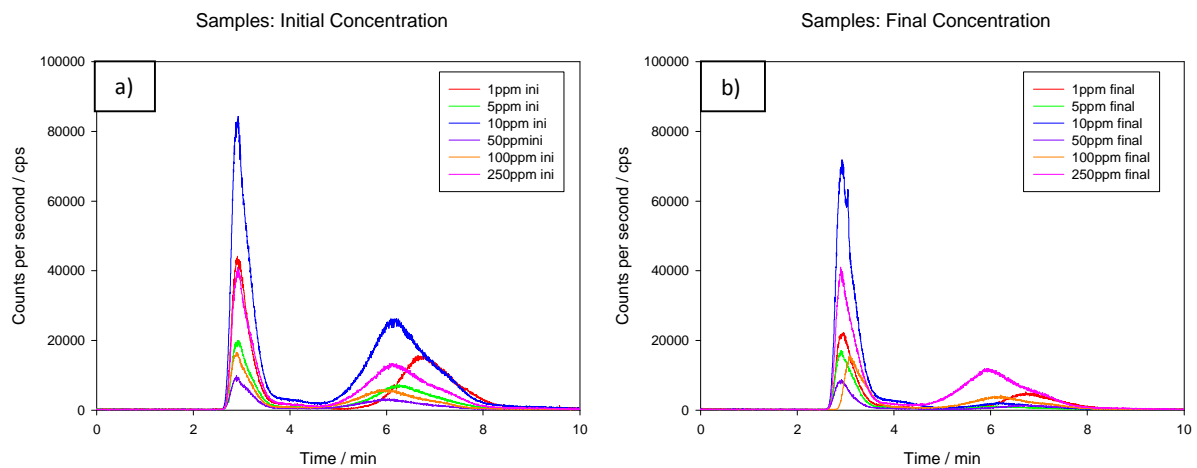
Figure 3.56. Arsenic speciation chromatogram of the initial (a) and final (b) samples for the maximum adsorption capacity experiments.

The Figure 3.57 shows that at very low concentration, 1 ppm, 41 % of adsorbed arsenic is arsenite and 59 % arsenate and at concentration range 5-250 ppm, arsenate is adsorbed in a percentage higher than 80 %.

Figure 3.57. Arsenite and arsenate adsorbed on the 3-MPA coated SPION to test different concentrations.

The recoveries, as given by the Table 3.20, were satisfactory with values ranging from 88 % to 95 %.

Table 3.20. Correlation between total arsenic adsorbed by ICP-MS and sum of adsorbed arsenite and arsenate by HPLC-ICP-MS in experiments at different concentrations.

Sample (pH 3.6)	As(III) (ppb) HPLC-ICP-MS	As(V) (ppb) HPCL-ICP-MS	As(III) + As(V) HPLC-ICP-MS	As total (ppb) ICP-MS	Recovery %
1 ppm As(III+V) initial	162,20	161,18	323,37	330,33	**98**
1 ppm As(III+V) final	48,70	81,55	130,26	134,95	**96**
5 ppm As(III+V) initial	74,08	69,09	143,18	147,09	**97**
5 ppm As(III+V) final	63,67	6,63	70,30	73,73	**95**
10 ppm As(III+V) initial	296,92	300,75	597,66	606,48	**98**
10 ppm As(III+V) final	266,02	15,65	281,67	317,26	**89**
50 ppm As(III+V) initial	36,39	33,15	69,54	70,12	**99**
50 ppm As(III+V) final	29,59	12,79	42,38	46,15	**92**
100 ppm As(III+V) initial	62,88	61,70	124,57	134,69	**92**
100 ppm As(III+V) final	57,40	42,66	100,05	103,66	**97**
250 ppm As(III+V) initial	143,81	146,27	290,09	297,94	**97**
250 ppm As(III+V) final	140,97	123,37	264,34	277,19	**95**

Therefore, taking into account these speciation results, 3-MPA coated SPION system confirms, in absence of interfering species, the adsorption system helps eliminating arsenate in presence of arsenite in contaminated solutions.

3.10.2. Arsenic speciation and contribution in the selectivity studies

In order to test selectivity results demonstrating the feasibility of this adsorbent system for possible applications in contaminated waters, different studies considering mixtures of arsenic species with other metal ions as well common anions in water were performed.

3.10.2.1. Effect of the presence of Metal Ions in the arsenic speciation

Arsenic speciation was studied in presence of metal ions. As shows the Figure 3.58, the presence of metal ions such as Cu^{2+}, Zn^{2+} or Ni^{2+} in the same solution, do not interfere the retention time of both arsenite and arsenate. Therefore, as it is expected, arsenite is resolved at retention time about 3.0 min while arsenate is resolved at 6.6 min. The references chromatograms and the spiked samples verify these results.
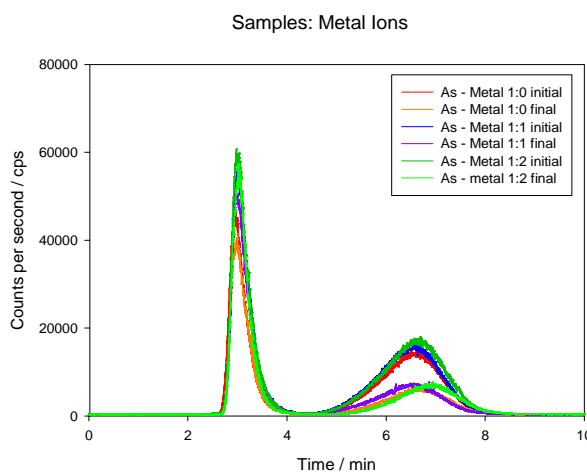
Figure 3.58. Arsenic speciation chromatograms in presence of different metal ions.

The Figure 3.59 shows that the arsenic selectivity is independent of metal ions concentration present in the contaminated solution and about 15 % of adsorbed arsenic is arsenite and the arsenate adsorbed reach to the 85 %. This is expected since the interaction with adsorbent material is anionic, and target metals are cations.

Figure 3.59. Arsenite and arsenate adsorbed on the 3-MPA coated SPION.

Like the other arsenic speciation experiments, the recoveries, as shows the Table 3.21, were satisfactory with values ranging from 95 % to 100 %.

Table 3.21. Correlation between total arsenic adsorbed by ICP-MS and combination of adsorbed arsenite and arsenate by HPLC-ICP-MS in interfering metal ions experiments.

Sample (As:Metal Ions)	As(III) (ppb) HPLC-ICP-MS	As(V) (ppb) HPCL-ICP-MS	As(III) + As(V) HPLC-ICP-MS	As total (ppb) ICP-MS	Recovery %
Ratio 1:0 initial	152.51	161.68	314.18	314.44	**100**
Ratio 1:0 final	134.58	62.48	197.06	207.05	**95**
Ratio 1:1 initial	181.54	160.35	341.89	342.69	**100**
Ratio 1:1 final	164.60	55.86	220.45	219.77	**100**
Ratio 1:2 initial	194.21	173.97	368.18	371.65	**99**
Ratio 1:2 final	176.78	69.54	246.32	255.64	**96**

3.10.2.2. Presence of interfering anions effect in the arsenic speciation

Arsenic speciation was studied in the presence of interfering anions. It must be taken into account that to perform these experiments only the samples at the optimum pH (pH 3.6 obtained in *Section 3.3.2.1*.) will be analyzed. As Figure 3.60 shows, the presence of chloride, nitrate, sulphate or phosphate do not interfere the retention time of both arsenite and arsenate like the metal ions in the previous experiment and thereby arsenite is resolved at retention time about 3.0 min while arsenate is resolved in a range of 6.0 and 6.6 min. The references chromatograms and the spiked samples verify these results. These values are

obtained for both types of samples, before (Figure 3.60a) and after (Figure 3.60b) the arsenic adsorption process.
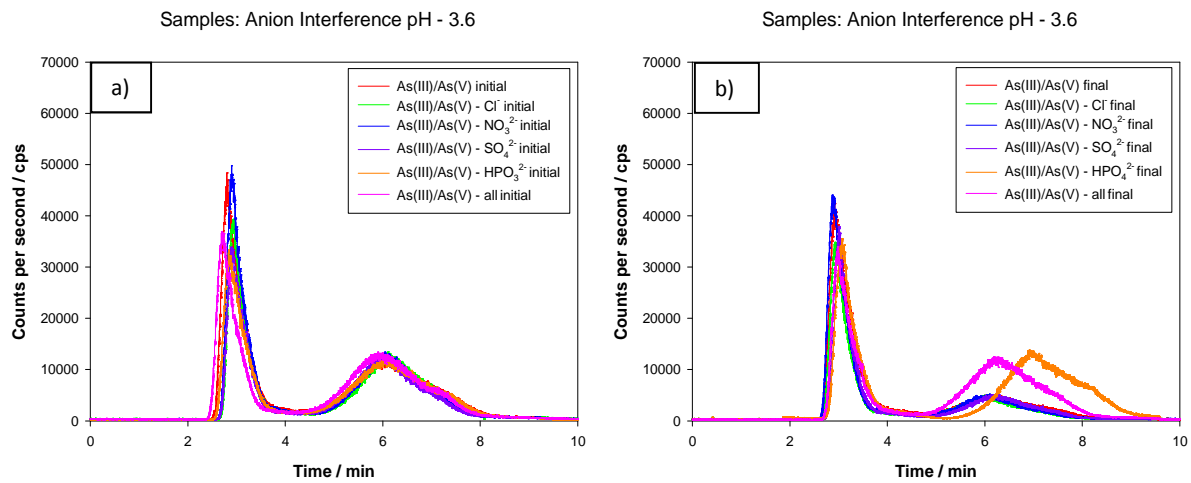
Figure 3.60. Arsenic speciation chromatograms of the initial (a) and final (b) samples for the anions interference experiments.

The Figure 3.61 confirms that without interfering anions, the adsorbent system is highly selective with a 10 % of adsorbed arsenic in form of arsenite and 90 % in form of arsenate. With the presence of interfering anions such as chloride and nitrate, which are the anions with less interference in the adsorption capacity, the arsenite adsorbed reach to 3-7 % and adsorbed arsenate up to 97-93 %. For the other interfering anions (sulphate and phosphate) the arsenite selectivity of the system decreases until 76-64 %. This fact can be derived from the affinity of the sulphate and phosphate anions which directly compete with the arsenate and not with the arsenite.

Figure 3.61. Arsenite and arsenate adsorbed on the 3-MPA coated SPION. The table shows the values of adsorption for each species in terms of concentration.

In this case, as Table 3.22 shows, the achieved recoveries are different from those obtained in previous experiments and in most of the samples. Recoveries reach 115-85 % and this recovery decrease until 70-77 % on few samples. It is noteworthy that the chromatographic system is based in anion exchange. Therefore, lower recoveries are reached in this case due to the presence of interfering anions that affect the exchange capacity of the column.

Table 3.22. Correlation between total arsenic adsorbed by ICP-MS and combination of adsorbed arsenite and arsenate by HPLC-ICP-MS in the interfering anions experiments.

Sample (As:Interf. Anions)	As(III) (ppb) HPLC-ICP-MS	As(V) (ppb) HPCL-ICP-MS	As(III) + As(V) HPLC-ICP-MS	As total (ppb) ICP-MS	Recovery %
As(III-V) initial	177.89	151.00	328.89	364.17	90
As(III-V) final	167.35	53.79	221.14	313.00	70
As - Chloride initial	123.80	145.45	269.25	284.66	95
As - Chloride final	116.12	42.82	158.94	137.57	115
As - Nitrate initial	157.56	147.35	304.91	358.67	85
As - Nitrate final	154.43	46.94	201.37	195.71	103
As - Sulphate initial	115.67	136.69	252.36	328.99	77
As - Sulphate final	50.03	119.38	169.41	169.49	71
As-phosphate initial	140.27	174.88	315.15	321.76	98
As-Phosphate final	128.15	153.25	281.40	320.53	88
As-All interf. initial	133.39	165.50	298.88	352.47	85
As-All interf. final	130.43	153.80	284.23	327.86	87

After the arsenic speciation, it can be conclude that 3-MPA coated SPION is an useful adsorbent system for the selective adsorption of As(V) in contaminated solutions with the presence of As(III), common interfering metal ions or common interfering anions, even though that this adsorbent system has the limitations described *Section 3.4*. Moreover, this indirect speciation technique has been verified as a useful technique for the arsenic speciation of this kind of liquid samples.

3.11. Direct Arsenic and Iron Speciation for SPION loaded Forager® Sponge by Synchrotron Radiation.

In this section, arsenic and iron speciation studies were performed with Forager® Sponge loaded SPION samples after the arsenic adsorption. Sponge samples loaded with different SPION amounts were used for the arsenic adsorption. On one hand, the studies at ESRF synchrotron (beamline BM25 SpLine at ESRF and beamline A1 at HASYLAB) were focused in the characterization of the arsenic adsorbed in the SPION loaded Forager® Sponge and it is expected to evaluate the arsenic speciation in order to develop a methodology to study arsenite and arsenate in the same sample. In the other hand, the studies at HASYLAB synchrotron were focused in the verification of SPION maintaining its structure during adsorption-desorption processes by studying iron speciation.

3.11.1. Arsenic speciation

Initial arsenic concentrations were analyzed by Field Portable X-Ray fluorescence equipment (FP-XRF) for both references and target samples in order to verify the Arsenic concentration level needed to perform the synchrotron experiments (Table 3.23). [96]

Table 3.23. Initial arsenic concentrations for references and samples by FP-XRF.

References [As] (mg/kg)				
$NaAsO_2$	210000±4000	Na_2HAsO_4	90000±1000	As(III)/As(V)	170000±3000
Samples [As] (mg/kg)					
As(III) 3.6 1i	410±8	As(V) 3.6 1i	9000±100	As(III+V) 3.6 1i	7400±80
As(III) 4.0 1i	420±8	As(V) 4.0 1i	6300±70	As(III+V) 4.0 1i	5100±60
As(III) 3.6 2i	420±8	As(V) 3.6 2i	10000±100	As(III+V) 3.6 2i	8000±100
As(III) 4.0 2i	420±8	As(V) 4.0 2i	7000±100	As(III+V) 4.0 2i	6300±70
As(III) 3.6 3i	500±9	As(V) 3.6 3i	11000±100	As(III+V) 3.6 3i	9000±100
As(III) 4.0 3i	380±8	As(V) 4.0 3i	9000±100	As(III+V) 4.0 3i	8000±100
As(III) 3.6 1iM	350±8	As(V) 3.6 1iM	9000±100	As(III+V) 3.6 1iM	6300±70

Sample concentration is lower than references concentration. This fact is due to the process of producing both references and target samples.

3.11.1.1. Arsenic reference compounds.

The arsenic K near-edge spectra for pure arsenic reference compounds of arsenite ($NaAsO_2$), arsenate (Na_2HAsO_4) and As(III)/As(V) mixture are shown in Figure 3.62. As expected, a shift of the edge position to higher energies becomes as arsenic is more oxidized, while k near-edge for As(III) is 11879.5 eV, k near-edge for As(V) is 11882.4 eV.
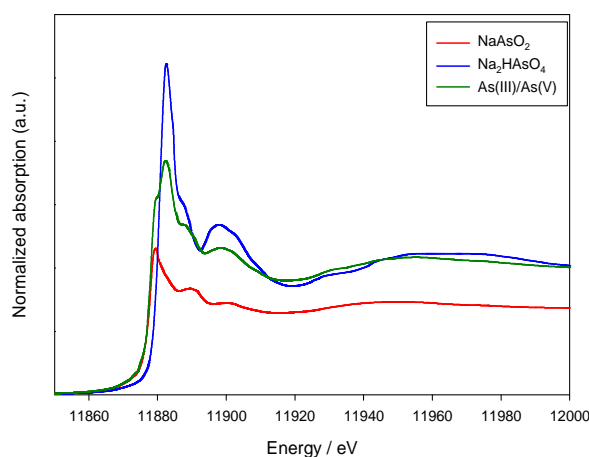
Figure 3.62. As K-edge XANES spectra of three reference compounds.

3.11.1.2. Arsenic adsorbed over Forager® Sponge loaded SPION.

The direct comparison of XANES spectra for arsenic references and arsenic adsorbed over SPION loaded Forager® Sponge samples was made. The first study was realised with only unique species at pH about 3.6 (optimum adsorption pH). The results show that the As(V) spectra were similar to the reference compound (Figure 3.63a) but As(III) spectra were different (Figure 3.63b). This difference was due to the interaction between Fe(III) of SPION and As(III) that produce a slight modifications in the spectra.[97]
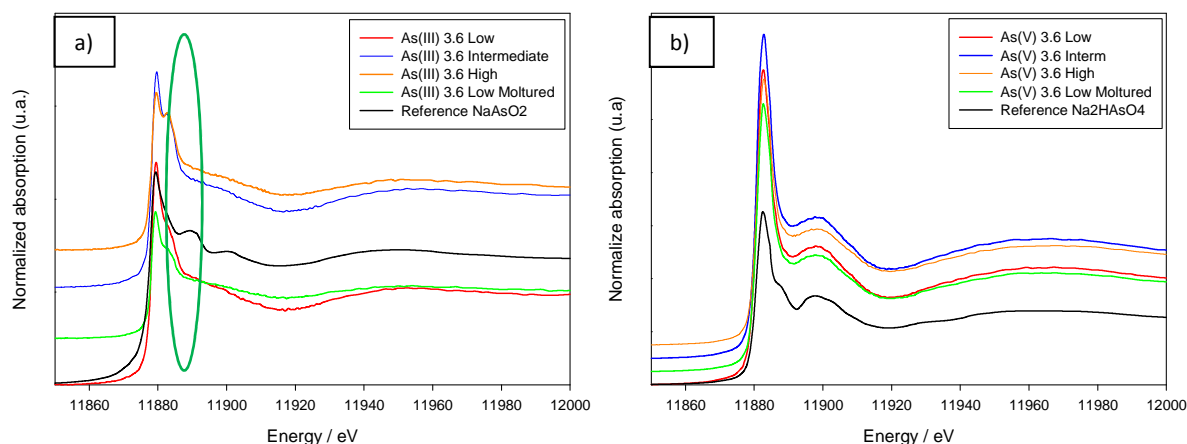
Figure 3.63. As K-edge XANES spectra for the As(V) (a) and As(III) (b) adsorption over Forager® Sponge loaded SPION. The green circle remarks the differences between As(III) references and samples.

The effect in the adsorption process of the presence of the two species of arsenic was studied by direct observation, as shown in Figure 3.64. All samples present same k near-edge, a fact indicating the presence of major component of Arsenic species in all samples. The comparison of XANES spectra for arsenic references and samples shows a negligible contribution of arsenite reference spectrum to the target samples that present spectra very similar to that of arsenate reference.
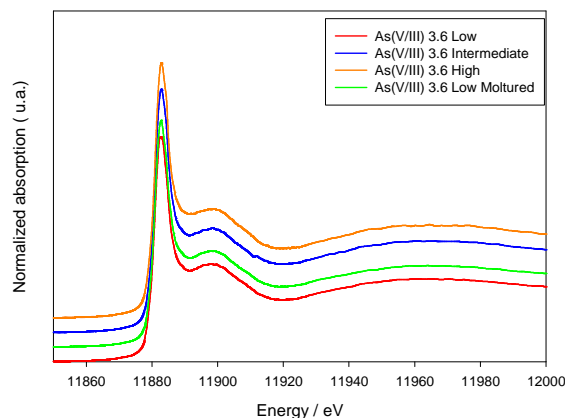
Figure 3.64. As K-edge XANES spectra for the As(III)/As(V) mixture adsorbed on SPION loaded Forager® Sponge.

Then, the effect of arsenic species in the adsorption process was quantitatively analysed by applying Principal Analysis Components (PCA) and linear combination fit using the software package XANES dactyloscope, as shown by the Figure 3.65, to ascertain the contribution of each Arsenic reference specie.

208
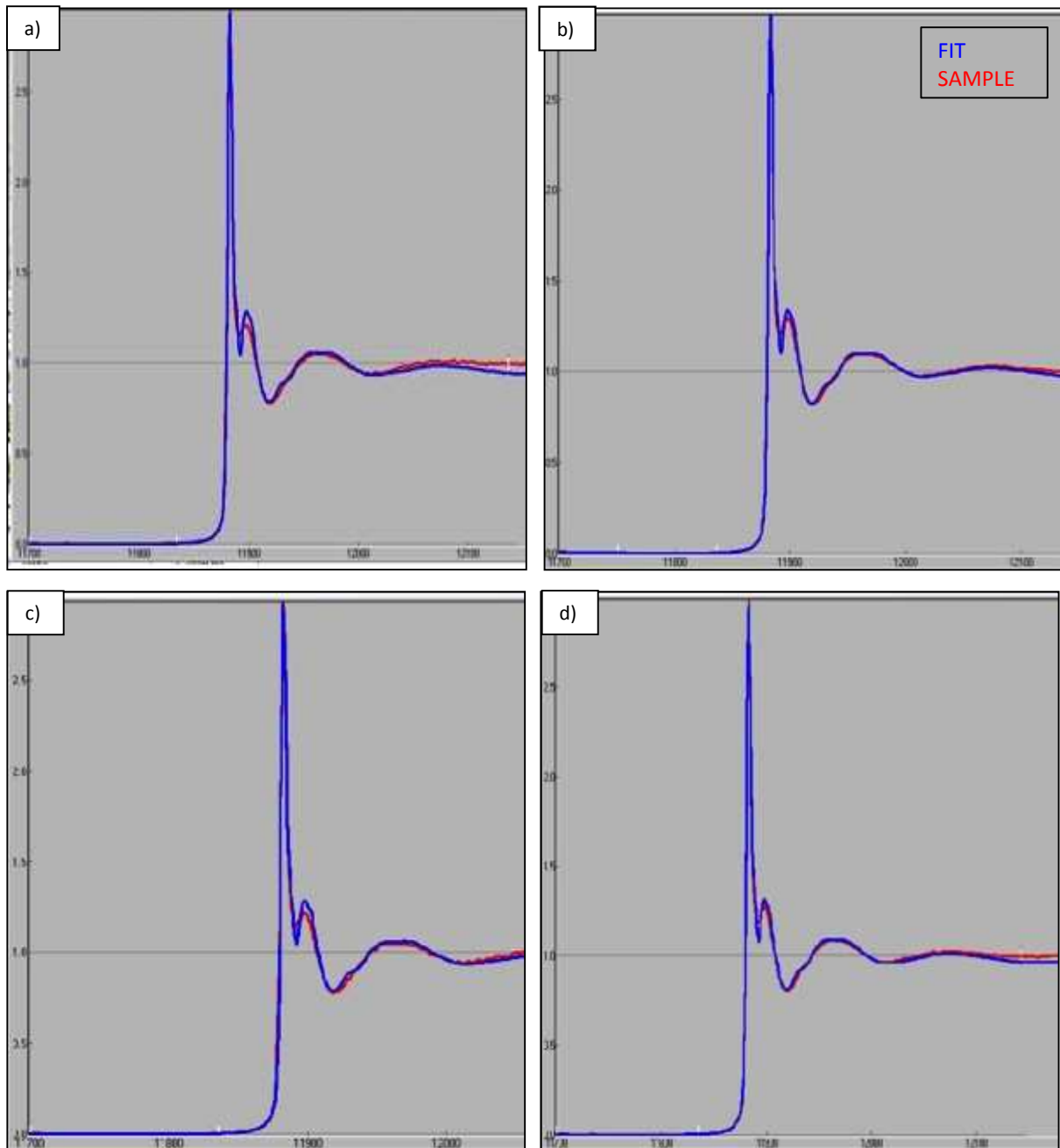
Figure 3.65. Fitting for the SPION loaded Forager® Sponge with low SPION concentration at different pHs, 2.0 (a), 3.6 (b), 5.6 (c) and 3.6 with previous milled sample (d).

The results confirm, for all analysed samples (SPION loaded Forager® Sponge with low SPION concentration at different pHs), that arsenate species is predominant reaching until 97 % (Figure 3.66). The sum of both species is 100±2 %. Then, arsenate is easily removed from the target solutions with this adsorbent system.

Figure 3.66. Total arsenite and arsenate distribution in Forager® Sponge loaded SPION normalized to percentage.

As speciation distribution shows, As(V) is easily removed of the target solutions with this adsorbent system and the analysis of these synthetic samples have validated the data analysis to be applied in real samples.

3.11.2. Iron speciation

As in the arsenic speciation experiments, initial iron concentrations were analyzed by Field Portable X-Ray fluorescence equipment (FP-XRF) for both references and samples in order to confirm the Fe concentration level to perform successfully the synchrotron experiments (

Table 3.24). [96]

Table 3.24. Initial iron concentrations for references and samples by FP-XRF.

References [Fe] (mg/kg)					
FeCl$_3$	32000±500	**FeCl$_2$**	41000±600	**FeCl$_3$/FeCl$_2$**	48000±700
SPION Standard	65000±700	**SPION-As(III)**	67000±700	**SPION-As(V)**	71000±800
Samples [Fe] (mg/kg)					
As(III) 3.6 1i	4400±70	**As(V) 3.6 1i**	3900±60	**As(III+V) 3.6 1i**	4300±70
As(III) 4.0 1i	4200±70	**As(V) 4.0 1i**	3800±60	**As(III+V) 4.0 1i**	5200±80
As(III) 3.6 2i	5800±90	**As(V) 3.6 2i**	7000±100	**As(III+V) 3.6 2i**	7900±100
As(III) 4.0 2i	5600±80	**As(V) 4.0 2i**	8000±100	**As(III+V) 4.0 2i**	9000±100
As(III) 3.6 3i	11000±100	**As(V) 3.6 3i**	10000±100	**As(III+V) 3.6 3i**	14000±200
As(III) 4.0 3i	8000±100	**As(V) 4.0 3i**	13000±200	**As(III+V) 4.0 3i**	9000±100
As(III) 3.6 1iM	3900±60	**As(V) 3.6 1iM**	4200±70	**As(III+V) 3.6 1iM**	4100±60

Sample concentration is lower than references concentration. This fact is due to the way of obtaining both standard (polyethylene impregnated with iron solution salts to a reasonable concentration level) and target samples (depending on the SPION loading process). For this study, additional reference samples are used; SPION references were used in order to have knowledge about its response in front of synchrotron radiation.

3.11.2.1. Iron reference compounds.

The iron K near-edge spectra for pure iron reference compounds of Fe^{3+} ($FeCl_3.6H_2O$), Fe^{2+} ($FeCl_2.4H_2O$), Fe^{3+}/Fe^{2+} mixture and SPION (Fe_3O_4) standard and SPION in presence of the different inorganic arsenic species are shown in Figure 3.67. A shift of the edge position to higher energies becomes as iron is more oxidized. This should appear in the comparison of $FeCl_3.6H_2O$ and $FeCl_2.4H_2O$. In this case, the XANES spectra shows, both k near-edges reach to 7136.0 eV indicating that $FeCl_2$ has suffered oxidation during the sample preparation and analysis process. On the other hand, for SPION standards the near-edge position is 7133.8 eV while k near-edge for iron salts is 7136.0 eV. This is due to the presence of Fe(II) in SPION that leads to lower value the edge energy
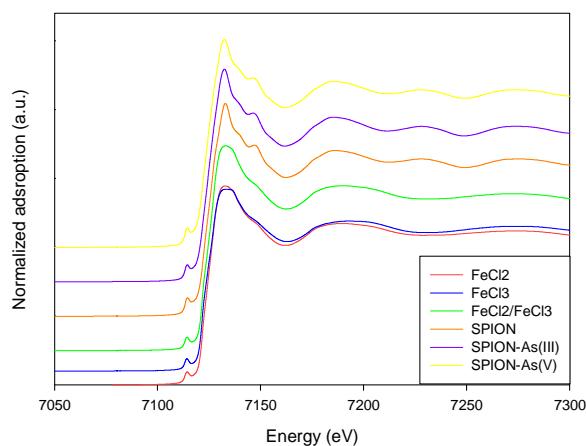
Figure 3.67. Fe XANES spectra of different reference compounds

Then, only the SPION standards are going to be used for the comparison with samples in the iron speciation.

3.11.2.2. Iron speciation in SPION from SPION loaded Forager® Sponge.

The direct comparison of XANES spectra for SPION standards and SPION loaded Forager® Sponge samples was made. This direct comparison, see Figure 3.68, determine that the SPION keeps the structure in the adsorption process in all cases, independently of the adsorbed species, As(III), As(V) or a mixture of both species.
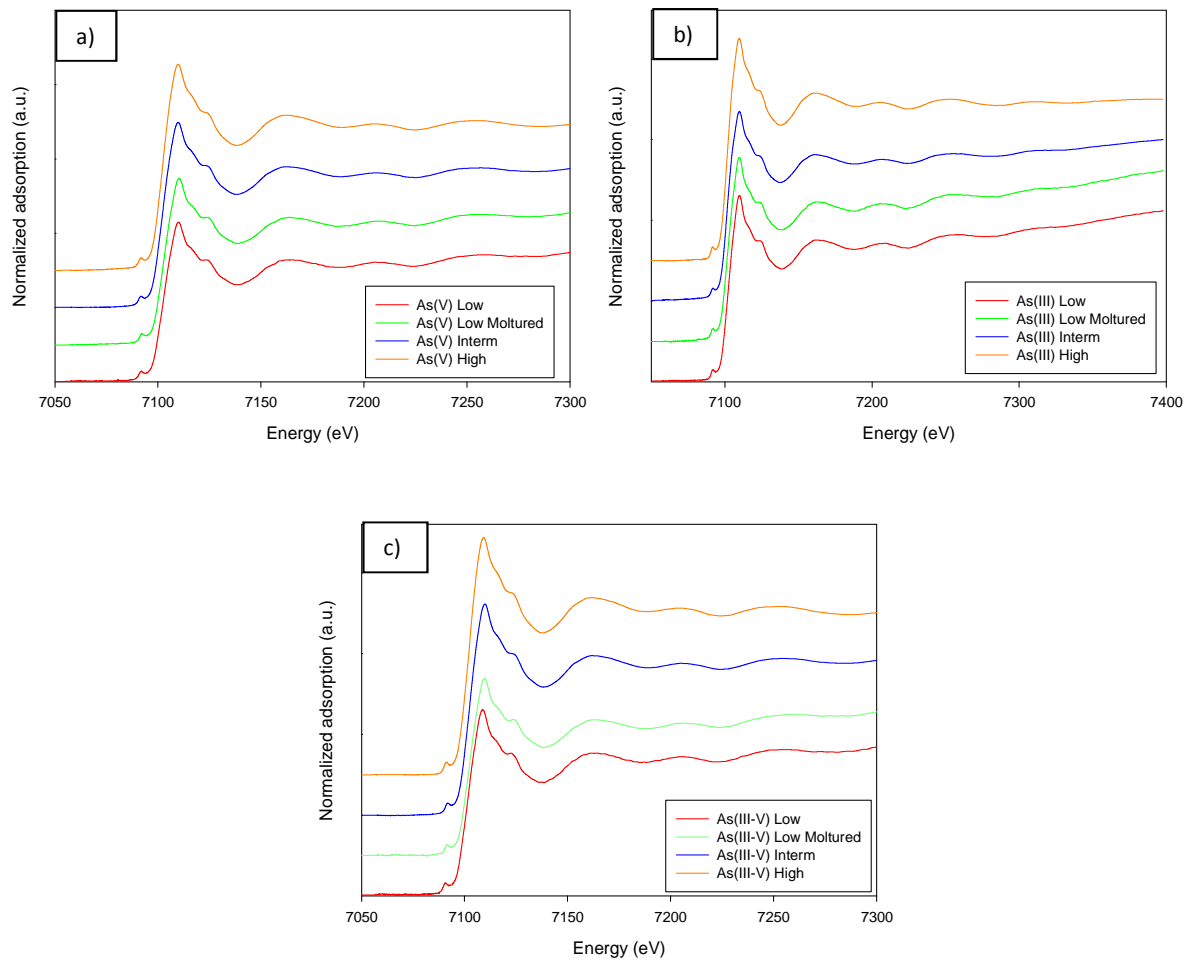
Figure 3.68. Fe k-edge XANES spectra for Forager® Sponge loaded SPION samples for each arsenic adsorption process: As(III) (a), As(V) (b) and As(III)/As(V) mixture (c).

Considering the obtained results, XANES was successfully applied as a method to direct characterization of the influence of arsenic speciation in water thanks to the sensitivity of the beamlines BM25 (ESRF) and A1 (HASYLAB).

References

1. Lafferty, B.K., Loeppert, R.H. Methyl arsenic adsorption and desorption behavior on iron oxides. *Environmental Science and Technology*, **2005**, *39*, 2120-2127.

2. Duxbury, J. M., A. B. Mayer, J. G. Lauren and N. Hassan. Food chain aspects of arsenic contamination in Bangladesh. *Journal of Environmental Science and Health, Part A*, **2003**, *38*, 61-69.

3. Fendorf, S., Eick, M. J., Grossl, P., Sparks, D. L. Arsenate and Chromate Retention Mechanisms on Goethite. 1. Surface Structure. *Environmental Science and Technology*, **1997**, *31 (2)*, 315-320

4. Manning, B. A., Fendorf, S. E., Goldberg, S. Surface Structures and Stability of Arsenic(III) on Goethite: Spectroscopic Evidence for Inner-Sphere Complexes. *Environmental Science and Technology,* **1998**, *32 (16)*, 2383-2388.

5. Waychunas, G. A., Rea, B. A., Fuller, C. C., Davis, J. A. Surface chemistry of ferrihydrite: Part 2. Kinetics of arsenate adsorption and Coprecipitation. *Geochimica et Cosmochimica Acta*, **1993**, *57*, 2251-2269.

6. Sun, X., Doner, H. E. An investigation of arsenate and arsenite bonding structures on goethite by FTIR. *Soil Science*, **1996**, *161*, 865-872.

7. Van der Hoek, E. E., Bonouvrie, P. A.; Comans, R. N. J. Sorption of As and Se on mineral components of fly ash: relevance for the leaching processes. *Applied Geochemistry*, **1994**, *9*, 403-412.

8. Grossl, P.; Eick, M. J.; Sparks, D. L.; Goldberg, S.; Ainsworth, C. C. Arsenate and Chromate Retention Mechanisms on Goethite. 2. Kinetic Evaluation Using a Pressure-Jump Relaxation Technique. *Environmental Science and Technology,* **1997**, *31 (2)*, 321-326.

9. Haron, M. J.; Wan Yunus, W. M. Z.; Yong, N. L.; Tokunaga, S. Sorption of arsenate and arsenate anions by iron(III)-poly(hydroxamic acid) complex. Chemosphere 1999, 39 (14), 2459-2466.

10. Khaodhiar, S.; Azizian, M. F.; Osathapahn, K.; Nelson, P., Water, O. Copper, chromium, and arsenic adsorption and equilibrium modeling in an iron-oxide-coated sand, background electrolyte system. *Water Air and Soil Pollution*, **2000**, *119 (1-4)*, 105-120.

11. Jain, A., and R. H. Loeppert. Effect of competing anions on the adsorption of arsenate and arsenite by ferrihydrite. *Journal of Environmental Quality*, **2000**, *29*, 1422-1430.

12. Loring, J.S., Sandström, M.H., Norén, K., Persson, P. Rethinking Arsenate coordination at the surface of goethite. *Chemical European Journal*, **2009**, *15*, 5063-5072.

13. Manceau, A. The mechanism of anion adsorption on iron-oxides- evidence for the bonding of arsenate tetrahedra on free Fe(O,OH)(6) edges, *Geochimica and Cosmochimica Acta*, **1995**, *59 (17)*, 3647-3653.

14. Petrone, L. Molecular surface chemistry in marine bioadhesion. *Advances in Colloid and Interface Science*, **2013**, *195-196*, 1-18.

15. Sun, X., Doner, H.E. An investigation of arsenate and arsenite bonding structures on goethite by FTIR. *Soil Science*, **1996**, *161 (12)*, 865–872.

16. Sherman, D.M., Randall, S.R. Surface complexation of arsenic(V) to iron(III) (hydr)oxides: structural mechanism from ab initio molecular geometries and EXAFS spectroscopy, *Geochimica and Cosmochimica Acta,* **2003**, *67 (22)*, 575-580.

17. Lumsdon, D.G., Fraser, A.R., Russel, J.D., Livesey, N.T. New infrared band assigments for the arsenate ion adsorbed on synthetic goethite (α-FeOOH), *Soil Science*, **1984**, *35*, 381–386.

18. Loeppert, R.H., Jain, A., El-Haleem, M.A.A., Biswas, B.K. Quantity and speciation of arsenic in soils by chemical extraction. *ACS Symposium Series*, **2003**, *835*, 42-56.

19. Jain, A., Raven, K.P., and Loeppert, R. H. Arsenite and arsenate adsorption on ferrihydrite: Surface charge reduction and net OH- release stoichiometry. *Environmental Science and Technology*, **1999**, *33*, 1179-1184.

20. Raven, K. P., A. Jain, and R. H. Loeppert. Arsenite and arsenate adsorption on ferrihydrite: kinetics, equilibrium, and adsorption envelopes. *Environmental Science and Technology*, **1998**, *32*, 344-349.

21. Shipley, H.J., Yean, S., Kan, A.T., Tomson, M.B. Adsorption of arsenic to magnetite nanoparticles: effect of particles concentration, pH, ionic strength and temperature. *Environmental Toxicology and Chemistry*, **2009**, *28* (3), 509–515.

22. Uheida, A., Salazar-Alvarez, G., Björkman, E., Zhang, Y., Muhammed, M. Fe_3O_4 and γ-Fe_2O_3 nanoparticles for the adsorption of Co^{2+} from aqueous solution. *Journal of Colloid Interface Science*, **2006**, *298*, 501-507.

23. Chin, A.B., Yacob, I.I. Synthesis and characterization of magnetic iron oxides nanoparticles via w/o microemulsions and Massart´s procedure. *Journal of Materials Processing Technology*, **2007**, *191*, 235-237.

24. JCPDS, *International Center for Power Diffraction Data: Swarthmore*, PA, Card **No, 19-629** (1989).

25. Fei, L., Peijiang, C., Huairuo, Z., Jifa, T., Congwen, X., Chengmin, S., Li, J., Gao, H. Novel nanopyramid arrays of magnetite. *Advanced Materials,* **2005**, *17*, 1893–1897.

26. García-Cerda, L.A., Rodríguez-Fernández, O.S., Betancourt-Galindo, R., Saldívar-Guerrero, R. Síntesis y propiedades de ferrofluidos de magnetita. *Superficies y Vacio*, **2003**, *16 (1)*, 28-31.

27. Han, C., Zhao, D., Deng, C., Hu, K. A facile hydrothermal synthesis of porous magnetite microspheres. Materials Letters, **2012**, *70*, 70–72.

28. Puigdomemech, I. Medusa, Royal Institut of Technology, Estocolm, (www.inorg.kth.se). Software, **1999**.

29. Santoyo-Salazar, J., Castellanos-Roman, M.A., Beatriz-Gómez, L. Structural and magnetic domains characterization of magnetic nanoproperties. *Material Science Engineering, C*, **2007**, *27*, 1317-1320.

30. Muñoz, J.A., Valiente, M., Gonzalo, A. Adsorción y Separación de Especies de Arsénico sobre material de Esponja con Selectividad y propiedades cinéticas mejoradas. Tabajo de Investigacion, Universitat Autònoma de Barcelona, **Diciembre 2001**.

31. Yan-Chu, H.. Arsenic in the environment. Part I: cycling and Characterization. J.O. Nriagu (Ed), John Wiley & Sons, New Cork, **1994**, p.17.

32. Jia, Y., Xu, L., Fang, Z., Demopoulos, G.P. Observation of Surface Precipitation of Arsenate on Ferrihydrite. *Environmental Science and Technol*ogy, **2006**, *40*, 3248-3252.

33. Muñoz, J.A., Gonzalo, A., Valiente, M. Arsenic adsorption by Fe(III)-loaded open-celled cellulose sponge. Thermodynamic and selectivity aspects. *Environmental Science and Technol*ogy, **2002**, *36*, 3405-3411.

34. Rau, I., Gonzalo, A., Valiente, M. Arsenic(V) adsorption by immobilized iron mediation. Modeling of the adsorption process and influence of interfering anions. *Reactive & Functional Polymers*, **2003**, *54*, 85-94.

35. Mohan, D., Pittman, C.U. Arsenic removal from water/wastewater using adsorbents - A critical review. *Journal of Hazardous Materials*, **2007**, *142*, 1-53.

36. Bruce, I.J., Taylor, J., Todd, M., Davies, M.J., Borioni, E., Sangregorio, C., Sen, T. Synthesis, characterisation and application of silica-magnetite nanocomposites. *Journal of Magnetism and Magnetic Materials*, **2004**, *284*, 145–160.

37. Nyquist, R.A., Kagel, R.O. Infrared spectra of ınorganic compounds. Academic Press, New York, **1971**.

38. Wei, S., Zhu Y., Zhang, Y., Xu, J. Preparation and characterization of hyperbranched aromatic polyamides/Fe$_3$O$_4$ magnetic nanocomposite. *Reactive and Functional Polymers*, **2007**, *66*, 1272–1277.

39. Yun, T.L., Kyoungja, W. Preparation of Water-dispersible and Biocompatible Iron Oxide Nanoparticles for MRI Agent. *IEE Transactions on nanotechnology*, **2008**, *7 (2)*, 111-114.

40. Rossi, L.M., Vono, L.L.R., Silva, F.P., Kiyohar, P.K., Duarte, E.L., Matos, J.R. A magnetically recoverable scavenger for palladium based on thiol-modified magnetite nanoparticles. *Applied Catalysis, A*., **2007**, *330*, 139-144.

41. Sivaraman, D. Synthesis and Characterization of thiol-functionalized chitosan based adsorbents for arsenic removal from water. *Doctoral Thesis*, **2004**.

42. Bellino, M.G., Calvo, E.J., Gordillo, G. Adsorption kinetics of charged thiol son gold nanoparticles. *Physical Chemistry Chemical Physics*, **2004**, *6*, 424-428.

43. De Abreu, R. T., Barros, F.C.F., Raulino, G.S.C., Moura, C.P., do Nascimento, R.F. Metal Ions Removal From Synthetic Solutions and Produced Water Using Activated Zeolite. *International Journal of Civil & Environmental Engineering*, **2012**, *12 (3)*, 20-25.

44. Sillén, L.G, Martell, A.E. Stability Constants, Special publications No.17, The chemical society, London, **1964**.

45. Arribas, J.S., Burriel, F., Méndez, J.H., Conde, F.L. Química Analítica Cualitativa, Ed. Paraninfo, **2006**.

46. Chanda, M., O'Driscoll, K.F., Rempel, G.L. Ligand exchange sorption of arsenate and arsenite anions by chelating resins in ferric ion form. *Reactive Polymers*, **1988**, *7*, 251-261.

47. Yoshida, I., Ueno, K., Kobayashi, H. Selective separation of arsenic(III) and (V) ions ferric complex of chelating ion-exchange resin. *Separation Science and Technology*, **1978**, *13 (2)*, 173-184.

48. Matsunaga, M., Yokoyama, T., Eldridge, R.J., Bolto, B.A. Adsorption characteristics of arsenic(III) and arsenic(V) on iron chelating resin having lysine – Nα, Nα, diacetic acid moiety. *Reactive and Functional Polymers*, **1996**, *29 (3)*, 167-174.

49. Rau, I., Gonzalo, A., Valiente, M. Arsenic (V) removal from aqueous solutions by iron(III) loaded chelating resin. *Journal of Radioanalytical Nuclear Chemistry,* **2000**, *246 (3)*, 597-600.

50. Li, X.Q., Zhang, W.X. Iron nanoparticles: the core-shell structure and unique properties for Ni(II) sequestration. *Langmuir*, **2006**, *22*, 4638-4642.

51. Pradeep, T. Nobel metal nanoparticles for water purification: a critical review. *Thin solid films*, **2009**, *517 (24),* 6441-6478.

52. Feng, L. Superparamagnetic high-surface-area Fe_3O_4 nanoparticles as adsorbents for arsenic removal. *Journal of Hazardous Materials*, **2012**, *217-218*, 439-446.

53. Chowdhury, S.R., Yanfu, E.K. Arsenic and chromium removal by mixed magnetite maghemite nanoparticles and the effect of phosphate no removal. *Journal of Environmental Management*, **2010**, *91*, 2238-2247.

54. Jin, Y., Liu, F., Tong, M., Hou, Y. Removal of arsenate by cetylthimethylammonuim bromide modified magnetic nanoparticles. *Journal of Hazardous Materials*, **2012**, *227-228,* 461-468.

55. Zhou, H., Green, T.B., Joo, Y.L. The thermal effects on electrospinning of polylactic acid melts. *Polymer*, **2006**, *47*, 7497–7505.

56. Deitzel, J.M., Kleinmeyer, J., Harris, D., Beck Tan, N.C. The effect of processing variables on the morphology of electrospun nanofibers and textiles. *Polymer*, **2001**, *42*, 261-272.

57. Mackay, M.E., Dao, T.T., Tuteja, A., Ho, D.L., Van Horn, B., Kim, H.C., Hawker, C.J. Nanoscale effects leading to non-Einstein-like decrease in viscosity. *Nature Materials*, **2003**, *2*, 762–766.

58. C. Fritzmann, C., Lowenberg, J., Wintgens, T., Melin, T. State of the Art of Reverse Osmosis Desalination, *Desalination*, **2007**, *216*, 1-76.

59. Zhou, W., He, J., Cui, S., Gao, W. Studies of Electrospun Cellulose Acetate Nanofibrous Membranes. *The Open Materials Science Journal*, **2011**, *5*, 51-55.

60. Tsioptsias, C., Sakellariou, K.G., Tsivintzelis, I., Papadopoulou, L., Panayiotou, C. Preparation and characterization of cellulose acetate–Fe_2O_3 composite nanofibrous materials. *Carbohydrate Polymers*, **2010**, *81*, 925–930.

61. He, J.X., Tang, Y.Y., Wang, S.Y. Differences in morphological characteristics of bamboo fibers and other natural cellulose fibers: studies on X-ray diffraction, solid state 13C-Cp/MAS NMR, and second derivative FTIR spectroscopy data. *Iranian Polymer Journal*, **2007**, *16 (12)*, 807-818.

62. Nataraj, S.K., Yang, K.S., Aminabhavi, T.M. Polyacrylonitrile-based nanofibers - A state of the art review. *Progress in Polymer Science*, **2012**, *37*, 487–513.

63. Zhang, L., Zhang, X., Li, P., Zhang, W. Effective Cd^{2+} chelating fiber based on polyacrylonitrile. *Reactive & Functional Polymers*, **2009**, *69*, 48–54.

64. Liu, R., Li, Y., Tang, H. Application of the Modified Polyacrylonitrile Fiber with Amino-Carboxyl-Tetrazine Groups for the Preconcentration of Trace Heavy Metal Ions. *Journal of Applied Polymer Science*, **1999**, *74,* 2631–2636.

65. Lian, N., Chang, X., Zheng, H., Wang, S., Dong, Y., Lai, S. Synthesis and efficiency of a chelating fiber for preconcentration and separation of trace Au(III) and Pd(IV) from solution samples. *Annali di Chimica*, **2005**, *95*, 677-683.

66. Shin, D.H., Ko, Y.G., Choi U.S., Kim, W.N. Design of High Efficiency Chelate Fibers with an Amine Group To Remove Heavy Metal Ions and pH-Related FT-IR Analysis. *Industrial & Engineering Chemical Research*, **2004**, *43,* 2060-2066.

67. Liu, R.X., Zhang, B.W., Tang, H.X. Synthesis and characterization of poly (acrylaminophosphoniccarboxyl-hydrazide) chelating fibre. *Reactive & Functional Polymers*, **1999**, *39,* 71–81.

68. Gong, B., Li, X., Wang, F., Xu, H., Chang, X. Synthesis of polyacrylacylaminourea chelating fiber and properties of concentration and separation of trace metal ions from samples. *Analytica Chimica Acta*, **2001**, *427,* 287–291.

69. Moroi, G., Bılba, D., Balba, N. Thermal behaviour of palladium complexing polyacrylamidoxime polymer. *Polymer Degradation and Stability*, **2001**, *72*, 525–535.

70. Soldatov, V.S., Shunkevich, A.A., Elinson, I.S., Johann, J., Iraushek, H. Chemically active textile materials as efficient means for water purification. *Desalination*, **1999**, *124,* 181-192.

71. Shin, D.H., Ko, Y.G., Choi U.S., Kim, W.N. Synthesis and characteristics of novel chelate fiber containing amine and amidine groups. *Polymers for Advanced Technology*, **2004**, *15,* 459-466.

72. Kampalanonwat P., Supaphol, P. Preparation and adsorption behavior of aminated electrospun polyacrylonitrile nanofiber mats for heavy metal ion removal. *Applied Materials and Interfaces,* **2010**, *2 (12),* 3619-3627.

73. Saeed, K., Park, S-Y., Oh, T-J. Preparation of Hydrazine-Modified Polyacrylonitrile Nanofibers for the Extraction of Metal Ions from Aqueous Media. *Journal of Applied Polymer Science*, **2011**, *121,* 869–873.

74. Zhang, H., Nie, H., Yu, D., Wu, C., Zhang, Y., White, C.J.B., Zhu, L. Surface modification of electrospun polyacrylonitrile nanofiber towards developing an affinity membrane for bromelain adsorption. *Desalination*, **2010**, *256,* 141–147.

75. Vatutsina, O.M., Soldatov, V.S., Sokolova, V.I., Johann, J., Bissen, M., Weissenbache, A. A new hybrid (polymer/inorganic) fibrous sorbent for arsenic removal from drinking water. *Reactive & Functional Polymers*, **2007**, *67,* 184–201.

76. Shunkevich, A.A., Akulich, Z.I., Mediak, G.V., Soldatov, V.S. Acid–base properties of ion exchangers. III. Anion exchangers on the basis of polyacrylonitrile fiber. *Reactive & Functional Polymers*, **2005**, *63,* 27–34.

77. Liu, R., Li, Y., Tang, H. Synthesis and Characteristics of Chelating Fibers Containing Imidazoline Group or Thioamide Group. *Journal of Applied Polymer Science*, **2002**, *83,* 1608-1616.

78. Moroi, G., Bilba, D., Bilba, N. Thermal degradation of mercury chelated polyacrylamidoxime. *Polymer Degradation and Stability*, **2004**, *84,* 207-214.

79. Gupta, M.L., Gupta, B., Oppermann, W., Hardtmann, G. Surface Modification of Polyacrylonitrile Staple Fibers via Alkaline Hydrolysis for Superabsorbent Applications. *Journal of Applied Polymer Science*, **2004**, *91,* 3127–3133.

80. Chang, X., Yang, X., Wei, X., Wu, K. Efficiency and mechanism of new poly(acryl-phenylamidrazone phenylhydrazide) chelating fiber for adsorbing trace Ga, In, Bi, V and Ti from solution. *Analytica Chimica Acta,* **2001**, *450*, 231–238.

81. McComb, M.E., Gesser, H.D. Passive monitoring of trace metals in water by in situ sample preconcentration via chelation on a textile based solid sorbent. *Analytica Chimica Acta*, **1997**, *341,* 229-239.

82. Gong, B. Synthesis of polyacrylaminoimidazole chelating fiber and properties of concentration and separation of trace Au, Hg and Pd from samples. *Talanta*, **2002**, *57,* 89-95.

83. Deng, S., Bai, R., Adsorption and desorption of humic acid on aminated polyacrylonitrile fibers. *Journal of Colloid and Interface Science*, **2004**, *280*, 36–43.

84. Zhang, G., Meng, H., Ji, S. Hydrolysis differences of polyacrylonitrile support membrane and its influences on polyacrylonitrile based membrane performance. *Desalination*, **2009**, *242,* 313–324.

85. Tran, T.D., Mori, S., Suzuki, M. Plasma modification of polyacrylonitrile ultrafiltration membrane. *Thin Solid Films*, **2007**, *515,* 4148–4152.

86. Dai, Z-W., Wan, L-S., Xu, Z-K. Surface glycosylation of polyacrylonitrile ultrafiltration membrane to improve its anti-fouling performance. *Journal of Membrane Science*, **2008**, *325,* 479–485.

87. Rahaman, M.S.A., Ismail, A.F., Mustafa, A. A review of heat treatment on polyacrylonitrile fiber. *Polymer Degradation and Stability*, **2007**, *92,* 1421-1432.

88. Sutasinpromprae, J., Jitjaicham, S., Nithitanakul, M., Meechaisue, C., Supaphol, P. Preparation and characterization of ultrafine electrospun polyacrylonitrile fibers and their subsequent pyrolysis to carbon fibers. *Polymer International*, **2006**, *55*, 825–833.

89. Lohokare, H.R., Muthu, M.R., Agarwal, G.P., Kharul, U.K. Effective arsenic removal using polyacrylonitrile-based ultrafiltration (UF) membrane. *Journal of Membrane Science*, **2008**, *320,* 159–166.

90. Deng, S., Bai R., Chen, J.P. Behaviors and mechanisms of copper adsorption on hydrolyzed polyacrylonitrile fibers. *Journal of Colloid and Interface Science*, **2003**, *260,* 265-272.

91. Kiani, G.R., Sheikhloie, H., Arsalani, N. Heavy metal ion removal from aqueous solutions by functionalized polyacrylonitrile. *Desalination*, **2011**, *269,* 266–270.

92. Li, G., Xiao, J., Zhang, W. Efficient and reusable amine-functionalized polyacrylonitrile fiber catalysts for Knoevenagel condensation in water. *Green chemistry*, **2012**, DOI: 10.1039/c2gc35483g. Consulted article in 21/07/2012.

93. Chatterjee, A. Determination of total cationic and total anionic arsenic species in oyster tissue using microwave-assisted extraction followed by HPLC–ICP-MS. *Talanta*, **2000**, *51*, 303–314.

94. Guerin, T., Astruc, M., Batel, A., Borsier, M. Multielemental speciation of As, Se, Sb and Te by HPLC-ICP-MS. *Talanta*, **1997**, *44*, 2201–2208.

95. Ronkart, S.N., Laurent, V., Carbonnelle, P., Mabon, N., Copin, A., Barthelemy, J-P. Speciation of five arsenic species (arsenite, arsenate, MMAAV, DMAAV and AsBet) in different kind of water by HPLC-ICP-MS. *Chemosphere*, **2007**, *66*, 738–745.

96. Chakraborty, S., Bardelli, F., Mullet, M., Greneche, J.M., Varma, S., Ehrhardt, J.J., Banerjee, D., Charlet, L. Spectroscopic studies of arsenic retention onto biotite. *Chemical Geology*, **2011**, *281*, 83-92.

97. Manning, B.A., Fendorf, S.E., Goldberg, S. Surface Structures and Stability of Arsenic(III) on Goethite: Spectroscopic Evidence for Inner-Sphere Complexes. *Environmental Science and Technology*, **1998**, *32 (16)*, 2383-2388.

4

Conclusions

---

4. CONCLUSIONS

Considering the objectives of the present studies, the results obtained in this work involve the improvement of SPION synthesis and the development of new adsorbent systems, based on SPION The new adsorbents include non-supported nanostructured systems, such as SPION in suspension or surface modified SPION as well as supported nanostructured systems, such as SPION loaded in either Forager® Sponge or CA and PAN nanofibers that were developed to obtain an efficient and innovative adsorbent system for arsenic removal in contaminated waters. These materials were fully characterized and applied to evaluate their arsenic adsorption capacity and selectivity.

Inorganic arsenic species, arsenite and arsenate, have been studied in order to determine the optimum adsorption parameters such as contact time, pH effect and concentration effect. Selectivity in presence of metal ions or interfering anions was studied using both direct and indirect speciation techniques. Specific conclusions, obtained from these results, can be summarized as follows.

Thanks to the application of characterization techniques to the different adsorbent systems and the different adsorption processes, it has been possible to obtain relevant information regarding the arsenic content in solution (by ICP-MS, ICP-AES and FP-XRF), the nanoparticles and nanofibers size, morphology and distribution (by TEM and SEM), magnetic (by SQUID) and structural properties (by TGA and ATR-FTIR) for the synthesized new adsorbent systems.

4.1. Non-supported SPION

1. A successful synthesis of SPION by the conventional co-precipitation was carried out, being remarkable the introduced modifications and improvements when compared with those existing methodologies such us that the partial oxidation of Fe^{2+} and a low reaction yield are avoided or a fractionated cleaning process, described in the literature.

2. Using synthetic solutions containing arsenite, arsenate and their mixtures, was determined the maximum adsorption for arsenate to be carried out in a short period of time (30 min) and in an acidic media (pH 3.6) when using SPION, while arsenite

adsorption is not pH dependent in a wide pH range. The maximum adsorption capacities were found to be 0.43 mmol As/g SPION and 0.91 mmol As /g SPION for arsenite and arsenate, respectively.

3. The presence of metal ions in solution such as, Zinc, Nickel and Copper in As(III)/As(V) mixtures were found not to interfere the arsenic adsorption on SPION. Up to twofold arsenic adsorption percentages (with molar ratio 1:1) are obtained when comparing to those achieved for the other metal ions such as Cu^{2+}. Such differences reach up to 4 times when using a higher molar ratio, 1:2.

4. In presence of interfering anions, the observed selectivity decreases as follows, phosphate >> sulphate ~ nitrate ~ chloride. Therefore, the results show that the adsorption capacity is similar in presence of all interfering anions except phosphate (adsorption capacity decrease in a 68%).

5. SPION provides an increase in the adsorption capacity against similar employed adsorbent materials. The reason lies on the nanometric size which specific surface area is remarkable higher than bulk Fe_3O_4 or other iron oxides, making SPION more reactive.

6. The main observed drawback is related to the partial aggregation of SPION, which reduces their potential loading capacity, being required the design of systems able to avoid such aggregation.

4.2. Functionalized Non-supported 3-MPA coated SPION

1. 3-mercaptopropionic acid was selected as extractant due to its potentiality to decrease the SPION aggregation by the role of the carboxylic and thiol groups and the novelty of such use for water treatment applications. The SPION functionalization with 3-MPA was successfully developed with an optimized 3.7 mmol 3-MPA/ g SPION coating the SPION surface.

2. The optimum adsorption parameters were evaluated and determined as in SPION studies and the results show that the adsorption process is faster (10 min) than using SPION suspension (30 min) in the same conditions. In this case, a pH dependence in As(III) adsorption is observed contrary to corresponding results on SPION suspension. The presence of thiol groups is the responsible of these effects. Then, the adsorption capacities are 1.03 mmol As/g SPION and 1.60 mmol As /g SPION for arsenite and

arsenate, respectively and improving the SPION suspension adsorption capacity for both arsenic species.

3. Adsorption selectivity in the presence of metal ions in solution such as, Zinc, Nickel and Copper in As(III)/As(V) mixtures determined successful results in particular for arsenate. While no arsenite selectivity is observed in presence of the proposed metal ions, arsenate is removed with high selectivity (95-96%) in both selected molar ratios without significant adsorption of Cu^{2+}, Zn^{2+} or Ni^{2+}.

4. Interfering anions reduces the observed selectivity as follows, phosphate >> sulphate ~ nitrate ~ chloride. Such results show a similar trend as in SPION suspensions, thus, i phosphate present the highest interfering effect (adsorption capacity decrease in a 90% for arsenite and 95% for arsenate) while the rest of anions have much less interference. This high interfering effect of phosphate is due to the effective competition with Arsenic oxoanions for the Fe(III) centers of the SPION..

5. Desorption process was successfully achieved using 1.0M HNO_3 solution. Up to a 97% of recovery for As(V), 89% for As(III) and 92% for mixtures is obtained, while 1.0M NaCl solutions was not useful for this application.

6. 3-MPA coated SPION provide an increase in the adsorption capacity against SPION suspension attributed to the reduction of nanoparticles aggregation because of the role of the organic functionalizing compound.

7. It is observed the impossibility to obtain a complete SPION dispersion despite the fact that the functionalization process Forager® Sponge was selected as tsupport for the SPION looking for a minimum aggregation process.

4.3. Forager® Sponge loaded SPION

1. SPION loaded Forager® Sponge was successfully developed and optimized to obtain a new adsorbent system with a fine and homogeneous SPION layer over the Forager® Sponge surface.

2. The optimum adsorption parameters were evaluated and determined as in previous adsorbent systems. Following the SPION suspension studies, the new adsorbent system works in optimum conditions to recover arsenate at pH 3.6, while arsenite adsorption is

not pH dependent and constant in a wide pH range. In this case, the adsorption capacities are 2.11 mmol As/g SPION and 12.09 mmol As /g SPION for arsenite and arsenate, respectively, improving those achieved adsorption capacities for non-supported SPION systems.

3. Selectivity against metal ions in solution such as, Zinc, Nickel and Copper in As(III)/As(V) mixtures determined successful results for the SPION loaded Forager® Sponge for arsenic. While arsenite is removed with a selectivity that reach up to 81% with low metal ions adsorption (4% with the higher molar ratio), arsenate is adsorbed with high selectivity (98-99%) in both selected molar ratios and no adsorption for Cu^{2+}, Zn^{2+} or Ni^{2+}.

4. Interfering anions entail the observed selectivity decrease as follows, phosphate >> sulphate ~ nitrate ~ chloride. Therefore, the results show that for As(III), the adsorption capacity is similar in the presence of all interfering anions and decrease between 65 and 80%. For arsenate, the presence of sulphate and phosphate present a more pronounced interfering effect (adsorption capacity decrease in a 80%). Like with previous adsorbent systems, the high interfering effect is because of the presence of phosphate.

5. Desorption process was successfully achieved using 1.0M HNO_3 due to is the only desorbing reagent that is able to desorb efficiently reaching to a 99.3 % of recovery for As(III), 98,2 % for As(V) and 97,2 % in mixtures without degrading the adsorbent system. . Other tested desorbing reagents such as NaOH, NaCl and H_3PO_4 become a problem for the adsorbent system due to removal of the SPION from the Sponge surface and degradation of SPION to Fe(II) and Fe(III).

6. A complete SPION dispersion is impossible to achieve despite the impregnation and dispersion process. In view of this situation, Forager® Sponge was selected as the support for the SPION with a reduced aggregation. The porosity and the obtained surface area by the milling process, makes that this support can provide the optimal conditions to develop an important role for these water treatment applications.

4.4. Cellulose Acetate – SPION nanofiber composites

1. 15% CA spinning solution with DMAc/Acetone mixture as solvent was determined to have a good spinnability. Specifically, the fibers were continuous and smooth without any beads or droplets in the surface of the electrospun membrane, and the diameter

ranged from 200-300 nm. In addition, electrospun CA-SPION nanofiber composites were successfully synthesized with SPION percentages of 0.3 and 3% (w/v) of SPION and with a similar diameter ranging from 200-300 nm.

2. Despite a low adsorption capacity for the designed CA-SPION nanofiber composites running under a continuous mode (0.06 mmol As(V)/g SPION), this study have demonstrated that CA-SPION nanofibers can be potentially applied for the removal of As(V) in water treatment applications.

4.5. SPION loaded HPAN nanofibers

1. 7.5–15 wt% PAN spinning solution with DMF as solvent was identified as the conditions for best spinnability. Specifically, the fibers were continuous and smooth without any beads or droplets in the surface of the electrospun membrane, and the diameter ranged among 300 nm to 1.5 μm.

2. In addition, surface modifications have been employed to activate the nanofiber surface through hydrolysis and hydrolysis combined with EDA. However, such modification was not useful for the SPION fixation and dispersion over the surface.

3. Taking into account the nanofiber size and the agglomeration after the hydrolysis to obtain HPAN nanofiber, the optimum nanofibers that can be electrospun are those PAN nanofibers prepared with the 10 wt% PAN solution with a diameter size of 350 nm.

4. The SPION fixation was developed and improved with a wide amount of the SPION within 0.5-14 mg per gram of HPAN nanofiber. The adsorption capacity increases to a very high values and the adsorption capacity reaches up to 32 mmol As(V) / g SPION, almost three times higher than the SPION loaded Forager® Sponge, with a SPION concentration of 0.5 mg SPION / g HPAN.

5. Adsorption experiments running under continuous mode by gravity with small size columns, 10x1.0 cm, were successfully realized. SPION loaded HPAN nanofibers with 0.29mg of SPION present an adsorption capacity about 52.6 mmol As(V) per gram of SPION, twice the observed adsorption for the same sample running under batch mode. It can be concluded that in continuous mode, the process is more efficient due to the operation mode (multiple separation mode) being the As(V) efficiently retained.

6. In gravity mode, nanofiber compression becomes a problem during the adsorption process that may block the solution flow. Thereby, a bigger column, 20x1.5 cm, was selected to increase the bed volume in order to observe the behaviour of the adsorbent system more close to conventional working conditions. As a result, the process was performed by counterflow to improve the contact between nanofiber and solution. Such modifications contribute to reach an adsorption capacity about 63 mol As(V) / g SPION. The achieved figures, in terms of adsorbent, means an adsorption capacity up to the 850mg of As(V) / g of adsorbent system.

7. Application to industrial water samples was carried out to verify the performance of the system in real environments in comparison with the synthetic experiments using counterflow mode. Obtained results were achieved in similar way as synthetic experiments when using samples of arsenic contaminated water from dumping lixiviation at Bailin. Under the experimental conditions employed, just one hour is required to remove all the As(V) entering the column..

4.6. Indirect Arsenic Speciation by HPLC-ICP-MS

1. Indirect speciation by HPLC-ICP-MS has been verified as a useful technique for the arsenic speciation in liquid samples.

2. Retention times were determined with a significant chromatographic resolution. While arsenite is the less retained species with a retention time of 3.0 min, while arsenate have a retention time of 6.6 min.

3. A good correlation is obtained between the speciation results for As(III) and As(V) by HPLC-ICP-MS and the total content by ICP-MS, with recoveries ranging from 95% to 100%.

4. From all the studied samples by this technique, it was possible to confirm that 3-MPA coated SPION is an useful adsorbent system for the selective adsorption of As(V) in contaminated solutions in the presence of As(III), common interfering metal ions or common interfering anions.

4.7. Direct Arsenic and Iron Speciation by Synchrotron radiation

1. Direct arsenic speciation by synchrotron radiation techniques has been carried out on adsorbent solid samples Thehe sensitivity of the beamlines BM25 (ESRF) and A1 (HASYLAB) allowed to analyze samples with low Arsenic content.

2. Specific software including Principal Components Analysis (PCA) and linear combination fit of corresponding reference spectra was applied to spectral data to evaluate the arsenic species content in the different target samples of SPION loaded Forager® Sponge at different pH values, revealing arsenate species to be predominant, and reaching up to a 97% of the total adsorbed Arsenic. This results confirm arsenate to be selectively removed from the contaminated water with the indicated adsorbent system

3. Direct speciation study of iron in the SPION samples reveals that SPION maintain its structure after the Arsenic adsorption process in all cases, independently of the adsorbed species, As(III), As(V) or a mixture of both species.

Future perspectives

Taking into account the work included in the PhD thesis, the future research will be focused on improving the adsorbent systems, especially those based in the SPION supported on nanofibers. Regarding the optimization of the nanofibers based adsorbent systems. Optimum SPION dispersion over the nanofibers surface is needed to achieve greater performance. Furthermore, the synthesis of PAN nanofibers with iron ions in the electrospinning solution to complete the SPION synthesis "in situ" either on or inside the nanofibers can be an interesting way to increase the dispersion and increase the specific surface area.

Regarding the adsorption processes, it is important to understand the behaviour of all adsorbent systems running under continuous mode to scale up the adsorption process to big wastewater volumes for their potential application to industrial water treatment (such as mining industry), one of the main arsenic contamination sources.

Regarding direct and indirect speciation, it will be important to analyze both samples, 3-MPA coated SPION and Forager® Sponge loaded SPION, by indirect and direct speciation

techniques trying to correlate the speciation methods. The main drawback concerning direct speciation by synchrotron radiation techniques is the availability of corresponding beamtime in the facility. On the other hand, it is noteworthy that in most cases, research time at European synchrotron facilities is financed by the European Commission.

ANNEX I

Articles to be submitted

I.1. SPION-Loaded Cellulose Sponge, a system for the arsenic removal from aqueous solution.

I.2. Arsenic (V) Removal with 3-Mercaptopropionic Acid Coated Superparamagnetic Iron Oxide Nanoparticles.

I.3. Cellulose-SPION nanofiber composites for water purification.

I.4. Arsenic speciation in the adsorption process of arsenate onto Forager® Sponge loaded SPION by XANES.

I.1. SPION-Loaded Cellulose Sponge, a system for the arsenic removal from aqueous solution.

SPION-Loaded Cellulose Sponge, a system for the arsenic removal from aqueous solution

D. Morillo Martín, G. Pérez González, M. Valiente Malmagro*

Departament de Química, Química Analítica, Universitat Autònoma de Barcelona, 08193 Bellaterra, Barcelona, Spain

CORRESPONDING AUTHOR FOOTNOTE.

Centre Grup de Tècniques de Separació en Química. Telephone number: +34 93 581 29 03, fax: +34 93 581 19 85, and e-mail address Manuel.Valiente@uab.es.

ABSTRACT.

Arsenic removal from contaminated waters is an important goal to accomplish environmental regulations. Decontamination process is made in several ways being adsorption process most efficient. In this concern, nanoparticles have been proposed as an appropriate material to increase the arsenic adsorption from contaminated waters. However, aggregation of nanoparticles has been detected as a main problem hindering the promising adsorption. To overcome this situation, a system to diminish aggregation based on the nanoparticles dispersion on an adequate supporting material is proposed. To this purpose, superparamagnetic nanoparticles have been fixed on a sponge of cellulose which helps to decrease the aggregation state and increase the adsorption of pollutants from aqueous effluents. This system has been applied to the adsorption of arsenate and arsenite, from

aqueous solutions. The experimental studies report a lower aggregation of supported superparamagnetic iron oxide nanoparticles over sponge than observed in the non-supported nanoparticles. Dispersion of the superparamagnetic iron oxide nanoparticles over sponge increases the adsorption capacity without modifying their properties. At this point, an increased adsorption capacity is observed for this sponge system than for superparamagnetic nanoparticles in suspension, maintaining their overall nanoproperties and demonstrating that sponge system is a suitable solution for the aggregation problem on superparamagnetic nanoparticles.

MANUSCRIPT TEXT.

INTRODUCTION

Arsenic is a relatively scarce element in the environment, atmosphere, water, soil and organisms, which is rarely found in elemental state. Usually it is found in combination with sulfur, oxygen and iron (1). Both natural (weathering, volcanism) and anthropogenic (mining industry, herbicides) are responsible for emissions of arsenic to the environment where it is redistributed to the atmosphere, lithosphere, hydrosphere and biosphere (2). Of the different arsenic oxidation states, in the environment, As(III) and As(V) as inorganic oxoanions species with acid characteristics in aqueous media dominate. In other hand, the oxidation states As(0) and As(-III) appear only under strongly reducing conditions and are very rare in the environment (3). The toxicity of arsenic depends of its oxidation state and decrease As(-III) >> As(III) >> As(V) >> organometalic arsenic >> As(0), being the MCL (Maximum Contaminant Level) from 50 μg/l to 10 μg/l (World Health Organization). The continuous strengthening of regulations, generate a demand for the improvement of existing methods (4, 5).

There are multiple methods to remove arsenic in contaminated effluents such as ion exchange (6), membrane processes (7) or selective adsorption (8). Numerous iron oxides have

demonstrated their affinity for arsenic but unlike them, the use of iron oxide nanoparticles provides an advantage due to increase contact specific area, allowing more active sites for adsorption (9).

The essence of nanoscience and nanotechnology is the ability to create materials, structures and systems which exhibit new properties for novel application, where combination of the desires properties and functionalities is achieved at nanometer scale (10). Small size gives nanoparticles a high surface area to volume ratio, a high surface reactivity, facilitating among other, new properties such as electrical, magnetic, optical, chemical etc…. In this sense, the interaction with different kinds of chemical species offer better kinetics for selective sorption of ions from aqueous solutions (11). At the nanoscale, inorganic metal oxides are potentially highly efficient agents for binding ions such as those of some pollutants (i.e arsenic). By tailoring the composition of the metal oxides, selective adsorption of different ions can be introduced, becoming the use of nanoparticles a very attractive new adsorption area for the recovery of ions from industrial wastes or natural water effluents.

However, magnetic material particles interact with each other forming large aggregates, reducing their adsorption capacity. By reducing the size of the magnetic nanoparticles below a few nanometers, the aggregation decreases and superparamagnetism occur, causing the atomic magnetic moments to fluctuate randomly. When a magnetic field is applied, the particles acquire a certain magnetization but, because of the high thermal energy, the long range order is lost when the field is removed, and the particles have no remanent magnetization (12). This makes superparamagnetic iron oxide nanoparticles, such as magnetite, excellent candidates for combing metal binding and selective adsorption properties with ease of phase separation.

A literature survey identify different nano-size iron oxides structures such as maghemite (γ-Fe2O3), siderite ($FeCO_3$) or fougerite ($[Fe(II)_4Fe(III)_2(OH)_{12}][CO_3 CO_3.2H_2O]$) being used to study the adsorption mechanisms and the extent of adsorption of arsenic ions (13, 14, 15). Also, other materials for arsenic adsorption such as resins or sponges loaded with iron(III) have been found(16).

The objective of the present work is to investigate the role and the effectiveness of nanosized magnetic particles, in this case, superparamagnetic iron oxide nanoparticles (Fe_3O_4) in the adsorption of arsenic(V) and arsenic(III) ions from aqueous solution, supporting this nanoparticles over a commercial ion exchange material (Forager Sponge, Dynaphore) based on an open-celled cellulose sponge and demonstrating the feasibility of using magnetic iron oxide nanoparticles for the binding and removal of arsenic(V) and arsenic(III).

EXPERIMENTAL SECTION

Chemicals and Reagents. Analytical grade solution of iron(III) chloride hexahydrate, Iron(II) chloride anhydrous, ammonium hydroxide, sodium acetate tryhydrate, acetic acid, sodium hydrogen arsenate heptahydrate, sodium metaarsenite and hydrochloric acid were used. Cellulose and polyamide chelating polymer sponge (Forager Sponge, Dynaphore) with tertiary amino and iminodiacetic groups to support the nanoparticles. Tetramethyl ammonium hydroxide (TMAOH, Fluka 25%) was used as redispersing agent and high purity water with a resistivity of 18 MΩ cm was used throughout all the experiments.

Characterization of adsorbent materials. Two types of adsorbent materials were used to remove arsenic from contaminated solutions. Superparamagnetic Iron Oxide Nanoparticles (SPION) were imaged with a transmission electron microscopy (TEM, JEOL JEM-2011 HRTEM). The crystallographic phase determination was also undertaken by analyzing the X-

ray powder diffraction (XRD) taken with a X-Pert Philips diffractometer, using a monochromatized X-ray beam with nickel-filtered CuKα radiation (λ = 0,154021 nm). The magnetization of both SPION and adsorbed SPION over cellulose was determined by Superconducting Quantum Interference Device (SQUID, MPMS-XL 7T) (17, 18, 19). To characterize the cellulose sponge and the SPION over the sponge surface TEM and Scanning Electron Microscopy (SEM, JEOL JSM-6300) was employed. Iron content was determined in order to control nanoparticles in the solution

Synthesis of adsorbent materials. The synthesis of 10 nm SPION was performed as described elsewhere (20, 21). The synthesis requires a constant bubbling of nitrogen to prevent oxidation of Fe(II) to Fe(III) and therefore, the generation of other iron oxides such as maghemite or ferrihydrite. A stock solution of Fe(III) in chloride medium was prepared by dissolving $FeCl_3.6H_2O$ in a deoxygenated HCl 0,2 M solution. A stock solution of NH_4OH 0,7 M was deoxygenated under nitrogen atmosphere and heated to 70º C. Later on, Fe(III) solution was added to the deoxygenated solution of NH_4OH. The reaction cause that the colour of the solution takes brown colour. After few minutes, anhydrous $FeCl_2$ was added and the solution was kept around 45 minutes under mechanical stirring and nitrogen bubbling for the ageing of nanoparticles. After cooling the sample in a water bath, the resulting solution was centrifuged at 2000 rpm, separating the nanoparticles by a magnet and washing with deoxygenated water four times. A subsequent redispersion step of the particles in an aqueous solution of TMAOH 0,01 M (≈pH 12) let to obtain SPION.

The synthesized nanoparticles were characterized through three techniques: by XRD analysis, in similar conditions that in the bibliography (2θ range to 10 – 60º, Step size 0.04, Time of step 4 minutes). The identification of SPION, particle size was studied by TEM and the magnetization by SQUID (22, 23, 24).

After SPION synthesis and SPION adsorption capacity determination, the sponge was loaded with SPION to improve the adsorbent material. The employed sponge improves the affinity for anionic or cationic species. A pretreatment of the commercial sponge was performed in order to facilitate the fixing of SPION by immersion in a hydrochloric acid for wiping their acidic form (16). Loading of the sponge with SPION was performed using a pneumatic nebulizer that generates the dispersion of the suspension of nanoparticles under a stream of nitrogen (30 psi). Different fixations were prepared depending on the number SPION impregnations on sponge (low, intermediate or high load).

The amount of SPION deposited was calculated by difference between the initial sponge acidic form weight and the weight of the loaded sponge as well as by the analysis of the Fe present in both the initial suspension of SPION and the corresponding washes by ICP-OES.

Adsorption experiment over SPION in suspension. The adsorption experiment was performed in batch by mixing aqueous solution of As(v) in Acetic/Acetate 0,2M media with aliquots of SPION using a rotatory shaker at room temperature. The pH of the solutions was controlled using hydrochloric acid and confirmed with pH measurements (pH meter, Crison). After mixing, the solid phase was removed from the supernatant by decantation with magnet and filtration with cellulose acetate Milipore filters of 0.22 μm. As and Fe content in the obtained supernatant was determined by inductively coupled plasma atomic emission spectroscopy (ICP-OES, Intrepid II, Thermo Fisher).

Adsorption over loaded sponge. The study and determination of adsorption capacity of the modified sponge was performed analogous to the procedure described for adsorption on SPION.

RESULTS AND DISCUSSION

Characterization of adsorbent materials. The morphology of the nanoparticles, primarily its size, determines its adsorption capacity. A 10.5 nm, optimal particle size for adsorption application it is hilighted in the literature (15, 21, 25). From the TEM micrograph (Fig.1.) a main spherical morphology for nanoparticles can be observed, which are partially aggregated when SPION are in suspension (Fig 1).
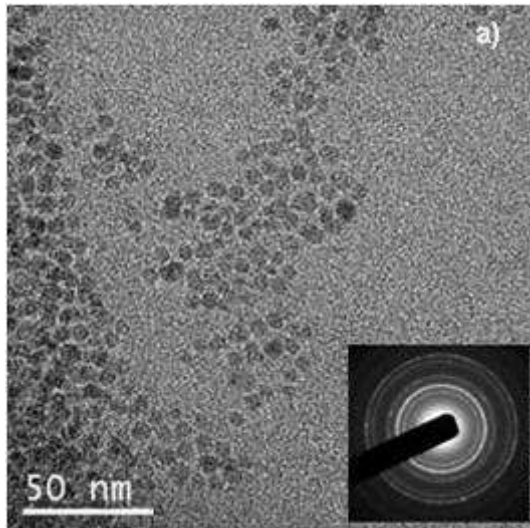
Figure 1. TEM micrograph of synthesized SPION with its diffractogram.

While, TEM micrographs of loaded sponges, indicate a greater specific surface, and therefore, greater adsorption capacity which could be obtained in nanoparticles loaded sponge due to the high dispersion of SPION.
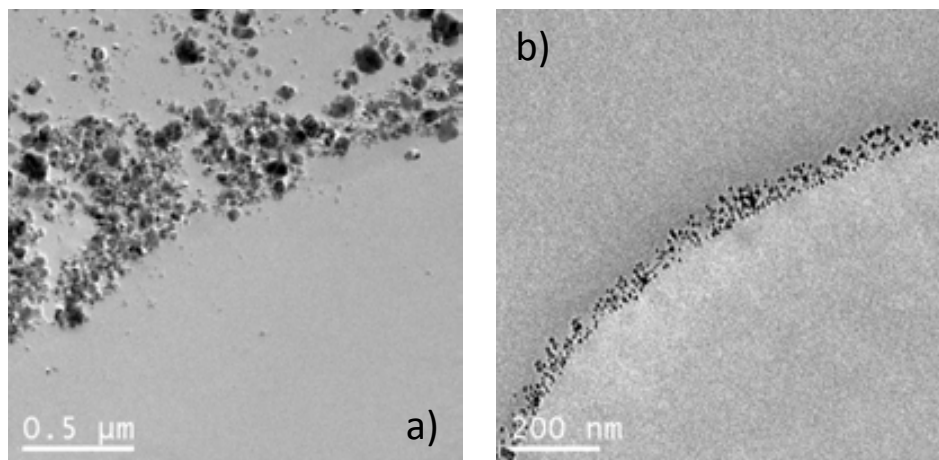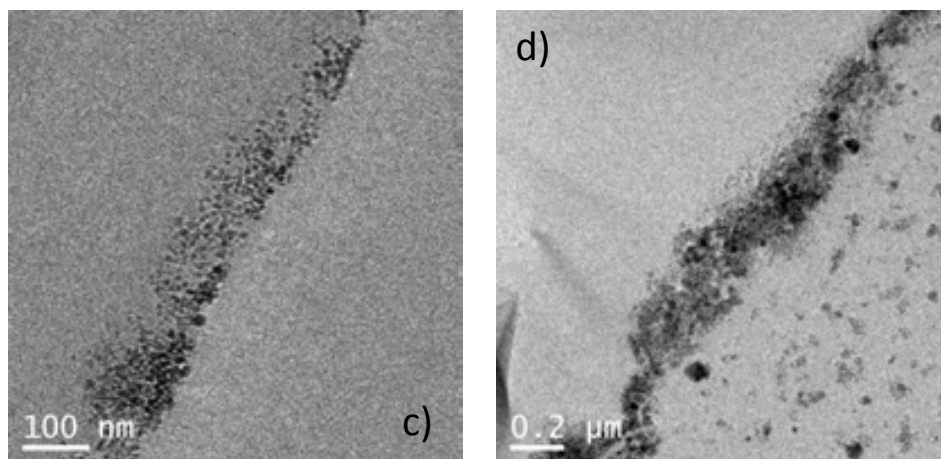
Figure 2. TEM micrograph of SPION loaded Sponge. Load during 24 h (a). Low load (b). Intermediate load (c). High load (d) of magnetite nanoparticles are distributed over the surface of the sponge.

The TEM micrographs of the different loads given in Fig 2 (a, b, c, d), although obtained at different resolution, show that longer loading processes (24 hours), provide a higher aggregation of SPION rather than using a pneumatic nebulizer. Moreover, lower load gives lower aggregation of SPION over the sponge. SEM was used to observe the distribution of MNPs over sponge. Thus, with a low load, a homogeneous and uniform SPION distribution on the surface of the sponge was observed that it was not observed for a high load.

The SPION diffractogram given in Figure 3 indicates the presence of a single phase corresponding to magnetite as compared to a magnetite standard found in the database (22).

Figure 3. Diffraction X-Ray spectra which shows the characteristic picks of the SPION and its crystallographic planes.

Finally, as shown in Figure 4, SQUID technique was used to determine the SPION magnetism. It was noted an approximately 80 emu/g magnetism, which corresponds to data reported in the literature (23). SQUID determined that nanoparticles still retained a certain magnetism (30 emu/g) when the nanoparticles are over the sponge. This decrease in the magnetism is due to magnetic analysis was performed over loaded sponge and in this case the SPION are more dispersed. Thus, reveal a remaining magnetic capacity of interest in order to recover the product when treating contamined solutions.
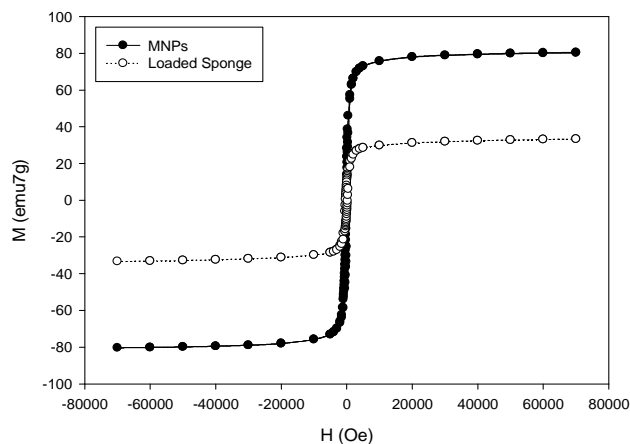
Figure 4. SQUID measurement for SPION and SPION loaded sponge.

Adsorption kinetic As(V) and As(III) over SPION. Maximum adsorption capacity of As(V), 0.91 mmols As / g SPION, was obtained at 60 minutes, observing small differences on the measures for 30 minutes. Longer kinetics (120 minutes) provides similar adsorption capacity (Fig 5a).

The maximum adsorption capacity of As(III), 0.43 mmols As / g SPION, present a variation with time less marked than in the case of As(V), although a the maximum adsorption at 60 minutes. In this case the adsorption is independent of pH, in the range studied, while the adsorption of As (V) is pH dependent (Fig 5b).
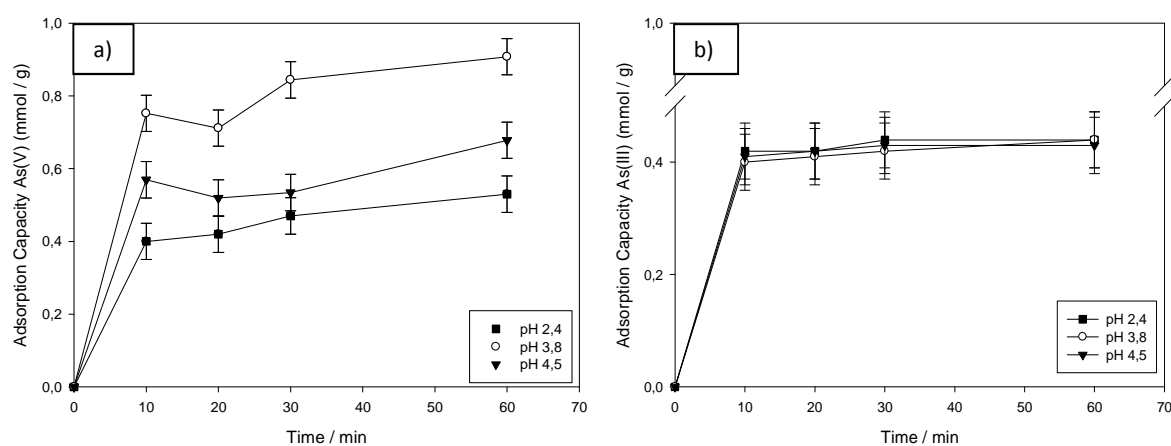
Figure 5. SPION adsorption capacity at different pH: As(V) (a), As(III) (b).

Effect of pH on the adsorption capacity over nanoparticles. A strong influence of pH is observed, especially at low pH values, in the case of As(V), reaching a maximum adsorption in the pH range 3.5 - 4.0, of 0.91 mmol As (V) / g SPION, shown in Fig 6. The acidity of arsenate species ($pKa1 = 2.2$) can be responsible of this fact, implying a relatively high proportion of deprotonated species at pH values of higher adsorption. Exceeded the maximum adsorption pH, a reduction at pH values 5.0-6.0 is observed, obtaining the same adsorption of lower pH values. In this case, the competitiveness of OH^- ions by Fe(III) decreases the adsorption of arsenate. pH does not affect the adsorption capacity of As(III) due to less acidic

species of arsenite (pKa1 = 9.2) and at the studied pH range, deprotonated species of arsenite are not present making not significant the pH effect.
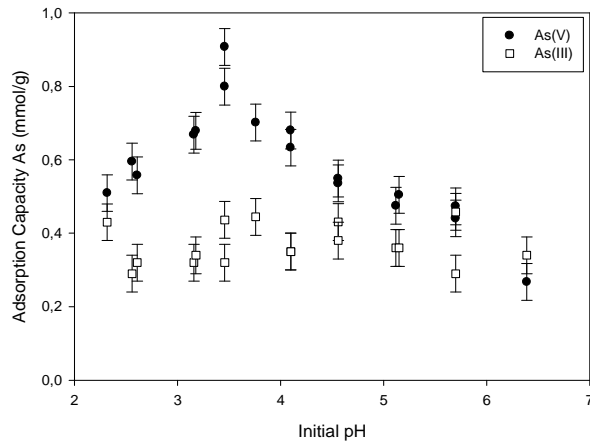
Figure 6. pH effect over As(V) and As(III) adsorption capacity with SPION.

Adsorption of As(V) and As(III) over loaded sponge. The effect of the load of SPION on the adsorption capacity of As(V) and As(III), was studied with the optimized conditions of time and pH (Fig 7).
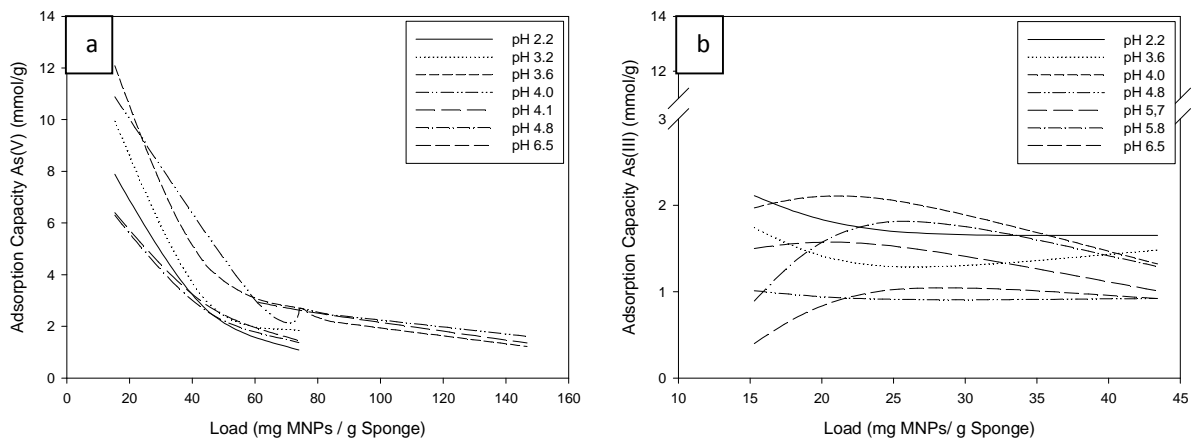
Figure 7. Adsorption capacity for SPION loaded sponge with different loads: As(V) (a). As(III) (b).

The observed behaviour can be interpreted based on an anion exchange of arsenic species corresponding to the protonated amine groups present in the matrix of the sponge (26).

However, there is a second process where an exchange of ligands provided by the ions Fe(III) of the SPION immobilized in the adsorbent material, is promoted. The affinity of arsenic oxoaniones for the iron on SPION is higher for the Fe(III) ions than Fe(II) ions.

As mentioned above, the differential behaviour of two species of arsenic is related to the different acidity of their respective oxoanions (27). This generate that may exist chemical forms of As(V) negatively charged in solution, which may be exchanged in the protonated amine groups of the sponge from a relatively acidic pH to basic pH values. Moreover, the difference in adsorption between the blank sponge and the sponge loaded with SPION it is attributed to the presence of ions of Fe(III) in the nanoparticles, which provide exchange adsorption centres for arsenic species. In this sense, the processes occurring during the arsenite and arsenate adsorption, at the studied pH, on cellulose sponge loaded with magnetite nanoparticles, could be explained by these equations (28):

R-Fe-OH + H$_2$AsO$_4^-$ $\leftrightarrow$ (R-Fe) HAsO$_4^-$ + H$_2$O   **log K = 2.5**

R-Fe-OH + H$_3$AsO$_3$ $\leftrightarrow$ (R-Fe) H$_2$AsO$_3$ + H$_2$O   **log K = 0.53**

With these data, the adsorption of As(V) on the SPION loaded sponge is favoured over the adsorption of As(III), similarly to the adsorption observed over other iron oxides (29). Finally, adsorption affinity follows solubility parameters, the anion being more prone to be adsorbed which form the more insoluble compound with the cation (30).

In this sense, the ion exchange and the adsorption of As is possible at any pH range, with a maximum of 0.4 mmol of As(V) / g sponge in the pH range (4-5). Moreover, only in basic solutions, As(III) may dominate. Under the working pH conditions, the operational capacity of the sponge is very small (0.15 mmol As(III) / g sponge), being the adsorption of As(III) on sponge virtually testimonial in all pH range.

The presence of SPION immobilized in the sponge enhances the adsorption capacity of both species of arsenic, so that the maximum adsorption of the sponge is 12,09 mmol As (V)/

g SPION at initial pH 3.6 and 2.11 mmol As (III)/ g SPION at pH 4.0, so this range confirm the optimum pH for maximum adsorption obtained for adsorption of arsenic on SPION suspension. This fact, coupled with the reduced adsorption of As(III) throughout the studied pH range, shows the possibility of separating both species of arsenic.

In this way, it can be concluded that the differential adsorption of As(V) and As(III) by SPION supported on sponge can be interpreted as a dual process consisting of an ion exchange of ammonium groups and an exchange of ligands on Fe(III) cores of the nanoparticles immobilized in the sponge. The use of supported SPION significantly improved both the adsorption capacity and selectivity of As(V) compared to the use of sponge. Losses of SPION are not significant in the studied pH range, becoming a potential application for removing As(V) from contaminated effluents. Increasing the number of impregnations of SPION over the sponge reduces the maximum adsorption capacity of the supported SPION due to increased aggregation.

Comparison of SPION suspension and loaded sponge adsorption capacity. Different adsorbent are compared in terms of adsorption capacities under optimized conditions of pH and time (Table 1). Significant differences between supports are observed, mainly SPION supported over sponge provide greater capacity for adsorption of As(V), up to four times higher than obtained both unsupported SPION and sponge without nanoparticles.

Table 1. Variation of the adsorption capacity of As(V) depending on the adsorbent material used.

	SPION	SPION loaded sponge	Sponge
Adsorption As(V) mmol As/g SPION	0,91	12,09	0,15
Adsorption As(III) mmol As/g SPION	0,43	2,11	0,1
pH reaction	3,76	3,6	4,0
Amount of sorbent (g)	0,05	0,1	0,1

The impregnation by pneumatic nebulisation of SPION supported over sponge produces the dispersion of particles and decreases the aggregation, improving the specific adsorption capacity of As(V). The role of the sponge is providing support for SPION on its surface, with a very weak contribution to the adsorption of As(V) species, 80 times smaller compared with the loaded sponge and 9 times smaller compared to SPION suspension.

Comparing the obtained results with similar studies employing the same type of sponge but loaded with iron(III), a high difference in adsorption is observed, being the SPION loaded sponge 35 times more effective for As(V) and 16 times higher for As(III) (16). The nanoparticles provide a more active adsorption sites accessible to both arsenite and arsenate. Something similar will happen in the case of different types of resins loaded with iron(III), where the SPION loaded sponge improves As(V) adsorption 19 times, while doubles the adsorption capacity of As(III) (31, 32, 33, 34).

REFERENCES.

(1) Azcue, J.M., Nriagu J. O., *Arsenic in the environment. Part I: cycling and Characterization,* J.O. Nriagu (Ed), John Wiley & Sons, New Cork, 1994.

(2) Smedley, P.L.; Kinniburgh, D.G. A review of the source, behaviour and distribution of arsenic in natural waters. *Applied Geochemistry,* **2002***, 17* (5), 517-568.

(3) Fergusson, J. E., *The heavy metals: chemistry, environment impact and health effects.* J.E. Fergusson, Pergamon Press: Oxford, 1990.

(4) Penrose, W.R. Arsenic in the marine and aquatic environments. Analysism, occurrence and significance. *CRC Crit. Rev. Environ Control,* **1974**, *4*, 465-482.

(5) USEPA United States Environmental Protection Agency. *Arsenic in drinking water, 2006; http://www.epa.gov/safety/arsenic/ (consulted 21/07/09).*

(6) Mohan, D.; Pittman C.U. Arsenic removal from water/wastewater using adsorbents; *Journal of Hazardous Materials,* **2007**, *142* (1-2), 1-53.

(7) Valcarcel, N., Gómez, A., *Técnicas Analíticas de Separación,* Reverté S.A., Barcelona, 1990

(8) McNeil, J. M., McCoy, D.E., Standard Hanbook of Hazardous Waste Treatment and Disposal, McGraw Hill book Company, New York, 1999, p.6.91.

(9) McNeil, J. M., McCoy, D.E., Standard Handbook of Hazardous Waste Treatment and Disposal, McGraw Hill book Company, New York, 1999, p.6.3.

(10) Siegel, R. W.; Hu, E.; Rocco, M. C. *Nanostructure Science and Technology, A worldwide Study*, WTEC; Loyola College Kluwer Academic, Baltimore, MD, 1999.

(11) Tsakalakos,T. NATO Sci. Ser., II: Math. Phys. Chem. (Nanostructures: Synthesis, Functional Properties an Applications), **2003**, *1*, 128.

(12) Goya, G. F.; Berquo, T. S.; Fonsec, F. C. Static and Dinamic magnetic properties of spherical magnetite nanoparticles. *J. Appl. Phys.*, **2003**, *94*, 3520-3528.

(13) Tuutijärvi, T.; Lu, J.; Sillanpää, M.; Chen, G. As(V) adsorption on maghemite nanoparticles. *Journal of Hazardous Materials*, **2009**, *166 (2-3)*, 1415-1420.

(14) Jönsson, J.; Sherman, D. M. Sorption of As(III) and As(V) to siderite, green rust (fougerite) and magnetite: Implications for arsenic release in anoxic groundwaste. *Chemical Geology*, **2008**, *255*, 173-181.

(15) Shipley, H. J.; Yean, S.; Kan, A. T.; Tomson, M. B. Adsorption of arsenic to magnetite nanoparticles: effect of particles concentration, pH, ionic strength and temperature. *Environmental Toxicology and Chemistry*, **2009**, *28* (3), 509–515.

(16) Muñoz, J. A.; Gonzalo, A.; Valiente, M. Arsenic adsorption by Fe(III)-loaded Open-Celled Cellulose Sponge. Thermodynamic and Selective Aspects. *Environ. Sci. Technol.,***2002**, *36*, 3405-3411.

(17) Adolphi, N. L. et al. *Characterization of magnetite nanoparticles for SQUID-relaxometry and magnetic needle biopsy*. Journal of Magnetism and Magnetic Materials, **2009**, *321*, 1459-1464.

(18) Garza, M.; Hinojosa, M.; Gonzalez, V. *Desarrollo de nanocomposites superparamagneticos de matríz biopolimérica.* CIENCIA UANL, **Abril-Junio 2009**, *Vol XII (2).*

(19) Kim, K. H. et al. *Synthesis and Magnetic properties of surface coated Magnetite superparamagnetic nanoparticles.* IEEE Transitiones on Magnetics, **2008**, *44* (11).

(20) Uheida, A.; Salazar-Alvarez, G.; Björkman, E.;Zhang, Y; Muhammed, M. Sorption of palladium(II), rhodium(III) and platinum(IV) on Fe_3O_4 nanoparticles. *J. Colloid Interface Sci.*, **2006**, *301*, 402-408.

(21) Uheida, A.; Salazar-Alvarez, G.; Björkman, E.;Zhang, Y; Muhammed, M. Fe_3O_4 and γ- Fe_2O_3 nanoparticles for the adsorption of Co^{2+} from aqueous solution. *J. Colloid Interface Sci.*, **2006**, *298*, 501-507.

(22) JCPDS, International Centre for Powder Diffraction Data: Swarthmore, PA, Card No. 19, (1989) 629.

(23) Cerda, L.A. G.; Fernández, S. R.; Galindo, R. B.; Guerrero, R. S. Síntesis y propiedades de ferrofluidos de magnetita. *Superficies y Vacio*, **2003**, *16* (1), 28-31.

(24) Salazar, J. S.; Roman, M.A. C.; Gomez, L. B. Structural and magnetic domains characterization of magnetic nanoproperties. *Materials Science and Engineering C*, **2007**, *27*, 1317-1320.

(25) Chin, A.B.: Yacob, I.I. Synthesis and characterization of magnetic iron oxides nanoparticles via w/o microemulsions and Massart´s procedure. *Journal of Materials Processing Technology*, **2007**, *191*, 235-237.

(26) Sillén, L.G, Martell, A.E. *Stability Constants, Special publications No.17,* The chemical society, London, 1964.

(27) Arribas, J.S., Burriel, F., Méndez, J.H., Conde, F.L. *Química Analítica Cualitativa*, Ed. Paraninfo, 2006.

(28) I. Puigdomemech, Medusa, Royal Institut of Technology, Estocolm, 1999 (www.inorg.kth.se). Software.

(29) Bhumbla, D.K., Keefer, R.F. *Arsenic in the environment. Part I: Cycling and characterization*, J.O. Nriagu, John Wiley & Sons, New York: 1994, p.51.

(30) N.B. Rainer, Process for the selective absorption of anions, US PATENT 5,187,200 (1993).

(31) Chanda, M.; O'Driscoll, K. F.; Rempel, G. L. *Ligand exchange sorption of arsenate and arsenite anions by chelating resins in ferric ion form*. React. Polym., **1988**, *7*, 251-261.

(32) Yoshida, I.; Ueno, K.; Kobayashi, H. *Selective separation of arsenic(III) and (V) ions ferric complex of chelating ion-exchange resin*. Sep. Sci. Technol., **1978**, *13* (2), 173-184.

(33) Matsunaga, M.; Yokoyama, T.; Eldridge, R. J.; Bolto, B. A. *Adsorption characteristics of arsenic(III) and arsenic(V) on iron chelating resin having lysine – N^{α}, N^{α}, diacetic acid moiety*. React. Funct. Polym, **1996**, *29* (3), 167-174.

(34) Rau,I.; Gonzalo, A.; Valiente, M. *Arsenic (V) removal from aqueous solutions by iron(III) loaded chelating resin*. J. Radianal. Nucl. Chem., **2000**, *246* (3), 597-600.

SPION-Loaded Cellulose Sponge, a system for the arsenic removal from aqueous solution

SUPLEMENTARY INFORMATION

RESULTS AND DISCUSSION

Characterization of SPION. The morphology of the nanoparticles, primarily its size, determines its adsorption capacity. The particle size was determined by TEM after performing the histogram, 10.5 nm as shows in Fig 1.
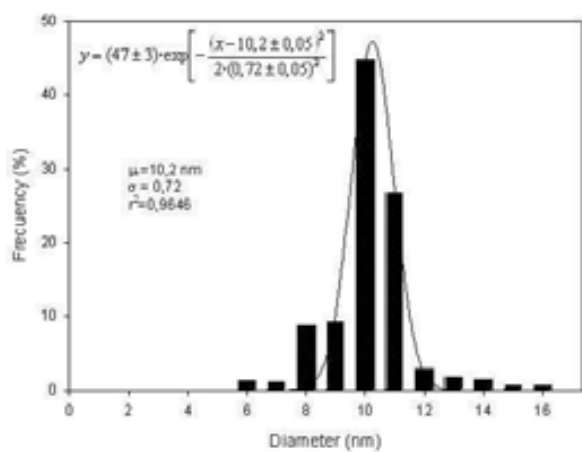
Figure 1. Distribution histogram of magnetite nanoparticles size.

For a better characterization, SEM technique was applied. As shown in the Figure 2 (a, b), SEM was used to observe how is the distribution of SPION over sponge and to this end we proceeded to perform micrographs and mapping of iron.
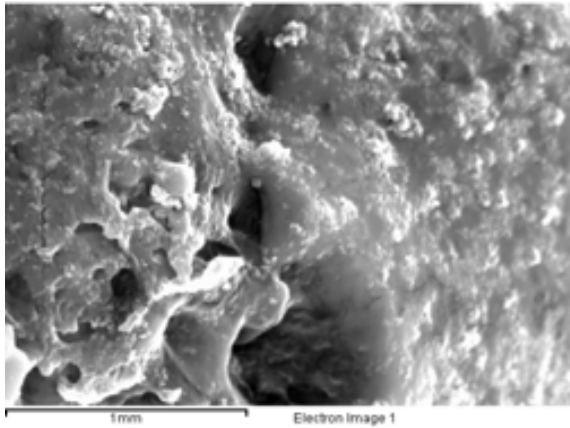
Figure 2. SEM micrograph of SPION loaded Sponge (a). SEM-mapping of Iron (b)

The observed behaviour can be interpreted based on an anion exchange of arsenic species corresponding to the protonated amine groups present in the matrix of the sponge. This will be a function of equilibrium pH of the aqueous solution, where Y is the species of arsenic exchanged by the counter ion (X), as it is shown in Figure 4.
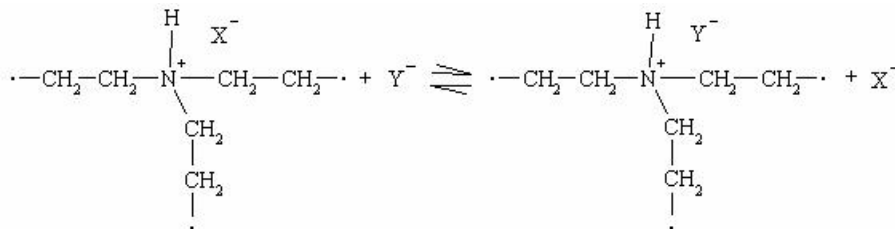
Figure 4. Anion-exchange process between arsenic and the amine groups.

However, there is a second process where an exchange of ligands provided by the ions Fe(III) of the SPION immobilized in the adsorbent material, sponge is promoted.

$$R - M - Z + X \rightarrow R - M - X + Z$$
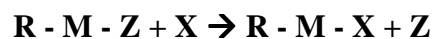
R is the matrix of the nanoparticles, M is the cation Fe(III), X is the chemical species of arsenic and Z is the ligand exchanged, OH⁻ions. The affinity of arsenic oxoaniones for the iron on SPION is higher for the Fe(III) ions than Fe(II) ions. This provides a higher activity of the ions Fe(III) with OH⁻.

I.2. Arsenic (V) Removal with 3-Mercaptopropionic Acid Coated Superparamagnetic Iron Oxide Nanoparticles

Arsenic (V) removal with 3-mercaptopropionic acid coated Superparamagnetic Iron Oxide Nanoparticles

D.MORILLO[a], A.UHEIDA[b], G. PÉREZ[a], M. MUHAMMED[b] and M. VALIENTE[a*]

[a]Universitat Autònoma de Barcelona, Centre GTS, Department of Chemistry, 08193 Bellaterra (Barcelona), Spain, Diego.morillo.martin@gmail.com, Gustavo.perez@uab.es and manuel.valiente@uab.cat*,

[b]Royal Institute of Technology (KTH), Functional Materials Division, 16440 Kista (Stochkolm), Sweden, salam@kth.se and mamoun@kth.se.

* Corresponding Author

ABSTRACT

In the present work, superparamagnetic iron oxides nanoparticles (SPION) surface coated with 3-mercaptoproponic acid (3-MPA) were prepared and their feasibility for the removal of arsenic (V) from dilute aqueous solutions was demonstrated. The synthesized 3-MPA coated SPION was characterized using Transmission Electron Microscopy (TEM), Thermogravimetric Analysis (TGA) and Fourier Transform Infra-Red Spectrometry (FTIR). Separation efficiency of the coated nanoparticles and the equilibrium isotherm of As(V) adsorption were investigated. The results obtained reveal the adsorption of As(V) to be highly pH-dependent and the maximum adsorption was attained in less than 60 minutes. The resulting increase of 3-MPA coated SPION loading capacity for As(V) as twice the adsorption capacity of SPION under the same conditions, is attributed to the increase of active adsorption sites. An adsorption reaction is proposed. On the other hand, efficient recovery of As(V) from the loaded nanoparticles was achieved using HNO_3 solution that also provides a concentration over the original As(V) solution

HIGHLIGHTS

- Feasibility of using SPION modified with 3MPA, for the removal of As(V).

- Adsorption pH is the main parameter controlling the As(V) removal.

- The absorption capacity for As(V) is twice of the corresponding SPION adsorption .

- The adsorbent system results in an effective sorption for selective As(V) removal.

KEYWORDS

1. Introduction

Nanotechnology and Nanoscience, the art of constructing systems and devices through the control of matter at the atomic and molecular level; have shown the positive potential to significantly enhance environmental quality and sustainability. Nanotechnology offers a superior protection for the environment through developing technologies that minimize undesirable derivatives, and remediation of contaminated water sources and existing waste sites. The nanotechnology industry is increasingly promoting nanotechnology as a "green" technology that will improve the environmental performance of existing industries by reducing consumption of energy and resources. A major challenge for Environmental Protection Agency (EPA) is to present cost-effective remediation method for adequate removal of hazardous substances for better protection of the environment. The EPA research focused is to create more effective systems in-terms of efficiency and cost (USEPA, 2003).

Rapid development in nanotechnology has allowed in-situ treatment technologies for groundwater contaminant source zones i.e., nanoparticles with unique and tuneable physical and chemical properties. Highly reactive nanoparticles such as nanosized sorbents (Tungittiplakorn et al., 2005; Tungittiplakorn et al., 2004) have been developed specifically to remediate contamination by heavy metal ion contaminants. Nanoparticles (10–500 nm) provide an opportunity to deliver these remedial agents to subsurface contaminants in situ, and provide access to contamination trapped in the smallest pores in an aquifer matrix. The high reactivity and the potential for facile delivery directly to the contaminant source, suggests that nanoparticles can accelerate the degradation rate of contaminants in the treated zone, and decrease the time and cost of remediation.

At the nanoscale, inorganic metal oxides are very efficient agents for binding ions such as arsenic and today's challenge is the translation of these achievements into an industrial

production environment which requires scale-up to a continuous and safe nanoparticle manufacturing process (Wegner, 2011; Strobel, 2009; Mädler, 2002). By tailoring the composition of the metal oxides, selective adsorption of different ions can be introduced. The utilization of nanoparticles for the recovery of metal ions from industrial wastes or natural water effluents has proved itself as superior new process.

Arsenic is a relatively scarce element in the environment, which is rarely found in elemental state. Usually it exists a compounding state with other elements, for example, with sulphur, oxygen and iron (Azcue and Nriagu, 1994) and the toxicity of arsenic depends of its oxidation state. According to the World Health Organization (WHO), the Maximum Contamination Level (MCL) of arsenic must be 10μg/l. The continuous strengthening of regulations, generate a demand for the improvement of existing methods (Penrose, 1974; USEPA, 2010). Several methods such as ion exchange, membrane processes, and selective adsorption have been studied for the removal of arsenic from contaminated effluents. (Mohan and Pittman, 2007; McNeil and McCoy, 1999a; McNeil and McCoy, 1999b; Valcarcel and Gómez, 1990).

In the present study the feasibility of using magnetite nanoparticles coated with 3-mercaptopropionic acid is demonstrated for selective sorption of arsenic (V) from aqueous solutions. The sorption properties were studied under static mode of operation.

2. Experimental section

2.1. Chemicals and Reagents

Stock solutions of As(V) were prepared from $Na_2HAsO_4.7H_2O$ (Sigma-Aldrich). Analytical grade $FeCl_2.4H_2O$, $FeCl_3.6H_2O$ (Sigma-Aldrich), ammonium hydroxide, toluene, sodium acetate trihydrate, acetic acid, nitric acid and sodium hydroxide were used as received.

Cu(NO$_3$)$_2$, Ni(NO$_3$)$_2$, Zn(NO$_3$)$_2$, NH$_4$Cl, NH$_4$(NO$_3$), K$_2$(SO$_4$) and NaH$_2$(PO$_4$) (Sigma-Aldrich) were used for the cationic and anionic selectivity experiments. 3-Mercaptopropionic acid (3-MPA, Sigma-Aldrich) and Tetramethyl ammonium hydroxide (TMAOH, Fluka 25% in water) were used without further purification. High purity water with a resistivity of 18 MΩ cm^{-1} was used throughout all the experiments.

2.2.   Characterization techniques for the adsorbent system

SPION and nanoparticle composites (NPCs) synthesized by functionalization of SPION with 3-MPA were imaged with a transmission electron microscopy (HR-FEG-TEM, JEOL JEM-2100, Tokyo, Japan). TEM-EDX for chemical composition determination was applied for the nanoparticles in dry form. The stability and the homogeneity of the SPION suspension in hydrodynamic mode were determined by Dynamic Light Scattering (DLS, Delsa Nano C, Beckman Coulter, Brea, CA, USA). To measure the weight variation and determine if the particles were load with the reagent Thermogravimetric Analysis (TGA, Q5000, TA instruments, New Castle, DE, USA) was employed. Fourier Transform Infra-red (FTIR, Nicolet Instruments model Avatar-100 equipped with ATR diamond at 303 K, Madison, WI, USA) was used to verify the interaction between SPION, 3-MPA and their bonding before and after the adsorption process (Adolphi et al., 2009; Garza et al., 2009; Kim et al., 2008).

2.3.   Synthesis of adsorbent materials

The synthesis procedure of SPION (~ 10 nm) has been described elsewhere (Morillo et al, 2009). A stock solution of iron(III) in chloride media was prepared by dissolving the respective salt with a deoxygenated 0.2M mol/L HCl aqueous solution. This solution was added to a deoxygenated solution of 0.7 mol/L NH$_4$OH under mechanical stirring. After few minutes, the respective salt of iron(II) in 2:1 ratio was added to avoid the partial oxidation of Fe(II). The particles were aged in the solution for about 45 min under mechanical stirring and

nitrogen bubbling, decanted by magnetic settling, and washed with deoxygenated water several times. A known amount of the synthesized particles was mixed with 3-MPA solution (150mM) in toluene using rotary shaker for 24 hours. After phase separation using magnetic settlement, the particles were washed with toluene three times to remove the excess of 3-MPA deposited on the surface of the particles. The particles were dried at room temperature (23C). FT-IR was used to check whether the reagent was bound to the surface of the particles, in a wavenumber range 4000-600 cm^{-1} (Ajay and Mona, 2005; Uzun et al., 2010). The TGA analysis was carried out with heating rate of 10 C/min in nitrogen until 900 C (Mahmoudi et al., 2009; Xuan and Chunfu, 2011).

2.4. Adsorption and Desorption Experiments

The adsorption experiments were performed by mixing a known amount of SPION coated 3-MPA with aqueous solutions of As(V) in 0.2 M Acetic/Acetate media using rotary shaker at room temperature (23 C). The pH of the solution was controlled using either HNO_3 or NaOH standardized solutions and confirmed by pH measurements (pH-meter, Crison, Barcelona, Spain). After mixing, the aqueous phase was separated from the solid phase by magnetic settlement and centrifugation at 14000 rpm using a centrifuge (Genofuge 16 M, Techne, Prinston, NJ, USA). The concentration of metal ions in the supernatant was determined by inductively coupled plasma atomic emission spectroscopy (ICP-AES, iCAP 6000, Thermo Fisher, Waltham, MA, USA). As(V) adsorption was calculated by mass balance and the effect of different parameters, such as time, pH and initial As(V) concentration have investigated. The dissolution of iron oxide was monitored by determining the concentration of iron in aqueous solutions.

In the desorption experiments, 10 ml of the elution solution (HNO_3 or NaCl) was added to an accurate quantity of 3-MPA coated SPION loaded with As(V). After 60 minutes of contact at

temperature 23 ± 1 C, the aqueous and the solid phases were separated by centrifugation and the concentration of As(V) in the supernatant was measured.

The sorption percentage and loading capacity of As(V) are defined as:

$$Sorption = \frac{(C_i + C_e)}{C_i} \times 100 \quad (\%) \tag{1}$$

$$q_e = (C_i + C_e) \times \frac{V}{m} \quad (mg/g) \tag{2}$$

where C_i is the initial As(V) concentration (mmol/L), C_e is the As(V) concentration in the aqueous solution (mmol/L), V is the volume of aqueous phase (mL), and m is the weight of 3-MPA coated SPION (g).

2.5.   Selectivity Experiments

Two different experiments were performed to study the selectivity of the adsorbent. In one hand, solutions of As(V) containing metal ions such as Cu(II), Ni(II) and Zn(II) in molar ratios 1:1 and 1:2 (As(V): metal ions) were treated in order to know if the adsorbent system can be used for As(V) removal in presence of metals. In the other hand, solutions of As(V) containing 0,25M of Cl^-, NO_3^-, SO_4^{2-} or PO_4^{3-} (ratio 20:1 respect of As(V) total in solution) were treated to observe the behaviour of the absorbent system in presence of interfering anions. The experiments were performed in the same way that the adsorption experiments by mixing a known amount of SPION coated 3-MPA with the solutions using rotary shaker at room temperature (23 C). The pH of the solution was controlled using either HNO_3 or NaOH standardized solutions and confirmed by pH measurements (pH-meter, Crison, Barcelona, Spain). After mixing, the aqueous phase was separated from the solid phase and the concentration of metal ions in the supernatant was determined by ICP-AES.

3. Results and discussion

3.1. Characterization of adsorbent material

The amount of 3-MPA coated on the surface of SPION was determined from the percentage weight loss measured by the thermogravimetric analysis (TGA). As shown in Fig. 1, the TGA curve for SPION shows a weight loss over 100–350º C of about 8%. This is most likely due to the loss of adsorbed water and dehydration of internal OH groups. However, for 3-MPA coated SPION, the TGA curve shows two weight loss steps. The first weight loss step over 100–180º C might be due to the loss of residual water adsorbed physically in the sample. The second weight loss over 200–800º C was due to the decomposition of 3-MPA. Based on the TGA data, the amount of 3-MPA coated on the surface of SPION is determined to be 3.7 mmol/g.

The TEM image of 3-MPA-coated SPION is shown in Fig. 2a. Energy Dispersive X-ray (EDX) analysis data (Fig. 2b) shows that the main compositions of the sample are Fe, O, (JCPDS File No. 19-629) and S. The presence of sulphur in the sample is a confirmation of the coating process (Cerda et al., 2003; Chin and Yacob, 2007; Salazar et al., 2007; Shipley et al., 2009; Uheida et al., 2006b).

In order to confirm the coating of the SPION surface with 3-MPA, FT-IR spectra of SPION, 3-MPA coated SPION, and 3-MPA were obtained (Fig. 3). As can be seen in Fig. 3, new bands were observed in the spectrum of 3-MPA coated SPION. However, their frequencies are shifted to lower values, indicating strong bonding of S. The reagent (3-MPA) has two important functional groups: thiol (SH) and carboxylic (COOH). The vibration of –SH group is at 2400 cm^{-1} and it was observed in all samples. The –COOH group has stretching vibration C=O at 1760-1690 cm^{-1} and the stretching vibration C-O at 1320-1210 cm^{-1}. The bending vibration O-H was not observed at 1440 and 950 cm^{-1}. A reasonable conclusion would therefore be that the reagent is bonded to the surface of SPION primarily through the

carboxylic group. In addition, at low wavenumber, 700-600 cm^{-1} the stretching vibration Fe-O was observed (Bruce et al., 2004; Nyquist and Kagel, 1971; Wei et al., 2007).

3.2. Proposed mechanism of 3MPA-SPION interaction

Taking into account the results obtained from the TGA and FT-IR analysis, a proposed mechanism for 3MPA coated SPION at acidic pH can be illustrated below (Yun et al., 2008):

$$(3)$$
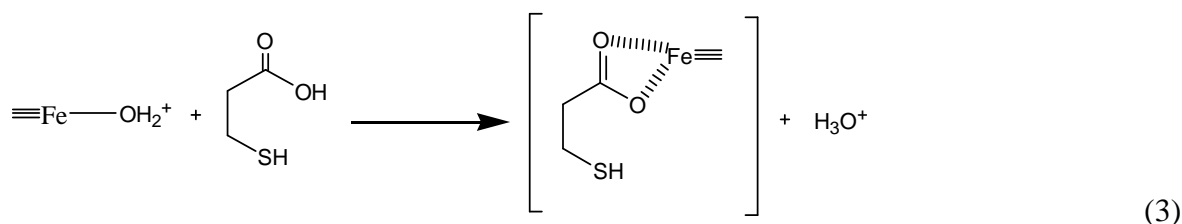
where Fe≡ represent the SPION.

The presence of a good leaving group as OH_2^+ on the SPION surface when producing the functionalization, is a key factor to this reaction leading to increase the amount of functionalized Fe atoms on the SPION surface. In this sense, the TGA results corroborate the high degradation of organic compounds between 200-800 C and the TEM-EDX showed quantitatively corresponding sulphur amount.

3.3. Sorption-desorption properties of As(V) on 3MPA-SPION.

This section includes results of different parameters, i.e., contact time, pH, and As(V) concentration affecting the adsorption process as well as its selectivity against most common interfering ions. As(V) desorption process is also described.

3.3.1. Effect of the contact time

In these experiments the effect of contact time on the adsorption of As(V) was studied. The experiments were carried out using 10 mg 3-MPA coated SPION at room temperature (23±1 C) and solution pH 4.0 with the contact time varying in the range of 10-360 min. The results obtained are presented in Fig. 4. As can be seen, the 3-MPA coated SPION synthesized at low

pH exhibit high sorption kinetics for As(V) than 3-MPA coated SPION synthesized at high pH, the 50% of the equilibrium sorption ($t_{1/2}$) being reached in less than 10 minutes. However, to ensure equilibrium, 1 hour contact time was maintained during the extraction studies.

3.3.2. Effect of pH

The adsorption of As(V) (Ci= 100 mg/L) using 3-MPA coated SPION was investigated by varying the solution pH in the range 2-11 (acetic/acetate media). The results obtained (Fig. 5) revealed that the adsorption of As(V) by 3-MPAcoated SPION is pH dependent. This is in agreement with the results obtained from solvent extraction studies using 3-MPA as extractant (Liane et al., 2007). This can be explained by the dependence of pH on the various As(V) species present in the aqueous solution.

A comparison of the observed pH effect with that obtained on previous reported As(V) adsorbant (Muñoz et al., 2002) respect to the SPION alone revealed similar behaviour with an adsorption maximum at pH 3.8. This similarity supports that Arsenic species responsible of the adsorption are the same.

As shown in the As(V) species diagram (Fig. 6), the acidity of arsenate species ($pKa_1 = 2.2$) can be responsible of the observed adsorption, since a relatively high proportion of deprotonated species are present at pH value 3.8 of highest adsorption. For lower pH values (2.0-3.0), the competition of H^+ species for arsenate leads to a lower adsorption. On the other hand, at pH > 5,0 the observed decrease on the As(V) adsorption is due to the increase of OH^- species to repress the process (see equation 3) .

3.3.3. Effect of Initial As(V) Concentration

In these experiments the effect of the initial As(V) concentration on the sorption of As(V) was studied in order to estimate the maximum loading capacity of 3-MPA coated SPION. The initial As(V) concentration was in the range of 1.3×10^{-5} mol/L and 1.3×10^{-2} mol/L. The relationship between the equilibrium aqueous concentration and the equilibrium loading capacity for As(V) is shown in Fig. 7. The experimental is in good agreement with the Langmuir adsorption model, as follows;

$$q_e = \frac{q_{max} k_L C_e}{1 + k_L C_e} \tag{4}$$

that can be written as:

$$\frac{C_e}{q_e} = \frac{1}{q_{max} k_L} + \frac{C_e}{q_{max}} \tag{5}$$

where q_e is the equilibrium loading capacity (mmol/g), C_e is the equilibrium metal concentration in the aqueous phase (mmol/ L), q_{max} is the maximum loading capacity (mmol/g) corresponding to a monolayer coverage, and k_L is Langmuir constant (L/mmol). The values of the maximum loading of As(V) and Langmuir constant are determined to be 2 mmol/g and 8.3 L/mmol respectively. The maximum loading capacity of As(V) corresponded to 54% (molar basis) of the total binding sites (3.7 mmol 3-MPA/g SPION). The major part of the reagent is likely to be accessible to As(V) ions.

With all parameters optimized, the mechanism can be described at pH=4, by the predominant specie of As ($H_2AsO_4^-$) (Puigdomenech, 1999; Muñoz et al, 2002):
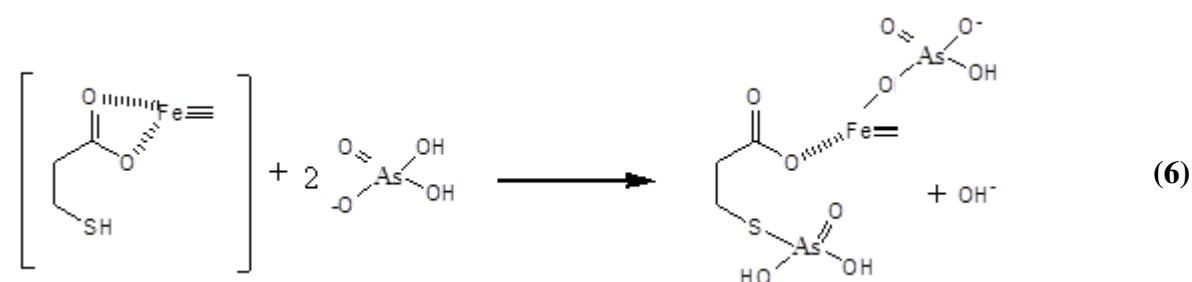
The observed increase of the solution pH supports the appropriateness of the proposed adsorption mechanism by reaction (6).

3.3.4. Selectivity

3.3.4.1. Selectivity with metal ions

In order to examine the separation of As(V) from a mixture containing metals, the selective sorption of As(V) from a solution containing mixture of Cu(II), Zn(II), and Ni(II) was investigated. The results obtained are listed in Table 1. The initial As(V) concentration was 7.5×10^{-4} mol L^{-1}. The results obtained are in agreement with that of solvent extraction studies (Uheida et al., 2006b). It indicates that 3-MPA coated SPION can be used to extract As(V) selectively from aqueous solutions under the experimental conditions studied.

3.3.4.2. Selectivity with interfering anions

The Fig. 8. Shows the effect of the pH in the adsorption of As(V) in the pH range 2-11 for the 3-MPA coated SPION for As(V) solutions with or without anions commonly presents in waste waters and potentially interfering in the As(V) adsorption such as chloride, nitrate, sulphate or phosphate. It can be emphasize that the interfering effect of these anions is very significant, due to the As(V) loading capacity in presence of one of these anions is always lower than the loading capacity without them. But the general tendency of varying the loading capacity with the pH is similar for all interfering anions, with an increase of the loading capacity when the pH increase until 4,5 or 5,0 and an stabilization until pH 11,0.

Because of the fact that is not existing a parameter that let us the interfering effect quantification of the different anions, it can be considered the values of loading capacity at pH 4,0 approximately (pH value in the zone where the loading capacity is higher). These values are registered in the Table. 2 with the values of the loading capacity decrease for each anion.

The selectivity decrease in order phosphate >> sulphate ~ nitrate ~ chloride. Therefore, the results show that the loading capacity is similar in presence of the all interfering anions except phosphate which present an interfering effect more pronounced. The high interfering effect of phosphate in the loading capacity of As(V) in all pH range is due to the effective competence for the Fe(III) centers of the SPION according with the similar affinity of phosphate and arsenate for Fe(III) and due to the major concentration of phosphate in ratio with the arsenate concentration (Yan-Chu, 1994).

As it is presented in the literature (De Abreu, 2012; Mohan, 2007), the comparative of the adsorption results between synthetic solution and real water present a greater efficiency for the metal ions removal from synthetic solution and this can be attributed to the matrix effect from real water which increase the ionic strength from solution as well the ions competition by the zeolite adsorption sites. Then, with the interfering anions, ionic strength of real solution have been simulated.

3.3.5. Desorption of As(V)

Different eluting solutions such as HNO_3 and NaCl were employed for the recovery of As(V) from the loaded 3-MPA coated SPION. The adsorption experiments were performed at pH 3.8 and initial As(V) concentration of 7.5×10^{-4} mol L^{-1}. Corresponding results are 97% for 1.0 M HNO_3 and 5% for 1.0 M NaCl. These results agree with the described pH effect on the adsorption process.

In addition, in the aqueous phases iron is not observed that means no striping of 3-MPA coated SPION is produced. Several 3-MPA coated SPION samples have been observed by SEM after the desorption process and all of them keep their structure with presence of mercaptopropionic agent on the SPION surface. That means that the absorbent material is stable after the treatment and it is ready to be used for adsorption – desorption cycles.

4. Conclusions

In this study, the feasibility of using 3-MPA coated SPION has been demonstrated for the removal of As(V) from diluted nitrate solutions. The time needed to reach maximum adsorption was attained in less than 1 hour and the loading capacity of 3MPAcoated SPION for As(V) was determined to be 2 mmol/g (150 mg/g). The adsorption behaviour of As(V) at 23+1 C was similar to Langmuir isotherm. The 3MPAcoated SPION have been shown to be selective for As(V) against base metals such as Cu(II), Zn(II), and Ni(II). FTIR analysis suggested that 3-MPA is bound to the SPION surface through the carboxylic group.

The possibility of combining the superparamagnetic properties of SPION with the selectivity of the reagent (3-MPA) could result in the development of a more effective sorbent for the selective recovery of As(V) from dilute solutions. In this work, sufficiently high loading capacity and high selectivity of As(V) were obtained using 3-MPAcoated SPION. As a result, this system provide a simple and efficient way to recover As(V) from dilute aqueous solutions. This system might be useful for treatment of process streams of As(V), especially since such streams usually contain low concentrations of these metals.

The experimental results are obtained at laboratory scale, in a pre-stage of pilot plant and for this reason no results at large scale are presented in this paper. Taking into account that it is possible to synthesize nanoparticles at industrial level, next step will be developed in this way.

5. Acknowledgment

6. References

Adolphi, N.L., et al., 2009. Characterization of magnetite nanoparticles for SQUID-relaxometry and magnetic needle biopsy. J. Magn. Magn. Mater. 321, 1459-1464.

Ajay, K.G., Mona, G., 2005. Cytotoxicity suppression and cellular uptake enhancement of surface modified magnetic nanoparticles, Biomaterials 26(13), 1565-1573.

Azcue, J.M., Nriagu, J.O., 1994. Arsenic in the environment. Part I: cycling and Characterization. J.O. Nriagu (Ed), John Wiley & Sons, New Cork, p.1.

Bruce, I.J., et al., 2004. Synthesis, characterisation and application of silica-magnetite nanocomposites. J. Magn. Magn. Mater. 284, 145–160.

Cerda, L.A.G., et al., 2003. Síntesis y propiedades de ferrofluidos de magnetita. Superficies y Vacio 16(1), 28-31.

Chin, A.B., Yacob, I.I., 2007. Synthesis and characterization of magnetic iron oxides nanoparticles via w/o microemulsions and Massart´s procedure. Journal of Mater. Proces. Technol. 191, 235-237.

De Abreu, R. T., et al, 2012. Metal Ions Removal From Synthetic Solutions and Produced Water Using Activated Zeolite. International Journal of Civil & Environmental Engineering, 12(3), 20-25.

Garza, M., et al., 2009. Desarrollo de nanocomposites superparamagneticos de matríz biopolimérica. CIENCIA UANL, Vol XII (2) (in Spanish).

Kim, K.H., et al., 2008. Synthesis and Magnetic properties of surface coated Magnetite superparamagnetic nanoparticles. IEEE Transition. Magn. 44 (11-1), 2940-2943.

Liane, M.R., et al., 2007. A magnetically recoverable scavenger for palladium based on thiol-modified magnetite nanoparticles. Appl. Catal., A 330, 139-144.

Mädler, L., et al., 2002. Controlled Synthesis of Nanostructured Particles by Flame Spray Pyrolysis, J. Aerosol Sci. 33(2), 369-289.

Mahmoudi, M., et al., 2009. Cell toxicity of superparamagnetic iron oxide nanoparticles. J. Colloid Interface Sci. 336, 510–518.

McNeil, J.M., McCoy, D.E., 1999a. Standard Handbook of Hazardous Waste Treatment and Disposal, McGraw Hill book Company, New York, p.6.3.

McNeil, J.M., McCoy, D.E., 1999b. Standard Hanbook of Hazardous Waste Treatment and Disposal, McGraw Hill book Company, New York, p.6.91.

Mohan, D., Pittman, C.U., 2007. Arsenic removal from water/wastewater using adsorbents, J. Hazard. Mater. 142(1-2), 1-53.

Morillo, D., Valiente, M., Perez, G., 2009. Avances en la adsorción de Arsénico con Nanopartículas, Proyecto de Investigación, Master Universitario en Ciencias y Tecnologías Químicas, Universitat Autònoma de Barcelona.

Muñoz, J.A., et al., 2002. Arsenic adsorption by Fe(III)-loaded Open-Celled Cellulose Sponge. Thermodynamic and Selective Aspects. Environ. Sci. Technol. 36, 3405-3411.

Nyquist, R.A., Kagel, R.O., 1971. Infrared spectra of ınorganic compounds. Academic Press, New York.

Penrose, W.R., 1974. Arsenic in the marine and aquatic environments. Analysism, occurrence and significance. CRC Crit. Rev. Environ. Control 4, 465-482.

Puigdomemech, I., 1999. Medusa, Royal Institut of Technology, Estocolm, (www.inorg.kth.se). Software.

Salazar, J.S., et al., 2007. Structural and magnetic domains characterization of magnetic nanoproperties. Mater. Sci. Eng., C 27, 1317-1320.

Shipley, H.J., et al., 2009. Adsorption of arsenic to magnetite nanoparticles: effect of particles concentration, pH, ionic strength and temperature. Environ. Toxicol. Chem. 28(3), 509-515.

Strobel, R., Pratsinis, S. E., 2009. Direct synthesis of maghemite, magnetite and wustite nanoparticles by flame spray pyrolysis. Advanced Powder Technology, 20(2), 190-194.

Tungittiplakorn, W., et al., 2005. Engineered Polymeric Nanoparticles for Bioremediation of Hydrophobic Contaminants. Environ. Sci. Technol. 39(5), 1354–1358.

Tungittiplakorn, W., et al. 2004. Engineered Polymeric Nanoparticles for Soil Remediation. Environ. Sci. Technol. 38(5), 1605–1610.

Uheida, A., et al., 2006a. Sorption of palladium(II), rhodium(III) and platinum(IV) on Fe3O4 nanoparticles. J. Colloid Interface Sci. 301, 402-408.

Uheida, A., et al., 2006b. Fe3O4 and γ- Fe2O3 nanoparticles for the adsorption of Co2+ from aqueous solution. J. Colloid Interface Sci. 298, 501-507.

USEPA, 2010. Arsenic in drinking water. U. S. Environmental Protection Agency. http://water.epa.gov/lawsregs/rulesregs/sdwa/arsenic/index.cfm (consulted 21/11/10).

USEPA, 2003. Proceedings: EPA Nanotechnology and the Environmental: Applications and Implications STAR Progress Review Workshop. U.S. Environmental Protection Agency, EPA Document Number: EPA/600/R-02/080.

Uzun, K. et al., 2010. Covalent immobilization of invertase on PAMAM dendrimer modified superparamagnetic iron oxide nanoparticles. J. Nanopart. Res. 12(8), 3057-3067.

Valcarcel, M., Gómez, A., 1990. Técnicas Analíticas de Separación, Reverté S.A., Barcelona.

Wei, S., et al., 2007. Preparation and characterization of hyperbranched aromatic polyamides/Fe3O4magnetic nanocomposite. React. Funct. Polym. 66, 1272–1277.

Xuan, X., Chunfu, Z., 2011. Controllable Assembly of Hydrophobic Superparamagnetic iron oxide nanoparticles with mPEG-PLA Copolymer and its effect on MR transverse Relaxation Rate. J. Nanomater. Article ID 152524, 7 pages.

Yan-Chu, H., 1994. Arsenic in the environment. Part I: cycling and Characterization. J.O. Nriagu (Ed), John Wiley & Sons, New Cork, p.17.

Yun, T.L., et al, 2008. Preparation of Water-dispersible and Biocompatible Iron Oxide Nanoparticles for MRI Agent. IEE Trans. nanotechnol. 7(2), 111-114.

Wegner, K., et al, 2011. Pilot Plants for Industrial Nanoparticle Production by Flame Spray Pyrolysis, KONA Powder and Particle 29, 251.

Figure 1
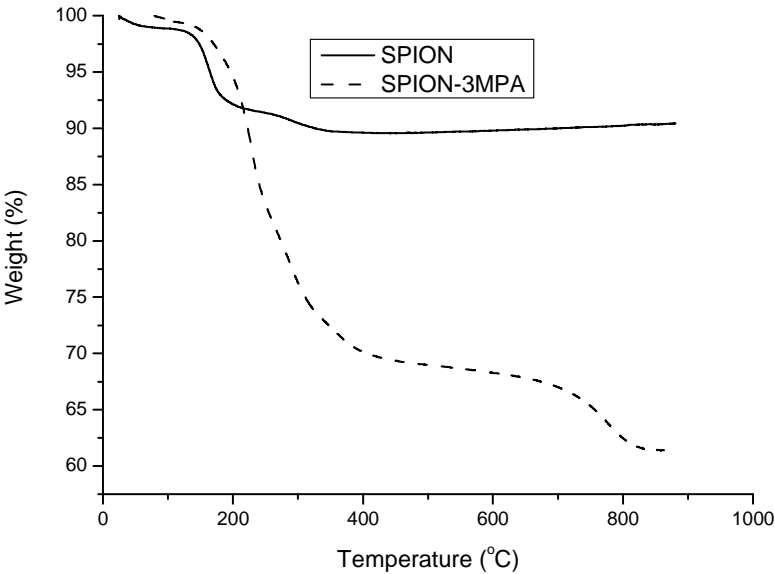
Figure 2
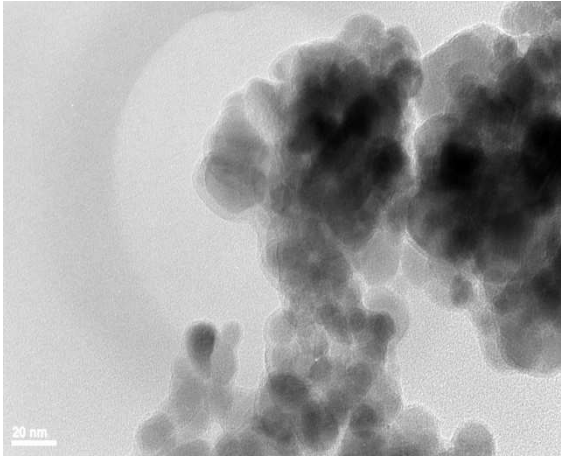
(a)
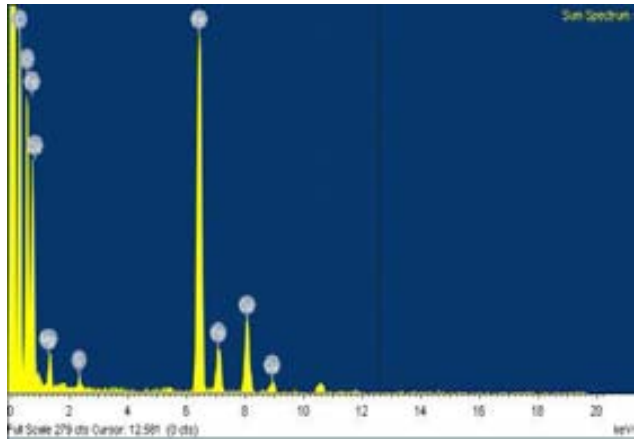
(b)

Figure 3
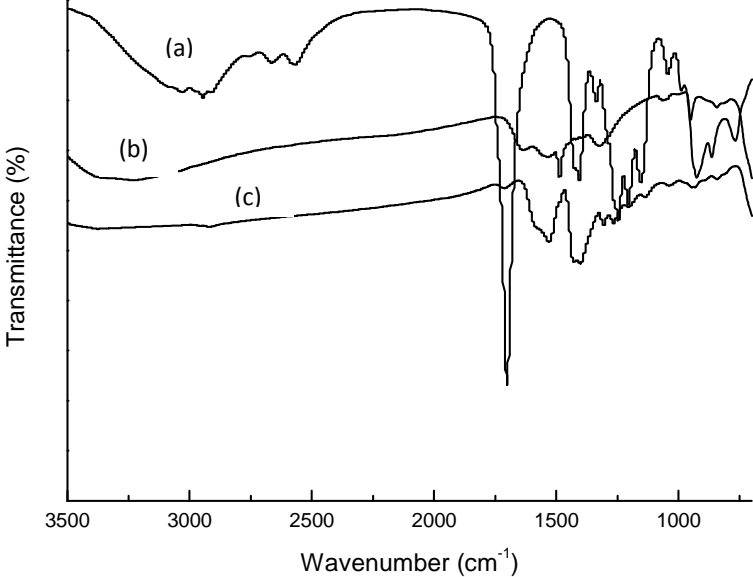
Figure 4
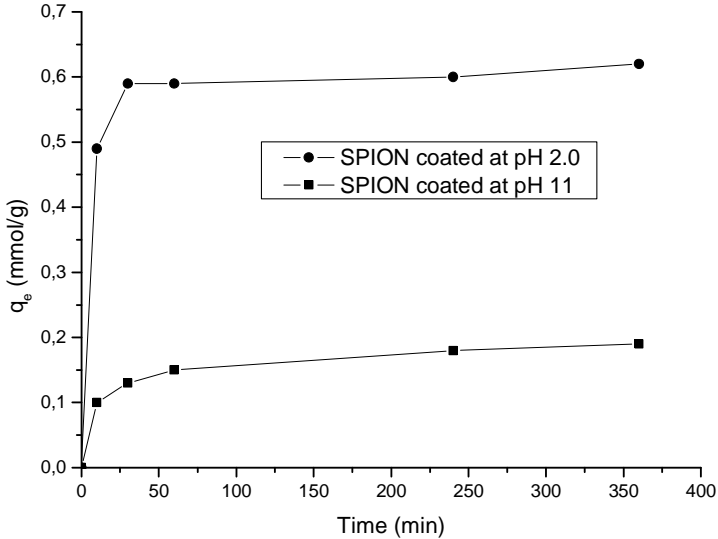
Figure 5
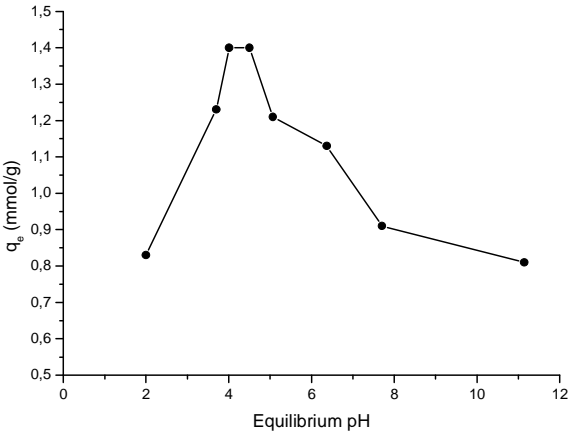
Figure 6
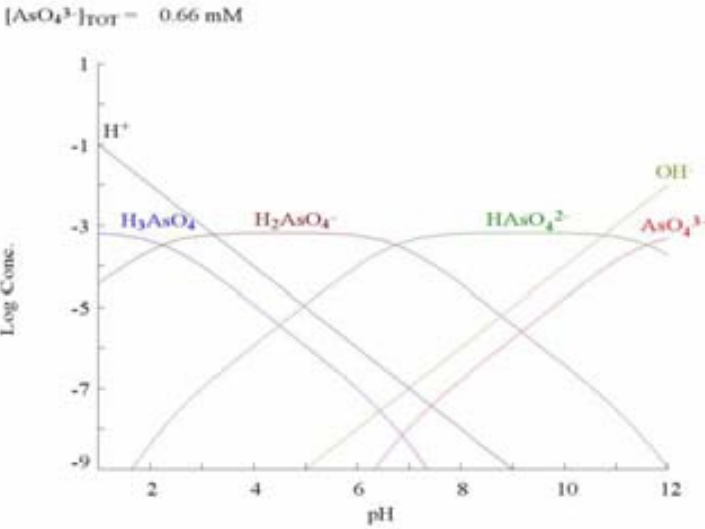
Figure 7
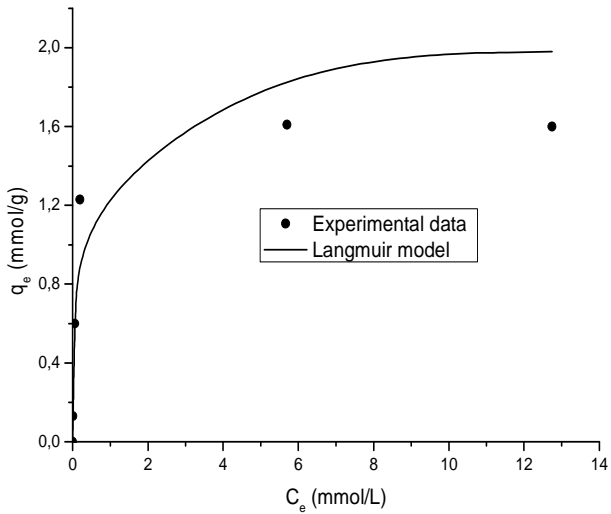
Figure 8
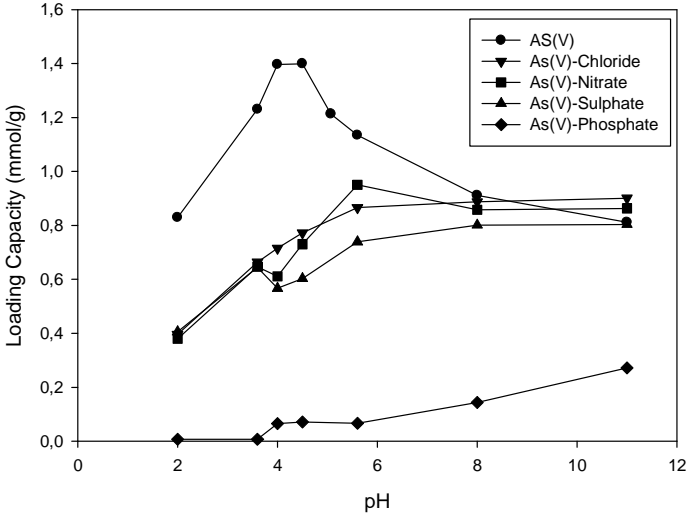
FIGURE CAPTIONS

Figure 1. TGA curves of SPION (pristine nanoparticles) and 3-MPA-coated SPION.

Figure 2. (a) TEM image of the SPION synthesized with co-precipitation method and surface coated with 3-MPA; (b) EDX analysis of the coated SPION.

Figure 3. FI-IR spectra of (a) 3-MPA, (b) SPION, (c) 3-MPA-coated SPION.

Figure 4. Effect of contact time on the removal of As(V) with SPION coated with 3-MPA at pH 2.0 and 11. As(V) initial concentration of 50 ppm and equilibrium pH of 4.0. The lines are guidelines.

Figure 5. Effect of pH on the removal of As(V) using SPION coated 3-MPA.

Figure 6. Diagram of the different species of As(V) in function of the pH.

Figure 7. Effect of initial As(V) concentration.

Figure 8. Effect of the presence of interfering anions on the As(V) removal with 3-MPA coated SPION in a pH range of 2.0 and 11.0. The lines are guidlines.

Metal ions	Sorption (%)	
	Molar ratio 1:1	Molar ratio 1:2
As(V)	95	96
Cu(II)	2	0.1
Ni(II)	0.5	2
Zn(II)	0.5	3

Table 1. Selective adsorption of As(V) from a mixture of base metals.

Sample	Loading Capacity (mmol/g)	% Decrease of Loading Capacity
Without Interference	1,400	-
Chloride	0,773	44,8
Nitrate	0,731	86,6
Sulphate	0,603	56,9
Phosphate	0,072	94,9

Table 2. Interfering effect of different anions in the loading capacity of As(V) at pH 4.0.

I.3. Cellulose-SPION nanofiber composites for water purification.

Cellulose-SPION nanofiber composites for water purification

D. Morillo[1], A. Uheida[2], G. Pérez[1], M. Mamoun[2], M. Valiente[1]*

[1]Departament de Química, Química Analítica, Universitat Autònoma de Barcelona, Bellaterra, Barcelona, Spain

[2]Functional Materials Division, KTH- Royal Institute of Technology, Kista, Stockholm, Sweden

ABSTRACT.

Water treatment purification is a field where the nanocomposites can be successfully applied. Nanocomposites can contribute to the removal of dangerous and carcinogenic pollutants from water such as arsenic. An example of these nanocompsites is cellulose acetate (CA) and cellulose acetate–Fe_3O_4 nanofibers, prepared by electrospinning technique from. CA solutions mixed with Fe_3O_4 nanoparticles, employing N,N-dimethylacetamide and acetone as the polymer solvent. In this study, the preparation of nanocomposites was optimized by both different CA nanofibers concentrations (10-20%) and Superparamagnetic Iron Oxide Nanoparticles concentrations (0,3% and 3.0% (w/v) to be dispersed in CA solution. Also the influence of Fe_3O_4 concentration on the size and morphology of the fibers was examined by scanning electron microscopy (SEM) and transmission electron microscopy (TEM). Preliminary studies of arsenic(V) adsorption in dynamic mode were made obtaining

interesting results that demonstrate that the adsorbent system is useful for this application, with a loading capacity of 0,09 mmol As(V) / g.

INTRODUCTION

Arsenic contamination of groundwater due to both natural (weathering reactions and biological activities) and anthropogenic (industrial wastewater effluents, primarily from metal processing and electroplating plants, as well power plants) sources is a widespread hazard affecting vast regions, being the maximum allowable arsenic level in drinking water set at 10 μg/L by the World Health Organization (2001) (1-4).

Among the vast amounts of information available in the literature there are several studies related to the removal of arsenic from contaminated groundwater at concentration levels of less than 1 mg/L, with a focus on preparing drinking or potable water, mainly employing adsorption treatments (3). Commonly used adsorbents include iron- and aluminum containing compounds such as hydrous ferric oxide; ferrihydrite; goethite; activated alumina, zeolites, sand (5-11), activated carbon granules and Fe-modified carbons (12-20). In these cases, precipitation or coprecipitation is the suitable treatment option, despite some disadvantages such as low removal efficiencies for arsenic requiring, preoxidation for better results or the production of toxic sludge, as well as their handling, storage, and treatment, which increase the final economical cost.

The development of new adsorbent system to remove As(V) from contaminated waters include the electrospinning as an established technique for the fabrication of micro- and nanofibrous polymer structures. Although the basic principle of the process is quite simple, there are too many parameters involved (e.g. applied voltage, concentration, conductivity and

viscosity of the solution), which has been studied (21, 22). The electrospinning technique has been widely employed, for preparing fibrous structures based on biocompatible–biodegradable polymers and polymer–inorganic composite materials, especially for biomedical applications (23-25).

Among the many materials employed in the manufacture of nanofibers, cellulose acetate (CA) is a well known derivative of cellulose, produced either by heterogeneous or homogeneous acetylation of cellulose (26, 27), used in a broad field of applications such as adhesive, film base in photography, in separation processes (e.g. filtering, reverse osmosis) (26), or ionic liquids as cellulose solvents (27-30) after homogeneous acetylation of cellulose. In contrast to cellulose, cellulose acetate possesses a much less crystalline structure and thus exhibits better solubility in common organic solvents such as acetone and porous structures based on CA have been developed (31, 32). Previously mentioned applications demand their synthetic preparation i.e by electrospinning. However, some parameters such as nature of solvent and applied voltage affect the fiber size and morphology (33, 34). While the generated CA in the form of nanofibers is applied for drug encapsulation (35, 36), as electrospun membranes are employed in separation processes (37, 38). CA–silver composite (39) and CA–polymer blends (35, 40) have been successfully electrospun for bacterial removal in water treatment or as tissue engineering scaffolds (41).

Another interesting alternative comprises the implementation of iron oxides, such as superparamagnetic iron oxide nanoparticles (SPION), in CA nanofibers. Such alternative would be interesting due to the exhibited biocompatibility and magnetic properties and the fact of increasing concern in the field of biomedical applications, for clinical diagnosis (imaging), cell labeling, drug targeting, and enzyme immobilization (42). Usually iron oxide nanoparticles are synthesized in situ in a polymer solution, obtaining a polymer–iron oxide composite. Although the in situ synthesis exhibits certain advantages (e.g. control of particle

size), it is mainly applied to water-soluble polymers. By this approach, a gelatin–iron oxide composite material has been developed and proposed as tissue engineering scaffold (43).

In short, considering the needs in the remediation As(V) polluted streams, cellulose acetate–iron oxide composite materials with nanofibrous structure were developed in this study via the electrospinning technique. The iron oxide nanoparticles were dispersed in the polymer solution at different concentrations. The influence of iron oxide concentration on the fiber size, morphology and thermal behavior was examined. The produced materials have potential use in adsorption and separation processes applications.

EXPERIMENTAL SECTION

Chemicals and Reagents. Sodium hydrogen arsenate heptahydrate, iron(III) chloride hexahydrate, Iron(II) chloride anhydrous, ammonium hydroxide, toluene, sodium acetate tryhydrate, acetic acid, nitric acid and sodium hydroxide were employed (Sigma-Aldrich). Tetramethyl ammonium hydroxide (TMAOH, Fluka 25%) was used as redispersing agent. Cellulose Acetate, N,N-dimethylacetamiede (DMA) and acetone as polymer solvents and high purity water with a resistivity of 18 $M\Omega\,cm^{-1}$ was used throughout all the experiments.

Characterization techniques for the adsorbent system. SPION were imaged by transmission electron microscopy (HR-FEG-TEM, JEOL JEM-2100) and the CA nanofibers were imaged by scanning electron microscopy (SEM, Zeiss Ultra 55, Gemini) and SEM to show the homogeneity of the electrospinning method as well as the distribution of the SPION on and into of the nanofiber. The stability and the homogeneity of the SPION suspension in hydrodynamic mode were determined by Dynamic Light Scattering (DLS, Delsa Nano C, Beckman Coulter).

Synthesis of adsorbent materials. The synthesis of 10nm SPION was performed as described elsewhere (44, 45). The synthesis requires a constant bubbling of nitrogen to prevent oxidation of iron(II) and therefore, the generation of other iron oxides such as maghemite or ferrihydrite. A stock solution of iron(III) in chloride media was prepared by dissolving the corresponding salt with a deoxygenated 0.2M HCl aqueous solution. This solution was added to a deoxygenated solution of 0.7M NH_4OH, heated to 70ºC, under mechanical stirring. After few minutes, the respective salt of iron(II) in a ratio 2:1 was added. The particles were aged in the solution for 45 min under mechanical stirring and nitrogen bubbling, decanted and washed with deoxygenated water several times. From this step, a subsequent redispersion step of the particles in an aqueous solution of TMAOH 0,01 M (≈pH 12) let to obtain SPION.

The synthesized nanoparticles were characterized through two techniques: by DLS preparing a dilution 1:100 v/v of the initial SPION suspension and by particle size determination through TEM (46-48).

The solutions used in the experiments had varying concentration of cellulose acetate between 10-20% (w/v) to determine which the best way to synthesize the nanofibers. The solvent was mixture of acetone and DMA in 2/1 v/v. Once the nanofibers were synthesized, different solutions were prepared with different concentration of SPION (0%, 0,3%, 3.0% (w/v)).

Two different procedures were compared when preparing nanocomposites. The first procedure involves the generation of a polymer dissolution and dispersion of Fe_3O_4 after accurately weighting cellulose acetate and adding an acetone/DMA mixture. The generated dissolution and dispersion are mixed and sonicated in order to obtain the electrospinning solution, shaking at room temperature to avoid sedimentation of the particles. Such procedure generates SPION particles inside CA nanofibers. The second procedure requires the CA

nanofiber dipping into the SPION suspension at different pH(3, 6.8, 11), for two hours under oscillatory shaking, generating SPION over the surface of the CA nanofibers. Afterwards, the obtained nanocomposites are rinsed with water and dried in a vacuum oven.

Electrospinning experiments. The electrospinning of the solutions was carried out by keeping constant flow solution rate (0.5 ml/h), constant needle to target distance (5 cm) and by applying two different voltages (9 and 12 kV) between the target and the needle. The target was a drum covered with aluminum foil. The samples were observed with SEM and TEM.

Adsorption experiment. The adsorption experiments were performed in dynamic mode by crossing aqueous solution of 100ppm of As(V) in 0.2M Acetic/Acetate media in a column 10x1 cm with a CA nanofiber, with a certain flow rate (1ml/min) of the arsenic solution. The pH of the solutions was controlled using 0.5M HNO_3 and 0.5M NaOH and confirmed with pH measurements (pH meter, Crison). After the experiment, the aliquot will be centrifuged (14000rpm) and decantation with external magnet. As and Fe ions content in the obtained supernatant was determined by inductively coupled plasma atomic emission spectroscopy (ICP-OES, iCAP 6000 ICP Spectrometer, Thermo Fisher).

Firstly, this experiment was realized with the CA nanofiber alone and later on, it was performed for the CA nanofiber with SPION

RESULTS AND DISCUSSION

Characterization of adsorbent material. The morphology of the nanoparticles, primarily its size, determines its adsorption capacity. A 10.5 nm, optimal particle size for adsorption application it is highlighted in the literature (45, 49, 50). From the TEM micrograph (Fig.1) a main spherical morphology for nanoparticles can be observed, which are partially aggregated

when SPION are in suspension. The homogeneity of the SPION suspension was verified by DLS analysis.

Figure 1. TEM micrograph of synthesized SPION.

Fibrous structure of CA nanofibers. SEM micrographs of CA-Nanofibers given in Fig 2 a, b, c, show the difference in diameter and the homogeneity of the nanofiber with the variation of concentration of the Cellulose Acetate. (51).

Figure 2. SEM micrograph of CA nanofiber at different CA concentration: 20% (a), 15% (b) and 10% (c) and at 9 kV.

SEM micrographs give us the information to determine the optimum CA concentration. As it can be observed in Fig. 2c, by decreasing the CA concentration the structure becomes less uniform. While 20%, provides a heterogenous fibers diameter and bubbles appear at 10% CA concentration, 15 % CA concentration generates the appropriate nanofibers to prepare the nanocomposites. High CA concentrations involve higher jet instability, which creates random fibers and thus non-uniform structures

The fibers are not homogeneous in diameter and at 10%, bubbles appear suggesting an unstable electrospinning as well as the generation of non-homogenous or reproducible nanofibers. It must be pointed out that the employed solvent mixture had a quite high boiling point and a reduced volatility (due to the addition of DMA) in contrast to common volatile organic solvents. Also, less time is available for solvent evaporation as the production of the fibers becomes more rapid. Subsequently, residual solvent remains in the fibers when they reach the target. This leads to coalescence of neighboring fibers and thus the produced structure is less uniform.

Fibrous structures of CA-SPION nanofiber composites by electrospinning. For the CA-SPION nanofiber composites, SEM and TEM were performed and the influence of iron oxide concentration on the fiber size can be analysed. Rather peculiar were the results considering the influence of iron oxide concentration on the fiber size. By adding only 0.3% of SPION in dry powder, an increase in the average fiber diameter is observed, as can be seen in Fig. 3a. However, further increase of the iron oxide content does not seem to have any major influence on the fiber size (Fig. 3b). Usually, by increasing the concentration of the solution, the fiber size is also increased, due to increase in the viscosity (21).

Figure 3. SEM micrograph of CA-SPION Nanofiber composites at 15% of CA and different SPION concentration: 0.3% (a), 3.% (b) at 9 kV.

It must be taken into account that the addition of the nanoparticles into the polymer solution has a double effect. Firstly, it is reasonable to expect increased viscosity due to the increase of the total dispersion concentration. However, the solid nanoparticles hinder polymer chain interactions by increasing their distance. The second phenomenon prevails in the 3.0% iron oxide dispersion, while with further increase of iron oxide content, the first phenomenon becomes dominant and the expected increase of the viscosity is observed. It should be mentioned here, that unexpected decrease in viscosity of polymer blend, due to nanoscale

effects, has been reported in the literature (52). Thus, when adding 3.0% of iron oxide, the decrease in the viscosity tend to decrease the nanofiber size.

TEM micrographs of the 0.3% SPION nanofiber composite are presented in Fig 4a and 4b. In this composite, the presence of SPION inside of the fibers can be seen and it shows that the electrospinning technique is useful for the preparation of this adsorbent materials. The problem is that with these characterization techniques its impossible say we are sure that the SPION is inside of the nanofiber.

Figure 4. TEM micrograph of CA-SPION nanofiber composites with 15% of CA and 0.3% of SPION (a, b) at 9 kV.

Fibrous structures of CA-SPION nanofiber composites by dipping. Representative SEM pictures of the composite materials are presented in Figure 5. In the pH 6.8 and 11.0 composite some iron oxide aggregates can be seen upon the fibers. In the composite of pH 3.0, iron oxide aggregates are hardly visible, while in the composites of neutral or basic pH, no aggregates can be seen.

Finally it is worth mentioning that all of the composite materials could be magnetized. Thus, they could possibly be used in advanced separation processes induced by external magnetic field (separation due to pore structure and due to magnetism.

Figure 5. SEM micrograph of CA-SPION nanofiber composites by dipping at different pHs: 3.0 (a), 6.8 (b) and 11.0 (c) with 0.3% of SPION at 9 kV.

Equilibrium time determination for CA-SPION nanofiber composite. 0.3% SPION and 15% CA nanofiber composite synthesized by electrospinning (Fig. 6a) and by dipping (Fig. 6b) was used for the adsorption experiment and the adsorption percentage determination. The equilibrium was acquired at 120 minutes of adsorption in continuous mode. It can show that with a higher load of SPION in the CA nanofiber, the system will work better.
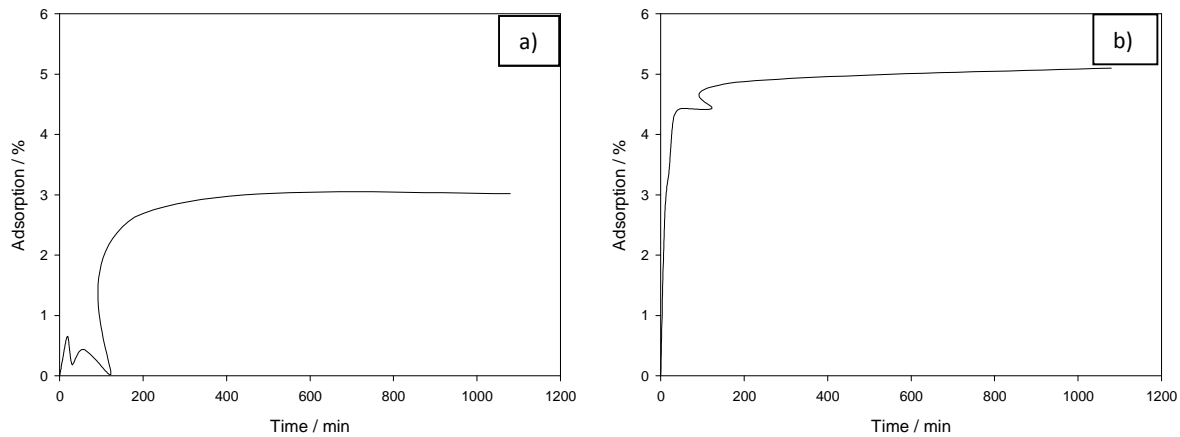
Figure 6. Equilibrium time study for the As(V) adsorption at pH 3,6 in CA-SPION nanofibers composites synthesized by electrospinning (a) and dipping (b).

CONCLUSIONS

The present studies have demonstrated that CA-SPION nanoparticles composites can be applied for the removal of As(V) in drinking water treatment or industrial water waste. An important study must be done to understand the mechanism and the real loading capacity due to the As(V) concentration was so high in this analysis and it's necessary to adjust the As(V) concentration to the maximum levels permited. It will be important for the development of this system and the final application. Thus, these nanofiber composites show certain magnetism that give an interesting ability to be recovered.

REFERENCES.

(1) Smedley, P. L.; Kinniburgh, D. G. A review of the source, distribution and behaviour of arsenic in natural waters. *Appl. Geochem.* **2002**, *17*, 517–568.

(2) Villaescusa, I.; Bollinger, J. C. Arsenic in drinking water: Sources, occurrence and health effects (a review). *ReV. EnViron. Sci. Biotechnol.* **2008**, *7*, 307–323.

(3) Mohan, D.; Pittman, C. U. Arsenic removal from water/wastewater using adsorbentssA critical review. *J. Hazard. Mater* **2007**, *142*, 1–53.

(4) Mandal, B. K.; Suzuki, K. T. Arsenic round the world: A review. *Talanta* **2002**, *58*, 201–235.

(5) Raven, K. P.; Jain, A.; Loeppert, R. H. Arsenite and arsenate adsorption on ferrihydrite: Kinetics, equilibrium, and adsorption envelope. *EnViron. Sci. Technol.* **1998**, *32*, 344–349.

(6) Singh, T. S.; Pant, K. K. Equilibrium, kinetic and thermodynamic studies for adsorption of As(III) on activated alumina. *Sep. Purif. Technol.* **2004**, *36*, 139–147.

(7) Guan, X. H.; Su, T.; Wang, J. Quantifying effects of pH and surface loading on arsenic adsorption on NanoActive alumina using a speciationbased model. *J. Hazard. Mater.* **2009**, *166*, 39–45.

(8) Lenoble, V.; Laclautre, C.; Deluchat, V.; Serpaud, B.; Bollinger, J. C. Arsenic removal by adsorption on iron(III) phosphate. *J. Hazard. Mater* **2005**, *123*, 262–268.

(9) Badruzzaman, M.; Westerhoff, P.; Knappe, D. R. U. Intraparticle diffusion and adsorption of arsenate onto granular ferric hydroxide (GFH). *Water Res.* **2004**, *38*, 4002–4012.

(10) Lo, S. L.; Jeng, T. H.; Chin, L. H. Characteristics and adsorption properties of an iron-coated sand. *Water Sci. Technol.* **1997**, *35* (7), 63–70.

(11) Onyango, M. S.; Kojima, Y.; Matsuda, H.; Ochieng, A. Adsorption kinetics of arsenic removal from groundwater by iron-modified zeolite. *J. Chem. Eng. Jpn.* **2003**, *36*, 1516–1522.

(12) Lorenzen, L.; Deventer, J. S. J.; Landi, W. M. Factors affecting the mechanism of the adsorption of arsenic species on activated carbon. *Miner. Eng.* **1995**, *8*, 557–569.

(13) Hong, H. J.; Kim, H.; Baek, K.; Yang, J. W. Removal of arsenate, chromate and ferricyanide by cationic surfactant modified powdered activated carbon. *Desalination* **2008**, *223*, 221–228.

(14) Dang, S. V.; Kawasaki, J.; Abella, L. C.; Auresenia, J.; Habaki, H.; Gaspillo, P. D.; Kosuge, H. Removal of arsenic from synthetic groundwater by adsorption using the combination of laterite and iron modified activated carbon. *J. Water EnViron. Technol.* **2008**, *6*, 43–54.

(15) Mondal, P.; Majumder, C. B.; Mohanty, B. Effects of adsorbent dose, its particle size and initial arsenic concentration on the removal of arsenic, iron and manganese from simulated ground water by Fe3+ impregnated activated carbon. *J. Hazard. Mater.* **2008**, *150*, 695–702.

(16) Gu, Z.; Fang, J.; Deng, B. Preparation and evaluation of GACbased iron containing adsorbents for arsenic removal. *EnViron. Sci. Technol.* **2005**, *39*, 3833–3843.

(17) Muñiz, G.; Fierro, V.; Celzard, A.; Furdin, G.; Gonzalez-Sanchez, G.; Ballinas, M. L. Synthesis, characterization and performance in arsenic removal of iron-doped activated carbons prepared by impregnation with Fe(III) and Fe(II). *J. Hazard. Mater.* **2009**, *165*, 893–902.

(18) Chen, W.; Parette, R.; Zou, J.; Cannon, F. S.; Dempsey, B. A. Arsenic removal by iron-modified activated carbon. *Water Res.* **2007**, *41*, 1851–1858.

(19) Zhang, Q. L.; Lin, Y. C.; Chen, X.; Gao, N. Y. A method for preparing ferric activated carbon composites adsorbents to remove arsenic from drinking water. *J. Hazard. Mater.* **2007**, *148*, 671–678.

(20) Jang, M.; Chen, W.; Cannon, F. S. Preloading hydrous ferric oxide into granular activated carbon for arsenic removal. *EnViron. Sci. Technol.* **2008**, *42*, 3369–3374.

(21) Deitzel, J.M., Kleinmeyer, J., Harris, D., & Beck Tan, N. C. (2001). The effect of processing variables on the morphology of electrospun nanofibers and textiles. *Polymer, 42, 261-272*.

(22) Tungprapa, S., Puangpam, T., Weerasombut, M., Jangchud, I., Fakum, P., Semongkhol, S., Meechaisue, C., & Supaphol, P.(2007). Electrospun cellulose acetate fibers: Effect of solvent system on morphology and fiber diameter. *Cellulose, 14, 563–575.*

(23) Dalton, P. D., Klinkhammer, K., Salber, J., Klee, D., & Moller, M. (2006). Direct in vitro electrospinning with polymer melts. *Biomacromolecules, 7, 686–690.*

(24) Fujihara, K., Kotaki, M., & Ramakrishna, S. (2005). Guided bone regeneration membrane made of polycaprolactone/calcium carbonate composite nanofibers. *Biomaterials, 26, 4139–4147.*

(25) Marras, S. I., Kladi, K. P., Tsivintzelis, I., Zuburtikudis, I., & Panayiotou, C. (2008). Biodegradable polymer nanocomposites: The role of nanoclays on the thermomechanical characteristics and the electrospun fibrous structure. *Acta Biomaterialia, 4, 756–765.*

(26) Rodrigues Filho, G., Monteiro, D. S., da Silva Meireles, C., Assuncao, R. M. N., Cerqueira, D. A., Barud, H. S., Ribeiro, S. J. L., & Messadeq, Y. (2008). Synthesis and

characterization of cellulose acetate produced from recycled newspaper. *Carbohydrate Polymers, 73, 74–82.*

(27) Wu, J., Jhang, H., He, J., Ren, Q., & Guo, M. (2004). Homogeneous acetylation of cellulose in a new ionic liquid. *Biomacromolecules, 5, 266–268.*

(28) Tsioptsias, C., & Panayiotou, C. (2008). Preparation of cellulose–nanohydroxyapatite composite scaffolds from ionic liquid solutions. *Carbohydrate Polymers, 74, 99–105.*

(29) Tsioptsias, C., Stefopoulos, A., Kokkinomalis, I., Papadopoulou, L., & Panayiotou, C. (2008). Development of micro- and nano-porous composite materials by processing cellulose with ionic liquids and supercritical CO_2. *Green Chemistry, 10, 965–971.*

(30) Viswanathan, G., Murugesan, S., Pushparaj, V., Nalamasu, O., Ajayan, P. M., & Linhardt, R. J. (2006). Preparation of biopolymer fibers by electrospinning from room temperature ionic liquids. *Biomacromolecules, 7, 415–418.*

(31) Fischer, F., Rigacci, A., Pirard, R., Berthon-Fabry, S., & Achard, P. (2006). Cellulose based aerogels. *Polymer, 47, 7636–7645.*

(32) Reverchon, E., & Cardea, S. (2007). Production of controlled polymeric foams by supercritical CO2. *The Journal of Supercritical Fluids, 40, 144–152.*

(33) Han, S. O., Youk, J. H., Min, K. D., Kang, Y. O., & Park, W. H. (2008). Electrospinning of cellulose acetate nanofibers using a mixed solvent of acetic acid/water: Effects of solvent composition on the fiber diameter. *Materials Letters, 62, 759– 762.*

(34) Tungprapa, S., Puangpam, T., Weerasombut, M., Jangchud, I., Fakum, P., Semongkhol, S., Meechaisue, C., & Supaphol, P. (2007). Electrospun cellulose acetate

fibers: Effect of solvent system on morphology and fiber diameter. *Cellulose, 14, 563–575.*

(35) Chen, C., Wang, L.,&Huang, Y. (2007). Electrospinning of thermo-regulating ultrafine fibers based on polyethylene glycol/cellulose acetate composite. *Polymer, 48, 5202–5207.*

(36) Tungprapa, S., Jangchud, I., & Supaphol, P. (2007). Release characteristics of four model drugs from drug-loaded electrospun cellulose acetate fiber mats. *Polymer, 48, 5030–5041.*

(37) Ma, Z., Kotaki, M., & Ramakrishna, S. (2005). Electrospun cellulose nanofibers as affinity membrane. *Journal of Membrane Science, 265, 115–123.*

(38) Zhang, L., Menkhaus, T. J., & Fong, H. (2008). Fabrication and bioseparation studies of adsorptive membranes/felts made from electrospun cellulose acetate nanofibers. *Journal of Membrane Science, 319, 176–184.*

(39) Son, W. K., Youk, J. H., & Park, W. H. (2006). Antimicrobial cellulose acetate nanofibers containing silver nanoparticles. *Carbohydrate Polymers, 65, 430–434.*

(40) Zhang, L., & Hsieh, Y. L. (2008). Ultra fine cellulose acetate/poly(ethylene oxide) biocomponent fibers. *Carbohydrate Polymers, 71, 196–207.*

(41) Entcheva, E., Bien, H., Yin, L., Chung, C. Y., Farrell, M., & Kostov, Y. (2004). Functional cardiac cell constructs on cellulose-based scaffolding. *Biomaterials, 25, 5753–5762.*

(42) Heymer, A., Haddad, D., Weber, M., Gbureck, U., Jakob, P. M., Eulert, J., & Noth, U. (2008). Iron oxide labeling of human mesenchymal stem cells in collagen hydrogels for articular cartilage repair. *Biomaterials, 29, 1473–1483.*

(43) Hu, S. H., Liu, T. Y., Tsai, C. H., & Chen, S. Y. (2007). Preparation and characterization of magnetic ferroscaffolds for tissue engineering. *Journal of Magnetism and Magnetic Materials, 310, 2871–2873.*

(44) Uheida, A.; Salazar-Alvarez, G.; Björkman, E.;Zhang, Y; Muhammed, M. Sorption of palladium(II), rhodium(III) and platinum(IV) on Fe_3O_4 nanoparticles. *J. Colloid Interface Sci.*, **2006**, *301*, 402-408.

(45) Uheida, A.; Salazar-Alvarez, G.; Björkman, E.;Zhang, Y; Muhammed, M. Fe_3O_4 and γ- Fe_2O_3 nanoparticles for the adsorption of Co^{2+} from aqueous solution. *J. Colloid Interface Sci.*, **2006**, *298*, 501-507.

(46) JCPDS, International Centre for Powder Diffraction Data: Swarthmore, PA, Card No. 19, (1989) 629.

(47) Cerda, L.A. G.; Fernández, S. R.; Galindo, R. B.; Guerrero, R. S. Síntesis y propiedades de ferrofluidos de magnetita. *Superficies y Vacío*, **2003**, *16* (1), 28-31.

(48) Salazar, J. S.; Roman, M.A. C.; Gomez, L. B. Structural and magnetic domains characterization of magnetic nanoproperties. *Materials Science and Engineering C*, **2007**, *27*, 1317-1320.

(49) Shipley, H. J.; Yean, S.; Kan, A. T.; Tomson, M. B. Adsorption of arsenic to magnetite nanoparticles: effect of particles concentration, pH, ionic strength and temperature. *Environmental Toxicology and Chemistry*, **2009**, *28* (3), 509–515.

(50) Chin, A.B.: Yacob, I.I. Synthesis and characterization of magnetic iron oxides nanoparticles via w/o microemulsions and Massart´s procedure. *Journal of Materials Processing Technology*, **2007**, *191*, 235-237.

(51) Zhou, H., Green, T. B., & Joo, Y. L. (2006). The thermal effects on electrospinning of polylactic acid melts. *Polymer, 47, 7497–7505.*

(52) Mackay, M. E., Dao, T. T., Tuteja, A., Ho, D. L., Van Horn, B., Kim, H. C., & Hawker, C. J. (2003). Nanoscale effects leading to non-Einstein-like decrease in viscosity. *Nature Materials, 2, 762–766.*

I.4. Arsenic speciation in the adsorption process of arsenate onto Forager® Sponge loaded SPION by XANES.

Arsenic speciation in the adsorption process of arsenate onto Forager® Sponge loaded SPION by XANES

D.MORILLO[a], G. PÉREZ[a] and M. VALIENTE[a]*

[a]*Universitat Autònoma de Barcelona, Centre GTS, Department of Chemistry, 08193 Bellaterra (Barcelona), Spain, diego.morillo.martin@gmail.com, Gustavo.perez@uab.es and manuel.valiente@uab.cat*,*

* Corresponding Author

ABSTRACT

In this paper, the arsenic speciation in the adsorption process onto Forager® Sponge loaded SPION by means of X-Ray Absorption Spectroscopy has been studied. This Forager® Sponge material present high as that enhances the exchange with Fe, and have been later applied to the adsorption of arsenate in order to profit the high affinity of Fe(III) towards arsenic inorganic species. Principal Analysis Components (PCA) and linear combination fit were applied to ascertain the contribution of each arsenic reference species and the results confirm, for analyzed Forager® Sponge loaded SPION at different pHs, that arsenate specie is predominant reaching until 97%. Then, arsenate is easily removed of the contaminated water with this adsorbent system. Regarding the SPION structure, Fe XANES studies reveals that SPION keeps the structure in the adsorption process in all cases, independently of the adsorbed species, As(III), As(V) or a mixture of both species. Then, direct speciation by synchrotron radiation technique had been verified as a useful technique for the arsenic speciation in solid samples.

INTRODUCTION

Arsenic biogeochemistry has received public and scientific attention due to environmental and public health disasters around the world [1,2,3]. Many types of adsorbents have been used for the removal of arsenic from aqueous effluents, many of them taking advantage of Fe(III) compounds affinity towards inorganic arsenic species. In this regard, many methodologies for arsenic removal involve the use of iron (hydr)oxydrates such as goethite (both natural or synthetic) [4, 5, 6], ferrihydrite [7, 8, 9] hematite [10, 11] or magnetite [12] and different Fe-bearing materials such as Fe(III)-exchange zeolites [13], aluminosilicates [14] or resins [15].

The understanding of the arsenic adsorption by iron (oxy)hydroxides and Fe-bearing materials is required to predict the long-term fate of arsenic and design new materials with improved capacity and efficiency for As sorption. In this context, XANES has become a valuable to provide key information about arsenic oxidation state in the sample,

In this sense, numerous remediation methodologies have been developed to remove As from drinking water (membranes, coagulation, anion exchange, etc.) although adsorption is the most commonly used due to its efficiency, capacity and relative low cost. Many different materials are being used for this purpose and the development of nanotechnology at the end of 20th century has widened the variety of adsorbents in several industrial and environmental applications. The nanosized iron oxide materials take advantage of the affinity of Fe(III) for aqueous inorganic arsenic species. The small size of nanoparticles provides several advantages, mainly related to the extremely high surface area which allows improving the removal capacity several orders of magnitude [16].

One fundamental difficulty in evaluating the leaching potential of As in the spent adsorbents is the accurate determination of its speciation in different solid phases and its possible presence as adsorbed surface complexes. X-ray absorption spectroscopy (XAS) including X-ray Absorption Near Edge Structure (XANES) and Extended X-ray Absorption Fine Structure (EXAFS) was developed as a quantitative, short-range structural probe in the 1970's following the pioneering work of [17]. XAS has since been applied widely in various fields of science and engineering to determine oxidation states and species of chemicals in solid, liquid, and biological samples. Among the most important applications of XAS in the environmental field is the study of As speciation and surface complexation in the aqueous phase and at liquid-mineral interfaces. [18,19,20,21,22] However, only limited reports have applied XAS in studying Ascontaining spent adsorbents. [23]

XANES can be used to determine arsenic speciation under in situ conditions. The excitation energy for As(III) is well-separated from As(V) by more than 3 eV. The organic As species can also be distinguished from inorganic As(III) and As(V).[24]

In this study, we carry out the contact of superparamagnetic iron oxide nanoparticles (SPION) with synthetic arsenic solutions in form of arsenate, arsenite or mixture of both. The study of the processes controlling arsenic adsorption expects to provide information to optimize the load of the Forager® Sponge with SPION and get adsorbent system with high loading capacity which proves the potential application to water treatment purification. The objective of the XAS studies is the characterization of the arsenic adsorbed in the Forager® Sponge loaded SPION and it is expected to evaluate the arsenic speciation in order to develop a methodology to study arsenite and arsenate in the same sample. To achieve this objective synchrotron radiation techniques based on X-Ray Absorption Near Edge Structure (XANES) are applied.

EXPERIMENTAL

In this work, powdered samples of the Fe(III)-bearing materials were reacted with solutions containing arsenic. The form in which the arsenic was taken up by each mineral was then investigated using X-Ray absorption spectroscopy.

Synthesis of the Forager® Sponge loaded SPION. The synthesis of 10 nm SPION is performed by co-precipitation method as described elsewhere.[25] A deoxygenated aqueous solution of tetramethylammonium hydroxide (TMAOH) 0.01 M (pH≈12) let to obtain SPION in a stable suspension for 6-8 months under deoxygenated atmosphere.

After SPION synthesis, Forager® Sponge is loaded with SPION to develop a new adsorbent material. A pretreatment, by immersion in a hydrochloric acid for wiping their acidic form, is performed in order to activate the amino groups and to facilitate SPION immobilization. [26] Having the SPION and the Forager® Sponge in acidic form, SPION load over the Forager® Sponge surface is performed. Such surface treatment is achieved using a pneumatic nebulizer that generates a homogeneous SPION dispersion, with the assistance of a peristaltic pump, under 30 psi of nitrogen.

Different fixations were prepared depending on the number of SPION impregnations and also the impregnation time. The Forager® Sponge appearance change completely and a colour change from orange-yellow to black after the SPION impregnation, was observed. Finally, a cleaning process is needed with deoxygenated water in order to remove the SPION excess that is not attached over the sponge surface. SPION loaded sponge is dried during 24 hours at 40 ℃ in oven and is kept in a desiccator until their use. The amount of SPION deposited was calculated by difference between the initial sponge acidic form weight and the weight of the loaded sponge as well as by the analysis of the Fe present in both the Forager® Sponge loaded SPION using microwave digestion and determining Fe by ICP-OES.

Arsenic Adsorption process on Forager® Sponge loaded SPION. The adsorption experiments were performed in batch mode by mixing aqueous solutions of 50ppm As(v) ($Na_2HAsO_4·7H_2O$, Sigma-Aldrich), As(III) ($NaAsO_2$, Sigma-Aldrich) or As(III)/As(V) mixture in 0.2M Acetic/Acetate media at room temperature (23±1 ℃) during 120 min with constant amounts of Forager® Sponge loaded SPION using a rotatory shaker. pH effect is interesting to observe its effect in the adsorption for the different arsenic species. Three pHs

were studied: 2.0; 3.6; 5.6. The pH of the solutions was controlled using 1.0M HNO_3 or 1.0M NaOH standardized solutions and confirmed with pH measurements.

Sample preparation of Forager® Sponge loaded SPION with adsorbed arsenic. After the adsorption process, Forager® Sponge loaded SPION of $Na_2HAsO_4·7H_2O$ (PANREAC) at pH=4 during 4h at 30 rpm. The suspension was filtered, thoroughly washed three times with distilled water and dried in an oven under air at 60ºC overnight.

Finally, each sample was milled to a fine powder and gently homogenized in an agate mortar with polyethylene (Sigma Aldrich, USA) which is transparent to X-rays, sieved below $< 2\mu m$. Each pellet has a total weight of 100 mg, 20 mg of standard sample and 80 mg of polyethylene. Samples were converted into pellets by hydraulic pressure (hydraulic press 25t RIIC, London) to be analyzed at the experimental station of the synchrotron facility. The obtained pellets were sealed between Kapton™ tape in order to avoid direct contact with the atmosphere and conserve the sample properties (**Figure 1**).

Figure 1. Example of samples encapsulated in Kapton® foils for the synchrotron experiments.

The standard samples for arsenic and iron species consist in a mixture and homogenization of standard samples with polyethylene to dilute and give consistence to the pellet. Later, the samples were homogenized, milled to a fine powder and converted into pellets by hydraulic pressure like the samples. The **Figure 2** shows the different compounds employed to synthetize the standard samples for arsenic and iron.

Figure 2. Studied arsenic and iron species

These species were selected as standard samples due to in arsenic experiments $NaAsO_2$ and Na_2HAsO_4 were those compounds employed to prepare the solutions for the adsorption process. For iron, chloride salts were used in the SPION synthesis and SPION reference is the principal standard to determine if any structural change is produced in the adsorption process. The content of Fe and As on each samples was determined by using a Field-Portable X-Ray Fluorescence equipment (FP-XRF, Innov-X Systems, model Alpha-6500R).

X-Ray Absorption Spectroscopy. The local environment of the arsenic was investigated by X-ray absorption near-edge structure (XANES). Arsenic absorption was recorded at the edge energy for its K line at 11689 eV and its fluorescence $K_{\alpha1}$ at 10543.4 eV and $K_{\beta1}$ at 11725.8 eV at beamline BM25 of ESRF facilities. In the same way, iron absorption was recorded at the edge energy for its K line at 7112 eV and its fluorescence $K_{\alpha1}$ at 6405.2 eV and $K_{\beta1}$ at 7059.3 eV at beamline A1 of DORIS III HASYLAB facilities. In both facilities, the monochromator consisted in a Si (111) double crystal and the detection was measured either by adsorption and by fluorescence using a 7-pixel Si(Li) detector over the energy range 11700-12700 eV. The monochromator was calibrated using the L(III) edge of a gold foil (11919 eV). Since, fluorescence data were of higher quality, they were selected for data treatment.

Data treatment. The XAS spectra were analyzed with XAS data analysis software IFEFFIT (developed by Matt Newville at CARS, Consortium for Advanced Radiation Sources, at The University of Chicago) and the data analysis is focused in XANES region which inform about the oxidation state for the arsenic adsorbed in Forager® Sponge loaded SPION samples during the adsorption process.

Spectral averages for the replicates of each standard and unknown sample were made, the energy is calibrated and background correction and edge normalization were performed.

Arsenic quantitative speciation is obtained by Principal Components Analysis (PCA) and Adjustment by least squares of the standard compounds. To study de sample composition as a lineal combination of the standard compounds, IFEFFIT software produces iterative combination until the combination of all components is 100% (a $\pm10\%$ error is admitted). [27] The relative quality of the fit was quantified by the residual value, a measure of how close the fit (x_{fit}) is to the data (x_{data}) based on a sum of squares. Determination of the fractional misfit is defined as **Equation 1** defines:

$$R = \sum \frac{(x_{fit} - x_{data})^2}{(x_{data})^2} \qquad (1)$$

RESULTS

Arsenic speciation

Arsenic adsorption onto Forager® Sponge loaded SPION. Initial arsenic concentrations were analyzed by Field Portable X-Ray fluorescence equipment (FP-XRF) for both standards and samples in order to verify if the standards and samples have enough arsenic concentration to perform the synchrotron experiments (**Table 1**).[28]

Table 1. Initial arsenic concentrations for standards and samples by FP-XRF.

Standards [As] (mg/kg)					
NaAsO$_2$	209971±4121	**Na$_2$HAsO$_4$**	89455±1135	**As(III)/As(V)**	169644±3005
Samples [As] (mg/kg)					
As(III) 3.6 1i	411±8	**As(V) 3.6 1i**	8801±96	**As(III-V) 3.6 1i**	7428±85
As(III) 4.0 1i	419±8	**As(V) 4.0 1i**	6329±71	**As(III-V) 4.0 1i**	5112±60
As(III) 3.6 2i	418±8	**As(V) 3.6 2i**	9551±105	**As(III-V) 3.6 2i**	8103±96
As(III) 4.0 2i	418±8	**As(V) 4.0 2i**	7148±82	**As(III-V) 4.0 2i**	6270±74
As(III) 3.6 3i	497±9	**As(V) 3.6 3i**	10390±116	**As(III-V) 3.6 3i**	9177±104
As(III) 4.0 3i	376±8	**As(V) 4.0 3i**	8979 103	**As(III-V) 4.0 3i**	8307±93
As(III) 3.6 1iM	353±8	**As(V) 3.6 1iM**	9349±106	**As(III-V) 3.6 1iM**	6288±68

Sample concentration is lower than standards concentration. This fact is because of the standards are composed from a pure salt slightly diluted with polyethylene and in the samples case, only the adsorbed arsenic is detected which is lower than in standards.

Arsenic reference compounds. The arsenic K near-edge spectra for pure arsenic reference compounds of arsenite (NaAsO$_2$), arsenate (Na$_2$HAsO$_4$) and As(III)/As(V) mixture are shown in **Figure 3**. As expected, a shift of the edge position to higher energies becomes as arsenic is more oxidized, while k near-edge for As(III) is 11879,5 eV, k near-edge for As(V) is 11882,4 eV.
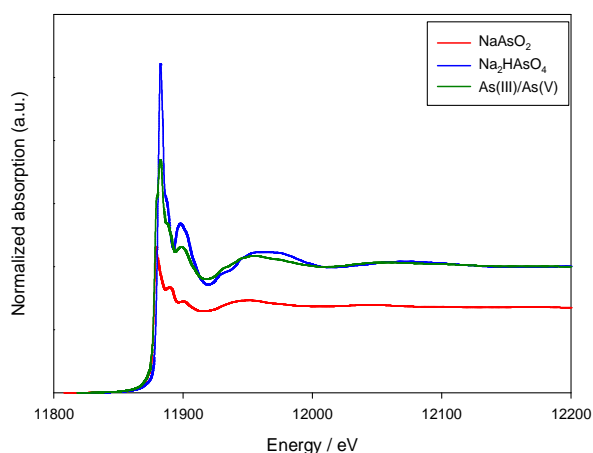
Figure 3. As K-edge XANES spectra of three reference compounds.

Arsenic adsorbed over Forager® Sponge loaded SPION. The direct comparison of XANES spectra for arsenic standards and arsenic adsorbed over Forager® Sponge loaded SPION samples was made. The first study was realised with only unique species at pH about 3.6 (optimum adsorption pH). The results show that the As(V) spectra were similar to the reference compound (**Figure 4a**) but As(III) spectra were different (**Figure 4b**). This difference was due to the interaction between Fe(III) of SPION and As(III) that produce a slight modifications in the spectra.[29]
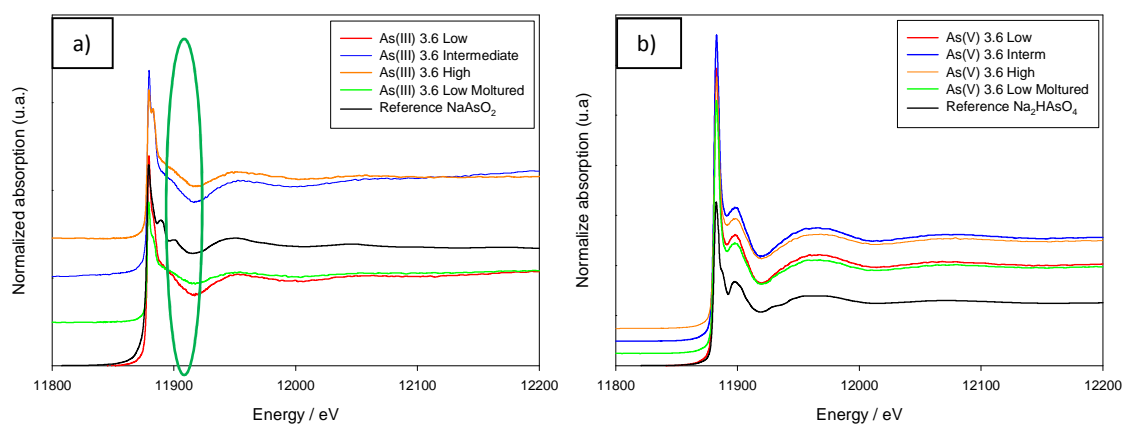
Figure 4. As K-edge XANES spectra for the As(V) (a) and As(III) (b) adsorption over Forager® Sponge loaded SPION. The green circle remarks the differences between As(III) standard and samples.

The effect in the adsorption process of the presence of the two species of arsenic was studied by the direct speciation study as shown by the **Figure 5**. All samples present same k near-edge, a fact that inform of the present of the same species in all samples. Direct comparison of XANES spectra for arsenic standards and samples shows that it is not observed a contribution

of arsenite standard in the real samples and the samples spectra are very similar to the arsenate standard.
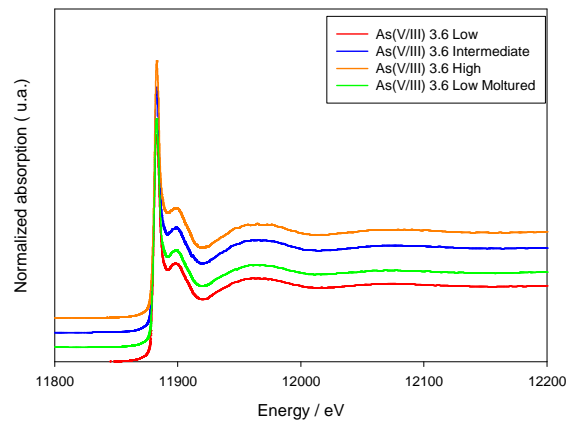
Figure 5. As K-edge XANES spectra for the As(III)/As(V) mixture adsorption over Forager® Sponge loaded SPION.

Then, the effect of arsenic species in the adsorption process was quantitatively analysed by applying Principal Analysis Components (PCA) and linear combination fit, as shown by the **Figure 6**, to ascertain the contribution of each As reference species.
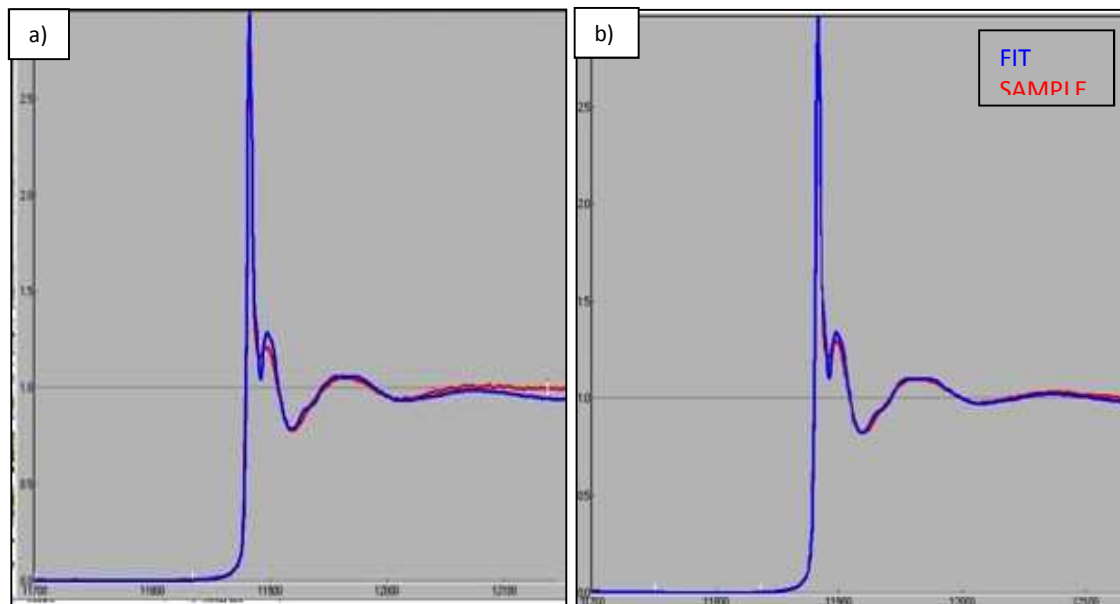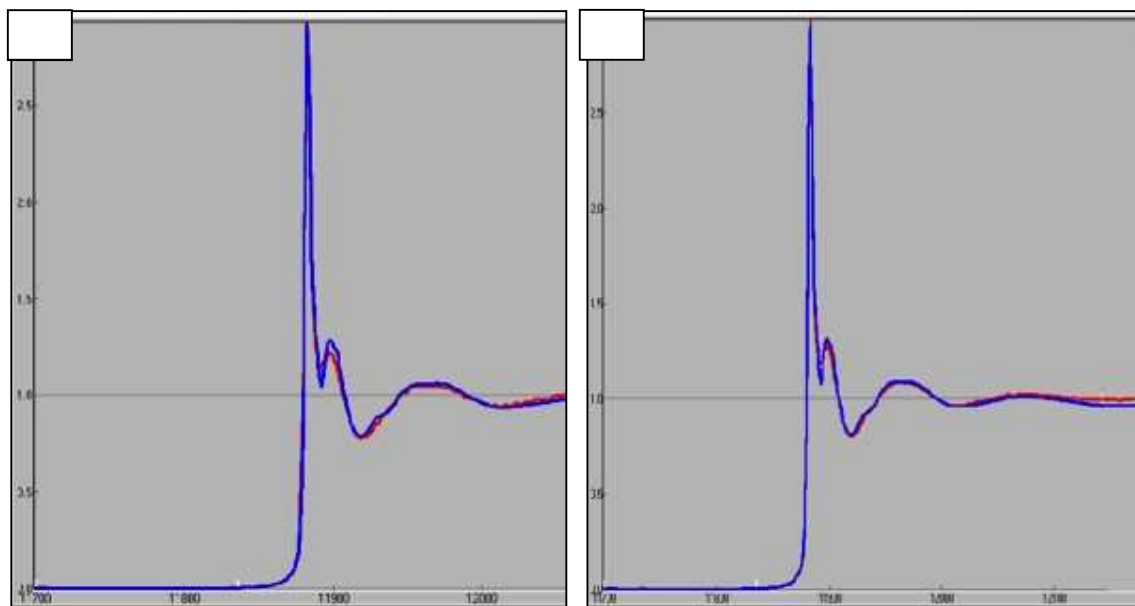
Figure 6. PCA analysis for the Forager® Sponge loaded SPION with low SPION concentration at different pHs, 2.0 (a), 3.6 (b), 5.6 (c) and 3.6 with previous milled sample (d).

The results confirm, for all analysed samples (Forager® Sponge loaded SPION with low SPION concentration at different pHs), that arsenate specie is predominant reaching until 97% (**Figure 7**). The sum of both species is 100 ± 2 %. Then, arsenate is easily removed of the contaminated water with this adsorbent system.

Figure 7. Total arsenite and arsenate distribution in Forager® Sponge loaded SPION normalized to percentage.

As speciation distribution shows, As(V) is easily removed of the contaminated solutions with this adsorbent system and the analysis of these synthetic samples have validated the data analysis to be applied in real samples.

Iron speciation

Like in the arsenic speciation experiments, initial iron concentrations were analyzed by Field Portable X-Ray fluorescence equipment (FP-XRF) for both standards and samples in order to verify if the standards and samples have enough Fe concentration to perform the synchrotron experiments (**Table 2**).[28]

Table 2. Initial iron concentrations for standards and samples by FP-XRF.

Standards [Fe] (mg/kg)					
FeCl$_3$	32257±473	**FeCl$_2$**	40838±609	**FeCl$_3$/FeCl$_2$**	47625±721
SPION	65092±722	**SPION-As(III)**	66918±730	**SPION-As(V)**	71376±801
Samples [Fe] (mg/kg)					
As(III) 3.6 1i	4416±71	**As(V) 3.6 1i**	3857±63	**As(III-V) 3.6 1i**	4308±72
As(III) 4.0 1i	4226±69	**As(V) 4.0 1i**	3792±61	**As(III-V) 4.0 1i**	5209±85
As(III) 3.6 2i	5841±91	**As(V) 3.6 2i**	7023±109	**As(III-V) 3.6 2i**	7961±128
As(III) 4.0 2i	5632±84	**As(V) 4.0 2i**	7655±119	**As(III-V) 4.0 2i**	8677±135
As(III) 3.6 3i	10887±163	**As(V) 3.6 3i**	9781±150	**As(III-V) 3.6 3i**	13941±210
As(III) 4.0 3i	7905±131	**As(V) 4.0 3i**	12836±198	**As(III-V) 4.0 3i**	9369±144
As(III) 3.6 1iM	3909±65	**As(V) 3.6 1iM**	4151±68	**As(III-V) 3.6 1iM**	4101±64

Sample concentration is lower than standards concentration. This fact is because of the standards are composed of a pure salt slightly diluted with polyethylene and in the samples case, only the Fe from SPION is detected. For this study, more standard samples are used; SPION standards were used in order to have knowledge about its response in front of synchrotron radiation.

Iron reference compounds. The iron K near-edge spectra for pure iron reference compounds of Fe^{3+} ($FeCl_3.6H_2O$), Fe^{2+} ($FeCl_2.4H_2O$), Fe^{3+}/Fe^{2+} mixture and SPION (Fe_3O_4) in presence of the different inorganic arsenic species are shown in **Figure 8¡Error! No se encuentra el origen de la referencia.**. A shift of the edge position to higher energies becomes as iron is more oxidized. This appears in the comparison of $FeCl_3.6H_2O$ and $FeCl_2.4H_2O$ and as the XANES spectra shows, both k near-edges reach to 7133.0 eV. Unique explanation is that $FeCl_2$ has suffered oxidation during the sample preparation and analysis process. By other side, there exists a shift position respect SPION standards and while k near-edge for iron salts is 7133.0 eV, k near-edge for SPION standards is 7136.8 eV.
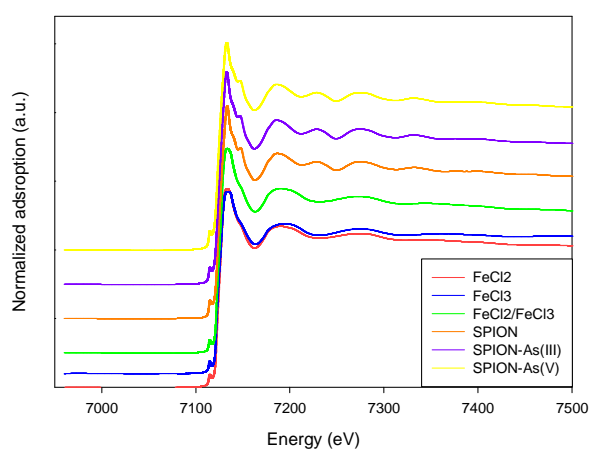
Figure 8. Fe XANES spectra of different reference compounds

Then, only the SPION standards are going to be used for the comparison with samples in the iron speciation.

Iron speciation in SPION from Forager® Sponge loaded SPION. The direct comparison of XANES spectra for SPION standards and Forager® Sponge loaded SPION samples was made. This direct comparison, see **¡Error! No se encuentra el origen de la referencia.**, determine that the SPION keeps the structure in the adsorption process in all cases, independently of the adsorbed species, As(III), As(V) or a mixture of both species.
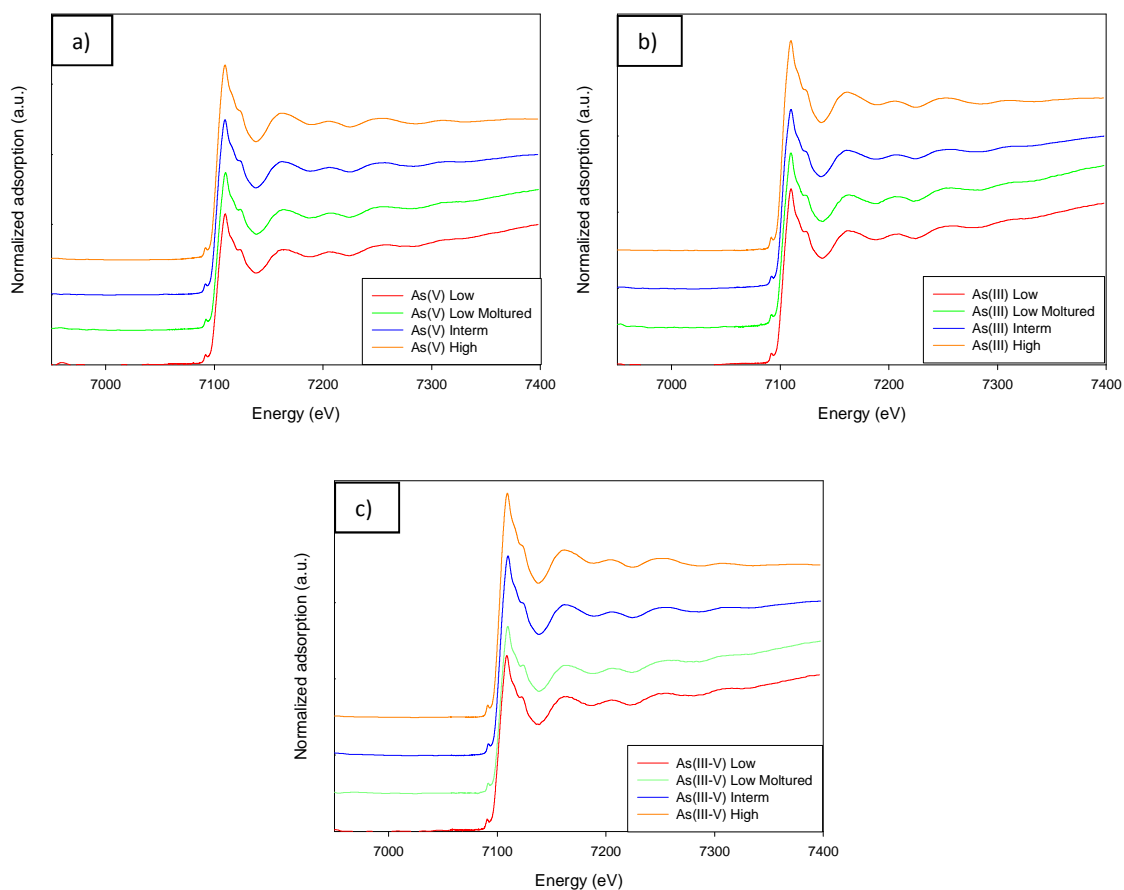
Figure 9. Fe k-edge XANES spectra for Forager® Sponge loaded SPION samples for each arsenic adsorption process: As(III) (a), As(V) (b) and As(III)/As(V) mixture (c).

CONCLUSIONS

Considering the obtained results, XANES was successfully applied as a method to better understand the influence of arsenic speciation in water due to the sensitivity of the beamlines BM25 (ESRF) and A1 (HASYLAB). Direct speciation by synchrotron radiation technique has been verified as a useful technique for the arsenic speciation in solid samples. Principal Analysis Components (PCA) and linear combination fit were applied to ascertain the contribution of each arsenic reference species and the results confirm, for analysed Forager® Sponge loaded SPION at different pHs, that arsenate specie is predominant reaching until 97%. Then, arsenate is easily removed of the contaminated water with this adsorbent system. The SPION keeps the structure in the adsorption process in all cases, independently of the adsorbed species, As(III), As(V) or a mixture of both species.

REFERENCES

1. Smedley, P.L., Kinniburgh, D.G. A review of the source, behaviour and distribution of arsenic in natural waters. *Applied Geochemistry,* **2002,** *17*, 517–568.

**2.** WHO, (World Health Organization) Toward a More Operational Response: Arsenic contamination in South and East Asian Countries. Technical Report No. 31303, 2005.

3. Bagla P, Kaiser J. India's spreading health crisis draws global arsenic experts. *Science*, **1996**, *274*, 174–175.

4. Fendrof, S., Eick, M. J., Grossl, P., Sparks, D.L. Arsenate and chromate retention mechanisms on goethite: I. Surface structure. *Environ. Sci. Technol.,* **1997**, *31*, 315-320.

5. Sherman, D.M., Randall, S.R. Surface complexation of arsenic (V) to iron (III) (hydr)oxides: Structural mechanism from ab initio molecular geometries and EXAFS spectroscopy. *Geochimica et cosmochimica Acta*, **2003**, *67*, 4223-4230.

6. Farquhar, M.L., Charnock, J.M., Livens, F.R., Vaughan, D.J. Mechanisms of arsenic uptake from aqueous solution by interaction with goethite, lepidocrocite, mackinawite, and Pyrite: An X-Ray Absorption Spectrescopy Study. *Environ. Sci. Technol.*, **2002**, *36*, 1757-1762.

7. Waychunas, G.A., Rea, B. A., Fuller, C. C., Davis, J.A. Surface chemistry of ferrihydrite: Part 1. EXAFS studies of the geometry of coprecipitated and absorbed absorbed arsenate. *Geochmica et Cosmochimica Acta*, **1993**, *57*, 2251-2269.

8. Jessen, S., Larsen, F., Koch, C.B., Arvin, E. Sorption and desorption of arsenic to ferrihydrite in a sand filter. *Environ. Sci. Technol.*, **2005**, *39*, 8045-8051.

9. Jia, Y., Xu, L., Fang, Z., Demopoulos, G.P. Observation of surface precipitation of arsenate on ferrihydrite. *Environ. Sci. Technol.* **2006**, *40*, 3248-3253.

10. Singh, D.B., Prasad, G., Rupainwar, D.C. Adsorption technique for the treatment of As(V)-rich effluents. *Colloids and Surfaces A.*, **1996,** 49-56.

11. Gimenez, J., Martinez, M., Pablo, J., Rovira, M., Duro, L. Arsenic sorption onto natural hematite, magnetite and goethite. *Journal of Hazardous Materials.,* **2007**, *141*, 575-580.

12. Shipley, H.J., Yean, S., Kan, A.T., Tomson, M.B. Adsorption of arsenic to magnetite nanoparticles: Effect of particle concentration, pH, ionic strength, and temperature. *Environmental Toxicology and Chemistry*, **2009**, *28(3)*, 509-515

13. Li, Z., Jean, J.S., Jiang, W.T., Chang, P.H., Chen, C.J. Removal of arsenic from water using Fe-Exchanged natural zeolite. *Journal of Hazardous Materials*, **2010**, *87(1-3)*, 318-323.

14. Dousova, B., Grygar, T., Martaus, A., Fuitova, L., Kolousek, D., Machovic, V. Sorption of As(V) on aluminosilicates treated with Fe(II) nanoparticles. *Journal of Colloid and Interface Science.*, **2006**, *302*, 424-431.

15. Rau, I., Gonzalo, A., Valiente, M. Arsenic(V) adsorption by immobilized iron mediation. Modeling of the adsorption process and influence of interfering anions. *Reactive & Functional Polymers*, **2003**, *54*, 85–94.

16. Muñoz, M., Gonzalo, A., Valiente, M. Arsenic(V) removal from aqueous solutions by iron(III) loaded chelating resin. *Environ, Sci. Technol.*, **2002**, *36*.

17. Sayers, D.E., Stern, E.A., Lytle, F.W. New technique for investigating noncrystalline structures. Fourier analysis of extended X-ray absorption fine structure. *Phys. Rev. Lett.*, **1971**, *27*, 1204–1207.

18. Manning, B.A., Fendorf, S.E., Goldberg, S. Surface structures and stability of arsenic(III) on goethite: spectroscopic evidence for inner-sphere complexes. *Environ. Sci. Technol*, **1998**, *32*, 2383–2388.

19. La Force, M.J., Hansel, C.M., Fendorf, S. Arsenic speciation, seasonal transformations, and co-distribution with iron in a mine waste-influenced palustrine emergent wetland. *Environ Sci Technol.*, **2000**, *33*, 3937–3943.

20. Farquhar, M.L., Charnock, J.M., Livens, F.R., Vaughan, D.J. Mechanisms of arsenic uptake from aqueous solution by interaction with goethite, lepidocrocite, mackinawite, and pyrite: an X-ray absorption spectroscopy study. *Environ Sci. Technol.*, **2002**, *36*, 1757–1762.

21. Smith PG, Koch I, Gordon RA, Mandoli DF, Chapman BD, Reimer KJ. X-ray absorption near-edge structure analysis of arsenic species for application to biological environmental samples. *Environ Sci Technol.*, **2005**, *39*, 248–254.

22. Ona-Nguema, G., Morin, G., Juillot, F., Calas, G., Brown, G.E. EXAFS analysis of arsenite adsorption onto two-line ferrihydrite, hematite, goethite, and lepidocrocite. *Environ Sci Technol.*, **2005**, *39*, 9147–9155.

23. Jing, C., Liu, S., Patel, M., Meng, X. Arsenic leachability in water treatment adsorbents. *Environ Sci Technol.*, **2005**, *39*, 5481–5487.

24. Jing, C., Meng, X., Liu, S., Baidas, S., Patraju, R., Christodoulatos, C., Korfiatis, G.P. Surface complexation of organic arsenic on nanocrystalline titanium oxide. *J Colloid Interface Sci.,* **2005**, *290*, 14–21.

25. Morillo, D., Valiente, M., Perez, G., **2009**. Avances en la adsorción de Arsénico con Nanopartículas, Proyecto de Investigación, Master Universitario en Ciencias y Tecnologías Químicas, Universitat Autònoma de Barcelona.

26. Muñoz, J.A., Gonzalo, A., Valiente, M. Arsenic adsorption by Fe(III)-loaded Open-Celled Cellulose Sponge. Thermodynamic and Selective Aspects. *Environmental Science and Technology*, **2002**, *36*, 3405-3411.

27. Kim, C.S., Bloom, N.S., Rytuba, J.J., Brown, G.E. Jr. Mercury speciation by X-ray adsorption fine structure spectroscopy and sequential chemical extractions: A comparison of speciation methods. *Environmental Science and Technology*, **2003**, *37*, 5102-5108.

28. Chakraborty, S., Bardelli, F., Mullet, M., Greneche, J.M., Varma, S., Ehrhardt, J.J., Banerjee, D., Charlet, L. Spectroscopic studies of arsenic retention onto biotite. *Chemical Geology*, **2011**, *281*, 83-92.

29. Manning, B.A., Fendorf, S.E., Goldberg, S. Surface Structures and Stability of Arsenic(III) on Goethite: Spectroscopic Evidence for Inner-Sphere Complexes. *Environmental Science and Technology*, **1998**, *32 (16)*, 2383-2388.

ANNEX II

Applied Spanish Patent

II.1. Superparamagnetic Iron Oxide Nanoparticles loaded PAN nanofibers as novel adsorbent of metals from contaminated water.

II.1. Superparamagnetic Iron Oxide Nanoparticles loaded PAN nanofibers as novel adsorbent of metals from contaminated water.

SOLICITUD DE PATENTE ESPAÑOLA

Núm. 201330144

Documentación aportada
con la solicitud

Título :	*"Filtro de tratamiento de líquidos con nanopartículas de magnetita y procedimientos correspondientes"*
Organismo Oficial :	Oficina Española de Patentes y Marcas (OEPM)
Titulares registrales:	ACONDICIONAMIENTO TARRASENSE y UNIVERSITAT AUTONOMA DE BARCELONA
Fecha de presentación :	6 febrero 2013

Para tratar cualquier extremo referente a este expediente,
sírvanse dirigirse a nuestra OFICINA de Barcelona haciendo constar
*la REFERENCIA **P201330144–SJP/mge***

Justificante de presentación electrónica de solicitud de patente

Este documento es un justificante de que se ha recibido una solicitud española de patente por vía electrónica, utilizando la conexión segura de la O.E.P.M. Asimismo, se le ha asignado de forma automática un número de solicitud y una fecha de recepción, conforme al artículo 14.3 del Reglamento para la ejecución de la Ley 11/1986, de 20 de marzo, de Patentes. La fecha de presentación de la solicitud de acuerdo con el art. 22 de la Ley de Patentes, le será comunicada posteriormente.

Número de solicitud:	P201330144
Fecha de recepción:	06 febrero 2013, 18:16 (CET)
Oficina receptora:	OEPM Madrid
Su referencia:	R-9699-P2013-01
Solicitante:	ACONDICIONAMIENTO TARRASENSE
Número de solicitantes:	2
País:	ES
Título:	FILTRO DE TRATAMIENTO DE LÍQUIDOS CON NANOPARTÍCULAS DE MAGNETITA Y PROCEDIMIENTOS CORRESPONDIENTES
Documentos enviados:	Descripcion-1.pdf (14 p.) Reivindicaciones.pdf (2 p.) Resumen-1.pdf (1 p.) Dibujos.pdf (4 p.) OLF-ARCHIVE.zip POWATT.pdf (1 p.) FEERCPT-1.pdf (1 p.) FEERCPT-2.pdf (1 p.)	package-data.xml es-request.xml application-body.xml es-fee-sheet.xml feesheet.pdf request.pdf
Enviados por:	CN=NOMBRE JORDA PETERSEN SANTIAGO - NIF 46117744F,OU=701002583,OU=FNMT Clase 2 CA,O=FNMT,C=ES
Fecha y hora de recepción:	06 febrero 2013, 18:16 (CET)
Codificación del envío:	A6:50:40:71:86:00:1A:D4:78:78:E3:B8:62:8D:77:8A:DA:CE:52:C4

/Madrid, Oficina Receptora/

(1) MODALIDAD:		
	PATENTE DE INVENCIÓN	[✔]
	MODELO DE UTILIDAD	[ ]

(2) TIPO DE SOLICITUD:		
	PRIMERA PRESENTACIÓN	[✔]
	ADICIÓN A LA PATENTE EUROPEA	[ ]
	ADICIÓN A LA PATENTE ESPAÑOLA	[ ]
	SOLICITUD DIVISIONAL	[ ]
	CAMBIO DE MODALIDAD	[ ]
	TRANSFORMACIÓN SOLICITUD PATENTE EUROPEA	[ ]
	PCT: ENTRADA FASE NACIONAL	[ ]

(3) EXP. PRINCIPAL O DE ORIGEN:	
MODALIDAD:	
N.º SOLICITUD:	
FECHA SOLICITUD:	

4) LUGAR DE PRESENTACIÓN:	
	OEPM, Presentación Electrónica

(5) DIRECCIÓN ELECTRÓNICA HABILITADA (DEH):	

(6-1) SOLICITANTE 1:	
DENOMINACIÓN SOCIAL:	ACONDICIONAMIENTO TARRASENSE
NACIONALIDAD:	España
CÓDIGO PAÍS:	ES
DNI/CIF/PASAPORTE:	G08360232
CNAE:	
PYME:	
DOMICILIO:	C/ de la Innovación, 2 Parc Científic i Tecnologic de Terrassa - Orbital 40
LOCALIDAD:	Terrassa
PROVINCIA:	08 Barcelona
CÓDIGO POSTAL:	08225
PAÍS RESIDENCIA:	España
CÓDIGO PAÍS:	ES
TELÉFONO:	
FAX:	
PERSONA DE CONTACTO:	

MODO DE OBTENCIÓN DEL DERECHO:	
INVENCIÓN LABORAL:	[✔]
CONTRATO:	[ ]
SUCESIÓN:	[ ]

(6-2) SOLICITANTE 2:	
DENOMINACIÓN SOCIAL:	UNIVERSITAT AUTONOMA DE BARCELONA
NACIONALIDAD:	España
CÓDIGO PAÍS:	ES
DNI/CIF/PASAPORTE:	Q0818002H
CNAE:	
PYME:	
DOMICILIO:	Edifici A, Campus Universitari UAB
LOCALIDAD:	Bellaterra
PROVINCIA:	08 Barcelona
CÓDIGO POSTAL:	08193
PAÍS RESIDENCIA:	España
CÓDIGO PAÍS:	ES
TELÉFONO:	
FAX:	

PERSONA DE CONTACTO:	
MODO DE OBTENCIÓN DEL DERECHO: INVENCIÓN LABORAL: CONTRATO: SUCESIÓN:	[✓] [ ] [ ]

(7-1) INVENTOR 1:

APELLIDOS:	Amantia
NOMBRE:	David
NACIONALIDAD:	Francia
CÓDIGO PAÍS:	FR
DNI/PASAPORTE:	X6176599H

(7-2) INVENTOR 2:

APELLIDOS:	Aubouy
NOMBRE:	Laurent
NACIONALIDAD:	Francia
CÓDIGO PAÍS:	FR
DNI/PASAPORTE:	X6630707Z

(7-3) INVENTOR 3:

APELLIDOS:	Faccini
NOMBRE:	Mirko
NACIONALIDAD:	Italia
CÓDIGO PAÍS:	IT
DNI/PASAPORTE:	Y0562856Z

(7-4) INVENTOR 4:

APELLIDOS:	Morillo Martín
NOMBRE:	Diego
NACIONALIDAD:	España
CÓDIGO PAÍS:	ES
DNI/PASAPORTE:	71023576-J

(7-5) INVENTOR 5:

APELLIDOS:	Pérez González
NOMBRE:	Gustavo
NACIONALIDAD:	España
CÓDIGO PAÍS:	ES
DNI/PASAPORTE:	34748082-G

(7-6) INVENTOR 6:

APELLIDOS:	Valiente Malmagro
NOMBRE:	Manuel
NACIONALIDAD:	España
CÓDIGO PAÍS:	ES
DNI/PASAPORTE:	38398789-J

(8) TÍTULO DE LA INVENCIÓN:	FILTRO DE TRATAMIENTO DE LÍQUIDOS CON NANOPARTÍCULAS DE MAGNETITA Y PROCEDIMIENTOS CORRESPONDIENTES
(9) PETICIÓN DE INFORME SOBRE EL ESTADO DE LA TÉCNICA: SI NO	[✓] [ ]
(10) SOLICITA LA INCLUSIÓN EN EL PROCEDIMIENTO ACELERADO DE CONCESIÓN SI NO	[ ] [✓]
(11) EFECTUADO DEPÓSITO DE MATERÍA BIOLÓGICA: SI NO	[ ] [✓]
(12) DEPÓSITO: REFERENCIA DE IDENTIFICACIÓN: INSTITUCIÓN DE DEPÓSITO: NÚMERO DE DEPÓSITO: ACCESIBILIDAD RESTRINGIDA A UN EXPERTO (ART. 45.1. B):	

(13) DECLARACIONES RELATIVAS A LA LISTA DE SECUENCIAS:	
LA LISTA DE SECUENCIAS NO VA MÁS ALLÁ DEL CONTENIDO DE LA SOLICITUD	[ ]
LA LISTA DE SECUENCIAS EN FORMATO PDF Y ASCII SON IDENTICOS	[ ]

(14) EXPOSICIONES OFICIALES:	
LUGAR:	
FECHA:	

(15) DECLARACIONES DE PRIORIDAD:	
PAÍS DE ORIGEN:	
CÓDIGO PAÍS:	
NÚMERO:	
FECHA:	

(16) AGENTE/REPRESENTANTE:	
APELLIDOS:	CURELL AGUILÀ
NOMBRE:	Mireia
CÓDIGO DE AGENTE:	0535/5
NACIONALIDAD:	España
CÓDIGO PAÍS:	ES
DNI/CIF/PASAPORTE:	35036646-X
DOMICILIO:	CURELL SUÑOL SLP - Passeig de Gràcia, 65 bis
LOCALIDAD:	Barcelona
PROVINCIA:	08_Barcelona
CÓDIGO POSTAL:	08008
PAÍS RESIDENCIA:	España
CÓDIGO PAÍS:	ES
TELÉFONO:	934875166
FAX:	934880321
CORREO ELECTRÓNICO:	mail@curellsunol.es
NÚMERO DE PODER:	

(17) RELACIÓN DE DOCUMENTOS QUE SE ACOMPAÑAN:	
DESCRIPCIÓN:	[✔] N.º de páginas: 14
REIVINDICACIONES:	[✔] N.º de reivindicaciones: 14
DIBUJOS:	[✔] N.º de dibujos: 4
RESUMEN:	[✔] N.º de páginas: 1
FIGURA(S) A PUBLICAR CON EL RESUMEN:	[✔] N.º de figura(s): 2
ARCHIVO DE PRECONVERSION:	[✔]
DOCUMENTO DE REPRESENTACIÓN:	[✔] N.º de páginas: 1
JUSTIFICANTE DE PAGO (1):	[✔] N.º de páginas: 1
JUSTIFICANTE DE PAGO (2):	[✔] N.º de páginas: 1
LISTA DE SECUENCIAS PDF:	[ ] N.º de páginas:
ARCHIVO PARA LA BUSQUEDA DE LS:	[ ]
OTROS (Aparecerán detallados):	

(18) EL SOLICITANTE SE ACOGE AL APLAZAMIENTO DE PAGO DE TASA PREVISTO EN EL ART. 162 DE LA LEY 11/1986 DE PATENTES, DECLARA: BAJO JURAMIENTO O PROMESA SER CIERTOS TODOS LOS DATOS QUE FIGURAN EN LA DOCUMENTACIÓN ADJUNTA:	[ ]
DOC COPIA DNI:	[ ] N.º de páginas:
DOC COPIA DECLARACIÓN DE CARENCIA DE MEDIOS:	[ ] N.º de páginas:
DOC COPIA CERTIFICACIÓN DE HABERES:	[ ] N.º de páginas:
DOC COPIA ÚLTIMA DECLARACIÓN DE LA RENTA:	[ ] N.º de páginas:
DOC COPIA LIBRO DE FAMILIA:	[ ] N.º de páginas:
DOC COPIA OTROS:	[ ] N.º de páginas:

(19) NOTAS:	
1) Poder General :	Se hace constar que en relación con el solicitante Universitat Autònoma de Barcelona, el representante cuenta con un Poder General nº 201203842
2) Firma :	Se hace constar que la presente

		solicitud ha sido firmada por Santiago Jordá Petersen Código de Agente 0978/4 "por mi compañero"
(20) FIRMA:		
	FIRMA DEL SOLICITANTE O REPRESENTANTE:	NOMBRE JORDA PETERSEN SANTIAGO - NIF 46117744F
	LUGAR DE FIRMA:	Barcelona
	FECHA DE FIRMA:	06 Febrero 2013

MINISTERIO
DE INDUSTRIA, ENERGIA
Y TURISMO

Oficina Española
de Patentes y Marcas

Identificación

Ejercicio: 2013

Nro. Justificante: 7915114874694

Sujeto Pasivo:

N.I.F.:   Apellidos y Nombre o Razón social:

Calle/Plaza/Avda.:   Nombre de la via pública: Nº   Esc   Piso   Puerta   Tfno.

Municipio: Provincia: Código Postal:

Agente o Representante legal: (1)

N.I.F.:   Apellidos y Nombre o Razón social:

B08503963   **CURELL SUÑOL SLP**

Calle/Plaza/Avda.:   Nombre de la via pública: Nº   Esc   Piso   Puerta   Tfno.

Municipio: Provincia: Código Postal:

Código de Agente o Representante: (2)   Digito de control:

0220

Autoliquidación

Titular del expediente si es distinto del pagador: **ACONDICIONAMIENTO TARRASENSE y UNIVERSITAT AUTONOMA DE BARCELONA**

Expediente Modalidad: **P**   Número: Tipo: (3)

Clave: **IE01**   Año: **2013**   Concepto: **Solicitud de Invenci por Internet**

Unidades: **1**   Importe: **62,43**

Referencia OEPM: **88072214294**

909992100200188072214294

Declarante

Fecha: **31/01/2013**

Firma:

CURELL SUÑOL SLP

Ingreso

Importe en Euros: **62,43**

Adeudo en cuenta: (X)

Entidad: Oficina: D.C.   Nro. Cuenta

2100

NRC Asignado: 7915114874694000000002

(1) Solo cuando el pago se realice con cargo a la cuenta corriente del representante o agente.

(2) En el caso de que tenga asignado un número por la OEPM.

(3)En el caso de patentes europeas, se pondrá una P si es el número de publicación o una S si es el número de solicitud.

(4) Una copia de este impreso se acompañará con la presentación de documentación en la OEPM.

Identificación

Ejercicio: 2013

Nro. Justificante: 7915114874694

Sujeto Pasivo:

N.I.F.: Apellidos y Nombre o Razón social:

Calle/Plaza/Avda.: Nombre de la via pública: Nº Esc Piso Puerta Tfno.

Municipio: Provincia: Código Postal:

Agente o Representante legal: (1)

N.I.F.: Apellidos y Nombre o Razón social:

B08503963 **CURELL SUÑOL SLP**

Calle/Plaza/Avda.: Nombre de la via pública: Nº Esc Piso Puerta Tfno.

Municipio: Provincia: Código Postal:

Código de Agente o Representante: (2) Digito de control:

0220

Autoliquidación

Titular del expediente si es distinto del pagador:

ACONDICIONAMIENTO TARRASENSE y UNIVERSITAT AUTONOMA DE BARCELONA

Expediente Modalidad: **P** Número: Tipo: (3)

Clave: **IE04** Año: **2013** Concepto: **Solicitud IET Internet**

Unidades: **1** Importe: **576,19**

Referencia OEPM: **88072214181**

909992100200188072214181

Declarante

Fecha: **31/01/2013**

Firma:

CURELL SUÑOL SLP

Ingreso

Importe en Euros: **576,19**

Adeudo en cuenta: ⊗

Entidad: Oficina: D.C. Nro. Cuenta

2100

NRC Asignado: 7915114874694000000001

(1) Solo cuando el pago se realice con cargo a la cuenta corriente del representante o agente.

(2) En el caso de que tenga asignado un número por la OEPM.

(3) En el caso de patentes europeas, se pondrá una P si es el número de publicación o una S si es el número de solicitud.

(4) Una copia de este impreso se acompañará con la presentación de documentación en la OEPM.

OFICINA ESPAÑOLA DE PATENTES Y MARCAS

Hoja informativa sobre pago de tasas de una solicitud de patente o modelo de utilidad

1. REFERENCIA DE SOLICITUD	R-9699-P2013-01	
2. TASAS	**Importe (en euros)**	
Concepto	**Código de barras asignado**	**Importe**
IE01 Solicitud de demanda de depósito o de rehabilitación.	88072214294	62,43
IE02 Solicitud de cambio de modalidad en la protección		0,00
IE04 Petición IET	88072214181	576,19
IE06 Prioridad extranjera (0)		0,00
El solicitante se acoge a la exención del pago de tasas	❏	
El solicitante es una Universidad pública	❏	
Importe total		638,62
Importe abonado		638,62

Se ha aplicado el 15% de descuento sobre la tasa de solicitud de acuerdo con la D. Adic. 8.2 Ley de Marcas.

CURELL SUÑOL
SOCIEDAD LIMITADA PROFESIONAL

Para la OEPM /For SPTMO	Represent. Ref.

ESPAÑA - PODER DE AGENTE
SPAIN - POWER OF ATTORNEY

NO REQUIERE LEGALIZACIÓN
NO LEGALIZATION REQUIRED

A. **OTORGANTE** (persona física o entidad otorgante)
   GRANTOR (authorizing natural person or entity)

Nombre(s): ACONDICIONAMIENTO TARRASENSE
Name(s)
Domicilio: C/ de la Innovación, 2 Parc Cientific i Tecnologic de Terrassa - Orbital 40
Address   08225 Terrassa (Barcelona)

B. **REPRESENTANTES**
   REPRESENTATIVES

Marcelino Curell Suñol, Mireia Curell Aguilà, Oscar Pirez Tarín, Santiago Jordá Petersen, Jordi Güell Serra indistintamente, todos ellos con domicilio profesional en Passeig de Gràcia 65 bis, Barcelona y sucursal en Madrid.
(Marcelino Curell Suñol, Mireia Curell Aguilà, Oscar Pirez Tarín, Santiago Jordá Petersen, Jordi Güell Serra severally, all with place of business in Passeig de Gràcia 65 bis, Barcelona and branch office in Madrid)

C. **NATURALEZA DEL PODER** (marcar la casilla apropiada)
   NATURE OF POWER (check the appropriate box)

☐ **Poder general:** Para todo tipo de procedimientos y actuaciones, como solicitante o titular, con relación a cualesquiera solicitudes y registros presentes o futuros, asi como para desistir de, o limitar, cualesquiera procedimientos o actuaciones efectuados en nombre del poderdante.
(General Power: For all proceedings and actions, as applicant or owner, in relation to all present or future applications or registrations, as well as to withdraw from, or restrict, any actions or proceedings undertaken in the name of the signatory.

☒ **Poder específico:** Para las solicitudes, registros y/o procedimientos indicados a continuación:
(Specific Power: For the following applications, registrations and/or proceedings):

solicitud de PATENTE DE INVENCION por "FILTRO DE TRATAMIENTO DE LÍQUIDOS CON NANOPARTÍCULAS DE MAGNETITA Y PROCEDIMIENTOS CORRESPONDIENTES"

D. **AMPLITUD:** El poder se extiende a todo tipo de actuaciones, procedimientos y fines, con plena facultad de delegación y sustitución.
   (EXTENT: Authorization is given for all type of actions, proceedings and purposes, with full power of delegation and substitution)

E. **FIRMANTE** (persona física que firma el poder)
   SIGNATORY (natural person signing this power)

Nombre: JOAN PARRA FARRÈ
Name
Cargo: DIRECTOR GERENTE
Position Y APODERADO

Fecha y firma:
Date and signature
06/02/2013

FILTRO DE TRATAMIENTO DE LÍQUIDOS CON NANOPARTÍCULAS DE MAGNETITA Y PROCEDIMIENTOS CORRESPONDIENTES

5 DESCRIPCIÓN

Campo de la invención

10 La invención se refiere a un filtro de tratamiento de líquidos, a un procedimiento de fabricación de un soporte para un filtro de tratamiento de líquidos y a un procedimiento de tratamiento de un líquido.

15 Estado de la técnica

La contaminación de las aguas por arsénico (usualmente en forma de As(III) y As(V) inorgánico) es un problema de salud pública en diversos lugares. Es conocido el empleo de óxidos de hierro para la eliminación de metales en general y del 20 arsénico en particular. Entre estos óxidos de hierro, la magnetita, en nanopartículas, es particularmente eficaz. Estas nanopartículas de magnetita se denominan habitualmente SPION (del inglés SuperParamagnetic Iron Oxide Nanoparticles – nanopartículas de óxido de hierro superparamagnético)

25 En el documento WO 2007/032860 se describe un filtro para la eliminación de arsénico en agua que comprende un soporte de poliacrilonitrilo (PAN) cargado con nanopartículas de hidróxido de hierro.

En el documento Morillo, D, Valiente, M., Perez, G., "Avances en la adsorción de 30 Arsénico con Nanopartículas", Proyecto de Investigación, Master Universitario en Ciencias y Tecnologías Químicas, Universitat Autònoma de Barcelona, Septiembre 2009, se describe el empleo de una esponja de celulosa como soporte, en la que se ha dispersado SPION, para la eliminación de arsénico en agua.

En el documento "Eletromagnetic properties of electrospun Fe_3O_4/carbon composite nanofibers". Bayat et a., Polymer 52 (2011)1645-53, se describen unas nanofibras de PAN que contienen diferentes cantidades de nanopartículas de magnetita.

En el documento "Polyacrylonitrile-based nanofibers- A state of the art review". Nataraj, et al. Progress in Polymer Science 37 (2012) 487-513, se describe la fabricación de nanofibras de PAN y se cita su posible uso como soporte de nanopartículas de óxidos de hierro para su aplicación como filtro.

Existe, sin embargo, la necesidad de seguir mejorando la eficiencia de los filtros basados en SPION para el tratamiento de aguas, y, en general, de líquidos.

Sumario de la invención

La invención tiene por objeto un filtro de tratamiento de líquidos caracterizado porque comprende un soporte de un material polimérico que presenta por lo menos un grupo funcional del grupo formado por carboxilo y tiol, cargado con SPION.

Efectivamente, se ha observado que unos filtros con unos soportes como los indicados presentan una capacidad de adsorción de arsénico muy superior a la que presentan filtros con soportes conocidos. Probablemente ello sea debido a que con los soportes indicados se consigue reducir la tendencia a la agregación de las partículas de SPION gracias a que los grupos carboxilo y/o tiol tienen una mejor capacidad de fijación de las partículas de SPION. De esta manera se consigue una superficie específica activa mayor y, en consecuencia, una mayor capacidad de adsorción de arsénico y, en general, de los metales que se desee eliminar. Además, esta mayor eficacia significa otras mejoras, como por ejemplo una reducción del volumen de almacenado de los residuos de filtrado.

Preferentemente el soporte son fibras de poliacrilonitrilo hidrolizado de fórmula general
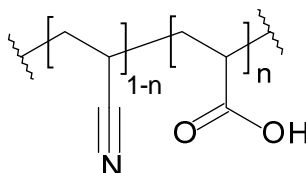
donde n está comprendido entre 0,01 y 1.

El empleo de fibras de PAN es conocido. Sin embargo, en la presente invención se ha descubierto que durante la reacción de hidrólisis (para dotar a las fibras de PAN de grupos carboxilo, de esta forma denominadas HPAN), las fibras resultantes experimentan un proceso de hinchado, lo que favorece el contacto y el paso del líquido a través de las mismas.

Ventajosamente el SPION tiene un tamaño de partícula medio comprendido entre 1 nm y 100 nm, y muy preferentemente entre 5 nm y 30 nm.

Ventajosamente las fibras tienen un tamaño medio comprendido entre 100 nm y 3 µm, y muy preferentemente entre 300 nm y 1µm. Se ha observado que dentro de estos rangos de tamaños de fibras hay un máximo de capacidad de adsorción. En general, en la presente descripción y reivindicaciones se hace referencia al tamaño de las fibras para referirse a su diámetro.

Ventajosamente el contenido de SPION es menor de 40 mg de SPION por g de fibra, y muy preferentemente es menor de 20 mg de SPION por g de fibra. Probablemente ello sea debido a que cantidades mayores de SPION favorecen la agregación del mismo, dificultando su aprovechamiento óptimo.

La invención también tiene por objeto un procedimiento de fabricación de un soporte para un filtro de tratamiento de líquidos caracterizado porque comprende:

[a] una etapa de electrohilatura en la que se prepara una solución de PAN en un disolvente que tiene un contenido de PAN comprendido entre 5 y 80% en peso, respecto del peso total de la solución y preferentemente comprendido entre 8,5 y 15% en peso, respecto del peso total de la solución,

5

[b] una etapa de hidrólisis de las fibras de PAN formadas en la etapa [a], y

[c] una etapa de carga de las fibras con SPION.

10 Efectivamente, este procedimiento ha permitido obtener el soporte cargado con SPION con las mejoras indicadas anteriormente.

Preferentemente la etapa de hidrólisis se realiza por inmersión de las fibras en una solución acuosa de un hidróxido alcalinotérreo que, ventajosamente tiene un pH

15 comprendido entre 11 y 13 y/o una temperatura comprendida entre 25ºC y 100ºC.

La invención tiene asimismo por objeto un procedimiento de tratamiento de un líquido, caracterizado porque se hace pasar el líquido a tratar por un filtro de acuerdo con la invención. Preferentemente el líquido es agua, y preferentemente el

20 líquido a tratar contiene As(III) y/o As(V).

Breve descripción de los dibujos

25 Otras ventajas y características de la invención se aprecian a partir de la siguiente descripción, en la que, sin ningún carácter limitativo, se relatan unos modos preferentes de realización de la invención, haciendo mención de los dibujos que se acompañan. Las figuras muestran:

30 Fig. 1, Efecto de la concentración de PAN en el tamaño de las fibras y en la modificación de éstas.

Fig. 2, Comparación de la capacidad de adsorción de HPAN-SPION y de SPION cargado en una esponja Forager.

Fig. 3, capacidad de adsorción de cada sistema adsorbente sintetizado.

Fig. 4, capacidad de adsorción respecto al tamaño de fibra.

Descripción detallada de unas formas de realización de la invención

1 - Metodología

1.1 - Síntesis de fibras de PAN

Se prepararon soluciones de electrohilatura (en inglés, "electrospinning") mediante soluciones de PAN de entre un 7 y un 15 % en peso en DMF (dimetilformamida). Se aplicó una agitación magnética durante 3 horas a 60ºC con el fin de obtener soluciones homogéneas de PAN. Se colocó la solución de electrohilatura en una jeringa de 10 ml con una aguja metálica de 0,020 mm de diámetro. Se utilizó una fuente de energía para proporcionar un elevado voltaje de 20 a 30 kV a la punta de la aguja de la jeringa y a un colector metálico. Se recogieron las fibras electrohiladas en una lámina de aluminio obteniendo un material textil con un tamaño de 60x20 cm. Se utilizó una distancia del colector a la punta comprendida entre 10 y 30 cm, y un caudal de solución comprendido entre 0,1 y 2,0 ml/h. Todos los procedimientos de electrohilatura se llevaron a cabo a temperatura ambiente (25ºC) con una humedad relativa del 50%. Las fibras obtenidas se secaron en un horno de vacío durante un periodo de 24 horas a 60 ºC para realizar caracterizaciones y experimentos de adsorción.

1.2 - Modificación de PAN y síntesis de fibras de HPAN cargadas con SPION

Se sumergieron fibras de PAN con una superficie de 200 cm^2 en 100 ml de NaOH al 15% durante 60 minutos a 50 ºC. Posteriormente, se lavó la membrana con agua

destilada y se colocó en 1,0 M de HCl a temperatura ambiente durante 120 minutos. El color de las fibras de PAN amarillentas hidrolizadas (las denominadas HPAN) pasó a ser blanco (el color inicial). Después de esto, la membrana se sumergió en 100 ml de una solución de etilendiamina (EDA) al 10% durante 60 minutos a temperatura ambiente (HPAN-EDA). Finalmente, se sumergieron las fibras de HPAN y de HPAN-EDA en 100 ml de una solución de 0,01 M de TMAOH con diferentes cantidades de nanopartículas SPION (de 0 a 15 mg de SPION) durante un periodo de 12 horas a temperatura ambiente.

Las fibras de PAN y de HPAN cargadas con SPION se caracterizaron utilizando un Microscopio Electrónico de Transmisión (TEM), un Microscopio Electrónico de Barrido (SEM) y un Espectrómetro de Infrarrojos de Transformada de Fourier de Reflectancia Total Atenuada (ATR-FTIR). No se caracterizaron las fibras de HPAN-EDA debido a la reducida capacidad de fijación de las nanopartículas SPION de dichas fibras, tal como se muestra más adelante.

1.3 - Adsorción de arsénico As(V) en discontinuo

Los primeros estudios de adsorción se llevaron a cabo en discontinuo. Se sumergieron 100 mg de fibra de HPAN cargada con SPION (esta cantidad se mantuvo constante en todos los experimentos, en modo continuo y en discontinuo) en 50 ml de una solución de arsenato a 100 ppm a un pH comprendido entre 3,6 y 4,0. La solución se agitó en una máquina vibratoria durante 1 hora. La cantidad de arsénico adsorbido en la fibra se determinó midiendo las concentraciones iniciales y finales de arsénico mediante un espectrofotómetro UV/Vis en una longitud de onda de 880 nm utilizando un reactivo colorimétrico. Los resultados obtenidos mediante la espectrofotometría UV/Vis se verificaron mediante la utilización de ICP-MS (Inductively coupled plasma mass spectrometry – espectrometría de masas por plasma acoplado inductivamente).

Estos estudios se llevaron a cabo en condiciones extremas debido a que la U.S. EPA ha reducido la máxima concentración permitida en agua a 10ppb. A

continuación, se realizan experimentos a 100ppm de As(V), a fin de saturar el sistema adsorbente y poder observar su capacidad de adsorción.

1.4 - Adsorción de arsénico As(V) en modo continuo

El segundo paso consistió en la mejora del sistema de adsorción mediante la utilización de un modo continuo con adsorción en columna. Se introdujeron 100mg de fibras de HPAN cargadas con SPION en dos columnas de tamaños diferentes (10x1,0 and 20x1,5 cm) y se hizo que 2 litros de 20ppm de As(V) atravesaran la columna con un caudal de 1ml/min durante 24 horas. Se realizó la recogida periódica de la muestra a los tiempos de: 0, 1, 2, 3, 4, 5, 10, 15, 20, 30, 60, 90, 120, 150, 180, 210, 240, 270, 300, 330, 360, 1320 y 1440 minutos.

1.5 - Aplicación del sistema adsorbente en una muestra real de aguas residuales

Se utilizó agua de lixiviación para realizar estos experimentos. Esta agua lixiviada (el pH de la solución es de aproximadamente 4) está exenta de As(V) y está dopada con 5 ppm de As(V) en solución. Las condiciones experimentales son las mismas que en el modo continuo con un tamaño de columna de 20x1,5 cm.
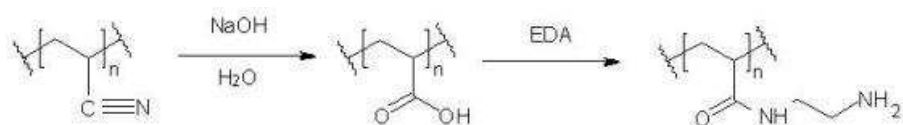
2 - Resultados y discusión

2.1 - Caracterización de fibras de PAN y de PAN hidrolizadas

Microscopio Electrónico de Transmisión (TEM).

Se utilizó el siguiente procedimiento para modificar las fibras de PAN obtenidas por electrohilatura:

Partiendo de PAN se obtuvo PAN hidrolizado (HPAN) tras una etapa de hidrólisis con NaOH. Adicionalmente se hizo reaccionar HPAN con etilendiamina (EDA) para obtener HPAN-EDA.

5   Con el fin de determinar la concentración óptima de PAN para realizar las fibras más útiles para esta aplicación se hicieron preparaciones de fibras a varias concentraciones de PAN..

Tal como muestra la Fig. 1, un aumento de la concentración de PAN de la solución
10   de electrohilatura produce un aumento del tamaño de las fibras, de manera que se llegan a obtener tamaños superiores a la micra cuando la concentración de PAN es elevada (15 % en peso).

2.2 - Caracterización de fibras de HPAN cargadas con SPION

15

El procedimiento de partida de la fijación de SPION sobre las fibras se desarrolló en los tres tipos de fibras electrohiladas: PAN, HPAN y HPAN-EDA. Estas preparaciones se llevaron a cabo para verificar lo recogido en la literatura relacionada, en la que se indica que las fibras de HPAN-EDA electrohiladas son
20   más eficaces para la fijación de SPION gracias a la presencia de los grupos amida y amina.

Sin embargo, sorprendentemente se ha observado que las fibras de PAN y HPAN-EDA presentan una fijación inferior de las nanopartículas SPION, tras 12 horas de
25   contacto, que las fibras de HPAN. Las fibras de HPAN muestran una fijación prácticamente total de las nanopartículas SPION de la suspensión (la cantidad máxima es 150 mg de SPION por gramo de fibra).

La cantidad de SPION que está fijada sobre la superficie de las fibras de HPAN se
30   cuantifica mediante la ICP-MS tras la preparación de muestras por medio del sistema de digestión por microondas. En la tabla siguiente se muestra la cantidad de SPION fijada sobre las fibras con respecto al teórico.

	Fe en muestra / mg	SPION en muestra / mg	SPION teórico/ mg
PAN - SPION	0,73	1,01	14,41
HPAN - SPION	10,12	13,98	14,41
HPAN-EDA - SPION	0,94	1,29	14,41

Los resultados muestran que un 97% de la cantidad inicial de SPION se fijó sobre la superficie de las fibras de HPAN frente a un 7% y un 9% que se fijó sobre las fibras de HPAN-EDA y PAN, respectivamente. Esto es particularmente sorprendente ya que en los documentos del estado de la técnica se propone la transformación de PAN en HPAN-EDA para mejorar la fijación de SPION y, si bien el proceso de formación de HPAN-EDA incluye una etapa de formación de HPAN, ni siquiera se sugiere la posibilidad de emplear HPAN como soporte para el SPION. Por lo tanto, el estado de la técnica, al descartar directamente el HPAN como soporte para el SPION está creando un prejuicio técnico contra esta posibilidad ya que la lectura de este documento desmotivaría al lector a intentar el empleo de HPAN como soporte para SPION.

2.3 - Adsorción de arsénico As(V) en discontinuo

Se desarrollaron distintos experimentos en discontinuo con el fin de analizar los distintos sistemas adsorbentes llevados a cabo y de determinar su capacidad de adsorción. Una comparación inicial con otro sistema adsorbente puede proporcionar información referente a la mejora de la capacidad de adsorción. El estudio del efecto de la concentración de PAN en la solución de electrohilatura sobre la capacidad de adsorción determinará el intervalo de tamaños de las fibras, en el que éstas proporcionan un mejor valor de la capacidad de adsorción.

2.3.1 - Comparación de la capacidad de adsorción de As(V) de las fibras de HPAN cargadas con SPION y nanopartículas SPION cargadas en una esponja Forager®.

De acuerdo con el estado de la técnica (ver documento "Master de D. Morillo" citado anteriormente), las nanopartículas SPION cargadas en una esponja Forager® constituyen un sistema adsorbente que muestra una elevada capacidad de adsorción gracias a una buena dispersión de SPION sobre la superficie celulósica de la esponja.

Tal como muestra la Fig. 2, las fibras de HPAN cargadas con SPION presentan un perfil de adsorción diferente con respecto a la esponja. El nuevo material adsorbente tiene una capacidad de adsorción reducida cuando la cantidad de SPION presente en la fibra de HPAN es elevada. Parece que el SPION se agrega en la superficie de la fibra de HPAN lo que no permite que el SPION trabaje de manera óptima (aumento de la agregación, descenso de la superficie específica y descenso de la capacidad de adsorción).

Sin embargo, cuando la cantidad de SPION está comprendida entre aproximadamente 5 y 40 mg por gramo de fibra de HPAN, la capacidad de adsorción aumenta de modo exponencial y la capacidad de adsorción alcanza 32 mmol As(V) / g de SPION, casi tres veces más que las nanopartículas SPION cargadas en la esponja Forager®.

2.3.2 - Adsorción de As(V) para diferentes tamaños de fibras de HPAN cargadas con SPION

La Fig. 3 presenta los resultados de la capacidad de adsorción de las distintas fibras de HPAN cargadas con SPION que han sido sintetizadas con distintas concentraciones de PAN en la solución de electrohilado. Como ya se ha comentado anteriormente, la concentración de PAN en la solución de electrohilado se traduce en un tamaño diferente de las fibras obtenidas. La diferencia entre el ensayo "HPAN 7 %" y el ensayo "HPAN 7d %" radica en el hecho que en el caso HPAN 7d se ha duplicado el tiempo de electrohilado, depositándose así una capa de fibras sobre el colector de electrohilado de doble grosor, manteniéndose el diámetro de las fibras.

La comparación de la capacidad de adsorción de As(V) que se obtiene bien con las nanopartículas SPION empleadas de una forma directa (es decir, directamente en suspensión del agua a tratar, sin ningún soporte), bien con las nanopartículas SPION cargadas en la esponja Forager®, respecto a los sistemas adsorbentes a base de fibras, muestran que éstos alcanzan una capacidad de adsorción similar o superior, excepto en el caso de las fibras de HPAN con un tamaño de 250 nm. En este caso parecen haberse producido dos efectos: por un lado, la aglomeración de fibras provoca el descenso de la penetración de la disolución a tratar en el sistema de adsorción y, por otro lado, la dispersión de SPION es menor que en otros casos.

Al comparar los compuestos de fibras sintetizados, las fibras de HPAN cargadas con SPION con fibras que tienen un tamaño de 350 nm presentan la máxima capacidad de adsorción y la cantidad óptima de SPION es de aproximadamente 2,9 mg de SPION por gramo de HPAN sobre la superficie de fibras. Al contrario de lo que cabría suponer, las fibras de menor tamaño presentan una capacidad de adsorción menor (Fig. 4). Esta menor capacidad de adsorción puede deberse a la distribución de las fibras de HPAN tal como muestran las imágenes de TEM en la Fig. 1. Así pues, la aglomeración de fibras afecta a la dispersión de SPION debido a que éstas disponen de una menor superficie de contacto para el SPION.

Una observación interesante e importante en el caso de las fibras de HPAN cargadas con SPION, con un tamaño de fibra de 350 nm, es que el compuesto de fibras crece en grandes proporciones (se hincha). Así, por ejemplo, 100 mg de fibras de HPAN cargadas con SPION pueden ocupar, en dos horas, un volumen de 500 ml de una solución acuosa.

2.4 - Adsorción de As(V) en modo continuo

Una vez se determinó el tamaño óptimo y la máxima capacidad de adsorción en discontinuo, se llevaron a cabo experimentos de adsorción en modo continuo, con el fin de observar el comportamiento del sistema adsorbente en un modo real de

trabajo de una futura aplicación y por este motivo, se emplearon diferentes tamaños de columna.

2.4.1 - Columnas de 10x1 cm:

5

Se realizan tres experimentos de adsorción en modo continuo por gravedad con fibras de HPAN cargadas con SPION que presentan distintas cantidades de SPION por gramo de HPAN (144,1 mg de SPION; 2,9 mg y un blanco de HPAN). Se observó que en las fibras de HPAN cargadas con SPION, cuanto mayor es la

10 cantidad de SPION, mayor es el aumento de la compresión de las fibras dentro de la columna. Este hecho resulta problemático para el proceso de adsorción, porque la superficie de contacto entre las fibras y la solución de arsénico disminuye y, en consecuencia, el tiempo de contacto es menor.

15 Asimismo se observa que las fibras de HPAN cargadas con SPION con 2,9 mg de SPION por gramo de HPAN presentan una capacidad de adsorción de aproximadamente 52,6 mmol de As(V) por gramo de SPION, lo que es aproximadamente el doble que la misma muestra en el ensayo en discontinuo (punto 2.3 anterior). Probablemente ello sea debido a que, en el modo continuo, la

20 solución puede penetrar más fácilmente en el compuesto de fibras, de manera que provoque que el As(V) sea más eficazmente retenido.

En este procedimiento de adsorción, aparecen dos problemas distintos: la compresión del compuesto de fibras y la adsorción rápida de As(V). Se ha

25 observado que a los 10 minutos, las fibras de HPAN cargadas con SPION están saturadas y la adsorción finaliza.

Los resultados muestran que las adsorciones en columna son más eficaces que las adsorciones en discontinuo.

30

2.4.2 - Columnas de 20x1,5 cm:

Se han realizado experimentos de adsorción en modo continuo tanto por gravedad como en contracorriente para los compuestos de fibras de HPAN-SPION con 2,9
5 mg de SPION por gramo de HPAN (cantidad óptima) en columnas de 20x1,5 cm. En este caso, el compuesto de fibras de HPAN-SPION no está comprimido durante todo el experimento. Este hecho resuelve un punto problemático en el proceso de adsorción cuando se utilizan columnas más pequeñas.

10 Tal como muestran los resultados de la tabla siguiente, mientras la adsorción en el modo de gravedad alcanza hasta 20,25 mol de As(V)/g de SPION, la adsorción en contracorriente obtiene una capacidad de adsorción de aproximadamente 63 mol de As(V)/g de SPION. Entonces, la capacidad de adsorción del sistema alcanza los 850 mg de As(V) / g del sistema adsorbente.

15

Este resultado es superior al de todos los sistemas adsorbentes estudiados y observados en la literatura. Este hecho podría deberse a que se dispone de un sistema con una gran superficie específica, que genera una alta dispersión del SPION, evitando la agregación debida al magnetismo de las nanopartículas, y que
20 permite que la disolución de arsénico circule por el sistema con mayor facilidad haciendo más efectivo el contacto con los centros de adsorción activos (SPION).

Parámetros	Gravedad	Contracorriente 1	Contracorriente 2
Desorbente	1,0M HNO_3	1,0M HNO_3	0,5M H_3PO_4
Tiempo de contacto (min)	20	60	60
As(V) adsorbido (mg)	28,4	83,9	86,1
Q max (mol As / g SPION)	20,25	62,30	64,51
Q Sistema (mg As / g HPAN-SPION)	317,7	830,1	851,7
Tiempo de desorción (min)	90	90	90
As(V) desorbido (mg)	0,32	8,48	6,64

Respecto al proceso de desorción, en este caso, únicamente el 10% del As(V) adsorbido había sido recuperado utilizando soluciones desorbentes, tales como ácido nítrico o ácido fosfórico. Esta etapa se realiza en un proceso de optimización con el fin de obtener un mayor porcentaje de recuperación.

5

Una consideración importante es el comportamiento del sistema a lo largo del tiempo. Los experimentos en contracorriente presentan un perfil distinto respecto al experimento de gravedad, al observarse que los experimentos en contracorriente proporcionan una mayor adsorción durante más tiempo. Este hecho puede deberse

10   a que en los ensayos en contracorriente, se elimina la posibilidad de que se generen canales de adsorción preferentes, forzando así a que la disolución de arsénico entre en contacto con toda la superficie del sistema adsorbente.

2.5 - Aplicación del sistema adsorbente en muestras reales de aguas residuales

15

Se llevaron a cabo experimentos de adsorción y desorción para estudiar el comportamiento de una muestra real y para comparar si el sistema adsorbente resultaba útil para esta aplicación cuando hay que tratar agua real contaminada.

20   Se realizó una comparación entre una muestra real (agua de lixiviado de vertedero) y el experimento sintético del comportamiento en contracorriente para observar si el sistema adsorbente funcionaba del mismo modo, comprobándose que ambos experimentos son similares.

REIVINDICACIONES

1 – Filtro de tratamiento de líquidos caracterizado porque comprende un soporte de un material polimérico que presenta por lo menos un grupo funcional del grupo formado por carboxilo y tiol, cargado con SPION.

2 – Filtro según la reivindicación 1, caracterizado porque dicho soporte son fibras de poliacrilonitrilo hidrolizado de fórmula general
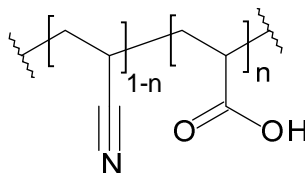
donde n tiene un valor comprendido entre 0,01 y 1.

3 – Filtro según una de las reivindicaciones 1 ó 2, caracterizado porque dicho SPION tiene un tamaño de partícula medio comprendido entre 1 nm y 100 nm

4 – Filtro según la reivindicación 3, caracterizado porque dicho SPION tiene un tamaño de partícula medio comprendido entre 5 nm y 30 nm.

5 – Filtro según cualquiera de las reivindicaciones 2 a 4, caracterizado porque dichas fibras tienen un tamaño medio comprendido entre 100 nm y 3 μm.

6 – Filtro según la reivindicación 5, caracterizado porque dichas fibras tienen un tamaño medio comprendido entre 300 nm y 1μm.

7 – Filtro según cualquiera de las reivindicaciones 2 a 6, caracterizado porque el contenido de SPION es menor de 40 mg de SPION por g de fibra.

8 – Filtro según la reivindicación 7, caracterizado porque el contenido de SPION es menor de 20 mg de SPION por g de fibra.

9 – Procedimiento de fabricación de un soporte para un filtro de tratamiento de líquidos caracterizado porque comprende:

[a] una etapa de electrohilatura en la que se prepara una solución de PAN en un disolvente que tiene un contenido de PAN comprendido entre 5 y 80% en peso, respecto del peso total de la solución y preferentemente comprendido entre 8,5 y 15% en peso, respecto del peso total de la solución,

[b] una etapa de hidrólisis de las fibras de PAN formadas en la etapa [a], y

[c] una etapa de carga de dichas fibras con SPION.

10 – Procedimiento según la reivindicación 9 caracterizado porque dicha etapa de hidrólisis se realiza por inmersión de dichas fibras en una solución acuosa de un hidróxido alcalinotérreo.

11 – Procedimiento según la reivindicación 10, caracterizado porque dicha solución acuosa tiene un pH comprendido entre 11 y 13.

12 – Procedimiento según una de las reivindicaciones 10 u 11, caracterizado porque dicha solución acuosa está a una temperatura comprendida entre 25ºC y 100ºC

13 – Procedimiento de tratamiento de un líquido, caracterizado porque se hace pasar el líquido a tratar por un filtro según cualquiera de las reivindicaciones 1 a 8.

14 – Procedimiento según la reivindicación 13, caracterizado porque el líquido a tratar contiene As(III) y/o As(V).
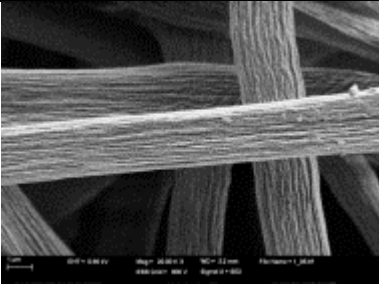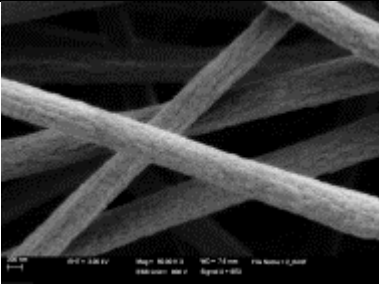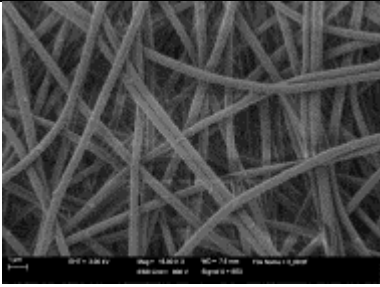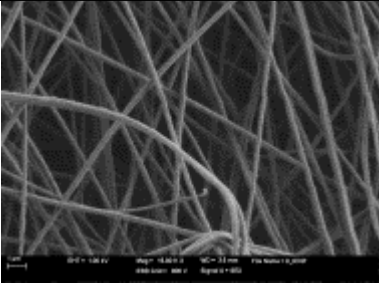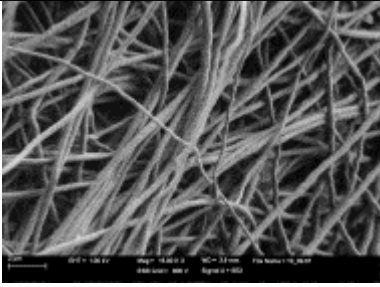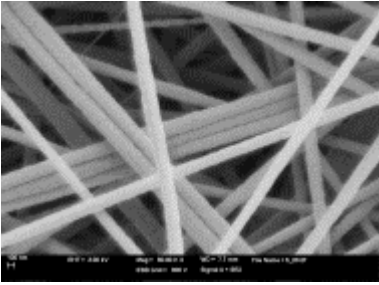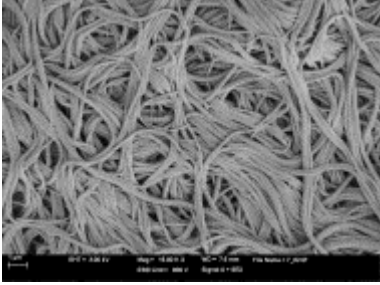
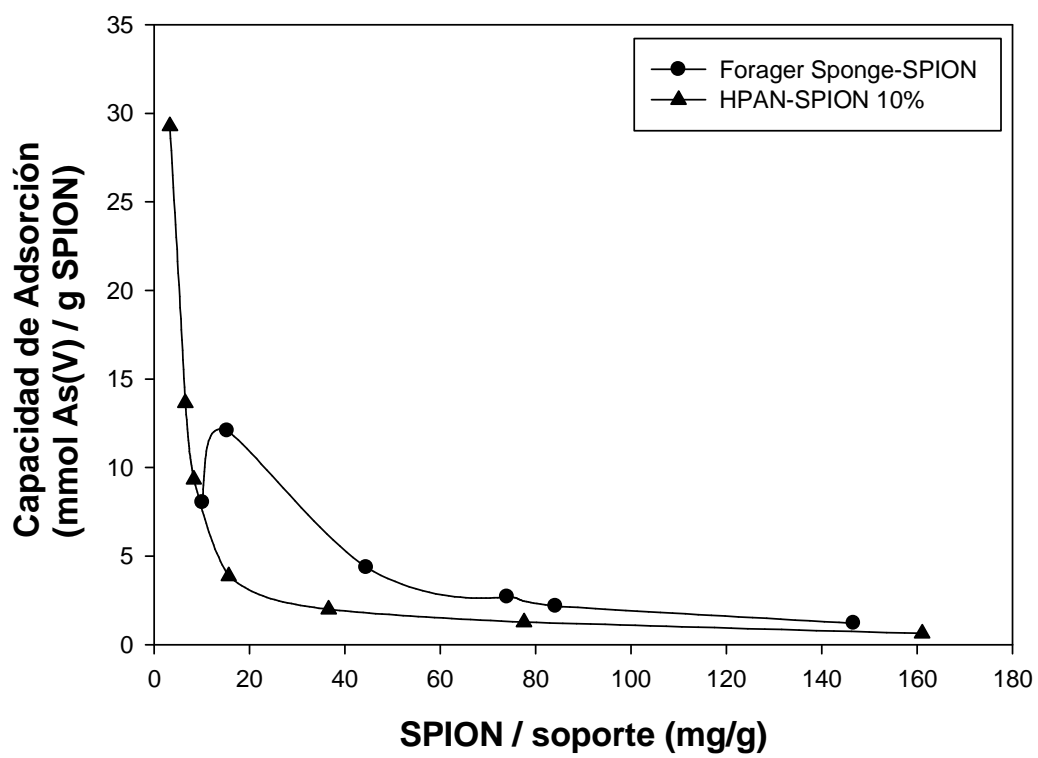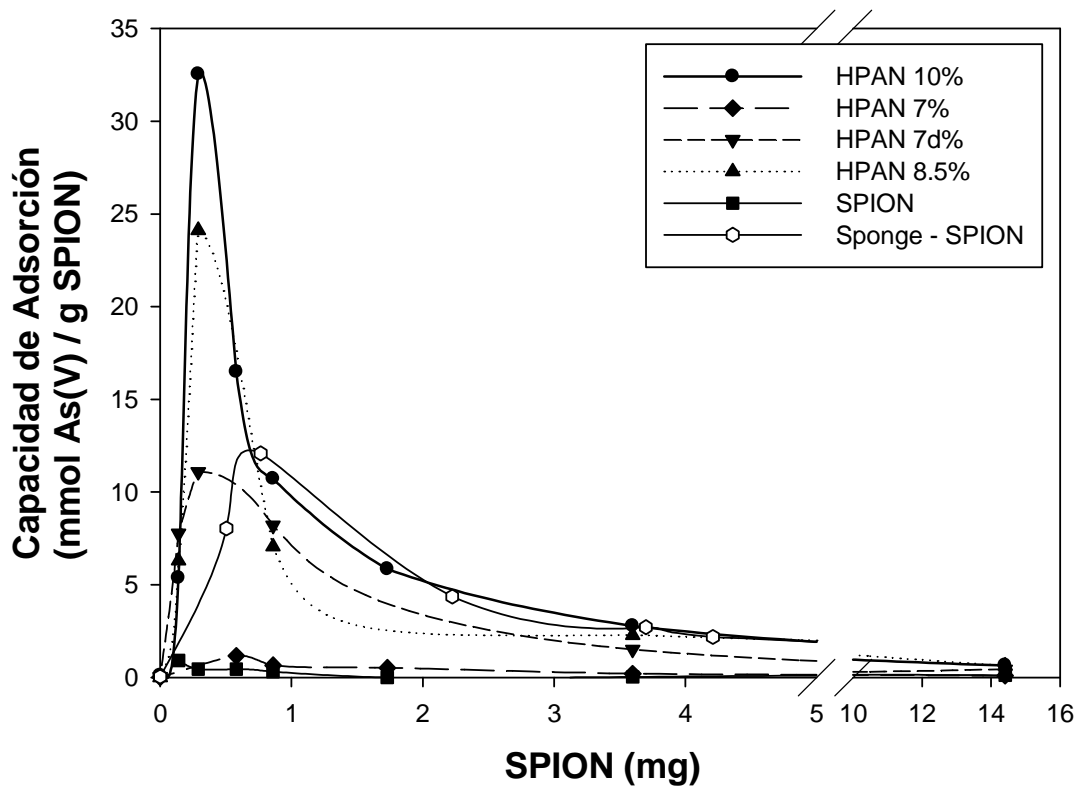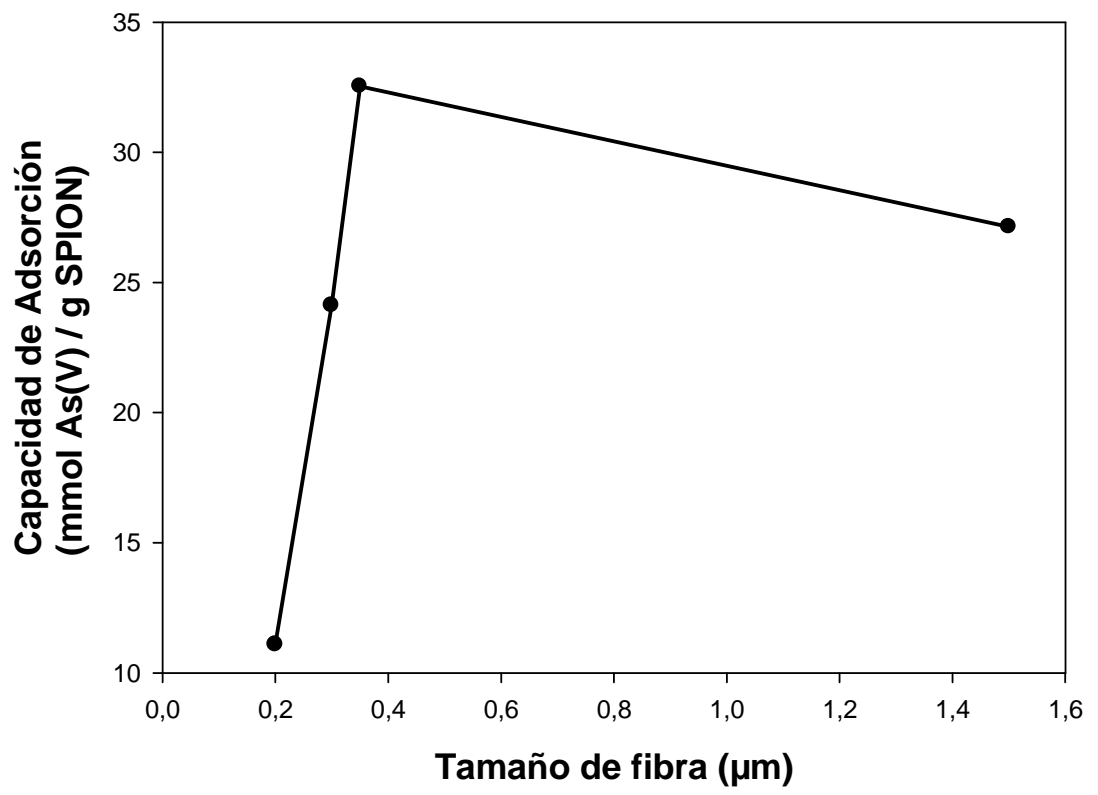| PAN % en peso	PAN	HPAN	Tamaño de la fibra
15			1,5 µm
10			350 nm
8,5			300 nm
7			200 nm

Fig. 1

Fig. 2

Fig. 3

Fig. 4

FILTRO DE TRATAMIENTO DE LÍQUIDOS CON NANOPARTÍCULAS DE MAGNETITA Y PROCEDIMIENTOS CORRESPONDIENTES

RESUMEN

5

Filtro de tratamiento de líquidos con nanopartículas de magnetita y procedimientos correspondientes. Filtro de tratamiento de líquidos que comprende un soporte de un material polimérico que presenta por lo menos un grupo funcional del grupo formado por carboxilo y tiol, cargado con SPION (SuperParamagnetic Iron Oxide Nano-

10 particles). El soporte es ventajosamente fibras de poliacrilonitrilo hidrolizado de fórmula general
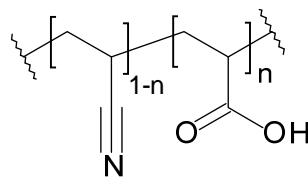
donde n tiene un valor comprendido entre 0,01 y 1, y donde el procedimiento de

15 fabricación comprende:

[a] una etapa de electrohilatura en la que se prepara una solución de poliacrilonitrilo en un disolvente que tiene un contenido de poliacrilonitrilo comprendido entre 5 y 80% en peso, respecto del peso total de la solución,

20

[b] una etapa de hidrólisis de las fibras de poliacrilonitrilo formadas en la etapa [a], y

[c] una etapa de carga de dichas fibras con SPION.

25

(Fig. 2)